Staphylococcal antimicrobial biosynthetic gene clusters and their impact on bacterial fitness

Dissertation

der Mathematisch-Naturwissenschaftlichen Fakultät

der Eberhard Karls Universität Tübingen

zur Erlangung des Grades eines

Doktors der Naturwissenschaften

(Dr. rer. nat.)

vorgelegt von

Sophia Krauß

aus Bad Windsheim

Tübingen

2022

Gedruckt mit Genehmigung der Mathematisch-Naturwissenschaftlichen Fakultät der Eberhard Karls Universität Tübingen.

Tag der mündlichen Qualifikation:	02.09.2022
Stellvertretender Dekan:	Prof. Dr. Thilo Stehle
1. Berichterstatter:	Prof. Dr. Andreas Peschel
2. Berichterstatter:	Prof. Dr. Christiane Wolz

Table of contents

Abstract

The human nasal microbiome comprises a distinct community of bacterial species and its composition is strongly influenced by microbe-microbe and microbe-host interactions. To overcome competitors and to finally achieve niche occupation, bacteria can produce antimicrobial compounds like bacteriocins inhibiting competing bacteria in the vicinity of the producer cell. Recent studies could demonstrate that biosynthetic gene clusters encoding secondary metabolites like bacteriocins are frequently found in staphylococci isolated from the human nasal microbiome. Furthermore, these gene clusters show strong signs of mobility mediated by horizontal gene transfer, due to their localisation on plasmids or mobile genetic elements. Thus, horizontal gene transfer allows bacteria to rapidly acquire bacteriocin biosynthetic gene clusters to either remain or invade new ecological niches. However, the metabolic costs which are associated with sudden bacteriocin production are barely studied. Here, we describe the mechanism of secretion and producer immunity of the microbiome-derived antimicrobial lugdunin, report about another novel antimicrobial compound produced by a human nasal *Staphylococcus epidermidis* isolate, called epifadin, and we describe that horizontal gene transfer of micrococcin P1 negatively effects bacterial fitness and central metabolism, which can be bypassed by adaptive mutation.

We demonstrate that secretion of and self-resistance to lugdunin, the first fibupeptide antibiotic isolated from the human nasal microbiome, is achieved by two distinct ABC transporters, which are encoded in the lugdunin operon. Our study could show the distinct but also overlapping roles of the two transporters and that both are required for full level lugdunin resistance. Epifadin is the first example of a staphylococcal bacteriocin produced by both, non-ribosomal peptide synthetases (NRPS) and polyketide synthases (PKS). It shows activity against a broad spectrum of major nasal microbiome members despite its very short half-life, making epifadin a very unusual antimicrobial molecule.

Furthermore, we report that horizontal gene transfer of the biosynthetic gene cluster encoding the thiopeptide micrococcin P1 in the lab strain *Staphylococcus aureus* RN4220 leads to a growth defect and disturbances of the cellular metabolism in the new host. Thus, we could demonstrate that sudden bacteriocin production is a burden for the new producer, which can be, however, reverted by adaptive mutation in *citZ*, encoding the citrate synthase, turning micrococcin P1 production into a benefit.

Our findings highlight the frequent occurrence and high mobility of bacteriocin biosynthetic gene clusters in the human nasal microbiome and the costs and benefits which are associated with acquisition of these gene clusters.

Zusammenfassung

Das humane nasale Mikrobiom besteht aus einer Vielzahl verschiedener Arten von Bakterien, dessen Zusammensetzung durch Interaktionen zwischen Bakterien untereinander aber auch durch Interaktionen mit dem Wirt beeinflusst wird. Um einen Vorteil gegenüber anderen konkurrierenden Bakterien zu erlangen und sich in der jeweiligen ökologischen Nische durchzusetzen, können Bakterien antimikrobielle Substanzen wie Bakteriozine produzieren, die es dem Produzenten ermöglichen Kontrahenten in ihrer Umgebung zu inhibieren. Studien haben gezeigt, dass Biosynthesegencluster die sekundäre Metabolite wie Bakteriozine kodieren, sehr häufig in nasalen Staphylokokken-Isolaten gefunden werden können. Darüber hinaus zeigen diese Gencluster aufgrund ihrer Lokalisierung auf Plasmiden oder mobilen genetischen Elementen Anzeichen von Mobilität durch horizontalen Gentransfer. Über horizontalen Gentransfer können Bakterien Biosynthesegencluster für Bakteriozine schnell erwerben, um sich entweder in ihrer ökologischen Nische zu behaupten oder in neue einzudringen. Der erhöhte metabolische Aufwand, der mit der plötzlichen Bakteriozinproduktion verbunden ist, ist jedoch kaum untersucht. Wir beschreiben hier den Mechanismus der Sekretion und Produzentenimmunität für den aus dem Mikrobiom stammenden antimikrobiellen Wirkstoff Lugdunin, berichten über eine weitere neuartige antimikrobiell wirksame Verbindung namens Epifadin, die von einem humanen nasalen *Staphylococcus epidermidis* Isolat produziert wird, und wir zeigen den negativen Einfluss des per horizontalem Gentransfer übertragenen Micrococcin P1 auf die Fitness und den zentralen Stoffwechsel des neuen Produzenten, welcher durch eine adaptive Mutation aufgehoben werden kann.

Wir können zeigen, dass die Sekretion und Selbstresistenz von Lugdunin, dem ersten aus dem menschlichen Nasenmikrobiom isolierten Fibupeptid-Antibiotikum, durch zwei unterschiedliche ABC-Transporter erreicht wird, die im Lugdunin-Operon kodiert sind. Unsere Studie konnte die unterschiedlichen, aber auch überlappenden Rollen der beiden Transporter zeigen und dass beide für eine vollständige Resistenz gegenüber Lugdunin erforderlich sind.

Epifadin ist das erste Beispiel eines Staphylokokken-Bakteriozins, das sowohl von nicht-ribosomalen Peptidsynthetasen (NRPS) als auch von Polyketidsynthasen (PKS) produziert wird. Es zeigt trotz seiner sehr kurzen Halbwertszeit Aktivität gegen ein breites Spektrum wichtiger Mitglieder des nasalen Mikrobioms, was Epifadin zu einem sehr ungewöhnlichen antimikrobiellen Molekül macht.

Darüber hinaus berichten wir, dass der horizontale Gentransfer des Biosynthesegenclusters für das Thiopeptid Micrococcin P1 in den Laborstamm *Staphylococcus aureus* RN4220 zu

einem Wachstumsdefekt und zu Störungen des zentralen Zellstoffwechsels im neuen Wirt führt. Somit können wir zeigen, dass die plötzliche Bakteriozin-Produktion eine Belastung für den neuen Produzenten darstellt, die jedoch durch eine adaptive Mutation in *citZ*, welches für die Citratsynthase kodiert, rückgängig gemacht werden kann, wodurch sich die Micrococcin P1 Produktion wieder in einen Vorteil umwandelt.

Unsere Ergebnisse unterstreichen das gehäufte Vorkommen und die hohe Mobilität von Bakteriozin-Biosynthesegenclustern im humanen nasalen Mikrobiom und geben einen Einblick in die Kosten und Nutzen die mit dem Erwerb dieser Gencluster verbunden sind.

Chapter 1 – General Introduction

Horizontal gene transfer of antimicrobial biosynthetic gene clusters in the human microbiome

The human microbiome

The human microbiome is the entity of genetic information from the whole spectrum of microorganisms living on and in the human body, also formerly defined as the microbiota. Bacteria display the most abundant members of the microbiome besides archaea, fungi, protozoans, and non-living viruses [1, 2]. The human microbiome has long been an understudied field, due to the non-cultivability of most members of the microbiome under lab conditions. Invention of high-throughput sequencing technologies led to a significant increase in knowledge about the composition and biological importance of the microbiome, by bypassing the non-culturable state of bacteria. Transcriptomics, proteomics, and metabolomics are further novel methods helping to characterize the microbiome [1, 3, 4]. Multiple studies revealed that microbes have a great influence on the overall human health and disease development and that the human microbiome is a highly sophisticated system. Thus, leading to the assumption that the global balance of the microbiome is more important than focusing on a single pathogen responsible for disease onset [5-8]. The Human Microbiome Project (HMP) was a global key initiative to collect and catalogue human microbial communities from various body sites like the oral cavity, nasal passages, skin, gastrointestinal tract, and urogenital tract. This project helped to define the basic composition of the human microbiome, which changes over time and varies between individuals as well as between body sites [9-11].

Antagonistic microbe-microbe interactions in the human nasal microbiome

The human nasal microbiome is comprised of a distinct community of bacterial species. Most of them acting as commensals, but some also as pathobionts, interacting with the human body from harmless to deadly, causing for instance mild middle ear infections but also serious blood stream infections [12]. Members of the nasal microbial community mainly belong to the phyla of Proteobacteria, Actinomycetota and Bacillota. *Cutibacterium acnes* and various species of *Corynebacterium* (*C. pseudodiptheriticum* or *C. accolens*), belonging to the Actinomycetota,

are prevalent in high frequency. For the phylum Bacillota, the most abundant bacteria are Staphylococcaceae (*Staphylococcus epidermidis* and *Staphylococcus aureus*), Carnobacteriaceae (*Dolosigranulum pigrum*) and Peptoniphilaceae (*Finegoldia magna*). *Moraxella catarrhalis* and *Haemophilus influenzae*, both members of the phylum Proteobacteria, comprise usually less than 10% of the whole community [11, 13]. The nasal microbiome displays a mixture of the microbiome of the skin and with a smaller proportion of the oral cavity [11, 14]. *S. aureus*, colonizing the anterior nares of approximately 30% of the human population, is a common nasal pathobiont and colonization is a risk factor for infection [12, 15, 16]. Three major determinants, namely the strain-dependent properties of the microbe itself, host related factors and the interaction of the bacterium with the nasal microbiome influence the highly dynamic and complex process of nasal carriage of *S. aureus* [17, 18]. Recent studies showed that the nasal cavities are poor in nutrients, suggesting that colonizing bacteria might be in strong competition with each other and may use a multitude of strategies to conquer competitors and to achieve niche occupation [19-21]. Establishment of efficient attachment mechanisms to host epithelial cells is important for nasal colonizers to remain in the nose and to not being removed by mucus flow and mucociliary clearance. Thus, competition for the limited number of binding sites located on the host nasal epithelium is thought to be one major competition strategy (Fig. 1a) [22-25]. As already mentioned, the nasal environment, compared to for example the gastrointestinal content, is scarce in nutrients. Therefore, bacteria might compete for nutrients released by the epithelial cells and glands (Fig. 1b) [19]. Studies showed that *S. aureus* can induce the release of pro-inflammatory molecules by induction of host inflammation in the nasal epithelium. Commensal bacteria, which are often more susceptible than *S. aureus*, are thus subsequently killed by antimicrobial molecules secreted locally by the host immune system (Fig. 1c) [26-29]. Another important factor of bacterial competition is the production of antimicrobial compounds, like bacteriocins, leading to bacterial death (Fig. 1d) [30].
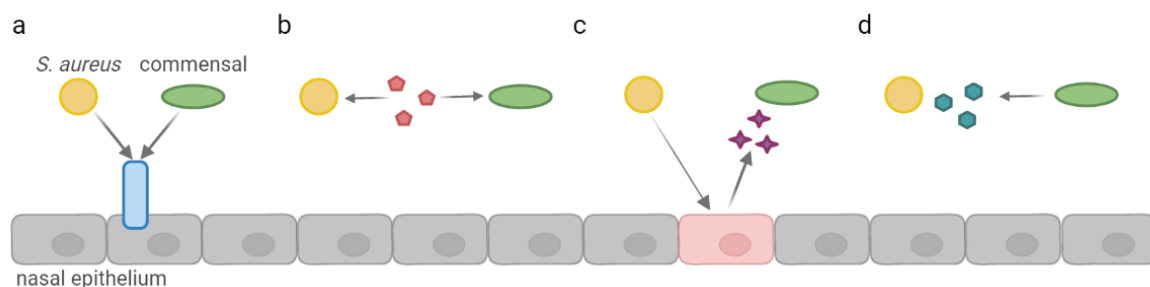

Figure 1: Bacterial competition in the human nasal microbiome. a) Competition for adhesion sites. b) Competition for nutrients. c) Activation of host immune system and killing of commensals by host antimicrobial substances. d) Competition via bacteriocin production.

Cooperation in bacterial communities: Importance of horizontal gene transfer

Besides the constant competition between bacteria in the microbiome, also cooperation in form of sharing public goods, mainly secondary metabolites, is ubiquitous in bacterial populations. Production and sharing of these public goods benefits all individuals in the community [31, 32]. These may be shared actively by secretion or passively by diffusion from the producing cell and range from large proteins to small metabolites. Extracellular digestive enzymes like proteases, surfactants promoting bacterial motility, toxins for host tissue damage, siderophores for iron scavenging, antibiotics or antibiotic-degrading enzymes, metabolites promoting cellular growth and molecules involved in virulence, biofilm formation or quorum sensing are commonly designated as public goods [32-34]. Interestingly, the benefit of public goods increases with population density, for example only if enough cells contribute to antibiotic production, the concentration is high enough to be effective against competitors [32]. To rapidly disseminate public goods in a population, bacteria make use of horizontal gene transfer (HGT), as genes encoding public goods are often located on mobile genetic elements (MGE). Thus, HGT is a major driver of bacterial adaptation, genetic variation, and evolution [35-38].

Mechanisms of horizontal gene transfer

Bacteria can transfer their DNA not only via reproduction, also called vertical gene transfer, but also via lateral gene transfer also known as HGT. HGT is facilitated by the occurrence of MGE, like plasmids, transposons, genomic islands, integrative and conjugative elements, and bacteriophages [39-41]. These elements can be transferred by three different mechanisms (Fig. 2). During transformation, bacteria take up extracellular double-stranded DNA fragments from their environment with subsequent integration into the genome or recirculation of the translocated DNA in case of plasmid DNA [40-42]. Bacteriophages facilitate the exchange of DNA via transduction. After infection of a donor cell, the bacteriophage propagates in the donor cell with either targeted (specialized transduction) or accidental (general transduction) uptake of donor DNA in the phage capsid. After lysis of the host cell the bacteriophage infects a recipient cell [43, 44]. Direct cell-to-cell contact via cell surface pili or adhesins are necessary for direct transfer of DNA sequences like plasmids via conjugation [40, 42, 45]. An "origin of transfer" (oriT) is necessary as recognition site for the conjugative machinery for successful transfer of DNA [46]. Recent studies identified further mechanisms of DNA transfer, like the release of DNA-containing membrane vesicles carrying DNA to new hosts [47, 48]. Also, gene transfer agents (GTA), DNA-containing particles similar to bacteriophages [49] and DNA transfer via intercellular connections like nanotubes were recently described [50]. Absorbed DNA needs to replicate in the new host to not getting lost during cell division. This is facilitated either by carrying an own or shared origin of replication to replicate independently from the

host chromosome or by integration into the host genome [51]. Integration of the new foreign DNA into the genome is mainly achieved by homologous recombination, where highly similar regions exist on the newly acquired DNA as well as on the genome, facilitating editing and exchange of these regions. Recombination can also lead to additive integration of DNA, where DNA can also integrate into regions with low or no sequence similarity leading to substitution of genetic information [39, 51, 52].
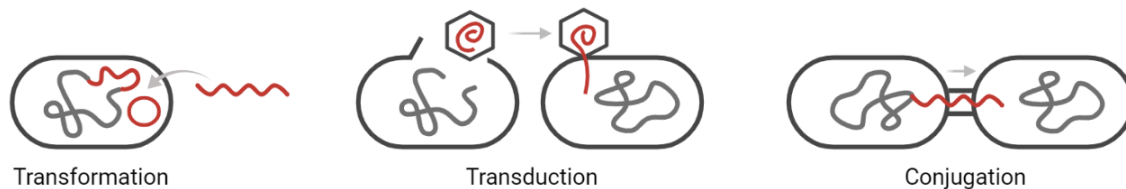

Figure 2: Schematic overview of the three mechanisms of horizontal gene transfer. Transformation is the uptake of free extracellular DNA and either integration into the genome or recirculation. Transduction is facilitated by bacteriophages, which take up DNA into their capsid and subsequently infect a recipient strain. Direct cell-to-cell contact via a cell surface pilus is necessary for DNA exchange via conjugation.

Bacteriocins are frequently found in the nasal microbiome and their BGCs show signs of HGT

Recent studies demonstrated the high frequency of biosynthetic gene clusters (BGCs) responsible for the production of secondary metabolites like bacteriocins in human metagenomic studies, where different human body sites like the nasal cavities were analysed [53]. Especially staphylococcal bacteriocin BGCs seem to be frequently transferred via HGT, due to their localisation on plasmids or MGEs on the chromosome [30]. Recombination events after bacteriocin BGC acquisition via HGT can lead to the generation of "new" BGCs. Besides integrating the whole BGC into the genome or keeping it as a full plasmid, recombination with another, already existing BGC can lead to the generation of a new bacteriocin BGC with altered activity. Another option is the sole acquisition of the resistance/immunity genes, thereby making the recipient resistant to a group of bacteriocins [54].

Bacteriocins are small, ribosomally synthesized peptides, with either broad or narrow-spectrum activity, whose BGCs also encode a producer-specific immunity mechanism against their own compound [55, 56]. Representing a very heterogeneous group of compounds, bacteriocins are divided into two classes: class I peptides undergo significant post-translational modifications and are thus also classified as ribosomally synthesised and post-translationally modified peptides (RiPPs) whereas class II peptides remain unmodified [55, 57]. Post-translational modifications include the formation of thiazole and oxazole heterocycles in certain microcins, lanthionine bridges in lantibiotics, or pyridine rings in thiopeptides [55]. Recently, the suggestion was made to regard all "microbiome-derived small-molecule antimicrobial

molecules" as bacteriocins, also when they are synthesized by non-ribosomal peptide synthetases (NRPS) [54]. Producer-immunity is generally limited to the produced compound or its derivatives and achieved by distinct mechanisms like export [58] or through expression of modified bacteriocin target proteins, like genetic alteration of the ribosomal protein L11 in case of thiopeptides [59]. Concerning the mode of action, bacteriocins exhibit many different mechanisms. However, they can be divided in peptides, which act at the cell envelope, by killing cells via pore formation or binding to lipid II und thus inhibiting peptidoglycan synthesis [60, 61], or those being primarily active inside the cell, affecting gene expression and protein production [62, 63].

Mobile bacteriocin BGCs identified in the human microbiome

In the following, bacteriocins are presented which were found in the metagenomes of nasal microbiome members or in species frequently present in the human nose and show signs of HGT.

The lantibiotic nukacin IVK45 was identified in *S. epidermidis* IVK45 with antimicrobial activity against bacterial species frequently found in human nasal microbiome. The BGC is located on a 22 kb plasmid and shows high similarity to BGCs responsible for the production of nukacins in *S. warneri* ISK-1 and *S. hominis* KQU-131 [30, 64, 65]. Comparison of the mature bacteriocin of nukacin IVK45 with nukacin ISK-1 or KQU-131 revealed that they differ by 5 or 6 amino acids, respectively. Peptides with lower similarities could also be identified in streptococci and lactococci, indicating that this BGC was transferred between different species and genera. This hypothesis is further supported by BLAST analysis of pIVK45 which revealed that large parts of the plasmid like the origin of replication show similarities to plasmids and other MGEs from *S. aureus*, *S. epidermidis*, and *S. lugdunensis*. The BGC itself is flanked by IS-like elements and transposases, whereas the precursor peptide is separated from the rest of the BGC by transposase fragments. This leads to the conclusion that multiple recombination events occurred in the generation of pIVK45 [30]. The authors conclude that these recombination events might have contributed to the generation of the described new bacteriocin nukacin IVK45, also exhibiting an altered activity spectrum compared to nukacin ISK-1 [30, 54]. Recently, nukacin KSE650 was identified in *S. epidermidis* KSE650, isolated from the human oral cavity, with 100% sequence identity of the mature peptide compared to nukacin IVK45. Located on a 6 kb larger plasmid but also with the precursor peptide separated from the BGC by transposases as in pIVK45, further highlights the mobility of this BGC [66].

Aureocin A70 is a heat-stable class II bacteriocin, which is originally produced by *S. aureus* A70. The BGC is located on an 8 kb plasmid (pRJ6) consisting of 3 transcriptional units which appear to be involved in bacteriocin production. The first transcript encodes the ATP-dependent transporter AurT showing similarity to lantibiotic exporters, and the second operon encodes the repressor protein AurR and the immunity protein AurI. The third operon consists of four genes, *aurABCD*, which encode four related small peptides. The four peptides show individual inhibitory activity and do not undergo post-translational modifications and are excreted by the ATP-dependent transporter AurT without processing. Aureocin A70 is thus the first described multi-peptide non-lantibiotic bacteriocin [67-69]. It could be demonstrated that the aureocin A70 genes can be transferred via conjugation amongst distinct staphylococcal strains via the four mobilization genes (*mobCDAB*) also localized on pRJ6. Studies on the *mob* region of pRJ6 revealed sequence similarity to *mob* regions of plasmids from several coagulase-negative staphylococci, which indicates that pRJ6 might have been transferred from coagulase-negative staphylococci to *S. aureus*. pRJ6 can be found in distinct *S. aureus* strains suggesting HGT among Staphylococci and represents the first known bacteriocinogenic mobilizable (Mob) plasmid of *S. aureus* [70-74].

The plasmid-encoded unmodified bacteriocin epidermicin NI01, identified in *S. epidermidis* 224 isolated from human skin, is another example for HGT in staphylococci. The BGC is comprised of nine genes, with high synteny to the aureocin A53 BGC. The only difference is the presence of an additional gene with unknown function. A three-component ABC transporter commonly found in staphylococci, two genes responsible for immunity and two genes with unclear function are associated with the structural gene encoding epidermicin NI01. The structural peptide however only shows 41% sequence identity to the peptide sequence of aureocin A53 [75, 76]. Recently, the epidermicin NI01 BGC was identified in *Staphylococcus capitis* TE8, also isolated from human skin, with similar genetic organization. In this strain, the BGC is located on a genomic island indicating HGT of this BGC over species boundaries [77].

Micrococcin P1 (MP1) is a class I bacteriocin, belonging to the subclass of thiopeptides [62]. It is one of the first described thiopeptide bacteriocins, isolated from *Micrococcus sp.* found in sewage in 1948 [78]. Over the years, MP1 was isolated from *Bacillus pumilus* found in soil [79], a food-borne *Staphylococcus equorum* WS2733 [80], *Bacillus cereus* ATCC14579 isolated in a farmhouse [81], the avian isolate *Macrococcus caseolyticus* 115 [59], the skin microbiome inhabitants *Staphylococcus hominis* S34-1 [82] and *Mammaliicoccus sciuri* IMDO-S72 [83], *S. aureus* MK65 isolated from pus and blood samples [84] and *Staphylococcus agnetis* 4244, a strain involved in bovine mastitis [85]. Comparison of the available BGCs from *Bacillus cereus* ATCC14579, *Macrococcus caseolyticus* 115 and *Staphylococcus hominis*

S34-1 reveals that the two last ones, which are located on a plasmid, are more similar to each other compared to the first one, which is chromosomally encoded (Fig. 3). In general, the BGC comprises various genes responsible for the posttranslational modification of MP1 showing similarities to enzymes modifying lantibiotics and cyanobactins/microcins and an immunity gene. Most interestingly, *B. cereus* ATCC14579 has four copies of the structural gene coding for the precursor peptide, allowing the generation of 7 other thiopeptides besides MP1, which makes the biggest difference to the other two BGCs. However, the C-terminal peptide sequence "SCTTCVCTCSCCTT" is identical in all BGCs. Concerning the two plasmid-encoded BGCs, the plasmids are comparable in size (~ 30 kb) and encode mobilization-associated genes indicating HGT of this plasmid [59, 81, 82, 86]. The MP1 BGC from *Mammaliicoccus sciuri* is also encoded on a plasmid and shows thus indications of HGT [83]. Given the frequent occurrence of this BGC even across different bacterial orders and the clear hints for MGE underline the advantage of acquisition and production of MP1 in various different ecological niches.
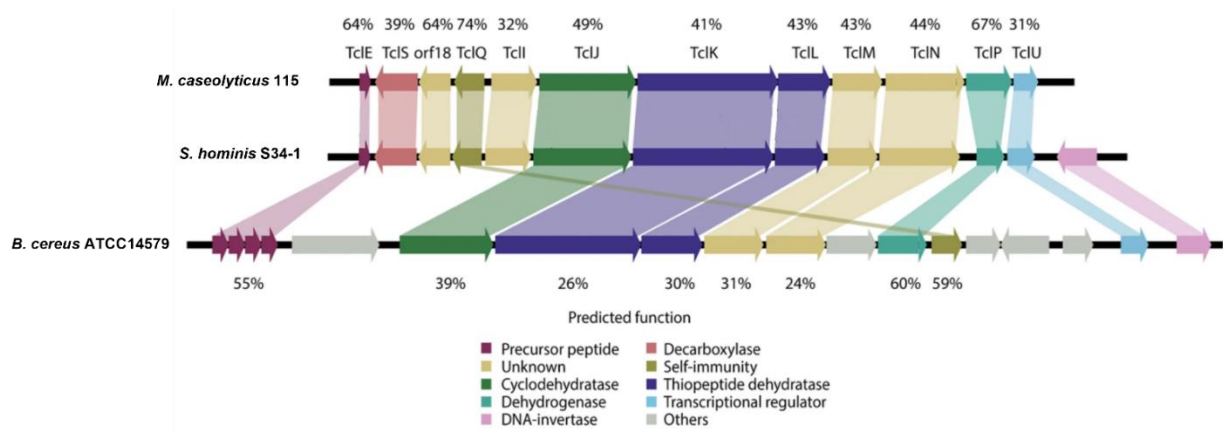

Figure 3: Alignment of MP1 BGC of M. caseolyticus 115, S. hominis S34-1 and B. cereus ATCC14579. Amino acid similarity of shown as well as putative protein function. Modified from Liu, Y., Liu, Y., Du, Z. et al., (2020), licensed by Creative Commons Attribution 4.0 International License.

1. Blum, H.E., *The human microbiome.* Adv Med Sci, 2017. **62**(2): p. 414-420.
2. Rogers, K., *"human microbiome"*, in *Encyclopedia Britannica*. 2022.
3. Hopson, L.M., et al., *Bioinformatics and machine learning in gastrointestinal microbiome research and clinical application.* Prog Mol Biol Transl Sci, 2020. **176**: p. 141-178.
4. Rackaityte, E. and S.V. Lynch, *The human microbiome in the 21(st) century.* Nat Commun, 2020. **11**(1): p. 5256.
5. E., B.J., *The Human Microbiome of Local Body Sites and Their Unique Biology*, in *Mandell, Douglas, and Bennett's Principles and Practice of Infectious Diseases*. 2020.
6. Le Chatelier, E., et al., *Richness of human gut microbiome correlates with metabolic markers.* Nature, 2013. **500**(7464): p. 541-6.
7. Nejman, D., et al., *The human tumor microbiome is composed of tumor type-specific intracellular bacteria.* Science, 2020. **368**(6494): p. 973-980.
8. Arrieta, M.C., et al., *The intestinal microbiome in early life: health and disease.* Front Immunol, 2014. **5**: p. 427.
9. Turnbaugh, P.J., et al., *The human microbiome project.* Nature, 2007. **449**(7164): p. 804-10.
10. Proctor, L.M., *The Human Microbiome Project in 2011 and beyond.* Cell Host Microbe, 2011. **10**(4): p. 287-91.
11. Human Microbiome Project, C., *Structure, function and diversity of the healthy human microbiome.* Nature, 2012. **486**(7402): p. 207-14.
12. Lemon, K.P., *Human nasal microbiota.* Curr Biol, 2020. **30**(19): p. R1118-R1119.
13. Wos-Oxley, M.L., et al., *A poke into the diversity and associations within human anterior nare microbial communities.* ISME J, 2010. **4**(7): p. 839-51.
14. Faust, K., et al., *Microbial co-occurrence relationships in the human microbiome.* PLoS Comput Biol, 2012. **8**(7): p. e1002606.
15. Kluytmans, J., A. van Belkum, and H. Verbrugh, *Nasal carriage of Staphylococcus aureus: epidemiology, underlying mechanisms, and associated risks.* Clin Microbiol Rev, 1997. **10**(3): p. 505-20.
16. von Eiff, C., et al., *Nasal carriage as a source of Staphylococcus aureus bacteremia. Study Group.* N Engl J Med, 2001. **344**(1): p. 11-6.
17. Brown, A.F., et al., *Staphylococcus aureus Colonization: Modulation of Host Immune Response and Impact on Human Vaccine Design.* Front Immunol, 2014. **4**: p. 507.
18. Johannessen, M., J.E. Sollid, and A.M. Hanssen, *Host- and microbe determinants that may influence the success of S. aureus colonization.* Front Cell Infect Microbiol, 2012. **2**: p. 56.
19. Krismer, B., et al., *Nutrient limitation governs Staphylococcus aureus metabolism and niche adaptation in the human nose.* PLoS Pathog, 2014. **10**(1): p. e1003862.
20. Hibbing, M.E., et al., *Bacterial competition: surviving and thriving in the microbial jungle.* Nat Rev Microbiol, 2010. **8**(1): p. 15-25.
21. Brugger, S.D., L. Bomar, and K.P. Lemon, *Commensal-Pathogen Interactions along the Human Nasal Passages.* PLoS Pathog, 2016. **12**(7): p. e1005633.
22. Schade, J. and C. Weidenmaier, *Cell wall glycopolymers of Firmicutes and their role as nonprotein adhesins.* FEBS Lett, 2016. **590**(21): p. 3758-3771.
23. Mulcahy, M.E., et al., *Nasal colonisation by Staphylococcus aureus depends upon clumping factor B binding to the squamous epithelial cell envelope protein loricrin.* PLoS Pathog, 2012. **8**(12): p. e1003092.
24. Weidenmaier, C., et al., *Role of teichoic acids in Staphylococcus aureus nasal colonization, a major risk factor in nosocomial infections.* Nat Med, 2004. **10**(3): p. 243-5.
25. Weidenmaier, C., C. Goerke, and C. Wolz, *Staphylococcus aureus determinants for nasal colonization.* Trends Microbiol, 2012. **20**(5): p. 243-50.
26. Herbert, S., et al., *Molecular basis of resistance to muramidase and cationic antimicrobial peptide activity of lysozyme in staphylococci.* PLoS Pathog, 2007. **3**(7): p. e102.

27. Hanzelmann, D., et al., *Toll-like receptor 2 activation depends on lipopeptide shedding by bacterial surfactants.* Nat Commun, 2016. **7**: p. 12304.

28. Cole, A.M., et al., *Determinants of Staphylococcus aureus nasal carriage.* Clin Diagn Lab Immunol, 2001. **8**(6): p. 1064-9.

29. Cole, A.M., et al., *Cationic polypeptides are required for antibacterial activity of human airway fluid.* J Immunol, 2002. **169**(12): p. 6985-91.

30. Janek, D., et al., *High Frequency and Diversity of Antimicrobial Activities Produced by Nasal Staphylococcus Strains against Bacterial Competitors.* PLoS Pathog, 2016. **12**(8): p. e1005812.

31. Ozkaya, O., et al., *Maintenance of Microbial Cooperation Mediated by Public Goods in Single- and Multiple-Trait Scenarios.* J Bacteriol, 2017. **199**(22).

32. Smith, P. and M. Schuster, *Public goods and cheating in microbes.* Curr Biol, 2019. **29**(11): p. R442-R447.

33. West, S.A., et al., *Social evolution theory for microorganisms.* Nat Rev Microbiol, 2006. **4**(8): p. 597-607.

34. Morris, J.J., *Black Queen evolution: the role of leakiness in structuring microbial communities.* Trends Genet, 2015. **31**(8): p. 475-82.

35. Gogarten, J.P. and J.P. Townsend, *Horizontal gene transfer, genome innovation and evolution.* Nat Rev Microbiol, 2005. **3**(9): p. 679-87.

36. Hall, R.J., et al., *Horizontal Gene Transfer as a Source of Conflict and Cooperation in Prokaryotes.* Front Microbiol, 2020. **11**: p. 1569.

37. Power, J.J., et al., *Adaptive evolution of hybrid bacteria by horizontal gene transfer.* Proc Natl Acad Sci U S A, 2021. **118**(10).

38. Hall, J.P.J., M.A. Brockhurst, and E. Harrison, *Sampling the mobile gene pool: innovation via horizontal gene transfer in bacteria.* Philos Trans R Soc Lond B Biol Sci, 2017. **372**(1735).

39. Rogers, K., *"horizontal gene transfer"*, in *Encyclopedia Britannica.* 2019.

40. Emamalipour, M., et al., *Horizontal Gene Transfer: From Evolutionary Flexibility to Disease Progression.* Front Cell Dev Biol, 2020. **8**: p. 229.

41. Burmeister, A.R., *Horizontal Gene Transfer.* Evol Med Public Health, 2015. **2015**(1): p. 193-4.

42. von Wintersdorff, C.J., et al., *Dissemination of Antimicrobial Resistance in Microbial Ecosystems through Horizontal Gene Transfer.* Front Microbiol, 2016. **7**: p. 173.

43. Goh, S., *Phage Transduction.* Methods Mol Biol, 2016. **1476**: p. 177-85.

44. Colavecchio, A., et al., *Bacteriophages Contribute to the Spread of Antibiotic Resistance Genes among Foodborne Pathogens of the Enterobacteriaceae Family - A Review.* Front Microbiol, 2017. **8**: p. 1108.

45. Guglielmini, J., F. de la Cruz, and E.P. Rocha, *Evolution of conjugation and type IV secretion systems.* Mol Biol Evol, 2013. **30**(2): p. 315-31.

46. Smillie, C., et al., *Mobility of plasmids.* Microbiol Mol Biol Rev, 2010. **74**(3): p. 434-52.

47. Yaron, S., et al., *Vesicle-mediated transfer of virulence genes from Escherichia coli O157:H7 to other enteric bacteria.* Appl Environ Microbiol, 2000. **66**(10): p. 4414-20.

48. Fulsundar, S., S. Domingues, and K.M. Nielsen, *Vesicle-Mediated Gene Transfer in Acinetobacter baumannii.* Methods Mol Biol, 2019. **1946**: p. 87-94.

49. Lang, A.S., O. Zhaxybayeva, and J.T. Beatty, *Gene transfer agents: phage-like elements of genetic exchange.* Nat Rev Microbiol, 2012. **10**(7): p. 472-82.

50. Dubey, G.P. and S. Ben-Yehuda, *Intercellular nanotubes mediate bacterial communication.* Cell, 2011. **144**(4): p. 590-600.

51. Thomas, C.M. and K.M. Nielsen, *Mechanisms of, and barriers to, horizontal gene transfer between bacteria.* Nat Rev Microbiol, 2005. **3**(9): p. 711-21.

52. Majewski, J. and F.M. Cohan, *DNA sequence similarity requirements for interspecific recombination in Bacillus.* Genetics, 1999. **153**(4): p. 1525-33.

53. Donia, M.S., et al., *A systematic analysis of biosynthetic gene clusters in the human microbiome reveals a common family of antibiotics.* Cell, 2014. **158**(6): p. 1402-1414.

54. Heilbronner, S., et al., *The microbiome-shaping roles of bacteriocins.* Nat Rev Microbiol, 2021. **19**(11): p. 726-739.

55.   Arnison, P.G., et al., *Ribosomally synthesized and post-translationally modified peptide natural products: overview and recommendations for a universal nomenclature.* Nat Prod Rep, 2013. **30**(1): p. 108-60.

56.   Cotter, P.D., R.P. Ross, and C. Hill, *Bacteriocins - a viable alternative to antibiotics?* Nat Rev Microbiol, 2013. **11**(2): p. 95-105.

57.   Simons, A., K. Alhanout, and R.E. Duval, *Bacteriocins, Antimicrobial Peptides from Bacterial Origin: Overview of Their Biology and Their Impact against Multidrug-Resistant Bacteria.* Microorganisms, 2020. **8**(5).

58.   Krauss, S., et al., *Secretion of and Self-Resistance to the Novel Fibupeptide Antimicrobial Lugdunin by Distinct ABC Transporters in Staphylococcus lugdunensis.* Antimicrob Agents Chemother, 2020. **65**(1).

59.   Bennallack, P.R., et al., *Characterization of a novel plasmid-borne thiopeptide gene cluster in Staphylococcus epidermidis strain 115.* J Bacteriol, 2014. **196**(24): p. 4344-50.

60.   Bierbaum, G. and H.G. Sahl, *Lantibiotics: mode of action, biosynthesis and bioengineering.* Curr Pharm Biotechnol, 2009. **10**(1): p. 2-18.

61.   Breukink, E. and B. de Kruijff, *Lipid II as a target for antibiotics.* Nat Rev Drug Discov, 2006. **5**(4): p. 321-32.

62.   Bagley, M.C., et al., *Thiopeptide antibiotics.* Chem Rev, 2005. **105**(2): p. 685-714.

63.   Parks, W.M., et al., *The action of the bacterial toxin, microcin B17, on DNA gyrase.* Biochimie, 2007. **89**(4): p. 500-7.

64.   Asaduzzaman, S.M., et al., *Nukacin ISK-1, a bacteriostatic lantibiotic.* Antimicrob Agents Chemother, 2009. **53**(8): p. 3595-8.

65.   Wilaipun, P., et al., *Identification of the nukacin KQU-131, a new type-A(II) lantibiotic produced by Staphylococcus hominis KQU-131 isolated from Thai fermented fish product (Pla-ra).* Biosci Biotechnol Biochem, 2008. **72**(8): p. 2232-5.

66.   Nakazono, K., et al., *Complete sequences of epidermin and nukacin encoding plasmids from oral-derived Staphylococcus epidermidis and their antibacterial activity.* PLoS One, 2022. **17**(1): p. e0258283.

67.   Netz, D.J., C. Bastos Mdo, and H.G. Sahl, *Mode of action of the antimicrobial peptide aureocin A53 from Staphylococcus aureus.* Appl Environ Microbiol, 2002. **68**(11): p. 5274-80.

68.   Coelho, M.L., et al., *Immunity to the Staphylococcus aureus leaderless four-peptide bacteriocin aureocin A70 is conferred by AurI, an integral membrane protein.* Res Microbiol, 2014. **165**(1): p. 50-9.

69.   Coelho, M.L., L.R. Fleming, and C. Bastos Mdo, *Insights into aureocin A70 regulation: participation of regulator AurR, alternative transcription factor sigma(B) and phage varphi11 regulator cI.* Res Microbiol, 2016. **167**(2): p. 90-102.

70.   de Oliveira, S.S., et al., *Genetic analysis of the bacteriocin-encoding plasmids pRJ6 and pRJ9 of Staphylococcus aureus by transposon mutagenesis and cloning of genes involved in bacteriocin production.* J Appl Microbiol, 1998. **85**(6): p. 972-84.

71.   Varella Coelho, M.L., et al., *Mobilization functions of the bacteriocinogenic plasmid pRJ6 of Staphylococcus aureus.* J Microbiol, 2009. **47**(3): p. 327-36.

72.   Coutinho, B.G., et al., *Revealing the latent mobilization capability of the staphylococcal bacteriocinogenic plasmid pRJ9.* J Mol Microbiol Biotechnol, 2011. **21**(3-4): p. 173-83.

73.   Ceotto, H., et al., *Aureocin A70 production is disseminated amongst genetically unrelated Staphylococcus aureus involved in bovine mastitis.* Lett Appl Microbiol, 2012. **54**(5): p. 455-61.

74.   Nascimento Jdos, S., et al., *Genomic fingerprinting of bacteriocin-producer strains of Staphylococcus aureus.* Res Microbiol, 2005. **156**(8): p. 837-42.

75.   Sandiford, S. and M. Upton, *Identification, characterization, and recombinant expression of epidermicin NI01, a novel unmodified bacteriocin produced by Staphylococcus epidermidis that displays potent activity against Staphylococci.* Antimicrob Agents Chemother, 2012. **56**(3): p. 1539-47.

76.   de Freire Bastos, M.D.C., et al., *Staphylococcins: an update on antimicrobial peptides produced by staphylococci and their diverse potential applications.* Appl Microbiol Biotechnol, 2020. **104**(24): p. 10339-10368.

77.   Kumar, R., et al., *Genome Analysis of Staphylococcus capitis TE8 Reveals Repertoire of Antimicrobial Peptides and Adaptation Strategies for Growth on Human Skin.* Sci Rep, 2017. **7**(1): p. 10447.

78.   Su, T.L., *Micrococcin, an antibacterial substance formed by a strain of Micrococcus.* Br J Exp Pathol, 1948. **29**(5): p. 473-81.

79.   Abraham, E.P., et al., *Probable identity of an antibiotic produced by a spore-bearing bacillus of the B. pumilus group with micrococcin.* Nature, 1956. **178**(4523): p. 44-5.

80.   Carnio, M.C., et al., *The macrocyclic peptide antibiotic micrococcin P(1) is secreted by the food-borne bacterium Staphylococcus equorum WS 2733 and inhibits Listeria monocytogenes on soft cheese.* Appl Environ Microbiol, 2000. **66**(6): p. 2378-84.

81.   Wieland Brown, L.C., et al., *Thirteen posttranslational modifications convert a 14-residue peptide into the antibiotic thiocillin.* Proc Natl Acad Sci U S A, 2009. **106**(8): p. 2549-53.

82.   Liu, Y., et al., *Skin microbiota analysis-inspired development of novel anti-infectives.* Microbiome, 2020. **8**(1): p. 85.

83.   Van der Veken, D., et al., *Genome-Based Characterization of a Plasmid-Associated Micrococcin P1 Biosynthetic Gene Cluster and Virulence Factors in Mammaliicoccus sciuri IMDO-S72.* Appl Environ Microbiol, 2022. **88**(4): p. e0208821.

84.   Kassem, M.A., et al., *Exploring clinically isolated Staphylococcus sp. bacteriocins revealed the production of amonabactin, micrococcin, and alpha-circulocin.* Iran J Microbiol, 2021. **13**(2): p. 212-224.

85.   Francisco, M.S., et al., *Draft genome sequence of Staphylococcus agnetis 4244, a strain with gene clusters encoding distinct post-translationally modified antimicrobial peptides.* J Glob Antimicrob Resist, 2021. **27**: p. 239-243.

86.   Ciufolini, M.A. and D. Lefranc, *Micrococcin P1: structure, biology and synthesis.* Nat Prod Rep, 2010. **27**(3): p. 330-42.

Chapter 2

Whole genome sequencing of bacterial isolates from the human nasal microbiota exhibiting antimicrobial activity

A library of nearly 2000 nasal isolates of diverse bacterial species, collected from hospitalized patients, students, university members and volunteers, was screened for antimicrobial activity on plates containing either *S. aureus* USA300 LAC, *Micrococcus luteus* (natural isolate) or *E. coli* DH5α as indicator strains under different media conditions. 21 isolates exhibiting strong inhibitory activity were identified on the species level by MALDI-TOF, whole genome sequencing (WGS) was performed by Illumina and the obtained sequences were analyzed using antiSMASH 5.0 (bacterial settings). The identified BGCs can be found in the supplement (table 1). In five staphylococcal species 15 different BGCs could be identified. Among them are already well known bacteriocins like BsaA1/2, epidermin, epilancin, nukacin ISK-1, aureocin A70, micrococcin P1 and lactococcin G which are either located on the chromosome or on a plasmid. The NRPS-encoded fibupeptide lugdunin could be identified in *S. lugdunensis* D2-37, another lugdunin producing isolate (*S. lugdunensis* IVK28) is part of this thesis (chapter 3). A so far not characterized BGC, with most likely three peptides forming the active compound, was found on the chromosome of two *S. epidermidis* (9-14,17-20) isolates. Epifadin, just recently identified in *S. epidermidis* IVK83 (chapter 4), was found in two other *S. epidermidis* isolates with almost 100% sequence identity. Pulcherriminic acid, a cyclic dipeptide already known for a long time, was identified in various *S. epidermidis* strains, most frequently found on a plasmid and only once on the chromosome (appendix). Interestingly, in five isolates, pulcherriminic acid is not the sole BGC and occurs for example together with epifadin, both encoded on separate plasmids. The micrococcin P1 producer *S. aureus* D4-19 was also further investigated in this thesis (chapter 5).

To conclude, the competition between bacteria of the human nasal microbiome due to poor nutrient supply, leads to the evolvement of various antimicrobial active substances, which are either more or less well characterised, and are often located on MGEs indicating HGT of these clusters. This thesis addresses four of the above-mentioned compounds and the remaining genome sequences might become a good basis for further studies to characterise the variety of antimicrobially active substances of the human nasal microbiome.

Chapter 3

Secretion of and self-resistance to the novel fibupeptide antimicrobial lugdunin by distinct ABC transporters in *Staphylococcus lugdunensis*

Sophia Krauss[1,2,3,§], Alexander Zipperer[1,2,§,*], Sebastian Wirtz[3,4], Julian Saur[3,4], Martin C. Konnerth[3,4,*], Simon Heilbronner[1,2,3], Benjamin O. Torres Salazar[1,2,3], Stephanie Grond[3,4], Bernhard Krismer[1,2,3,#], Andreas Peschel[1,2,3]

1. Interfaculty Institute of Microbiology and Infection Medicine, Infection Biology, University of Tübingen, Germany.
2. German Center for Infection Research (DZIF), partner site Tübingen, Germany.
3. Cluster of Excellence EXC 2124 Controlling Microbes to Fight Infection.
4. Organic Chemistry, University of Tübingen, Germany.
§ Sophia Krauss and Alexander Zipperer contributed equally to this manuscript
* Present address: Alexander Zipperer, Roche Innovation Center Basel, F. Hoffmann-La Roche Ltd., Roche Pharma Research & Early Development, Basel, Switzerland; Martin C. Konnerth, EMC Microcollections GmbH, Tübingen, Germany.

Running Title: Lugdunin secretion and self-resistance

Address correspondence to Bernhard Krismer (b.krismer@uni-tuebingen.de)

Abstract

Lugdunin is the first reported non-ribosomally synthesized antibiotic from human microbiomes. Its production by the commensal *Staphylococcus lugdunensis* eliminates the pathogen *Staphylococcus aureus* from human nasal microbiomes. The cycloheptapeptide lugdunin is the founding member of the new class of fibupeptide antibiotics, which have a novel mode of action and represent promising new antimicrobial agents. How *S. lugdunensis* releases and achieves producer self-resistance to lugdunin has remained unknown. We report that two ABC transporters encoded upstream of the lugdunin-biosynthetic operon have distinct yet overlapping roles in lugdunin secretion and self-resistance. While deletion of the *lugEF* transporter genes abrogated most of the lugdunin secretion, the *lugGH* transporter genes had a dominant role in resistance. Yet, all four genes were required for full-level lugdunin resistance. The small accessory putative membrane protein LugI further contributed to lugdunin release and resistance levels conferred by the ABC transporters. Whereas LugIEFGH also conferred resistance to lugdunin congeners with inverse structure or with amino acid exchange at position six, they neither affected the susceptibility to a lugdunin variant with an exchange at position two nor to other cyclic peptide antimicrobials such as daptomycin or gramicidin S. The obvious selectivity of the resistance mechanism raises hopes that it will not confer cross-resistance to other antimicrobials or to optimized lugdunin derivatives to be used for the prevention and treatment of *S. aureus* infections.

Introduction

The dynamic changes in microbiome composition are governed by multiple antagonistic or mutualistic microbial interactions [1]. Several microbiome members achieve fitness benefits in competition with other bacteria through the production of bacteriocins or related antimicrobials [2, 3]. The biosynthetic genes for the production of antimicrobials are located in highly variable and often mobile clusters, which usually also include genes conferring self-resistance to the producer strain [4, 5]. Such mechanisms can confer resistance to a more or less narrow range of antimicrobials thus defining the capacity of antimicrobials-producing bacterial strains to tolerate their own compound plus, potentially, those from competitors. The capacity to produce bacteriocins and related molecules has been found to be particularly abundant in microbiome members from nutrient-poor habitats such as the human nose [6]. We are only beginning to understand the diversity and relevance of such molecules [7].

We have recently reported that most isolates of *Staphylococcus lugdunensis*, a colonizer of the human skin and nasal mucosa, produce lugdunin, the founding member of a new class of circular antimicrobial peptides named fibupeptides [8, 9]. Lugdunin is synthesized by non-

ribosomal peptide synthetases and inhibits target bacteria by dissipating their membrane potential, probably in a protonophore-like fashion [9]. In addition to its direct antimicrobial activity, lugdunin stimulates human skin cells to produce antibacterial host defense peptides that synergize with lugdunin in the elimination of susceptible microbes [10]. Lugdunin-producing *S. lugdunensis* can eradicate the major human pathogen *Staphylococcus aureus* and nasal carriage of *S. lugdunensis* strongly reduces the rate of nasal colonization by *S. aureus* [8]. The suitability of lugdunin as a potential new drug for *S. aureus* decolonization and therapy depends also on the risk of resistance development. We found that *S. aureus* cannot develop spontaneous resistance to lugdunin even after several passages in cultures with increasing subinhibitory concentrations of lugdunin [8]. It has remained unclear though how *S. lugdunensis* achieves self-resistance to its product and if potential resistance genes could be mobilized and transferred to *S. aureus* or other pathogens.

Here we analyzed the *lugEFGH* genes encoded next to the lugdunin biosynthesis genes and show that the four ABC-transporter encoding genes are necessary and sufficient to confer lugdunin resistance. LugEFGH and the accessory small putative membrane protein LugI were required for both, optimal secretion of endogenous lugdunin and resistance to exogenous lugdunin and even slight changes in lugdunin structure abrogated the capacity of the ABC exporters to protect against these compounds.

Results

The lugdunin gene cluster includes 13 genes, many of which encode proteins of unknown functions

The recent identification of the lugdunin gene cluster comprising the biosynthetic *lugABCD* genes and the putative regulator *lugR* [8] prompted us to elucidate the boundaries of the cluster and identify additional genes potentially involved in lugdunin synthesis, export, regulation, and self-resistance. The cluster plus some of the adjacent genes has a significantly lower G+C content than the rest of the chromosome (26.7 vs. 33.8%, respectively), and the region spanning *lugH* and *lugR* has even less than 24% G+C (Fig. 1a) suggesting that *lugRABCD* plus nine additional genes form the full gene cluster (Fig. 1b). *lugD*, coding for the starter unit in lugdunin biosynthesis, is flanked by the genes encoding LugT, a putative type-II thioesterase that may repair stalled peptidyl carrier protein (PCP) domains [11], and LugZ, which is homologous to 4'-phosphopantetheinyl transferases and probably converts apo-PCP to the active holo-form by attachment of the 4-phosphopantetheine cofactor [11]. Further downstream, probably forming a separate transcriptional unit, *lugM* encodes a putative monooxygenase the role of which in the biosynthesis process remains unclear.
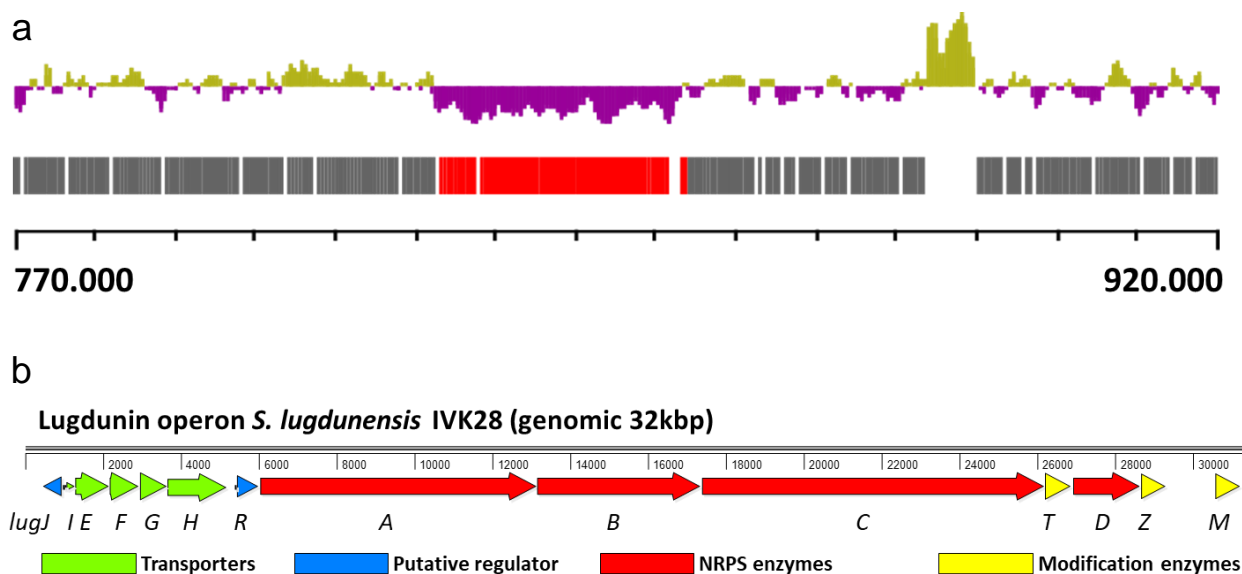
Figure 1. Decreased G+C content (a) and genetic organization (b) of the lugdunin gene cluster. The *S. lugdunensis* IVK28 chromosomal section between nucleotides 770,000 and 920,000 (NCBI accession number PRJNA669000) along with the encoded open reading frames in red (lugdunin gene cluster *lugJ* to *lugM*) and gray (other genes) and the corresponding G+C content in purple (below average; 26.7% for the lugdunin operon) and green (above average; 33.82% for the entire genome) is shown in (a). Organization of the lugdunin gene cluster with functional assignment in different colors is shown in (b). Protein accession numbers are listed in supplementary Table S1.

Upstream of *lugR* five genes (*lugIEFGH*) form another operon (Fig. 1b). LugI is predicted to encode a 79-amino acids long integral membrane protein with two transmembrane helices and no similarity to proteins of known function (Suppl. Fig.S1). LugE and LugG contain conserved 'Walker' motives probably representing the ATP-binding components of ABC transporter complexes [12]. LugF and LugH are related to the integral membrane parts of putative ABC transporters of other Firmicutes, with LugF containing six and LugH twelve putative transmembrane segments (Suppl. Fig.S1). According to the canonical architecture of ABC transporter complexes, the four proteins could form two distinct transporters, one as a LugEF homodimer and a second with a LugG homodimer linked to one LugH copy. Upstream of *lugI*, the gene *lugJ* is encoded in opposite direction, which may constitute a second regulator gene in addition to *lugR*. LugJ most likely belongs to the winged-helix type HTH-containing transcriptional regulators. Most antibiotic biosynthetic gene clusters encode proteins conferring self-resistance to the producing strain. Usually, these are either antibiotic-insensitive variants of target proteins, enzymes for the modification of target structures (e.g. rRNAs), or antibiotic exporters [13]. None of the genes in the lugdunin cluster seemed to reflect the first two types of self-resistance genes while the putative ABC transporter genes were regarded as

19

candidates for accomplishing lugdunin secretion and self-resistance and were analyzed further.

ABC transporters encoded in the *lug* gene cluster mediate lugdunin release and confer resistance to lugdunin

To analyze a potential role of the ABC transporters in lugdunin export and self-resistance, different combinations of *lugEFGH* and the co-transcribed gene *lugI* were deleted in the lugdunin-producing strain *S. lugdunensis* IVK28. To avoid polar effects on downstream transcripts an allelic replacement strategy with no insertion of foreign DNA fragments was used. When inhibition zones around spotted bacterial suspensions with identical diameters of the wild type and mutants on agar containing lugdunin-susceptible *S. aureus* cells were compared (Fig. 2a), the *lugIEFGH* mutant (Δ*lugIEFGH*) showed no inhibition, indicating that some or all of the five genes are required for lugdunin export. Deletion of only *lugEFGH* strongly reduced but did not abolish lugdunin release. The inhibitory distance was about 25% compared to the wild type (Fig. 2a), suggesting that LugI has a very modest but LugEFGH-independent role in lugdunin release. However, the sole inactivation of *lugI* caused no reduction in lugdunin release. Deletion of *lugEF* had a significant impact on the level of lugdunin export, which was almost as strong as in the Δ*lugEFGH* mutant, indicating that LugEF have a dominant role in lugdunin export. In contrast, the Δ*lugGH* mutant released even slightly higher amounts of lugdunin (about 38%) and exhibited a growth defect in liquid culture compared to the wild type (Fig. 2b), suggesting a role in resistance to lugdunin rather than export. Accordingly, the other *lugGH*-deficient mutant strains Δ*lugEFGH* and Δ*lugIEFGH* displayed similar growth defects (Fig. 2b).

To investigate the role of LugIEFGH in lugdunin self-resistance, several combinations of the genes were deleted in *S. lugdunensis* Δ*lugD*, which does not produce lugdunin [8], and the susceptibility of the resulting mutants to lugdunin was analyzed. Deletion of the entire gene set (*lugIEFGH*) strongly decreased the minimal inhibitory concentration (MIC) to exogenous lugdunin from 10.5 µg/ml to 2.0 µg/ml, indicating that the genes are involved in producer self-resistance to lugdunin (Fig. 3). Deletion of either *lugEF* or *lugGH* also led to reduced lugdunin MIC values indicating that both ABC transporters play a role in lugdunin self-resistance. Deletion of *lugI* led to a decrease of the MIC to the identical level as the *lugGH* deletion. Deletion of *lugEF*, *lugIEF*, or *lugIEFGH* led to a stepwise MIC decrease to the lowest observed level. Δ*lugEFGH*, still expressing *lugI*, showed the same MIC level as the *lugIEFGH* mutant, indicating that although *lugI* deletion has an effect on the overall MIC level, LugI seems to rely on the presence of one of the transporters to modulate lugdunin self-resistance (Fig. 3a). The lugdunin MIC of the *S. lugdunensis lugEFGH* deletion mutant was at the same level as those

of a representative panel of nasal *S. aureus* and *S. epidermidis* strains (2.7 µg/ml on average; Suppl. Fig. S2) suggesting that there is probably no additional self-resistance system involved.
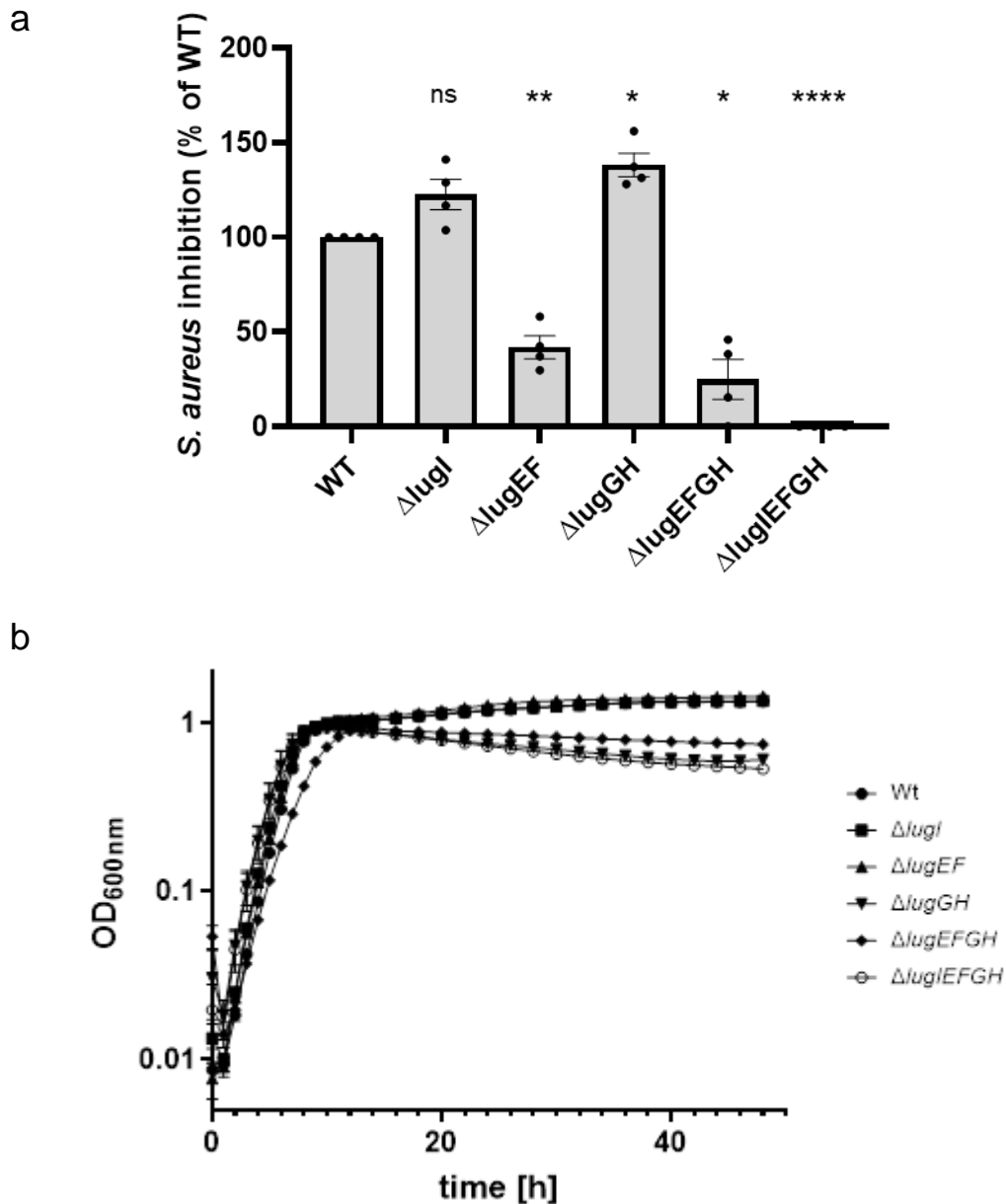

Figure 2. Impact of combinations of deletions of the luglEFGH genes on S. lugdunensis lugdunin secretion (a) and growth (b). (a) Differences in inhibition zone distances around colonies of S. lugdunensis wild type (WT), set to 100%, or mutants with the indicated deletions on agar containing lugdunin-susceptible S. aureus. (b) Growth in broth culture of the strains shown in (a). Means and SEM of at least 4 (a) or 3 (b) independent experiments are shown. Significant differences were calculated by one-way ANOVA (Dunnett's multiple comparisons test) (*, $P \leq 0.05$; **, $P \leq 0.01$; ***, $P \leq 0.005$).

To confirm the capacity of *lugIEFGH* to confer lugdunin resistance, the genes were cloned in different combinations in the pRB474 vector downstream of a constitutive promoter and introduced into *S. aureus* N315. *lugGH* expression led to a significantly increased lugdunin MIC (Fig. 3b), which confirms the important contribution of this subset of genes to lugdunin resistance. The additional expression of *lugEF* further raised the resistance of *S. aureus* to lugdunin, which supports the notion that full lugdunin resistance depends on the presence of all four ABC transporter genes. However, expression of *lugEF* alone did not cause a notable level of resistance. The presence of the entire operon *lugIEFGH* increased the lugdunin MIC to the highest observed level of 15.9 µg/ml indicating that the small *lugI* also contributes to resistance. When *lugI* was expressed in combination with *lugEF* (pRB474-lugIEF) no increased MIC compared to lugEF expression alone was observed. In contrast, *lugI* expression with *lugGH* (pRB474-lugIGH) enhanced the MIC to the same level as *lugEFGH* expression indicating that LugI might have a supporting effect with LugGH rather than with LugEF. Accordingly, the exclusive expression of *lugI* did not alter the susceptibility to lugdunin. The lugdunin MIC reached in *S. aureus* pRB474-lugIEFGH was identical to or even higher than that of *S. lugdunensis* IVK28, probably as a consequence of the high plasmid copy number (Fig. 3b).

The resistance conferred by the ABC transporters LugIEFGH is largely specific for native lugdunin

While some ABC drug exporters have broad substrate specificities, others are highly selective for only certain compounds [14]. The *lugIEFGH* genes were assessed for their capacity to protect *S. aureus* against lugdunin derivatives (see chemical structures 1-4 in Suppl. Fig. S3) and other antimicrobial compounds to elucidate the transporters' substrate range. The three derivatives enantio-lugdunin, 6-Trp-lugdunin and 2-Ala-lugdunin were selected, because they had similar activities as native lugdunin. 6-Trp-lugdunin was even slightly more active than native lugdunin. Since most other lugdunin derivatives showed no or only residual activity, we could include only the two active versions (9). The constitutive expression of LugIEFGH did not affect the susceptibility of *S. aureus* to the membrane-active cyclic peptide antibiotics daptomycin, and gramicidin S, or to the small non-peptide protonophors CCCP and nigericin, indicating that the resistance mechanism has a strict preference for the structure of lugdunin (Fig. 4a). LugIEFGH also conferred some degree of resistance to the lugdunin enantiomer (enantio-lugdunin), which has the same structure as regular lugdunin but an inverse D-/L-amino acid configuration [8, 9], albeit with a much lower efficacy as to native lugdunin. Similar though even less pronounced findings were obtained with 6-Trp-lugdunin, which contains a D-tryptophan at position six instead of a D-valine [9].
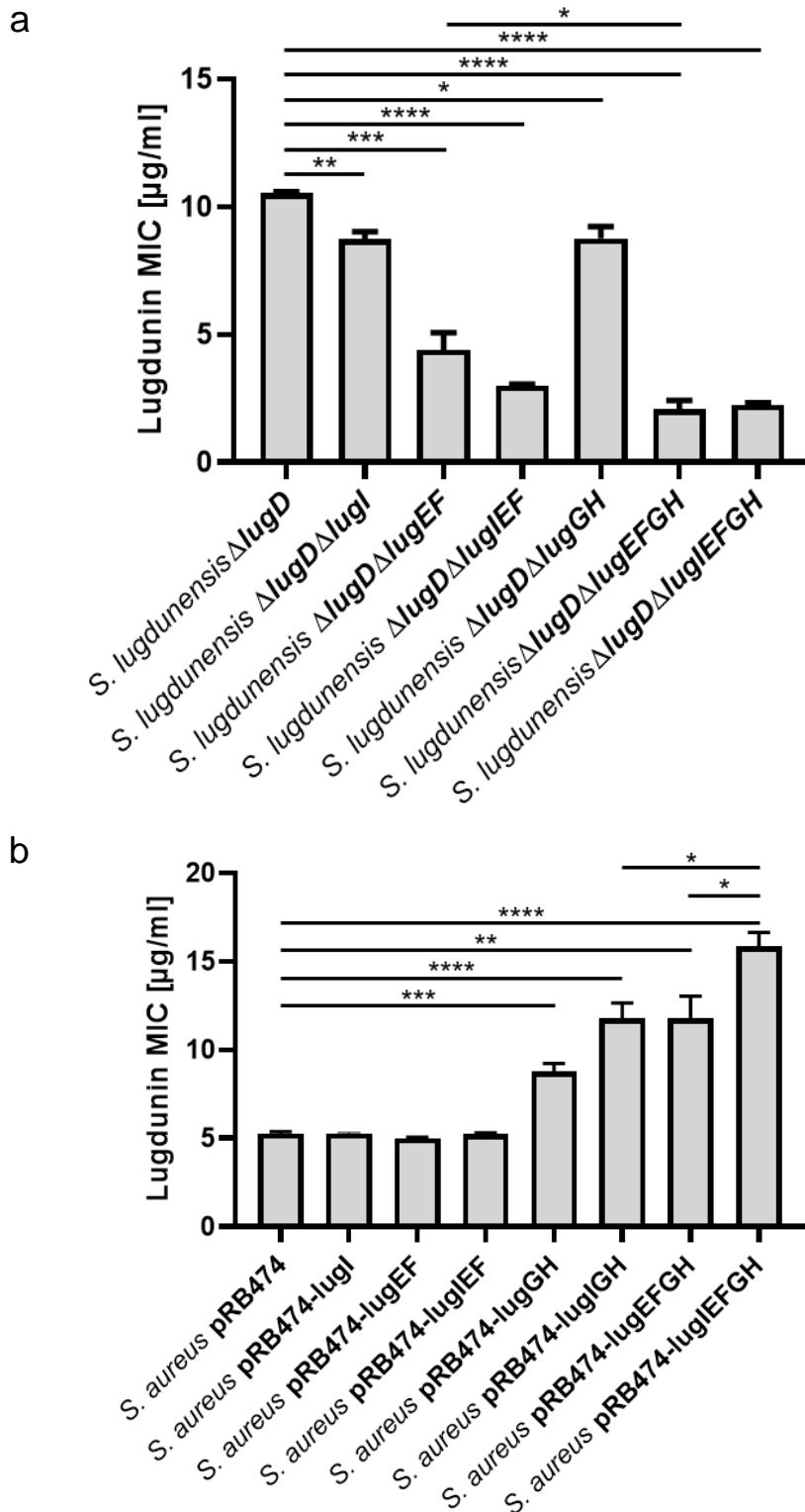
Figure 3. Impact of *lugIEFGH* deletion in the *S. lugdunensis* Δ*lugD* strain (a) or constitutive expression in *S. aureus* (b) on lugdunin susceptibility. Means and SEM of at least five independent experiments are shown. Significant differences were calculated by one-way ANOVA (Brown-Forsythe and Welsh) (*, P ≤ 0.05; **, P ≤ 0.01; ***, P ≤ 0.005).

In contrast, 2-Ala-lugdunin (D-alanine instead of D-valine at position two) [9] had equal antimicrobial activity against *S. aureus* with or without LugIEFGH, implying that no resistance against the 2-Ala congener was conferred. Thus, LugIEFGH are largely specific for lugdunin in its native structure, and lugdunin alterations at position two are less well tolerated by the transporter than alterations at position six.
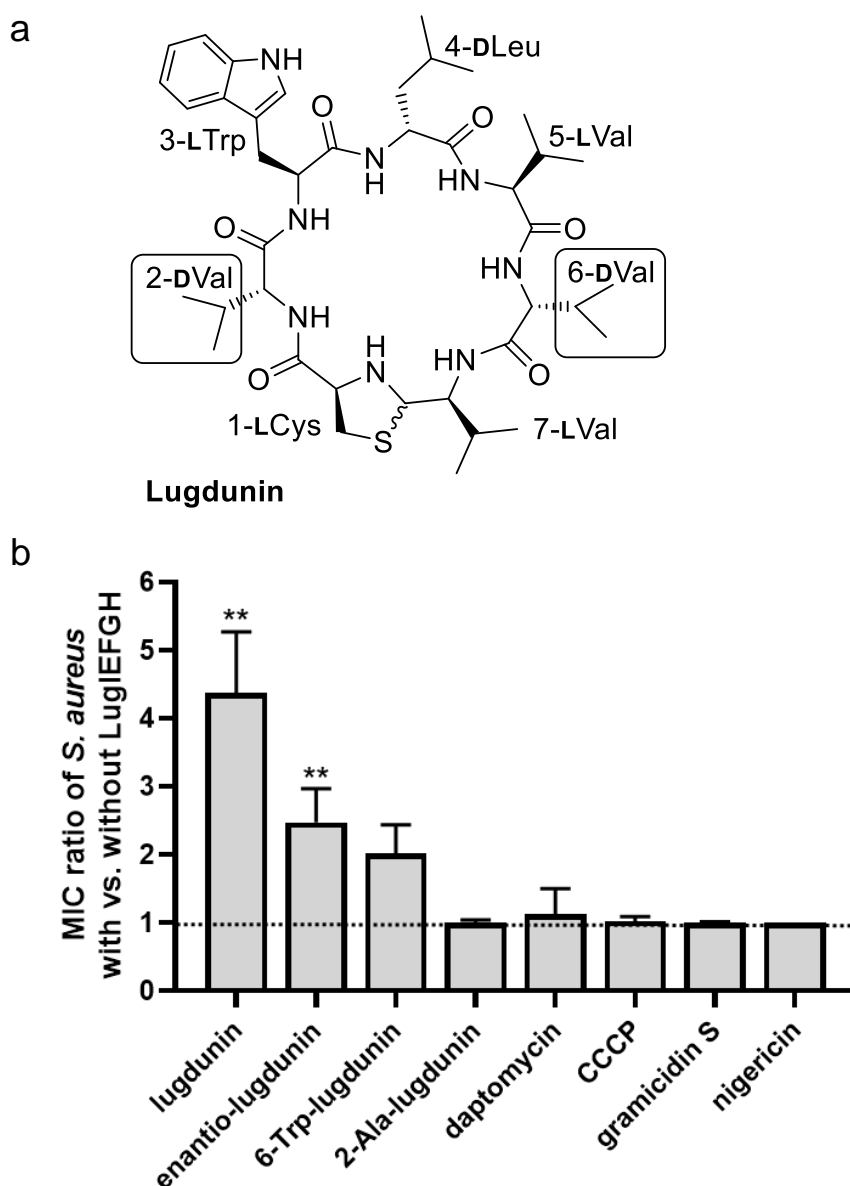
a

Lugdunin

b

Figure 4. Impact of *lugIEFGH* on *S. aureus* susceptibility to lugdunin variants and other cyclic peptide antimicrobials. Chemical structure of lugdunin and positions of alterations in derivatives used in (b) are shown in (a). The ratios of MICs elucidated for *S. aureus* pRB474-lugIEFGH vs. *S. aureus* pRB474 is shown in (b). Means +/- SEM from at least three independent experiments and significant differences between MICs for the two strains, calculated by Student's multiple unpaired t-test (with Holm-Sidak correction) are shown (**, $P \leq 0.01$). Mean MIC values for all compounds and both strains are listed in supplementary Table S2.

Discussion

Lugdunin, the first non-ribosomally synthesized antibiotic from human microbiomes, has a novel structure and an unusual protonophore-like mode of action, which distinguishes it from most of the antibiotics in clinical use [9]. Lugdunin causes proton leakage in synthetic, protein-free membrane vesicles, suggesting that it does not need to target a proteinaceous molecule to exert its antibacterial activity [9]. The atypical mode of action raised the question whether the bacterial producer strains would also use an unusual mechanism to achieve self-resistance to lugdunin. As shown for other cyclic peptides, lugdunin may be able to oligomerize in membranes [15-17], which might also have an influence on its recognition by the lugdunin transporters. We demonstrate that *S. lugdunensis* uses the four ABC transporter proteins LugEFGH for lugdunin secretion and self-resistance (Fig. 5), which is reminiscent of several other antimicrobial molecule producers [2, 18]. The use of two separate ABC transporters for antimicrobial secretion and self-resistance has previously been documented for instance for several lantibiotics and other bacteriocins [18]. Moreover, the phenol-soluble modulin (PSM) peptides produced by most *Staphylococcus* species are secreted by an ABC transporter complex, which is encoded by four genes most probably forming two separate transporters, PmtAB and PmtCD [19]. They confer self-resistance to PSMs and several other membrane-damaging cationic antimicrobial peptides (CAMPs) [20].
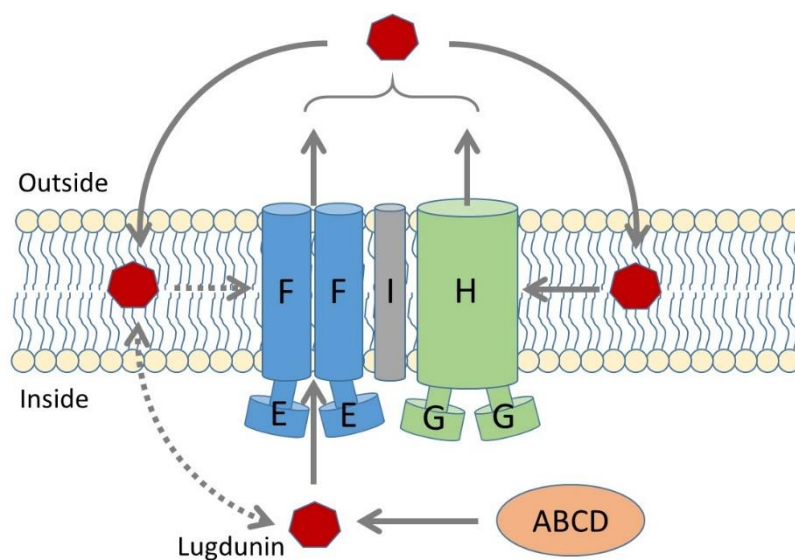

Figure 5. Model for the roles of LugIEFGH in lugdunin secretion and self-resistance. LugEF has a dominant role in lugdunin secretion and a minor role in lugdunin resistance. In contrast, LugGH is mostly responsible for self-resistance, presumably by taking lugdunin up from the membrane bilayer. LugI contributes to secretion and resistance by collaborating with the ABC transporters in a currently unclear fashion. Putative minor lugdunin passage ways are shown as dashed arrows. ABCD depicts the intracellular lugdunin-biosynthetic enzymes.

The roles of LugEF and LugGH in lugdunin export and self-resistance overlapped to some degree, which is also reminiscent of some bacteriocin-synthetic systems with two separate ABC transporters [21, 22]. LugGH had a dominant role in lugdunin resistance in *S. aureus*, which was even enhanced by the presence of LugI. Accordingly, LugGH had only a weak effect on lugdunin release in *S. lugdunensis.* Although deletion of *lugGH* in *S. lugdunensis* had only a minor effect on the MIC compared to *lugEF* deletion, it had a strong impact on the growth and fitness of lugdunin-producing *S. lugdunensis,* which is in agreement with its capacity to protect the producer against its product. The *S. lugdunensis lugGH* mutant released even slightly more lugdunin than the wild type for unclear reasons, maybe as a consequence of dysregulation of the lugdunin-biosynthetic process in these highly stressed mutant bacteria. This might also be the explanation for the unexpected strong impact of *lugEF* deletion in *S. lugdunensis* on the MIC, although LugEF does not change the MIC level in *S. aureus*. As for several other ABC exporters conferring resistance to membrane-active compounds, it can be assumed that LugH takes up its cargo from the membrane bilayer by opening the channel laterally (Fig. 5). In contrast to LugGH, LugEF did not seem to affect the producer's fitness but had a dominant impact on lugdunin release, probably by acquiring lugdunin from the biosynthetic machinery (LugABCD) in the cytoplasm. Nevertheless, LugEF also contributed to lugdunin resistance, maybe by exporting excess cytoplasmic or membrane-embedded lugdunin (Fig. 5). It is currently not clear if the two transporter systems form indeed a complex together with LugI. It is possible that LugEF may be associated with the biosynthesis machinery formed by LugABCD to directly export newly synthesized lugdunin, which, in addition to the stoichiometry of the LugIEFGH products, remains to be explored.

It remains unclear how LugI may contribute to lugdunin secretion and self-resistance, but it is obvious that its role in resistance depends on the presence of both ABC transporters. Accessory membrane proteins have been described for other ABC transporters, for instance the *S. aureus* VraDEH system, which confers resistance to CAMPs. In addition to the ATPase VraD and the integral membrane component VraE the system includes the small VraH protein, which is required for high-level resistance to gallidermin and daptomycin and has been denoted a "peptide resistance ABC transporter activity modulator" [23], a term also appropriate for LugI. VraH has a similar size and predicted membrane topology as LugI, but no obvious sequence similarity. Accessory integral membrane proteins are also known to complement ABC transporters secreting and conferring producer self-resistance to the lantibiotics epidermin and gallidermin [21, 22].

Only inversion of the lugdunin structure in enantio-lugdunin or a minor change at amino acid position six of lugdunin were tolerated by the resistance mechanism although resistance to these congeners was much less pronounced than for native lugdunin. In contrast, changes at

position two abrogated the capacity of LugIEFGH to confer resistance completely. The high selectivity distinguishes the lugdunin resistance mechanism from those to other antimicrobial molecules such as PSMs or from multi-drug ABC exporters such as Sav1866 [24] or AbcA [25, 26]. Slight modifications of lugdunin that maintain or even increase its antimicrobial activity will therefore make it difficult for LugIEFGH to neutralize such variants if they would be developed for clinical use, even if *lugIEFGH* could spread horizontally between different bacterial species. More detailed studies will be necessary to elucidate the molecular basis for the selectivity and elucidate if and which mutations in the self-resistance proteins might alter or broaden its preferences for peptide cargo.

LugIEFGH have never been found outside the *lug* operon of *S. lugdunensis*, neither in *S. aureus* nor other nasal microbiome members. Only a few members of the Bacillales order, mainly from the environmental or intestinal bacterial genera *Salinicoccus*, Planococcus, *Exiguobacterium,* or *Gracilibacillus*, respectively, harbor homologs of the *lugIEFGH* cluster, albeit without the lugdunin biosynthesis genes. Additionally, *Streptococcus mutans* genomes encode an ABC transporter with homology to LugGH, but lack LugI or LugEF homologs. Despite its lower G+C content, the *lug* gene cluster does not seem to constitute a promiscuous genetic element, which may restrict its mobility among species other than *S. lugdunensis.*

Materials and Methods

Strains and growth conditions. The *Staphylococcus* strains used in this study were *S. aureus* N315, *S. aureus* USA300 LAC, and *S. lugdunensis* IVK28. Further strains used for MIC determination were *S. aureus* N315 with plasmids pRB474, pRB474-lugI, pRB474-lugEF, pRB474-lugIEF, pRB474-lugGH, pRB474-lugIGH, pRB474-lugEFGH, and pRB474-lugIEFGH. The construction of the plasmids is described below. *E. coli* DC10B was used as the cloning host for further transformation in *S. aureus* N315 (expression of transporter genes) or *S. aureus* PS187 for subsequent phage transduction into *S. lugdunensis* IVK28 [27].

Basic medium (BM: 1% soy peptone A3 (Organotechnie SAS, France), 0.5% OHLY KAT yeast extract (Deutsche Hefewerke GmbH, Germany), 0.5% NaCl, 0.1% glucose and 0.1% K_2HPO_4, pH 7.2) was used as the standard growth medium and for MIC determinations. If necessary, antibiotic was used at a concentration of 10 µg ml^{-1} for chloramphenicol. *E. coli* transformants were grown in lysogeny broth (LB; Lennox)-medium (1% tryptone, 0.5% yeast extract, 0.5% NaCl; Carl Roth GmbH, Germany) supplemented with 100 µg ml^{-1} ampicillin or corresponding LB agar.

To analyze growth curves strains were grown overnight in BM with suitable antibiotics under continuous shaking at 37°C. Each strain was adjusted to OD_{600} =1 in MHB and 2.5 µl of the

bacterial stock solutions were pipetted to 500 µl MHB in a 48-well microtiter plate. The plates were incubated for 48 h under continuous shaking in a microplate reader and OD_{600} was measured every 15 minutes.

Synthetic lugdunin congeners and control compounds. All synthetic lugdunin derivatives were synthesized as described elsewhere [9]. Daptomycin (Cubicin) was purchased from MSD Sharp & Dohme GmbH (Haar, Germany), CCCP, gramicidin S and nigericin were obtained from SigmaAldrich (now Merck, Germany).

Generation of *S. lugdunensis* IVK28 knockout mutants. DNA manipulation, isolation of plasmid DNA, and transformation of *E. coli* were performed by use of standard procedures. Enzymes for molecular cloning were obtained from Thermo Fisher Scientific and New England Biolabs. For the generation of knock-out mutants the temperature-sensitive shuttle-vector pBASE6 was used and mutants were generated by allelic replacement as described previously [28]. Flanking regions of the genes to be deleted were amplified by PCR (Table 1), and ligated to shuttle vector pBASE6 after digestion with suitable restriction enzymes. Cloning was performed in *E. coli* DC10B from where sequence-verified plasmids were transferred to *S. aureus* PS187 by electroporation. Phage φ187 was used for transduction of *S. lugdunensis* IVK28 as described elsewhere [27]. Mutations in *S. lugdunensis* were confirmed by PCR amplification of the entire *lugJIEFGH* region with control primers and analysis of the fragment sizes in comparison to the wild type. For the construction of the *lugIGH* mutant the confirmed *lugGH* mutant was transduced with the plasmid for *lugI* deletion and the second deletion was performed in the Δ*lugGH* background.

Expression of ABC transporter genes in *S. aureus* N315. The transporters of *S. lugdunensis* IVK28 were cloned in pRB474 as follows. For the *lugEF* construct, the primers ABC1-down and ABC2-up (Table 2) were used to amplify *lugEF*, and the primers ABC regulator forw and ABC2-up were used to amplify *lugIEF.* To express only *lugI* the gene was amplified with primers ABC regulator forw and lugI rev. *lugGH* was generated with the primers ABC3-down and ABC4-up. For the generation of the *lugIGH* construct the plasmid pRB474-lugGH was digested with PstI and treated with alkaline phosphatase. Here, *lugI* was amplified with the primers ABC regulator forw and lugI rev Pst, digested with PstI and ligated into the PstI digested pRB474-lugGH. The correct orientation of *lugI* in front of *lugGH* was confirmed by sequencing. *lugEFGH* was generated with the primers ABC1-down and ABC4-up. The PCR fragment for *lugIEFGH* was amplified with the primers ABC regulator forw and ABC4-up. All PCR products and plasmid pRB474 were digested with PstI and SacI, to ligate the PCR fragments into pRB474. The resulting constructs pRB474-lugI, pRB474-lugEF, pRB474-

lugIEF, pRB474-lugGH, pRB474-lugIGH, pRB474-lugEFGH, and pRB474-lugIEFGH were transferred into *E. coli* DC10B [29] and, subsequently into *S. aureus* N315.

Analysis of lugdunin secretion. To analyze the capacity of *S. lugdunensis* IVK28 and its isogenic mutants to export lugdunin, an *S. aureus* inhibition assay was performed. *S. aureus* USA300 LAC was grown overnight in BM, and BM agar, cooled down to 50°C after autoclaving, was inoculated to a final OD of 0.00125 with this overnight culture. From this suspension defined 15 ml agar plates with 8.4 cm diameter were poured. *S. lugdunensis* strains were grown overnight in BM, centrifuged, and washed in 1/10 volume phosphate buffered saline (PBS) to remove residual cell-associated lugdunin. After a second centrifugation step, cultures were adjusted to an optical density (600 nm) of 20, and 10 µl of the suspensions were spotted on the solidified BM agar plates containing *S. aureus*. After drying of the spots, the plates were incubated at 37°C for 24 h and inhibition zones were photographed and analyzed with ImageJ software (version 1.8.0_112). For each experiment all strains to be analyzed were spotted on the same agar plate and the inhibition zone, defined as the distance between the *S. lugdunensis* IVK28 colony and the growing *S. aureus* cells, was defined as 100%.

MIC determination. Strains used for MIC determinations were grown overnight in BM, with chloramphenicol for plasmid containing strains, under continuous shaking at 37°C. Each strain was adjusted to OD_{600}=0.0625 in BM. The antimicrobial molecule stock solutions were serially diluted in BM in 96-well microtiter plates. Each well with 100 µl medium, and chloramphenicol if required, was inoculated with 2 µl of the OD_{600}=0.0625 bacterial stock solution. The plates were incubated at 37 °C for 24 hours under continuous shaking (160 rpm). OD_{600} of each well was measured with a microplate reader and the concentration leading to a 75%-growth reduction was calculated and defined as MIC value.

Statistics. Statistical analyses were performed using Graph Pad Prism 8.01. One-way ANOVA was used to compare MIC levels of individual strains against the reference strain, and t-tests were used for the comparison of MIC levels against various compounds with or without transporter genes.

Acknowledgements

References

1.   Krismer B, Weidenmaier C, Zipperer A, Peschel A. The commensal lifestyle of Staphylococcus aureus and its interactions with the nasal microbiota. Nat Rev Microbiol. 2017;15(11):675-87. Epub 2017/10/13. doi: 10.1038/nrmicro.2017.104. PubMed PMID: 29021598.

2.   Cotter PD, Hill C, Ross RP. Bacteriocins: developing innate immunity for food. Nat Rev Microbiol. 2005;3(10):777-88. Epub 2005/10/06. doi: 10.1038/nrmicro1273. PubMed PMID: 16205711.

3.   Otto M. Staphylococci in the human microbiome: the role of host and interbacterial interactions. Curr Opin Microbiol. 2020;53:71-7. Epub 2020/04/17. doi: 10.1016/j.mib.2020.03.003. PubMed PMID: 32298967.

4.   Arnison PG, Bibb MJ, Bierbaum G, Bowers AA, Bugni TS, Bulaj G, et al. Ribosomally synthesized and post-translationally modified peptide natural products: overview and recommendations for a universal nomenclature. Nat Prod Rep. 2013;30(1):108-60. Epub 2012/11/21. doi: 10.1039/c2np20085f. PubMed PMID: 23165928; PubMed Central PMCID: PMCPMC3954855.

5.   Medema MH, Kottmann R, Yilmaz P, Cummings M, Biggins JB, Blin K, et al. Minimum Information about a Biosynthetic Gene cluster. Nat Chem Biol. 2015;11(9):625-31. Epub 2015/08/19. doi: 10.1038/nchembio.1890. PubMed PMID: 26284661; PubMed Central PMCID: PMCPMC5714517.

6.   Janek D, Zipperer A, Kulik A, Krismer B, Peschel A. High Frequency and Diversity of Antimicrobial Activities Produced by Nasal Staphylococcus Strains against Bacterial Competitors. PLoS Pathog. 2016;12(8):e1005812. doi: 10.1371/journal.ppat.1005812. PubMed PMID: 27490492; PubMed Central PMCID: PMCPMC4973975.

7.   Sugimoto Y, Camacho FR, Wang S, Chankhamjon P, Odabas A, Biswas A, et al. A metagenomic strategy for harnessing the chemical repertoire of the human microbiome. Science. 2019;366(6471). Epub 2019/10/05. doi: 10.1126/science.aax9176. PubMed PMID: 31582523.

8.   Zipperer A, Konnerth MC, Laux C, Berscheid A, Janek D, Weidenmaier C, et al. Human commensals producing a novel antibiotic impair pathogen colonization. Nature. 2016;535(7613):511-6. doi: 10.1038/nature18634. PubMed PMID: 27466123.

9.   Schilling NA, Berscheid A, Schumacher J, Saur JS, Konnerth MC, Wirtz SN, et al. Synthetic Lugdunin Analogues Reveal Essential Structural Motifs for Antimicrobial Action and Proton Translocation Capability. Angew Chem Int Ed Engl. 2019;58(27):9234-8. Epub 2019/05/07. doi: 10.1002/anie.201901589. PubMed PMID: 31059155; PubMed Central PMCID: PMCPMC6618241.

10.   Bitschar K, Sauer B, Focken J, Dehmer H, Moos S, Konnerth M, et al. Lugdunin amplifies innate immune responses in the skin in synergy with host- and microbiota-derived factors. Nat Commun. 2019;10(1):2730. Epub 2019/06/23. doi: 10.1038/s41467-019-10646-7. PubMed PMID: 31227691; PubMed Central PMCID: PMCPMC6588697.

11.   Kotowska M, Pawlik K. Roles of type II thioesterases and their application for secondary metabolite yield improvement. Appl Microbiol Biotechnol. 2014;98(18):7735-46. Epub 2014/08/02. doi: 10.1007/s00253-014-5952-8. PubMed PMID: 25081554; PubMed Central PMCID: PMCPMC4147253.

12.   Locher KP. Mechanistic diversity in ATP-binding cassette (ABC) transporters. Nat Struct Mol Biol. 2016;23(6):487-93. Epub 2016/06/09. doi: 10.1038/nsmb.3216. PubMed PMID: 27273632.

13.   Mungan MD, Alanjary M, Blin K, Weber T, Medema MH, Ziemert N. ARTS 2.0: feature updates and expansion of the Antibiotic Resistant Target Seeker for comparative genome mining. Nucleic Acids Res. 2020. Epub 2020/05/20. doi: 10.1093/nar/gkaa374. PubMed PMID: 32427317.

14.   Orelle C, Mathieu K, Jault JM. Multidrug ABC transporters in bacteria. Res Microbiol. 2019;170(8):381-91. Epub 2019/06/30. doi: 10.1016/j.resmic.2019.06.001. PubMed PMID: 31251973.

15.   De Riccardis F, Izzo I, Montesarchio D, Tecilla P. Ion transport through lipid bilayers by synthetic ionophores: modulation of activity and selectivity. Acc Chem Res. 2013;46(12):2781-90. doi: 10.1021/ar4000136. PubMed PMID: 23534613.

16.   Duax WL, Griffin JF, Langs DA, Smith GD, Grochulski P, Pletnev V, et al. Molecular structure and mechanisms of action of cyclic and linear ion transport antibiotics. Biopolymers. 1996;40(1):141-55.   doi: 10.1002/(SICI)1097-0282(1996)40:1%3C141::AID-BIP6%3E3.0.CO;2-W. PubMed PMID: 8541445.

17.   Ghadiri MR, Granja JR, Buehler LK. Artificial transmembrane ion channels from self-assembling peptide nanotubes. Nature. 1994;369(6478):301-4. doi: 10.1038/369301a0. PubMed PMID: 7514275.

18.   Bierbaum G, Sahl HG. Lantibiotics: mode of action, biosynthesis and bioengineering. Curr   Pharm   Biotechnol.   2009;10(1):2-18.   Epub   2009/01/20.   doi: 10.2174/138920109787048616. PubMed PMID: 19149587.

19.   Chatterjee SS, Joo HS, Duong AC, Dieringer TD, Tan VY, Song Y, et al. Essential Staphylococcus aureus toxin export system. Nature medicine. 2013;19(3):364-7. Epub 2013/02/12. doi: 10.1038/nm.3047. PubMed PMID: 23396209; PubMed Central PMCID: PMCPMC3594369.

20.   Cheung GYC, Fisher EL, McCausland JW, Choi J, Collins JWM, Dickey SW, et al. Antimicrobial Peptide Resistance Mechanism Contributes to Staphylococcus aureus Infection. J Infect Dis. 2018;217(7):1153-9. Epub 2018/01/20. doi: 10.1093/infdis/jiy024. PubMed PMID: 29351622; PubMed Central PMCID: PMCPMC5939666.

21.   Peschel A, Schnell N, Hille M, Entian KD, Gotz F. Secretion of the lantibiotics epidermin and gallidermin: sequence analysis of the genes gdmT and gdmH, their influence on epidermin production and their regulation by EpiQ. Mol Gen Genet. 1997;254(3):312-8. Epub 1997/04/16. doi: 10.1007/s004380050421. PubMed PMID: 9150266.

22.   Hille M, Kies S, Gotz F, Peschel A. Dual role of GdmH in producer immunity and secretion of the Staphylococcal lantibiotics gallidermin and epidermin. Appl Environ Microbiol. 2001;67(3):1380-3. Epub 2001/03/07. doi: 10.1128/aem.67.3.1380-1383.2001. PubMed PMID: 11229936; PubMed Central PMCID: PMCPMC92739.

23.   Popella P, Krauss S, Ebner P, Nega M, Deibert J, Gotz F. VraH Is the Third Component of the Staphylococcus aureus VraDEH System Involved in Gallidermin and Daptomycin Resistance and Pathogenicity. Antimicrob Agents Chemother. 2016;60(4):2391-401. doi: 10.1128/AAC.02865-15. PubMed PMID: 26856834; PubMed Central PMCID: PMCPMC4808217.

24. Velamakanni S, Yao Y, Gutmann DA, van Veen HW. Multidrug transport by the ABC transporter Sav1866 from Staphylococcus aureus. Biochemistry. 2008;47(35):9300-8. doi: 10.1021/bi8006737. PubMed PMID: 18690712.

25. Costa SS, Viveiros M, Amaral L, Couto I. Multidrug Efflux Pumps in Staphylococcus aureus: an Update. Open Microbiol J. 2013;7:59-71. Epub 2013/04/10. doi: 10.2174/1874285801307010059. PubMed PMID: 23569469; PubMed Central PMCID: PMCPMC3617543.

26. Yoshikai H, Kizaki H, Saito Y, Omae Y, Sekimizu K, Kaito C. Multidrug-Resistance Transporter AbcA Secretes Staphylococcus aureus Cytolytic Toxins. J Infect Dis. 2016;213(2):295-304. Epub 2015/07/15. doi: 10.1093/infdis/jiv376. PubMed PMID: 26160745.

27. Winstel V, Kuhner P, Rohde H, Peschel A. Genetic engineering of untransformable coagulase-negative staphylococcal pathogens. Nat Protoc. 2016;11(5):949-59. Epub 2016/04/23. doi: 10.1038/nprot.2016.058. PubMed PMID: 27101516.

28. Geiger T, Francois P, Liebeke M, Fraunholz M, Goerke C, Krismer B, et al. The stringent response of Staphylococcus aureus and its impact on survival after phagocytosis through the induction of intracellular PSMs expression. PLoS pathogens. 2012;8(11):e1003016. doi: 10.1371/journal.ppat.1003016. PubMed PMID: 23209405; PubMed Central PMCID: PMCPMC3510239.

29. Monk IR, Shah IM, Xu M, Tan MW, Foster TJ. Transforming the untransformable: application of direct transformation to manipulate genetically Staphylococcus aureus and Staphylococcus epidermidis. mBio. 2012;3(2). doi: 10.1128/mBio.00277-11. PubMed PMID: 22434850; PubMed Central PMCID: PMCPMC3312211.

30. Omasits U, Ahrens CH, Muller S, Wollscheid B. Protter: interactive protein feature visualization and integration with experimental proteomic data. Bioinformatics. 2014;30(6):884-6. doi: 10.1093/bioinformatics/btt607. PubMed PMID: 24162465.

Supplemental Information

Table S1: Accession numbers of the proteins involved in lugdunin biosynthesis, transport and putative regulation

Protein	Accession number
LugJ	WP_002460039.1
LugI	WP_002460038.1
LugE	WP_002478838.1
LugF	WP_002478839.1
LugG	WP_002460034.1
LugH	WP_002460033.1
LugR	WP_002460032.1
LugA	WP_002492248.1
LugB	WP_081094477.1
LugC	WP_037540567.1
LugT	WP_002460022.1
LugD	WP_002478846.1
LugZ	WP_002478847.1
LugM	WP_002492211.1

Table S2: Mean MIC values in BM-medium of all tested compounds for *S. aureus* pRB474 and pRB474-lugIEFGH

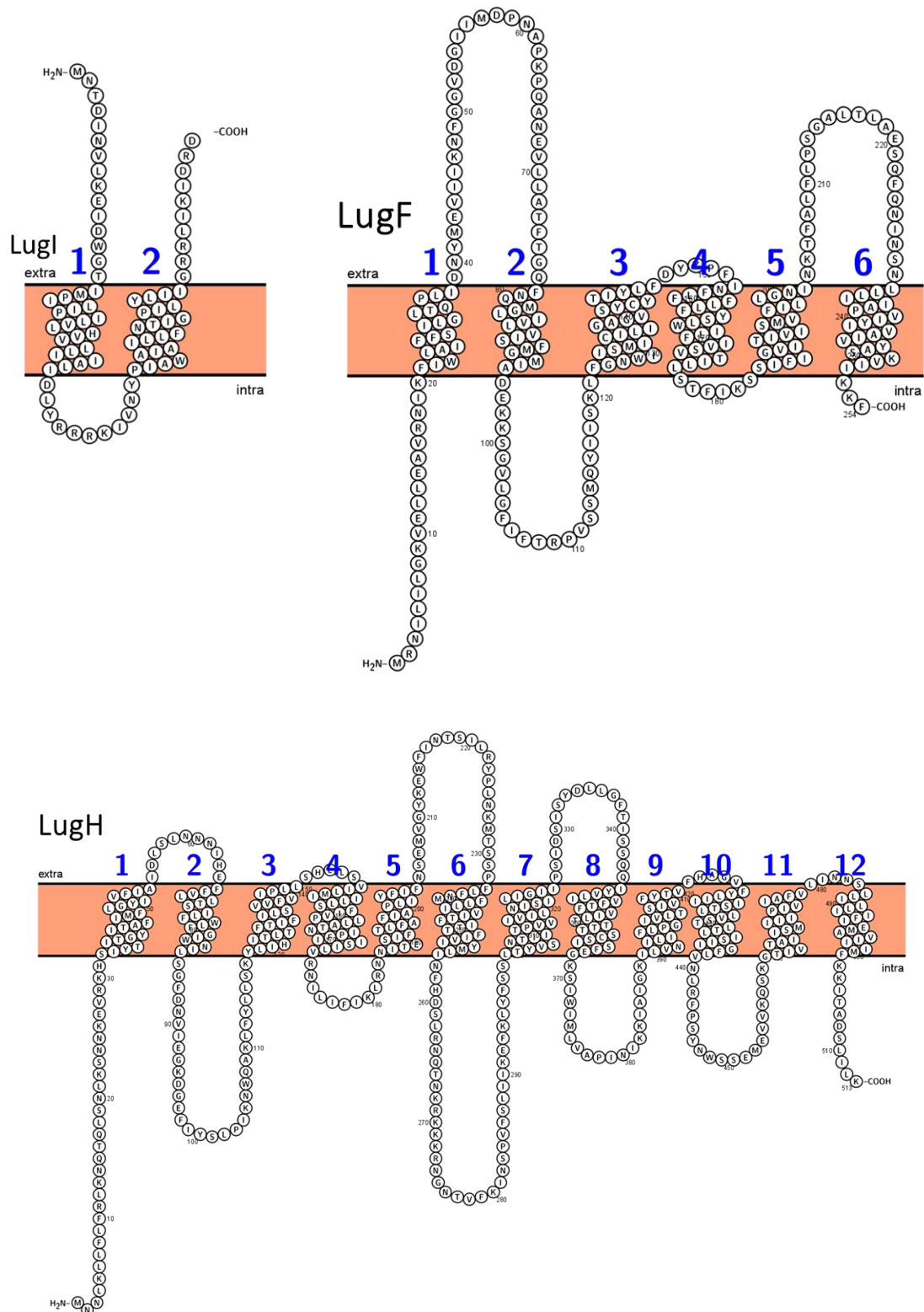| Compound	MIC *S. aureus* pRB474	MIC *S. aureus* pRB474-lugIEFGH	Ratio
lugdunin	8.15	33.68	4.13
Enantio-lugdunin	31.3	69.75	2.23
6-Trp-lugdunin	16.43	31.05	1.89
2-Ala-lugdunin	40.17	39.93	0.99
daptomycin	2.17	2.17	1
CCCP	0.63	0.64	1.02
gramicidin S	2.75	2.74	1.00
nigericin	0.25	0.25	1.00

Fig. S1: Predicted transmembrane topologies of LugI, LugF, and LugH. The transmembrane topology for LugI, LugF, and LugH was predicted with the help of PROTTER (version 1.0; http://wlab.ethz.ch/protter/start/) [30].
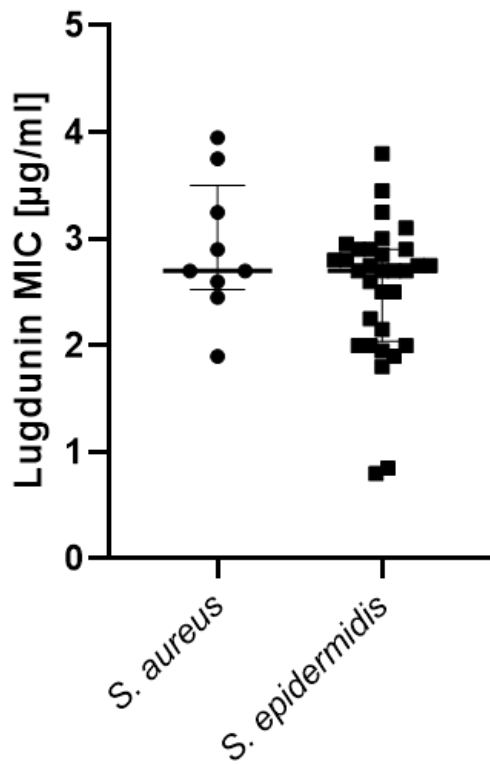
Fig. S2: Comparison of lugdunin susceptibility of individual nasal *S. aureus* and *S. epidermidis* isolates. The MIC of lugdunin was tested against representative nasal *S. aureus* and *S. epidermidis* isolates. Shown are the medians with interquartile range for the two groups.
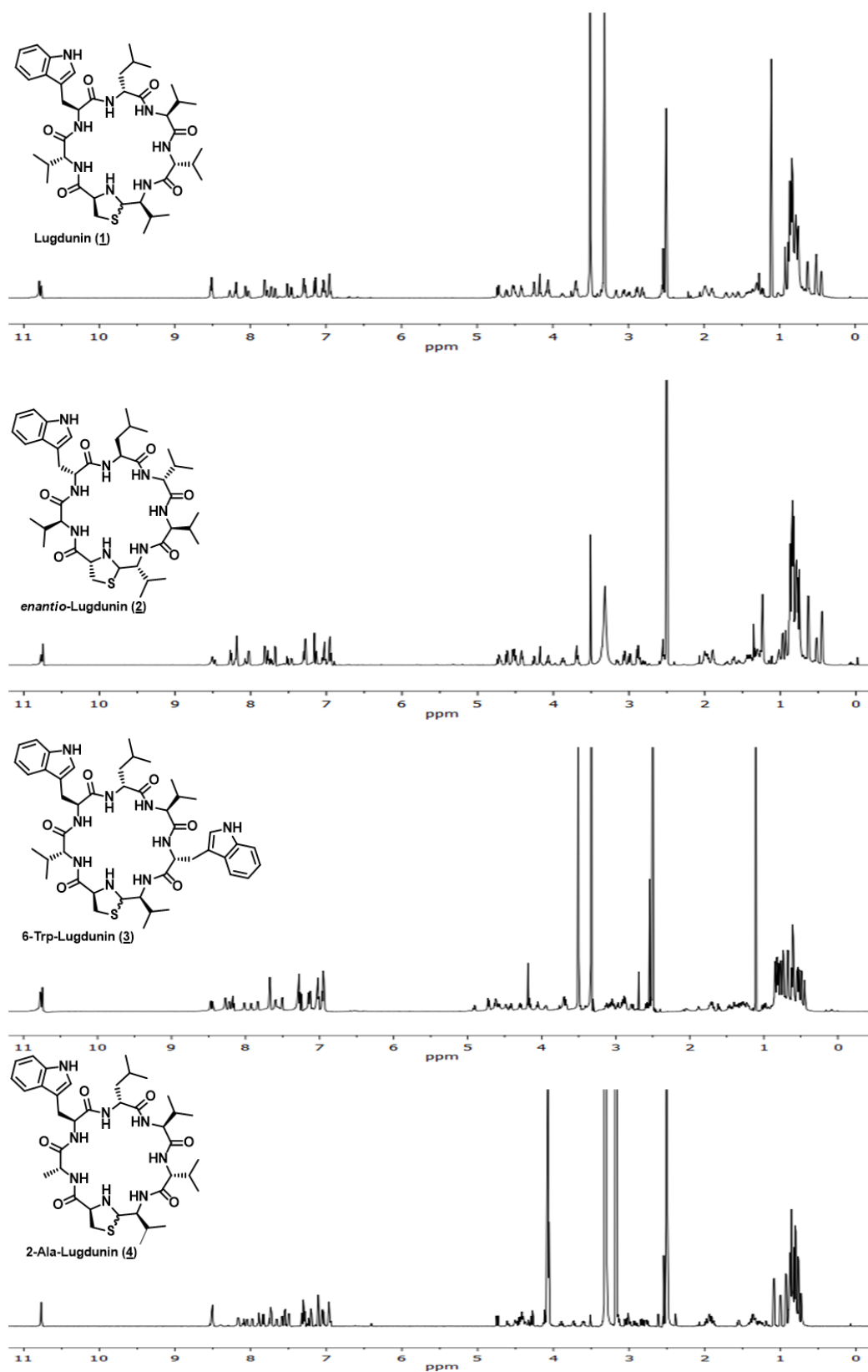
Fig. S3: Chemical structural formula of synthetic lugdunin analogues **1** – **4** and ^{1}H NMR spectra thereof (d$_6$-dmso, 700 MHz, 303K).

Chapter 4

Extremely short-lived peptide-polyene antimicrobial enables nasal commensal to eliminate *Staphylococcus aureus*

Benjamin O. Torres Salazar[a,b,c], Taulant Dema[d,#], Nadine A. Schilling[b,d,#], Daniela Janek[a,b,c], Anne Berscheid[c,e], Sophia Krauss[a,b,c], Min Li[f], Malcolm J. Horsburgh[g], Tillmann Weber[h], José Manuel Beltrán-Beleña[b,d], Heike Brötz-Oesterhelt[c,e], Stephanie Grond[b,d*], Bernhard Krismer[a,b,c*]; Andreas Peschel[a,b,c].

[a] Department of Infection Biology, Interfaculty Institute of Microbiology and Infection Medicine, University of Tübingen, Tübingen, Germany; [b] Cluster of Excellence EXC 2124 Controlling Microbes to Fight Infections; [c] German Center for Infection Research (DZIF), partner site Tübingen; [d] Institute of Organic Chemistry, University of Tübingen, Tübingen, Germany; [e] Department of Microbial Bioactive Compounds, Interfaculty Institute of Microbiology and Infection Medicine, University of Tübingen, Tübingen, Germany; [f] Department of Laboratory Medicine, Renji Hospital, School of Medicine, Shanghai Jiaotong University, Shanghai, China; [g] Department of Infection Biology and Microbiomes, University of Liverpool, Liverpool, UK; [h] The Novo Nordisk Foundation Center for Biosustainability, Technical University of Denmark, Kongens Lyngby, Denmark

*corresponding authors
#these authors contributed equally

Abstract

Antagonistic bacterial interactions often rely on antimicrobial bacteriocins, which attack only a narrow range of target bacteria. However, in rapidly changing microbiomes, antimicrobials with broader activity may be advantageous. We report a new type of antimicrobial, epifadin, produced by nasal *Staphylococcus epidermidis*. It has an unprecedented architecture with a non-ribosomally synthesized peptide, a polyketide, and a modified terminal amino acid moiety. Epifadin combines a wide antimicrobial target spectrum with an extraordinarily short life span. It is highly unstable under *in vivo*-like conditions, presumably as a means to limit collateral damage of bacterial mutualists. However, *Staphylococcus aureus* is effectively eliminated by epifadin-producing *S. epidermidis* during co-cultivation *in vitro* and *in vivo* indicating that epifadin-producing commensals could help prevent nasal *S. aureus* carriage. We describe a new microbiome-derived antimicrobial class and suggest that limiting the half-life of an antimicrobial may help to balance its beneficial and detrimental activities.

Introduction:

The microbiomes of human skin and upper airways play crucial roles in human health and predisposition to various diseases. Microbiome compositions govern susceptibility to and severity of chronic diseases such as atopic dermatitis and acne, and microbiomes can include facultative bacterial pathogens such as *Staphylococcus aureus*, which colonizes the anterior nares of ca. 30% of the human population [1-3]. Microbiome dynamics are shaped by both, antagonistic and mutualistic interactions between microbiome members, but the elucidation of underlying molecular mechanisms has remained in its infancy [4].

Staphylococcus epidermidis is the most abundant member of human skin and nasal microbiomes [5,6]. The mechanisms underlying its ecological success have remained largely unclear. *S. epidermidis* can modify its surface glycopolymers to alter its adhesive properties to different host surfaces [7] and it produces phenol-soluble modulin peptides, which modulate inflammatory reactions in skin and epithelia that seem to promote *S. epidermidis* persistence and may impair the fitness of its major competitors [8-10]. Moreover, *S. epidermidis* is a particularly frequent producer of bacteriocins, antibacterial peptides with highly variable structures and activity against potential target species [11-14]. Bacteriocins have traditionally been defined as ribosomally synthesized post-translationally modified peptides (RIPPs), but this term is increasingly used to encompass microbiome-derived small-molecule antibacterial agents including also, for instance, non-ribosomally synthesized peptides (NRPs) [4].

Bacteriocin production is often beneficial but can also cause collateral damage to the producer when other bacteria, which are necessary for the function of mutualistic networks, are also

killed. Moreover, several bacteriocins can damage host cells, leading to inflammation and increased local antimicrobial defense [15,16]. Bacteria can pursue different strategies to limit such bacteriocin-mediated collateral damage. They can use, for instance, bacteriocins with an extremely narrow and specific target range, such as most microcins, which would spare many important mutualists [17,18]. Another strategy relies on contact-dependent bacteriocins such as effectors secreted by type-V-VII secretion systems, which rely on specific interbacterial adhesion mechanisms, sparing mutualistic bacteria that do not physically bind to the bacteriocin producer [19,20]. Theoretically, bacteria could also produce bacteriocins with limited lifetime, precluding their accumulation at a wider distance to the producing micro-colony. The latter strategy would not rely on a high selectivity of the compound for specific competitors, which may be difficult to ensure in a dynamic microbiome context. However, it would ensure that the producer inhibits only bacteria in close proximity but maintains long-distance interaction networks and the integrity of host cells. Such a strategy can only work if community density is relatively low and individual bacteria are not constantly mixed, which is usually the case in skin and anterior nares habitats.

Here we present a novel bacteriocin-like antimicrobial, epifadin, produced by certain *S. epidermidis* strains, that combines an exceptionally wide target range with a very short half-life thereby reflecting an unusual and previously unrecognized antimicrobial strategy. It is the first antimicrobial produced by a common member of the human microbiota that combines moieties synthesized by non-ribosomal peptide synthetases (NRPS) and polyketide synthases (PKS) and it allows *S. epidermidis* to eliminate its competitor *S. aureus* from the same habitat, both *in vitro* and *in vivo*.

Results:

S. epidermidis IVK83 produces a new type of antimicrobial agent.

We previously reported that more than 95% of *S. epidermidis* isolates from the human nose produce antimicrobial molecules with activity against one or several other bacterial skin and nose microbiome members [11]. Whereas most inhibited only a limited number of test bacteria, isolate IVK83 was unique in its capacity to strongly inhibit most of the test strains, including representatives of Firmicutes, Actinobacteria, and γ-Proteobacteria. A transposon mutant library of IVK83 was generated, and a mutant failing to inhibit *S. aureus* USA300 and other test strains was identified. The transposon had disrupted an unknown biosynthetic gene cluster (BGC) operon, composed of ten putative genes, which encompassed about 40 kb on a 55-kb plasmid (Fig. 1a), named pIVK83. The BGC encoded an unusual set of a putative NRPS (EfiA), PKS (EfiB, EfiC, EfiD), and a combined PKS/NRPS (EfiE). An oxidoreductase (EfiO) was

encoded between *efiD* and *efiE*, along with further genes required for NRP synthesis including a phosphopantetheinyl transferase (EfiP) and a thioesterase (EfiT). In addition, two genes encoded the components of a putative ABC transporter, EfiF and EfiG, (Fig. 1). The transposon had disrupted *efiA*, the first gene of the operon. Deleting *efiTP* in IVK83 abrogated antibacterial activity, which was restored by complementation with a plasmid-encoded *efiTP* copy, thereby confirming that the BGC is required for the capacity of IVK83 to inhibit other bacteria (Fig. 1b).

Screening of *S. epidermidis* strain collections identified four additional isolates, from Tübingen, Shanghai (China), and Liverpool (UK), with largely identical antimicrobial activities, plasmids, and BGCs. They belonged to four different multi-locus sequence types (STs), ST575 (IVK83, Tübingen), ST549 and ST615 (additional Tübingen strains), and ST73 (Shanghai and Liverpool). The plasmid with its BGC was absent from all *S. epidermidis* genomes in public sequence databases, but present in two *Staphylococcus saccharolyticus* genomes [21] indicating that it is an infrequent accessory genetic element.

Epifadin is a new, highly unstable, small-molecule antimicrobial agent. Culture filtrates of IVK83 contained antibacterial activity, but initial typical isolation strategies via extraction and chromatography failed. The activity could be enriched by acidic precipitation with hydrochloric acid (pH=2), drying under vacuum, and dissolution in DMSO. However, within a short time, the antimicrobial activity decreased profoundly under standard laboratory conditions, which impeded further purification of the compound, e.g., via chromatography. Systematic variation of incubation conditions revealed rapid loss of antimicrobial activity by storage for instance in aqueous solution, at room temperature, exposure to light, or pH values above 5 (Fig. 2). However, the antibacterial activity remained largely constant when the extract was maintained under acidic conditions, protected from oxygen and light, and stored at –80°C under argon atmosphere with addition of 0.05% of the oxidation inhibitor palmitoyl ascorbate (PA). In an aqueous solution at pH 7, 37°C, and laboratory light exposure, the antimicrobial activity quickly faded and was completely lost after three hours (Fig. 2). In contrast, other microbiome-derived antimicrobial peptides such as lugdunin from *Staphylococcus lugdunensis* [22], gallidermin from *Staphylococcus gallinarum* [23], or nisin A from *Lactococcus lactis* [24], did not lose activity under the same conditions within the six hours observation period.

Reversed-phase high-performance liquid chromatography with ultraviolet light detection (RP-HPLC-UV) of DMSO-PA extracts, obtained from acid-precipitated culture supernatants revealed no obvious difference between the IVK83 wild type and *efiTP* mutant strain at the peptide-bond specific wavelength of 215 nm, although the genes for NRPS pointed to the presence of multiple peptide bonds. However, wild type and mutant differed in a major and in some adjacent minor peaks at 383 nm, indicating the presence of an expanded unsaturated

system with double bonds (Figs. 3a-c). The antimicrobial activity corresponded well to the major 383-nm peak fraction. RP-HPLC coupled with high resolution mass spectrometry (RP-HPLC- HR-MS) revealed a quasi-molecular ion ([M+H]$^+$, *m/z* 964.4472) corresponding to $C_{51}H_{62}N_7O_{12}^+$ (*m/z* 964.4451) and an elementary composition of $C_{51}H_{61}N_7O_{12}$ of the antibacterial agent (Fig. 4a). This formula was unknown in scientific literature, indicating that IVK83 produces a novel compound, which was named epifadin to reflect its origin from *S. epidermidis* and its rapidly fading activity at typical environmental conditions.

Epifadin is a complex natural product with unprecedented structure, synthesized by a combination of NRPS and PKS enzymes. The epifadin BGC was analyzed with antiSMASH 5.0 (bacterial settings) [25], which predicted a three-partite composition with an N-terminal NRP part followed by a polyketide (PK) moiety and a C-terminal single amino acid residue (Fig. 1c). The order of adenylation, condensation, and epimerization domains in the NRPS enzyme EfiA suggested the biosynthesis of a penta-peptide sequence starting with aromatic amino acids, followed by aspartate, asparagine, and an aliphatic amino acid (see Suppl. Information) (Fig. 1c).

Epifadin was repeatedly purified from 100 L IVK83 culture supernatant as outlined above, immediately followed by preparative RP-HPLC in the dark and collecting the eluate at -77°C under inert argon gas, finally yielding 6 mg of the transiently intact pure compound. RP-HPLC-HR-MS confirmed the fast degradation of epifadin under regular laboratory conditions within a few hours. A peptide amide Phe-Phe-Asp-Asn-NH$_2$ with the neutral sum formula $C_{26}H_{32}N_6O_7$ ([M+H]$^+$, *m/z* 541.2422, in accordance with $C_{26}H_{33}N_6O_7^+$ (*m/z* 541.2405)), represented a dominant decomposition fragment, likely resulting from spontaneous, distinct chemical decomposition at the originally fifth amino acid (Extended Data Fig. 1a). Since this fragment was not accessible to common Marfey`s analysis, for the assignment of the D-, L-configuration of the phenylalanine moieties, we synthesized L-Phe-D-Phe-L-Asp-D-Asn-NH$_2$ (FfDn-NH$_2$). Synthetic FfDn-NH$_2$ showed identical physicochemical properties in RP-HPLC-UV, and MS/MS analysis compared to the natural tetrapeptide amide fragment of epifadin (Extended Data Fig. 1). The L-D-L-D-amino acid configuration of the peptide amide was also supported by antiSMASH prediction. Nuclear magnetic resonance (NMR) spectroscopy of the pure tetrapeptide amide confirmed the sequence, which lacked antimicrobial activity (see Suppl. Information, Extended Data Fig. 2). Additionally, multidimensional NMR experiments of purified, intact epifadin provided evidence that the fifth amino acid is a modified alanine (Extended Data Fig. 3,4a) with a carbon double bond (-NH-C(CH$_3$)=C) instead of the C-terminal carbonyl group (-NH-CH(CH$_3$)-C=O).

Two-dimensional NMR (Extended Data Fig. 3) revealed the direct linkage of the decarbonylated pentapeptide to a polyene structure, with a tetraene at C_α of the original alanine unit, linked to a saturated methylene unit, overall building an octaketide bridge ($C_{16}H_{20}$), which is presumably formed by the trans-acetyltransferase (AT) type PKS modules of EfiC, EfiD, and EfiE (Fig. 1c,d and Extended Data Fig. 4a). Detailed structure elucidation of the polyene part was achieved by sets of two-dimensional NMR yielding additional spatial information, despite limitations due to the instability of epifadin.

The NRPS domain of EfiE was predicted to link an aspartate as the sixth amino acid to the hydrophobic PK chain of epifadin and was suggested to allow for further modification, a terminal cyclization (Fig. 1c). HR-MS (MS/MS) analyses of epifadin combined with the predicted enzymatic properties of EfiE underline the Dieckmann-like cyclization of the terminal amino acid to form a tetramic acid as structural feature of epifadin (Suppl. Information). Distinct signals from ^{13}C-NMR spectroscopy and MS analyses yielded a characteristic signal pattern for the deduced tetramic acid moiety with well-assigned fragment ions (e.g., [M+H]$^+$, m/z 158.0454, assigned to $C_6H_8NO_4^+$ (m/z 158.0448); [M+H]$^+$, m/z 140.0348, for a $C_6H_6NO_3^+$ moiety (m/z 140.0342) (Fig. 4a; Extended Data Fig.5; Supplementary Table S1). The tetramic acid moiety is further supported by the predicted adenylation domain specificity of A_5 (Asp) and the presence of a C-terminal condensation domain in EfiE. A similar cyclization mechanism was proposed for malonomycin [26] and fungal PKS-NRPS derived products such as cAATrp [27].

Remarkably, none of the epifadin PKS contains a cognate AT domain. The single, discrete acyltransferase (EfiB) presumably loads the extender units to the acylcarrier protein (ACP) domains of EfiCDE. Since only three PKS modules are responsible for incorporation of nine malonyl-CoA building blocks, epifadin biosynthesis seems to involve an iterative trans-AT PKS system for the generation of the polyene moiety. To the best of our knowledge, such an iterative trans-AT PKS system has been described only once, for biosynthesis of the macrocyclic chejuenolide [28].

The provided results represent strong evidence for the given epifadin structure (Fig. 1c, 4b), which combines all results from HPLC-UV coupled with high-resolution MS, yielding sum formulae, fragmentation patterns, and UV spectrum (Fig. 3,4; Extended Data Fig. 1,5,6,9; Supplementary Table S1); from multidimensional NMR analyses of full epifadin and synthetic epifadin fragments with spatial elucidations (Extended Data Fig. 3,4a); and from sequence-based prediction of EfiA-P enzyme reactions (Fig. 1c, Suppl. Information). Moreover, we will focus on a chemical total synthesis to elucidate more structural details of the C_6H_{10} bridge in the polyene moiety, which will require further efforts though and remains challenging because of the extraordinary instability of epifadin. By all means, we demonstrate that epifadin is the

first NRP/PK antimicrobial isolated from the human microbiome and the founding member of a new structural class of peptide-polyene-tetramic acids.

Epifadin is a potent, broad-spectrum, bactericidal antimicrobial. A large panel of microorganisms from human nasal microbiomes was analyzed for susceptibility to epifadin by monitoring inhibition zones around the epifadin producer IVK83. Epifadin activity was tested also against selected bacterial isolates with the limited amounts of purified, non-decomposed epifadin in the dark to sustain the stability of epifadin. Most of the tested Firmicutes (several *Staphylococcus* species, *Streptococcus pyogenes*) and Actinobacteria (several *Corynebacterium* species, *Cutibacterium acnes*, *Micrococcus luteus*, *Kocuria* spec.) were susceptible albeit with some intra-species variability (Fig. 5a). Notably, all tested *S. aureus* strains were susceptible to epifadin, whereas 9 of 16 tested nasal *S. epidermidis* isolates were resistant. Most of the tested γ-Proteobacteria were resistant but *Raoultella ornithinolytica* was inhibited. Since the antifungal agents amphotericin A, a natural derivative of amphotericin B, and nystatin A_1 contain similar polyene moieties as epifadin [29], *S. epidermidis* IVK83 was also tested for its impact on *Candida albicans* and *Saccharomyces cerevisiae*. Both fungal species were inhibited by the wild-type strain (Fig. 5a) but not by the isogenic mutant Δ*efiTP*. Thus, epifadin has a very broad activity spectrum including Gram-positive and some Gram-negative bacteria and yeasts.

Epifadin turned out to be a potent inhibitor of *S. aureus* with MIC values between 0.9 and 1.5 μg/mL (Fig. 5b). Interestingly, among all the tested *Staphylococcus* species, epifadin was most active against *S. aureus* and had significantly higher MIC values between 3.7 and 8.6 μg/mL even for susceptible strains of *S. epidermidis*, *Staphylococcus hominis*, *Staphylococcus sciuri* (now *Mammaliicoccus sciuri*), and *Staphylococcus warneri*. Purified epifadin was bactericidal - a tenfold MIC reduced the number of viable *S. aureus* cells by three orders of magnitude within four hours of incubation (Extended Data Fig. 7a). Epifadin targets a cellular mechanism or structure that can also be essential in fungal cells. In contrast, epifadin impaired human HeLa cells only at ca. 20-fold MIC (Extended Data Fig. 7b), suggesting the lack of major cytotoxic potential for human cells.

Epifadin allows *S. epidermidis* to eliminate *S. aureus* during *in vitro* and *in vivo* co-cultivation. The particularly strong, bactericidal activity of epifadin against *S. aureus* raised the question if epifadin can help *S. epidermidis* to outcompete *S. aureus*. The mutant *S. epidermidis* Δ*efiTP* was overgrown by *S. aureus* during co-cultivation on agar plates or in liquid broth within 24 hours (Fig. 6a,b, Extended Data Fig. 8), which is in agreement with the

previously documented capacity of *S. aureus* to grow faster or utilize nutrients better than *S. epidermidis* [30]. In contrast, the IVK83 wild type eradicated *S. aureus* within 24 hours, indicating that epifadin was effective enough under the used conditions to confer a significant fitness advantage over *S. aureus*. *S. aureus* had almost completely vanished after 24 hours, underlining the bactericidal activity of epifadin. Complementation of the mutant with a plasmid-encoded copy of *efiTP* restored the *S. aureus*-eradicating ability of IVK83 Δ*efiTP*, confirming that it is indeed epifadin that allowed *S. epidermidis* to outcompete *S. aureus* (Fig. 6c, Extended Data Fig. 8).

The ability of epifadin to promote the competitive capacity of *S. epidermidis in vivo* was analyzed in the cotton rat-based model of nasal colonization[31]. The IVK83 wild type and Δ*efiTP* strains were similarly proficient in nasal colonization (Fig. 6d). When either the IVK83 wild type or the *efiTP* mutant were instilled into the noses together with equal numbers of *S. aureus* Newman, the number of viable *S. aureus* cells was significantly reduced after five days with the IVK83 wild type-colonized compared to the Δ*efiTP*-colonized animals (Fig. 6e), indicating that epifadin-producing *S. epidermidis* can effectively interfere with *S. aureus* nasal colonization.

Discussion

Recent metagenome- and cultivation-dependent screening approaches have revealed an increasing number of BGCs for complex natural products among bacteria from microbiomes [32,33]. These include several NRP compounds such as lugdunin [22] and PK compounds such as wexrubicin [33]. We here report epifadin, the first example of an antimicrobial peptide-polyene consisting of both, NRP and PK moieties produced by a common member of the human microbiome. Epifadin is the founding member of a new compound class. Previously, hybrid NRP/PK molecules have been associated predominantly with environmental or soil bacteria. Our study further supports the notion that the antibacterial compounds produced by environmental and host-associated bacterial communities rely on equally unique and complex chemical architectures [34].

Epifadin is an amphiphilic, charged compound with an unprecedented alternation of a polar peptide, a non-polar polyene, and, again, a polar and charged amino acid-derived building block. Its antimicrobial mechanism remains to be elucidated in the future, but the molecular target appears to be shared by bacterial and fungal cells. It also remains unclear why only fungal but not human HeLa cells were affected by epifadin. The extraordinary instability of epifadin may cause a higher impact on cells that take the compound up quickly, while slow uptake may spare cells due to the rapid loss of structural integrity. The types of immunity (or

self-protection) proteins encoded in a BGC can help to propose the mode of action of a new antibiotic. However, the epifadin BGC encodes only the two ABC transporter components EfiFG as potential resistance proteins, which may act as drug exporters and do not shed light on the antibacterial target.

The high instability remains challenging for future studies with epifadin congeners. While the full epifadin molecule may persist refractory to NMR analysis due to the labile enamide moiety, chemical synthesis of epifadin analogues, and comparison of chromatographic, spectroscopic, and antimicrobial properties with those of native epifadin may confirm structural details and provide molecular knowledge of the mechanism of antimicrobial action. However, this will be a long-term endeavor with strategies needed for chemical synthesis of the complex and unstable enamide polyene tetramic acid in epifadin. Such a proof of structure - only by chemical synthesis - of a fungal propargyl tetramic acid natural product has been exemplified recently [35].

Previous approaches for the isolation of new microbiome-derived bacteriocins and related compounds focused on stable compounds, which are comparable easy to purify and to characterize [4]. Short-lived antimicrobial compounds may have been overlooked in many of these studies and purification attempts may have remained unsuccessful. The *Bacillus* antimicrobial bacillaene, for instance, is also highly unstable because of its polyene-enamide structure [36]. At first thought, it may seem paradox and a waste of energy for a bacterium to produce an antimicrobial with such a short lifespan. However, limited stability may help to minimize collateral damage of bacterial mutualists and host cells. Mounting evidence indicates that bacterial interactions in complex communities are not only shaped by antagonistic but also by multifactorial mutualistic interdependencies [37]. Bacterial life on mammalian skin and in the nares is challenging because nutrient supply is poor and many of the important cofactors and building blocks need to be released from larger polymers or synthesized *de-novo* [30,38]. All these constraints require that bacteria use antagonistic mechanisms with great care. Other strategies than using short-lived antimicrobials may be equally costly but even less effective. For instance, bacteriocins with a very narrow target spectrum may work only in a community with defined and stable composition while its transfer to other, even slightly different microbiomes may easily lead to loss of a competitive advantage. Likewise, contact-dependent bacteriocin delivery requires a huge and complex secretion machinery, which are also costly to synthesize and maintain [39]. A short-lived but broad-spectrum antimicrobial such as epifadin may be much more versatile and advantageous in microbiomes with limited physical proximity between antimicrobial producer and potential target bacteria. Such low bacterial densities and large spatial separation of individual bacterial microcolonies can be found for instance on human skin and upper airways. It should be noted that the human antimicrobial host defense also

relies on short-lived compounds, reactive oxygen and nitrogen derivatives, with broad toxicity to microbial and even host cells [40]. If produced at the right place and the right time, the beneficial consequences of such compounds outweigh the detrimental effects. It remains to be analyzed under which conditions epifadin is produced by *S. epidermidis* as the BGC does not encode a potential regulator (Fig. 1A).

The epifadin BGC is located on a conjugative plasmid, which probably disseminates horizontally because it was found in different *S. epidermidis* clonal lineages and in *S. saccharolyticus* isolates [21]. The fact that we found epifadin produced by *S. epidermidis* isolates from three different geographical regions underscores its evolutionary success and fitness benefit. Related gene clusters have also been found in *Lactococcus lactis* [41] and *Streptococcus mutans* [42]. However, antimicrobial activities have not been reported for these strains. Moreover, these two BGCs lack EfiO and the gene order is different from the epifadin BGC suggesting that the product is not identical to epifadin.

Epifadin-producing *S. epidermidis* IVK83 had a strong capacity to eliminate the opportunistic pathogen *S. aureus* in experimental nasal colonization studies similar to the recently reported *S. lugdunensis* strain IVK28 producing lugdunin [22]. Although epifadin is too unstable in its native form to be considered as a new drug, epifadin-producing commensal bacteria could be used as probiotics that would eliminate *S. aureus* from the nares of at-risk patients. The search for fugacious bacteriocins should be extended to other microbes to identify further previously overlooked, short-lived antimicrobials, which could hold promise for the eradication of facultative pathogens in human microbiomes.

Materials and Methods

Bacterial strains and growth conditions. The bacterial strains used in this study are listed in Supplementary Table S2. Tryptic soy broth (TSB) and tryptic soy agar (TSA) or basic medium (BM: 1% soy peptone, 0.5% yeast extract, 0.5% NaCl, 0.1% glucose and 0.1% K_2HPO_4, pH 7.2) and BM agar (BM with 1.5% agar) were used for bacterial cultivation. For corynebacteria, 5% sheep blood (Oxoid) was added. Cutibacteria were incubated under anaerobic conditions using an anaerobic jar including an AnaeroGen™ bag (Thermo Fisher Scientific). When appropriate, antibiotics were used at concentrations of 250 µg/mL for streptomycin, 10 µg/mL chloramphenicol, 100 µg/mL ampicillin or 2.5 µg/mL erythromycin. All media were prepared with water purified by a VEOLIA PureLab Chorus2 water purification system.

Antimicrobial spectrum of IVK83. The antimicrobial activity of *S. epidermidis* IVK83 was assessed by spotting *S. epidermidis* IVK83 on TSA agar plates containing lawns of the

bacterial test strains listed in Supplementary Table S2. To this end, the test strains from fresh agar plates were resuspended in phosphate-buffered saline (PBS, Gibco), adjusted to an OD_{600} of 0.5 and streaked out evenly on TSA or TSA + blood plates with a cotton swab. *S. epidermidis* IVK83 grown on TSA was resuspended in PBS, adjusted to an OD_{600} of 1, and 10 µl were spotted on the bacterial lawn. Plates were incubated for 24 h to 48 h at 37°C, anaerobic bacteria were grown under anaerobic conditions as above, and diameters of inhibition zones were measured.

Transposon mutagenesis for the identification of the epifadin BGC. Identification of the epifadin BGC was performed via transposon mutagenesis as described earlier [43]. Briefly, *S. epidermidis* IVK83 was transformed with vector pTV1ts [44,45] containing the transposon Tn917 with an erythromycin resistance gene (*ermB*). After growing in TSB supplemented with 10 µg/mL chloramphenicol at 30°C overnight, the culture was diluted (1:1000) in TSB containing 2.5 µg/mL erythromycin, and cultivated at 42°C overnight. This step was repeated once more with 2.5 µg/mL erythromycin and once without erythromycin and the cells were subsequently plated on TSA containing 2.5 µg/mL erythromycin. Erythromycin-resistant but chloramphenicol-sensitive mutants, which probably had *Tn*917 integrated and the plasmid lost, were screened for loss of antimicrobial activity against *S. aureus*. The insertion sites were identified by sequencing upstream and downstream-flanking regions of the transposon of genomic DNA isolated from non-inhibiting clones with primers Tn917 up and Ptn2 down.

Whole-genome analysis of *S. epidermidis* IVK83. Whole-genome sequence of *S. epidermidis* IVK83 was determined by Illumina short-read and PacBio long-read sequencing. Illumina reads were *de-novo* assembled by velvet (version 1.2.10) [46], and *S. epidermidis* IVK83 was also sequenced using the PacBio Sequel platform. SMRTbell libraries were constructed using standard procedures (Pacific Biosciences) and the genome was *de-novo* assembled using the Hierarchical Genome Assembly Process (HGAP4) workflow in SMRT Link (v.5.1.0.26411; Pacific Biosciences). Alignment of the two *de-novo* assemblies with MAUVE [47] (version 2.4.0) and subsequent manual curation allowed us to generate the final genome, which was confirmed by mapping the Illumina reads to the final assembly. The circular chromosome and the plasmid were annotated using the NCBI Prokaryotic Genome Annotation Pipeline (version 5.3) and deposited at NCBI.

Construction of an epifadin production-deficient mutant and complementation. In order to generate a production-deficient mutant of *S. epidermidis* IVK83, the thermosensitive plasmid pBASE6 [48] and the primers listed in Supplementary Tables S3 and S4 were used. For its construction, DNA fragments up- and downstream of the genes *efiP* (phosphopantetheinyl-transferase) and *efiT* (thioesterase) were amplified by PCR using primers 83 KO Acc65I with 83 KO EcoRI, and 83 KO BssHII with 83 KO SalI, respectively. After digestion of the upstream

fragment with restriction enzymes EcoRI/Acc65I (Thermo) and of the downstream fragment with BssHII/SalI (Thermo), the two fragments and the Acc65I-BssHII-digested erythromycin resistance cassette from plasmid pEC2 [49] were ligated into the EcoRI/SalI-digested vector pBASE6. The resulting plasmid pBASE6_KO83 was cloned in *E. coli* DC10B, isolated, and used to transform IVK83. Homologous recombination was monitored according to established procedures [48] resulting in the epifadin-deficient mutant IVK83 Δ*efiTP*.

For mutant complementation, the genes Δ*efiTP* were amplified by PCR using primers 83 compl BamHI and 83 compl EcoRI. After digestion with BamHI/EcoRI (Thermo), the DNA fragment was ligated into BamHI/EcoRI-digested pRB474 [50]. After transformation and amplification of the resulting vector pRB474-83compl *in E. coli* DC10B, the vector was used to transform the epifadin-deficient IVK83 Δ*efiTP* and clones were screened for antimicrobial activity against *S. aureus*.

Purification of epifadin. All steps of the purification process were performed under reduced light exposure. An overnight culture of IVK83 in TSB was used to inoculate fresh TSB 1:1,000, which was incubated for 4 h at 37°C and constant shaking at 160 rpm to obtain bacteria in exponential growth phase. Subsequently, fresh TSB containing 5 g/L glucose was inoculated with an OD_{600} of 0.00125 of IVK83 and incubated for 44 h at 30°C with constant shaking at 160 rpm. Cultures were centrifuged and the supernatant adjusted to pH 2 using 37% HCl (Thermo Fisher Scientific) for 2 h at 4°C. The acidified supernatants were centrifuged at 8,000 x g for 15 min at 4°C, the clear supernatant was discarded, and the obtained precipitate was resuspended in small volumes of deionized water and frozen at –80°C. The precipitate was lyophilized at –20°C and 1 mbar until water was completely removed. DMSO (Merck) supplemented with 0.05% palmitoyl ascorbate (PA) was added 20:1 (mL vol/g weight) to the precipitate to extract the active compound from the insoluble particles of the precipitate. After gentle vortexing and centrifugation, the DMSO supernatant was transferred to a new vial. Extraction of the precipitate was repeated once more. DMSO extracts were combined, lyophilized, and the dry extract resuspended in a 1:2 mixture of system A buffer (99.95% H_2O, 0.05% trifluoroacetic acid (TFA)) and system B buffer (80% acetonitrile (Baker), 19.95% H_2O, 0.05% TFA). Subsequently, the solution was injected to a preparative, RP-HPLC column (Kromasil 100 C18, 7 μm, 250x4 mm, Dr. Maisch GmbH) and HPLC was performed with a gradient ranging from 50% system B to 100% system B within 30 min at 383 nm (diode-array detector). The product-containing fractions were collected at –77°C (dry ice isopropyl alcohol cooling bath) under argon atmosphere, lyophilized, and stored at –80°C until further use.

Stability analysis of epifadin. The effect of different incubation conditions on the bioactivity of epifadin was analyzed by agar diffusion assays on lawns of the sensitive indicator strain *S. aureus* USA300 LAC. To this end, liquid TSA was inoculated with an overnight culture of

USA300 at an OD_{600} of 0.00125. After solidification of the agar, a cork borer was used to punch wells into the agar with 5 mm diameter. TSB media with 50 mM sodium citrate (pH 5 and 6) or 50 mM tris(hydroxymethyl)aminomethane (pH 8 and 9) were prepared. Epifadin-containing precipitate was dissolved in DMSO (12 mg/mL) and insoluble particles were removed by centrifugation. The supernatant was added to the prepared TSB media at a final concentration of 750 µg precipitate per mL. (37.5 µg in 50 µL). Media were incubated for six hours at 21°C, 30°C, or 37°C with or without laboratory light exposure, and constant shaking at 500 rpm in a thermomixer (Eppendorf). As controls, 70 µg/mL (3.5 µg in 50 µl) lugdunin, 24 µg/mL (1.2 µg in 50 µL) gallidermin, and 100 µg/mL (5 µg in 50 µL) nisin were used. At different time points, 50 µl of each sample were pipetted into the wells of the agar plates. After incubation at 37°C overnight, zones of inhibition were analyzed with ImageJ software (version 1.8.0_112).

Analysis of epifadin by HPLC-UV-HR-MS. Mass spectra were recorded on a HPLC-UV-HR-MS (MaXis4G with Performance Upgrade kit with ESI-Interface, Bruker Daltonics) with time-of-flight (TOF) detection. In order to obtain HR-MS data, DMSO extracts were lyophilized, resuspended in an acetonitrile-water mixture (1:1), and applied to a Dionex Ultimate 3000 HPLC system (Thermo Fisher Scientific), coupled to the MaXis 4G ESI-QTOF mass spectrometer (Bruker Daltonics). The ESI source was operated in ESI (+) mode at a nebulizer pressure of 2.0 bar, and dry gas was set to 8.0 L·min^{-1} at 200°C. MS/MS spectra were recorded in auto-MS/MS mode with collision energy stepping enabled. Sodium formiate was used as internal calibrant in each analysis. The routine gradient was from 90% deionized H_2O and 10% methanol with 0.1% formic acid to 100% methanol with 0.1% formic acid in 20 min with a flow rate of 0.3 mL/min on a Nucleoshell® EC RP-C_{18} (150 x 2 mm, 2.7µm) from Macherey-Nagel.

NMR spectroscopy. ^{1}H-NMR was performed on Bruker AMX-600 (600 MHz) and Bruker AvanceIII-700 (700 MHz) instruments. Chemical shifts were monitored as δ-values (ppm) relative to the solvent DMSO-d_6 as internal standard. Coupling constants (*J*) were monitored in Hertz (Hz). Abbreviations for multiplicity description are as follows: s: singlet, d: duplet, dd: duplet of a duplet, m: multiplet. ^{13}C-NMR was performed on a Bruker AMX-600 (150.3 MHz) and Bruker AvanceIII-700 (176.1 MHz) instrument. Chemical shifts were monitored as δ-values (ppm) relative to the solvent DMSO-d_6 as internal standard. Homonuclear correlation experiments are based on ^{1}H-^{1}H-Rotating Frame Overhauser Effect Spectroscopy (ROESY).

Chemical solid-phase peptide synthesis (SPPS) of FfDn-NH$_2$. Fmoc-D-Asn(Trt) resin (loading: 0.23 mmol·g^{-1}, 150 mg, 34.5 µmol scale, TG S RAM, Rapp Polymere) was swollen in 2 mL dimethylformamide (DMF) for 30 min. The Fmoc group was removed by treatment with a solution of 2% DBU/10% morpholine (v/v) in DMF (2 mL) for 3 min and additional 12 min. The resin-bound residue was submitted to iterative peptide assembly (Fmoc-SPPS) using 2%

DBU/10% morpholine (v/v) in DMF (2 mL, 3 + 12 min) for Fmoc-deprotection and Fmoc-D/L-AA$_x$-OH (Fmoc-D-Asp(O*t*Bu)-OH, Fmoc-D-Phe-OH and Fmoc-L-Phe-OH) (6 equiv.), HATU (6 equiv.), HOBt (6 equiv.) and NMM (8 equiv.) in DMF (2 mL) for 45 min to couple each amino acid. After full assembly of linear peptide amide on the solid-support, the resin was washed with DMF (3 x 2 mL), DCM (3 x 2 mL), toluene (3 x 2 mL), IPA (3 x 2 mL), diethylether (Et$_2$O) (3 x 2 mL) and dried under reduced pressure for 3 h. The peptide was cleaved by treatment with TFA/TIPS/H$_2$O (95:5:5 v/v/v, 2 mL) for 3 x 1 h and one washing step with TFA (2 mL) for 10 min. The solvents were removed under reduced pressure, the residue was washed with Et$_2$O (3 x 2 mL) and centrifuged. The pale orange precipitate was lyophilized using *tert*-butanol/water (1:1 v/v, 10 mL).

Acetylation of the tetra-peptide amide via chemical reaction with epifadin extract. To 10 mg precipitate of IVK83 wild type culture supernatant 200 µL 50 mM ammonium bicarbonate and 500 µL acetylation reagent (25% acetic acid anhydride in methanol) were added and stirred at room temperature for one hour. 100 µL of the reaction solution were taken, lyophilized, and dissolved in 50 µL methanol (LC MS grade) for HPLC-MS analytics.

Esterification of the tetra-peptide amide via chemical reaction of epifadin extract with methanol. To 10 mg precipitate of IVK83 wild type culture supernatant, 1 mL methanol and a droplet of sulfuric acid were added and stirred at room temperature overnight. After centrifugation of the reaction solution 100 µL were taken for HPLC-MS analytics.

Determination of the inhibitory concentration (IC) of epifadin. Due to the low stability of epifadin under standard culture conditions and resulting low yields after purification, minimal inhibitory concentration (MIC) determination via standardized laboratory approaches such as microdilution or standard agar dilution was not feasible. Instead, a miniaturized assay was developed. Molten TSA, kept below 42°C, was inoculated with different test strains at an OD$_{600}$ of 0.00125. 17.5 mL were poured into petri dishes, resulting in agar layers of ~3.16 mm thickness. After solidification, a cork borer was used to punch wells of 4-mm diameter into the agar. 35 µl of purified epifadin in DMSO-PA (2.4 µg, 1.2 µg, 0.6 µg, 0.3 µg, 0.15 µg and 0.075 µg) were pipetted into the wells and agar plates were incubated for 24 h at 37°C in the dark. Diameters of the zones of inhibition were measured and the volume containing the inhibitory epifadin concentration was calculated, using the following formula for cylinder volume:

$$V_c = \pi \ x \ r^2 \ x \ h \qquad V_c = \text{cylinder volume}$$

$$V_i = (\pi r_z^2 x \ h_a) - (\pi r_w^2 x h_a) \qquad V_i = \text{inhibited volume}$$

r_z^2 = radius (diameter/2) zone of inhibition

r_w^2 = radius (diameter/2) of well

h_a = height of agar

The volume of agar showing inhibition of the test strain was then correlated with the included amount of epifadin, and the epifadin concentration necessary to inhibit test strain growth in a 1-mL volume was calculated to yield IC values. If e.g., 2.4 µg of epifadin lead to an inhibited volume of 480 µl, in order to inhibit a volume of 1 mL, 5 µg epifadin is needed, which corresponds to an IC of 5 µg/mL. These calculations were conducted for the lowest amount of epifadin that led to a zone of inhibition to minimize the necessary epifadin amounts and the calculation error due to the gradient within the inhibition zone. As a control, the same assay was used to determine the IC for vancomycin and daptomycin under these conditions.

Minimal bactericidal concentration determination (MBC). Fresh TSB was inoculated 1:1,000 with an overnight culture of *S. aureus* USA300 LAC and incubated for 4 h at 37°C and constant shaking at 160 rpm. Bacteria were centrifuged and washed once with PBS. Subsequently, cells were resuspended in PBS to an OD_{600} 0.00125 (1 x 10^6 CFU/mL) and different concentrations of purified epifadin in DMSO-PA were added. Bacteria were incubated for 4 h at 37°C and shaking in the dark (500 rpm, thermomixer). Every 30 min, samples were taken and serial dilutions were plated on TSA. After 24 h incubation at 37°C, CFUs were counted.

***In vitro* competition assay.** *S. epidermidis* IVK83 wild type, *S. epidermidis* IVK83 Δ*efiTP*, *S. epidermidis* IVK83 Δ*efiTP* pRB474-83compl, and a streptomycin-resistant *S. aureus* Newman strain were grown overnight in TSB at 37°C and constant shaking at 160 rpm. The bacteria were washed once with TSB and adjusted to 5 x 10^8 CFU/mL in TSB. For liquid culture-based competition, 10 mL of *S. aureus* and 10 mL *S. epidermidis* suspension were mixed in shaking flasks and incubated at 37°C and constant shaking at 160 rpm. After 24 h of incubation, fresh TSB was inoculated to an OD_{600} 0.5 with the previous culture (to ensure nutrient availability for antimicrobial production by IVK83) and further incubated at 37°C; this procedure was repeated twice. Samples were taken at 0 h, 24 h, 48 h, and 72 h and serial dilutions were plated on TSA and TSA supplemented with streptomycin for *S. aureus* Newman selection. After overnight incubation at 37°C, CFUs were counted, and bacterial ratios were calculated.

For agar-based competition, overnight cultures of *S. aureus* and *S. epidermidis* were washed once with PBS and adjusted to 1 x 10^8 CFU/mL in PBS. 500 µL of *S. aureus* and 500 µl of *S. epidermidis* were mixed and 3 x 20 µL drops were spotted on TSA and incubated at 37°C. After 24 h incubation, grown bacterial cells were scraped off from the three spots, individually resuspended in PBS, and adjusted to an OD_{600} 0.5 in 1 mL PBS, from which again 3 x 20 µl were spotted on fresh TSA and incubated at 37°C; this procedure was repeated twice. Samples of bacteria were taken at 0 h, 24 h, 48 h and 72 h, resuspended, and serial dilutions were plated on TSA and TSA supplemented with streptomycin. After overnight incubation at 37°C, CFUs were counted, and bacterial ratios were calculated.

Animal models and ethics statement. All animal experiments were conducted in strict accordance with the German regulations of the Gesellschaft für Versuchstierkunde/Society for Laboratory Animal Science (GV-SOLAS) and the European Health Law of the Federation of Laboratory Animal Science Associations (FELASA) in accordance with German laws after approval by the local authorities (IMIT 1/15, Regierungspräsidium Tübingen). Animal studies were carried out at the University Tübingen and conformed to institutional animal care and use policies. No randomization or blinding was necessary for the animal colonization model, and no samples were excluded. Animal studies were performed with cotton rats of both genders, 8–12 weeks old, respectively.

Colonization and co-colonization of cotton rat noses. Spontaneously streptomycin-resistant *S. epidermidis* IVK83 and *S. epidermidis* IVK83 Δ*efiTP* mutants were generated by incubating and passaging those strains on TSA supplemented with 250 μg/mL streptomycin. For co-colonization of cotton rat noses, these strains and streptomycin-resistant *S. aureus* Newman were used. The cotton rat colonization model has been described previously [31]. In previous experiments, Zipperer et al. have shown that an inoculum of 1×10^7 CFU/nose are required to achieve stable colonization of $1 \times 10^3 – 1 \times 10^4$ CFU/nose for *S. aureus* Newman, while other staphylococcal species such as *S. lugdunensis* may require a higher inoculum [22]. Since the capability of *S. epidermidis* IVK83 and *S. epidermidis* IVK83 Δ*efiTP* to colonize cotton rat noses were unknown, the inoculum required to achieve stable colonization was determined first. In brief, overnight cultures were washed twice in PBS and inocula were adjusted to 1×10^8 CFU/10 μl. Subsequently, cotton rats were anaesthetized with isoflurane and instilled intranasally with 1×10^8 CFU/nose. After 5 days, the cotton rats were euthanized, and the noses were removed and covered in 1 mL PBS. After heavy vortexing for 30 s, dilutions of the samples were plated on BM agar supplemented with 250 μg/mL streptomycin and incubated overnight at 37°C to obtain CFU/nose. Whereas an inoculum of 1×10^7 CFU/nose is sufficient for *S. aureus* Newman to establish colonization, *S. epidermidis* IVK83 and IVK83 Δ*efiTP* had to be instilled with 1×10^8 CFU/nose to obtain comparable colonization levels. Based on these parameters, co-colonization was performed with tenfold increased inoculum for IVK83 and IVK83 Δ*efiTP*.

For co-colonization experiments, cotton rats were instilled intranasally with a mixture of 1×10^7 CFU/nose of *S. aureus* Newman and either 1×10^8 CFU/nose IVK83 or IVK83 Δ*efiTP*. 5 days after instillation, bacteria were extracted from cotton rat noses as described above and the bacterial ratio was calculated; *S. aureus* (yellow) and *S. epidermidis* (white) were distinguished by color and colony size.

Cytotoxicity assay in HeLa cells. The human cervical carcinoma HeLa cell line was cultivated in RPMI cell culture medium (Thermo Fisher Scientific) supplemented with 10% fetal bovine serum (Thermo Fisher Scientific) at 37°C, 5% CO_2, and 95% relative humidity. A two-

fold serial dilution of epifadin in RPMI was prepared in a microtiter plate and trypsinized HeLa cells were added at a final cell concentration of 1 x 10^4 per well. After 24 h incubation, 7-hydroxy-3H-phenoxazin-3-one-10-oxide (resazurin) was added at a final concentration of 200 μM and cells were again incubated for 24 h. Cell viability was evaluated by determining the reduction of resazurin to the fluorescent resorufin (λex 560 nm, λem 600 nm) in relation to an untreated control in a TECAN Infinite M200. Cycloheximide served as a positive control.

Reporting Summary. Further information on research design is available in the Nature Research Reporting Summary linked to this article.

Data availability. WGS data obtained for *S. epidermidis* IVK83 were deposited in the NCBI Sequence Read Archive (genome available under accession number CP088002, plasmid pIVK83 under CP088003). Sequence of strain *S. epidermidis* B155 (Liverpool, UK) was deposited as BioSample SAMEA12384066 (BioProject PRJEB50307). Additional information can be obtained from the corresponding authors upon reasonable request.

References

1   Paller, A. S. *et al.* The microbiome in patients with atopic dermatitis. *J Allergy Clin Immunol* **143**, 26-35, doi:10.1016/j.jaci.2018.11.015 (2019).
2   Totté, J. E. *et al.* Prevalence and odds of Staphylococcus aureus carriage in atopic dermatitis: a systematic review and meta-analysis. *Br J Dermatol* **175**, 687-695, doi:10.1111/bjd.14566 (2016).
3   Lee, Y. B., Byun, E. J. & Kim, H. S. Potential Role of the Microbiome in Acne: A Comprehensive Review. *J Clin Med* **8**, 987, doi:10.3390/jcm8070987 (2019).
4   Heilbronner, S., Krismer, B., Brotz-Oesterhelt, H. & Peschel, A. The microbiome-shaping roles of bacteriocins. *Nat Rev Microbiol*, doi:10.1038/s41579-021-00569-w (2021).
5   Kloos, W. E. & Musselwhite, M. S. Distribution and persistence of Staphylococcus and Micrococcus species and other aerobic bacteria on human skin. *Appl Microbiol* **30**, 381-385 (1975).
6   Coates, R., Moran, J. & Horsburgh, M. J. Staphylococci: colonizers and pathogens of human skin. *Future Microbiol* **9**, 75-91, doi:10.2217/fmb.13.145 (2014).
7   Du, X. *et al.* Staphylococcus epidermidis clones express Staphylococcus aureus-type wall teichoic acid to shift from a commensal to pathogen lifestyle. *Nat Microbiol* **6**, 757-768, doi:10.1038/s41564-021-00913-z (2021).
8   Cogen, A. L. *et al.* Staphylococcus epidermidis antimicrobial delta-toxin (phenol-soluble modulin-gamma) cooperates with host antimicrobial peptides to kill group A Streptococcus. *PLoS One* **5**, e8557, doi:10.1371/journal.pone.0008557 (2010).
9   Cogen, A. L. *et al.* Selective Antimicrobial Action Is Provided by Phenol-Soluble Modulins Derived from Staphylococcus epidermidis, a Normal Resident of the Skin. *Journal of Investigative Dermatology* **130**, 192-200, doi:https://doi.org/10.1038/jid.2009.243 (2010).
10   Otto, M. Phenol-soluble modulins. *Int J Med Microbiol* **304**, 164-169, doi:10.1016/j.ijmm.2013.11.019 (2014).
11   Janek, D., Zipperer, A., Kulik, A., Krismer, B. & Peschel, A. High Frequency and Diversity of Antimicrobial Activities Produced by Nasal Staphylococcus Strains against Bacterial Competitors. *PLoS Pathog* **12**, e1005812, doi:10.1371/journal.ppat.1005812 (2016).
12   O'Sullivan, J. N., Rea, M. C., O'Connor, P. M., Hill, C. & Ross, R. P. Human skin microbiota is a rich source of bacteriocin-producing staphylococci that kill human pathogens. *FEMS Microbiology Ecology* **95**, doi:10.1093/femsec/fiy241 (2018).
13   Götz, F., Perconti, S., Popella, P., Werner, R. & Schlag, M. Epidermin and gallidermin: Staphylococcal lantibiotics. *International Journal of Medical Microbiology* **304**, 63-71, doi:https://doi.org/10.1016/j.ijmm.2013.08.012 (2014).
14   Ekkelenkamp, M. B. *et al.* Isolation and structural characterization of epilancin 15X, a novel lantibiotic from a clinical strain of Staphylococcus epidermidis. *FEBS Letters* **579**, 1917-1922, doi:10.1016/j.febslet.2005.01.083 (2005).
15   Molloy, E. M., Cotter, P. D., Hill, C., Mitchell, D. A. & Ross, R. P. Streptolysin S-like virulence factors: the continuing sagA. *Nature Reviews Microbiology* **9**, 670-681, doi:10.1038/nrmicro2624 (2011).
16   Van Tyne, D., Martin, M. J. & Gilmore, M. S. Structure, function, and biology of the Enterococcus faecalis cytolysin. *Toxins (Basel)* **5**, 895-911, doi:10.3390/toxins5050895 (2013).
17   Cascales, E. *et al.* Colicin biology. *Microbiol Mol Biol Rev* **71**, 158-229, doi:10.1128/MMBR.00036-06 (2007).
18   Baquero, F., Lanza, V. F., Baquero, M.-R., del Campo, R. & Bravo-Vázquez, D. A. Microcins in Enterobacteriaceae: Peptide Antimicrobials in the Eco-Active Intestinal Chemosphere. *Frontiers in Microbiology* **10**, doi:10.3389/fmicb.2019.02261 (2019).

19   Klein, T. A., Ahmad, S. & Whitney, J. C. Contact-Dependent Interbacterial Antagonism Mediated by Protein Secretion Machines. *Trends Microbiol* **28**, 387-400, doi:10.1016/j.tim.2020.01.003 (2020).

20   Cao, Z., Casabona, M. G., Kneuper, H., Chalmers, J. D. & Palmer, T. The type VII secretion system of Staphylococcus aureus secretes a nuclease toxin that targets competitor bacteria. *Nat Microbiol* **2**, 16183, doi:10.1038/nmicrobiol.2016.183 (2016).

21   Brüggemann, H. *et al.* Staphylococcus saccharolyticus Isolated From Blood Cultures and Prosthetic Joint Infections Exhibits Excessive Genome Decay. *Frontiers in Microbiology* **10**, doi:10.3389/fmicb.2019.00478 (2019).

22   Zipperer, A. *et al.* Human commensals producing a novel antibiotic impair pathogen colonization. *Nature* **535**, 511-516, doi:10.1038/nature18634 (2016).

23   Schnell, N. *et al.* Prepeptide sequence of epidermin, a ribosomally synthesized antibiotic with four sulphide-rings. *Nature* **333**, 276-278, doi:10.1038/333276a0 (1988).

24   Rogers, L. A. & Whittier, E. O. LIMITING FACTORS IN THE LACTIC FERMENTATION. *Journal of bacteriology* **16**, 211-229 (1928).

25   Blin, K. *et al.* antiSMASH 5.0: updates to the secondary metabolite genome mining pipeline. *Nucleic Acids Res* **47**, W81-w87, doi:10.1093/nar/gkz310 (2019).

26   Law, B. J. C. *et al.* A vitamin K-dependent carboxylase orthologue is involved in antibiotic biosynthesis. *Nat Catal* **1**, 977-984, doi:10.1038/s41929-018-0178-2 (2018).

27   Fujii, I. Functional analysis of fungal polyketide biosynthesis genes. *J Antibiot (Tokyo)* **63**, 207-218, doi:10.1038/ja.2010.17 (2010).

28   Ng, B. G., Han, J. W., Lee, D. W., Choi, G. J. & Kim, B. S. The chejuenolide biosynthetic gene cluster harboring an iterative trans-AT PKS system in Hahella chejuensis strain MB-1084. *J Antibiot (Tokyo)* **71**, 495-505, doi:10.1038/s41429-017-0023-x (2018).

29   Cavassin, F. B., Baú-Carneiro, J. L., Vilas-Boas, R. R. & Queiroz-Telles, F. Sixty years of Amphotericin B: An Overview of the Main Antifungal Agent Used to Treat Invasive Fungal Infections. *Infectious Diseases and Therapy* **10**, 115-147, doi:10.1007/s40121-020-00382-7 (2021).

30   Krismer, B. *et al.* Nutrient limitation governs Staphylococcus aureus metabolism and niche adaptation in the human nose. *PLoS Pathog* **10**, e1003862, doi:10.1371/journal.ppat.1003862 (2014).

31   Baur, S. *et al.* A Nasal Epithelial Receptor for Staphylococcus aureus WTA Governs Adhesion to Epithelial Cells and Modulates Nasal Colonization. *PLoS Pathog* **10**, e1004089, doi:10.1371/journal.ppat.1004089 PPATHOGENS-D-13-03084 [pii] (2014).

32   Donia, M. S. *et al.* A systematic analysis of biosynthetic gene clusters in the human microbiome reveals a common family of antibiotics. *Cell* **158**, 1402-1414, doi:10.1016/j.cell.2014.08.032 (2014).

33   Sugimoto, Y. *et al.* A metagenomic strategy for harnessing the chemical repertoire of the human microbiome. *Science* **366**, doi:10.1126/science.aax9176 (2019).

34   Donia, M. S. & Fischbach, M. A. HUMAN MICROBIOTA. Small molecules from the human microbiota. *Science* **349**, 1254766, doi:10.1126/science.1254766 (2015).

35   Myrtle, J. D., Beekman, A. M. & Barrow, R. A. Ravynic acid, an antibiotic polyeneyne tetramic acid from Penicillium sp. elucidated through synthesis. *Org Biomol Chem* **14**, 8253-8260, doi:10.1039/c6ob00938g (2016).

36   Moldenhauer, J., Chen, X.-H., Borriss, R. & Piel, J. Biosynthesis of the Antibiotic Bacillaene, the Product of a Giant Polyketide Synthase Complex of the trans-AT Family. *Angewandte Chemie International Edition* **46**, 8195-8197, doi:https://doi.org/10.1002/anie.200703386 (2007).

37   Pacheco, A. R. & Segrè, D. A multidimensional perspective on microbial interactions. *FEMS microbiology letters* **366**, fnz125, doi:10.1093/femsle/fnz125 (2019).

38   Byrd, A. L., Belkaid, Y. & Segre, J. A. The human skin microbiome. *Nature Reviews Microbiology* **16**, 143-155, doi:10.1038/nrmicro.2017.157 (2018).

39   Garcia-Bayona, L. & Comstock, L. E. Bacterial antagonism in host-associated microbial communities. *Science* **361**, doi:10.1126/science.aat2456 (2018).

40   Moghadam, Z. M., Henneke, P. & Kolter, J. From Flies to Men: ROS and the NADPH Oxidase in Phagocytes. *Front Cell Dev Biol* **9**, 628991, doi:10.3389/fcell.2021.628991 (2021).

41   Khayatt, B. I., van Noort, V. & Siezen, R. J. The Genome of the Plant-Associated Lactic Acid Bacterium Lactococcus lactis KF147 Harbors a Hybrid NRPS-PKS System Conserved in Strains of the Dental Cariogenic Streptococcus mutans. *Curr Microbiol* **77**, 136-145, doi:10.1007/s00284-019-01799-1 (2020).

42   Wu, C. *et al.* Genomic island TnSmu2 of Streptococcus mutans harbors a nonribosomal peptide synthetase-polyketide synthase gene cluster responsible for the biosynthesis of pigments involved in oxygen and H2O2 tolerance. *Appl Environ Microbiol* **76**, 5815-5826, doi:10.1128/AEM.03079-09 (2010).

43   Neubauer, H., Pantel, I. & Götz, F. Molecular characterization of the nitrite-reducing system of Staphylococcus carnosus. *Journal of bacteriology* **181**, 1481-1488, doi:10.1128/JB.181.5.1481-1488.1999 (1999).

44   Gutierrez, J. A. *et al.* Insertional mutagenesis and recovery of interrupted genes of Streptococcus mutans by using transposon Tn917: preliminary characterization of mutants displaying acid sensitivity and nutritional requirements. *J Bacteriol* **178**, 4166-4175, doi:10.1128/jb.178.14.4166-4175.1996 (1996).

45   Youngman, P. J., Perkins, J. B. & Losick, R. Genetic transposition and insertional mutagenesis in Bacillus subtilis with Streptococcus faecalis transposon Tn917. *Proc Natl Acad Sci U S A* **80**, 2305-2309, doi:10.1073/pnas.80.8.2305 (1983).

46   Zerbino, D. R. & Birney, E. Velvet: algorithms for de novo short read assembly using de Bruijn graphs. *Genome Res* **18**, 821-829, doi:10.1101/gr.074492.107 (2008).

47   Darling, A. E., Mau, B. & Perna, N. T. progressiveMauve: multiple genome alignment with gene gain, loss and rearrangement. *PLoS One* **5**, e11147, doi:10.1371/journal.pone.0011147 (2010).

48   Geiger, T. *et al.* The stringent response of Staphylococcus aureus and its impact on survival after phagocytosis through the induction of intracellular PSMs expression. *PLoS Pathog* **8**, e1003016, doi:10.1371/journal.ppat.1003016 (2012).

49   Brückner, R. Gene replacement in Staphylococcus carnosus and Staphylococcus xylosus. *FEMS Microbiol Lett* **151**, 1-8, doi:10.1111/j.1574-6968.1997.tb10387.x (1997).

50   Bruckner, R. A series of shuttle vectors for Bacillus subtilis and Escherichia coli. *Gene* **122**, 187-192, doi:10.1016/0378-1119(92)90048-t (1992).

Acknowledgments

Author Contributions

B.O.T.S. performed and analyzed most of the bacteriological, molecular, and compound isolation experiments with help by D.J., S.K. and B.K., who originally isolated strain IVK83; animal experiments were performed by B.O.T.S. and B.K.; T.D., N.A.S., and S.G. elucidated the structure of epifadin with support from J.M.B.-B.; A.B. analyzed epifadin toxicity.; M.L., M.J.H. and S.K. identified and provided epifadin-producing *S. epidermidis* strains.; T.W. analyzed the potential epifadin biosynthesis enzymes; H.B.-O., S.G., B.K., and A.P. supervised the experiments and wrote the manuscript.

Competing interest

The authors declare no competing interest.

Figures (1-6):
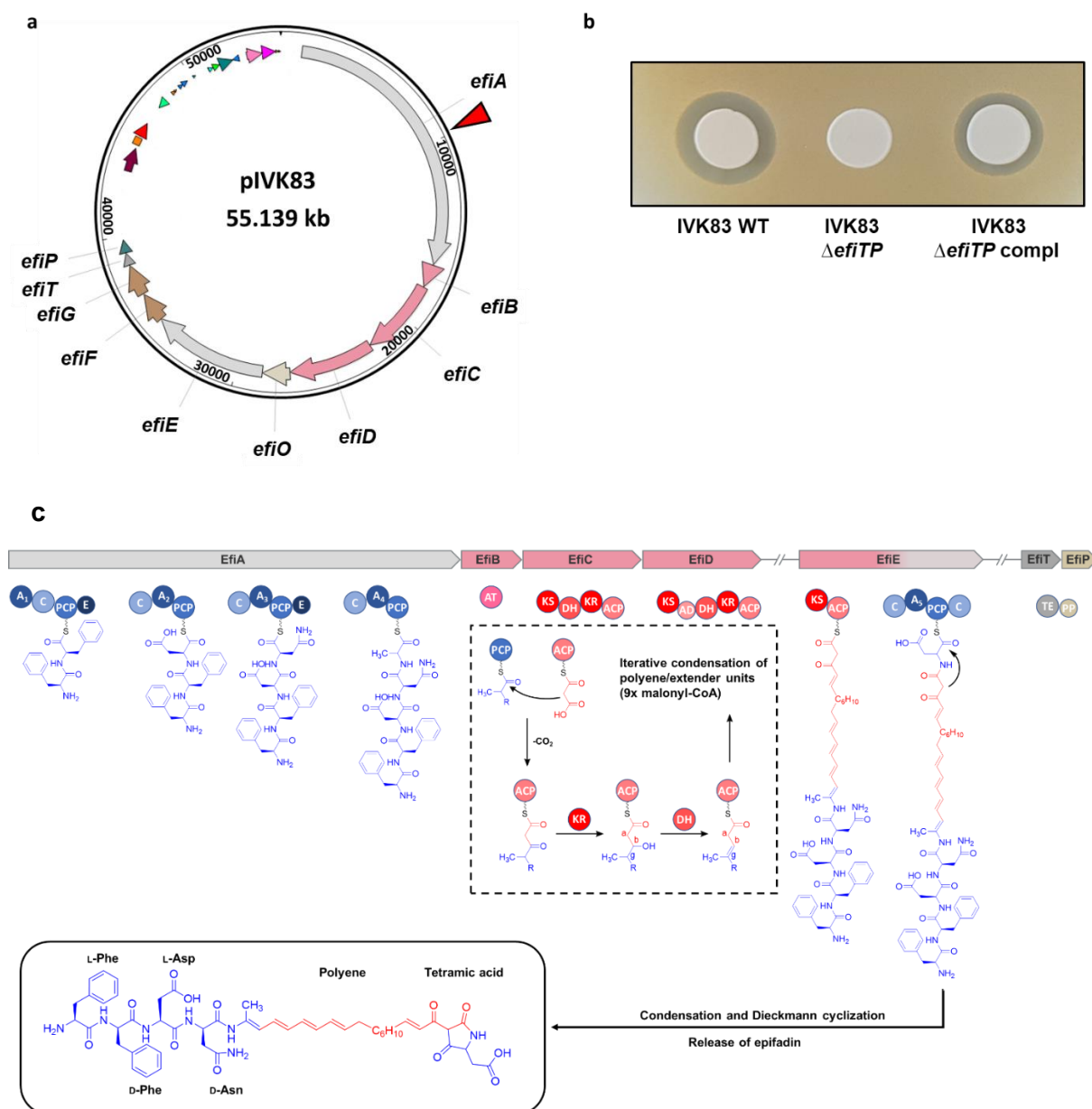
Figure 4. Plasmid and epifadin BGC composition, biosynthetic modules, and domain organization of the epifadin NRPS/PKS enzymes of IVK83. a, Plasmid map of pIVK83 (~55 kbp) harboring the epifadin operon (~40 kbp). The cluster consists of genes encoding a putative NRPS (*efiA*), three PKS (*efiB*, *efiC*, *efiD*), a hybrid PKS/NRPS (*efiE*), a putative NAD(P)- or FAD-dependent oxidoreductase (*efiO*) located between *efiD* and *efiE*, a thioesterase (*efiT*), a phosphopantetheinyl transferase (*efiP*), and two ABC transporter genes (*efiF*, *efiG*). Red arrow indicates the insertion site of Tn917, generating an epifadin-deficient mutant. **b**, Antimicrobial activity of IVK83 wild type (WT), isogenic Δ*efiTP* mutant and complemented strain towards *S. aureus* USA300. **c**, Domain organization of the NRPS and PKS EfiA, EfiB, EfiC, EfiD, EfiE, EfiT, and EfiP involved in epifadin biosynthesis and proposed biosynthesis pathway. Functional domains: A, adenylation; C, condensation; PCP, peptidyl carrier protein; E, epimerization; AT, acyltransferase; KS, ketosynthase; DH, dehydratase; KR, ketoreductase; ACP, acylcarrier protein; AD, trans-AT docking; TE, thioesterase; PP, 4'-phosphopantetheinyl transferase. In the final structure of epifadin the given tetramic acid

additionally undergoes keto-tautomerisation. NRPS and PKS modules and their domains as well as their products are depicted in blue and red, respectively.
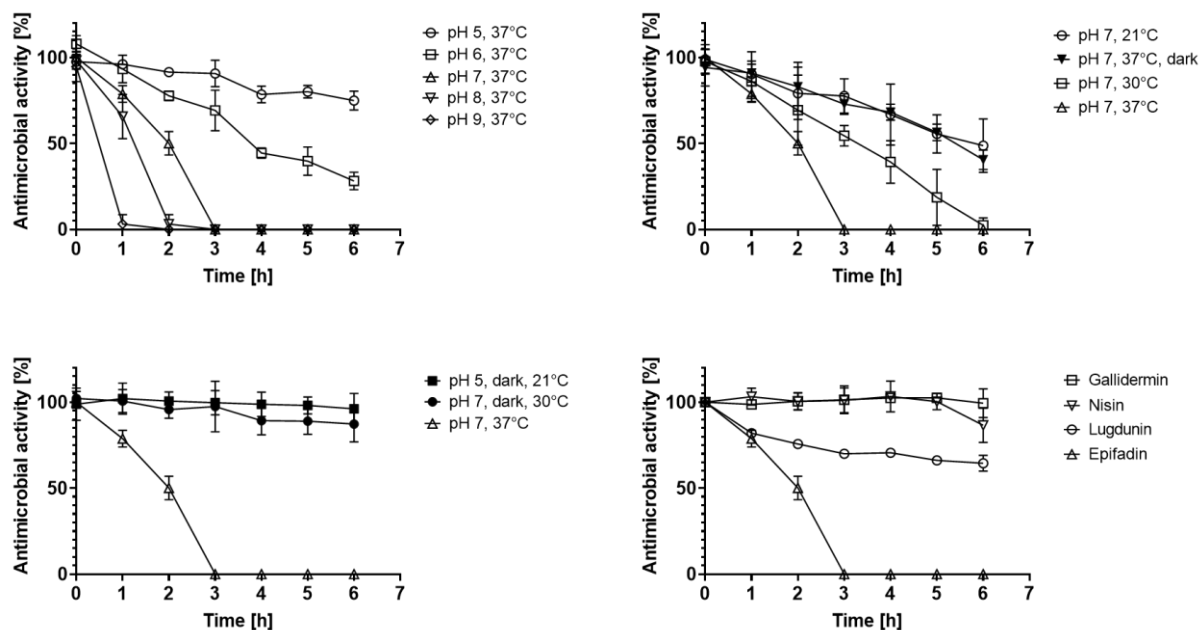
Figure 5. High instability of epifadin under *in-vivo* like conditions. DMSO extract of HCl-precipitate of IVK83 culture supernatants containing epifadin was diluted in TSB and incubated for the indicated time periods under constant shaking under the indicated conditions and subsequently tested for activity towards *S. aureus* USA300. **a**, different pH values with ambient laboratory light exposure at 37°C; **b**, different temperatures with/without laboratory light exposure at pH 7 and **c**, combinations of the conditions used for **a** and **b**, under which the culture filtrate containing epifadin showed the highest stability. **d**, Stability of epifadin compared to other antibacterial agents under *in-vivo* like cultivation conditions (37°C, pH 7, laboratory light exposure). Conditions at pH 7, 37°C, and 0 h were used as reference for 100% stability.
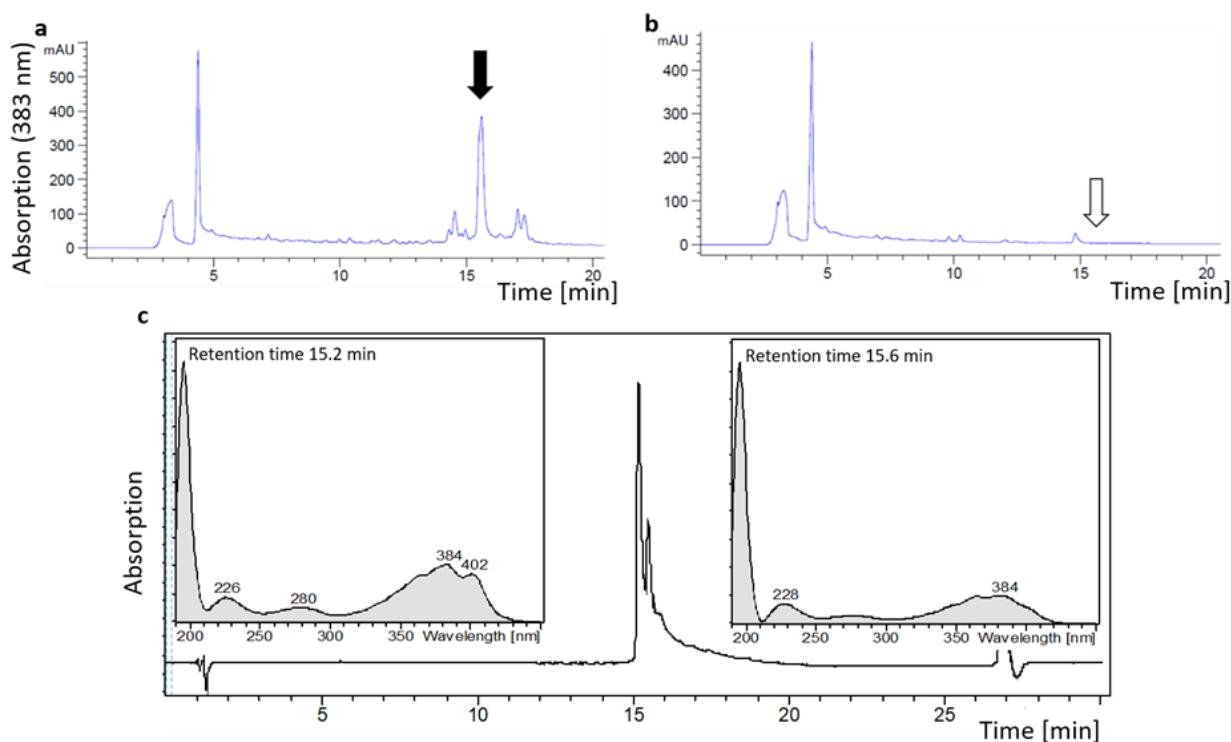
Figure 3. Detection, isolation, and absorption spectrum of epifadin. Chromatogram (a, b) and absorption spectrum (c) of epifadin on RP-HPLC column. **a,b**, HPLC-UV chromatograms (λ = 383 nm) of DMSO-PA extract of IVK83 wild type (**a**) and $\Delta efiTP$ mutant (**b**). A prominent peak (black arrow) of epifadin is only present in the wild-type sample with a retention time of ~15 min at 383 nm. **c,** UV-chromatogram (383 nm) of the epifadin peak is shown. UV-spectra of the active compound at 15.2 min and 15.6 min from 190 nm to 450 nm are shown (methanol as a solvent causes a strong absorbance at 200 nm). The absorption maxima of the epifadin peak are indicated (peptide bond, 210-230 nm; phenylalanine, 280 nm; and polyene moiety, 330-410 nm).
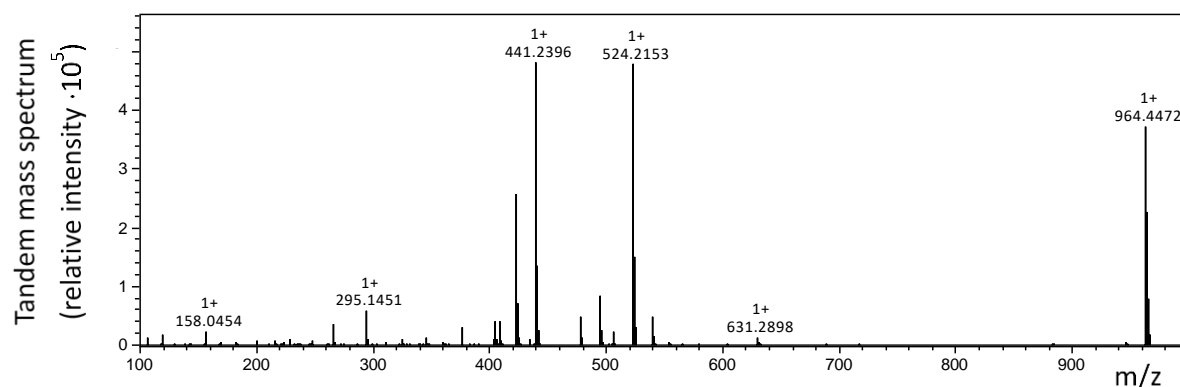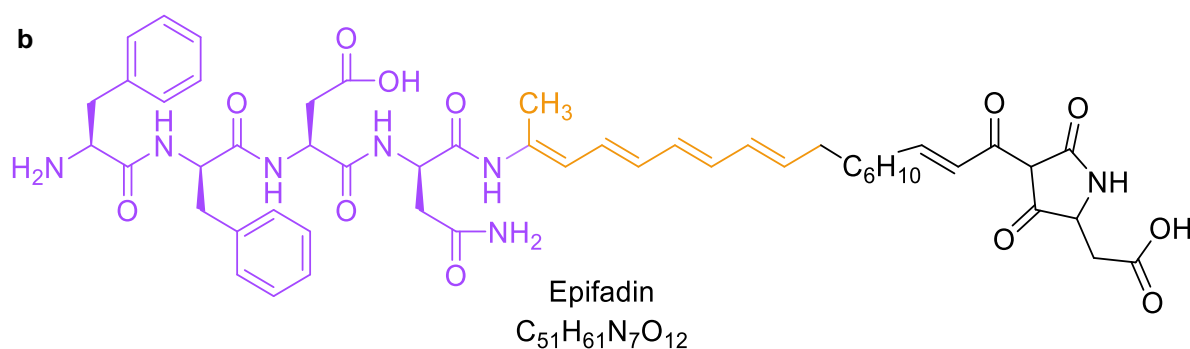
Figure 4. Molecular mass and structure of epifadin. **a**, MS/MS spectrum of intact epifadin (HR-ESI(+) time-of-flight (TOF) mass spectrometry) indicates a mass of intact epifadin of 964.4472 Da. **b**, purple moiety elucidated by NMR and MS, orange moiety by NMR, and tetramic acid moiety (black, inferred from genetic-, single NMR, and MS data in accordance with detailed MS mechanistic considerations. The structure is not depicted in its keto-tautomeric form).

a

Species	Zone of inhibition
Bacillus cereus 2/3	(grey)
Bacillus cereus 1/3	(yellow)
Citrobacter freundii 2/2	(grey)
Citrobacter koseri 5/5	(grey)
Corynebacterium accolens 2/2	(grey)
Corynebacterium aurimucosum 1/1	(grey)
Corynebacterium pseudodiphteriticum 4/29	(grey)
Corynebacterium pseudodiphteriticum 1/29	(green)
Corynebacterium pseudodiphteriticum 19/29	(yellow)
Corynebacterium pseudodiphteriticum 4/29	(red)
Cutibacterium acnes 3/3	(yellow)
Cutibacterium avidum 1/1	(grey)
Dermabacter hominis 1/1	(grey)
Dolosigranulum pigrum 1/1	(grey)
Enterococcus faecalis 8/8	(grey)
Enterococcus faecium 9/9	(green)
Escherichia coli 2/2	(grey)
Klebsiella oxytoca 2/2	(grey)
Klebsiella pneumoniae 3/3	(grey)
Kocuria spp. 1/1	(yellow)
Micrococcus luteus 9/9	(yellow)
Raoultella ornithinolytica 1/2	(grey)
Raoultella ornithinolytica 1/2	(yellow)
Rothia mucilaginosa 1/1	(yellow)
Staphylococcus aureus 1/5	(green)
Staphylococcus aureus 4/5	(yellow)
Staphylococcus capitis 3/3	(grey)
Staphylococcus caprae 2/2	(grey)
Staphylococcus carnosus 1/1	(green)
Staphylococcus epidermidis 9/16	(grey)
Staphylococcus epidermidis 3/16	(green)
Staphylococcus epidermidis 4/16	(yellow)
Staphylococcus hominis 3/3	(yellow)
Staphylococcus pettenkoferi 1/1	(yellow)
Staphylococcus warneri 2/2	(yellow)
Staphylococcus lugdunensis 1/2	(grey)
Staphylococcus lugdunensis 1/2	(green)
Staphylococcus xylosus 1/1	(yellow)
Streptococcus pyogenes 1/1	(yellow)
Candida albicans 1/1	(yellow)
Saccharomyces cerevisiae 1/1	(yellow)

No inhibition
<1 mm (green)
1-3 mm (yellow)
3-5 mm (red)

b

Antibiotic	Strain	IC* (µg/ml)
Epifadin	*S. aureus* USA300LAC	1,5
	S. aureus USA300 JE2	1,5
	S. aureus Newman	1,5
	S. aureus RN4220	0,9
	S. aureus NCTC 8325	0,9
	S. epidermidis IVK7	6,0
	S. hominis 9VPs_KB1	4,6
	S. hominis 89VPS_B7	8,6
	S. capitis 50VAS_KB6	4,6
	S. warneri 1929	3,7
	S. warneri 1930	6,0
	M. luteus	7,4
	S. pyogenes	0,6
Vancomycin	*S. aureus* USA300 LAC	6,0
	S. aureus USA300 JE2	3,7
Daptomycin	*S. aureus* USA300 LAC	4,0
	S. aureus USA300 JE2	4,3

Figure 5. Broad antimicrobial activity of epifadin-producing *S. epidermidis* IVK83. a, Sizes of inhibition zones caused by IVK83 on lawns of test strains listed on the left are given in color code: grey (no inhibition); green (below 1 mm); yellow (1 mm to 3 mm); or red (3 mm to 5 mm). The numbers of isolates with a specific degree of susceptibility to epifadin among all tested isolates is given behind species names. The IVK Δ*efiTP* mutant mediated no inhibition. **b**, Inhibitory concentration (IC*) of epifadin against the listed bacterial strains. Assays were performed on TSA inoculated with the indicated bacterial strain.

* IC was determined by an agar diffusion assay as described in the Materials and Methods section.
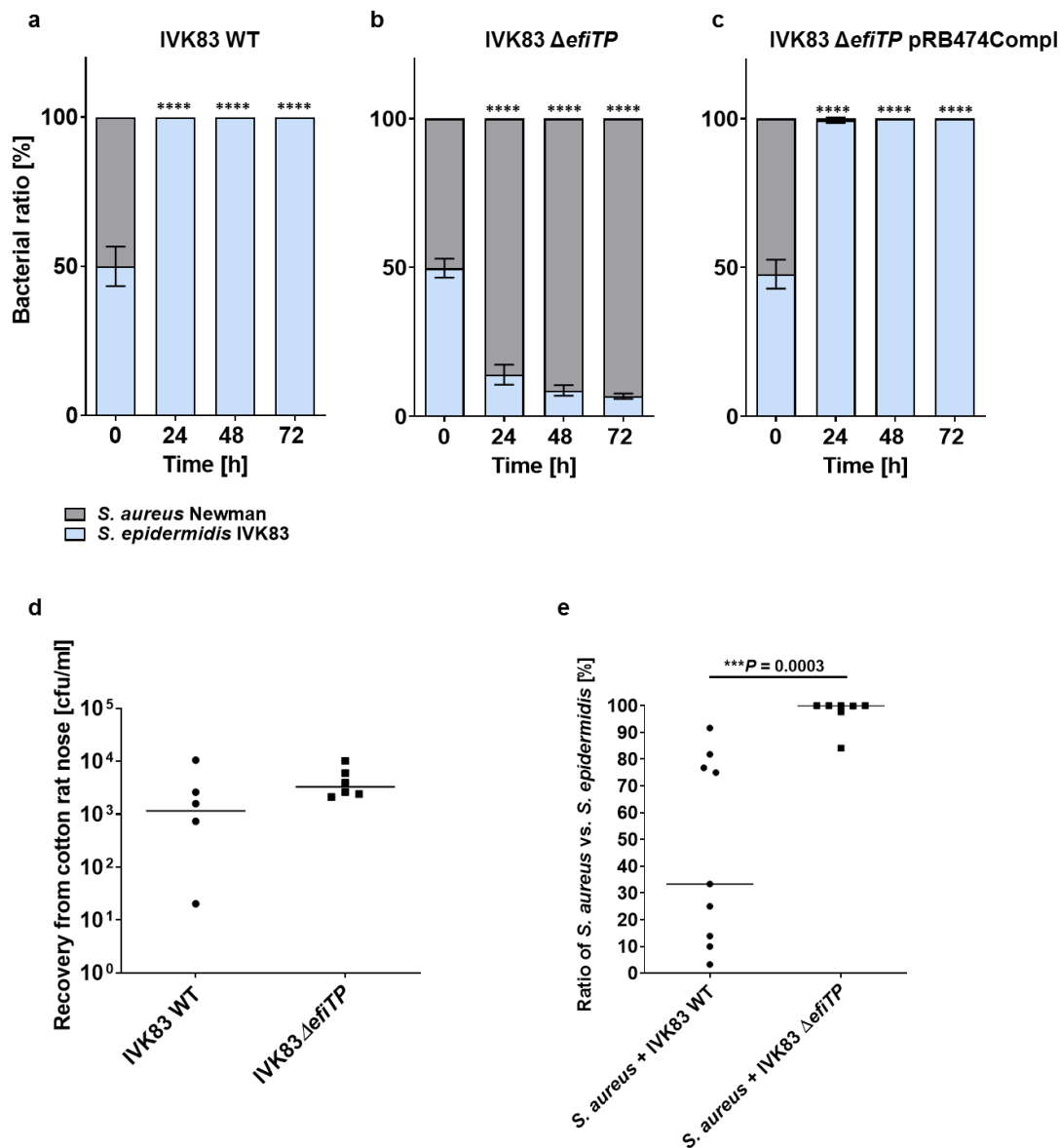
Figure 6. Epifadin-producing *S. epidermidis* IVK83 restricts *S. aureus* growth *in vitro* and *in vivo* in cotton rats. a-c, in *vitro* competition assays on TSA. **a,** *S. aureus* growth is inhibited by IVK83 wild type (WT) (grey or light blue bars, respectively) after 24 h of incubation on TSA. **b,** in contrast, the mutant IVK83 Δ*efiTP* is overgrown by *S. aureus* over time. **c,** Complementation (pRB474Compl) restored the wild-type phenotype. Data points represent mean values ± SD of three independent experiments. Significant differences between starting condition and indicated time points were analyzed by one-way ANOVA (**P < 0.01; ***P < 0.001; ****P < 0.0001). **d**, Nasal colonization capability of IVK83 wild type and IVK83 Δ*efiTP* in cotton rats. Bacterial CFUs found in cotton rat noses five days after instillation are shown. Horizontal lines represent the median of each group. **e**, Epifadin-producing IVK83 reduces *S. aureus* carriage in cotton rat noses. Percentage of *S. aureus* cells from cotton rat noses was significantly lower when *S. aureus* was co-colonized with IVK83 wild type compared to the Δ*efiTP* mutant five days after instillation. Horizontal lines represent medians of each group. Significant differences were calculated by the Mann-Whitney test (***P = < 0.001).
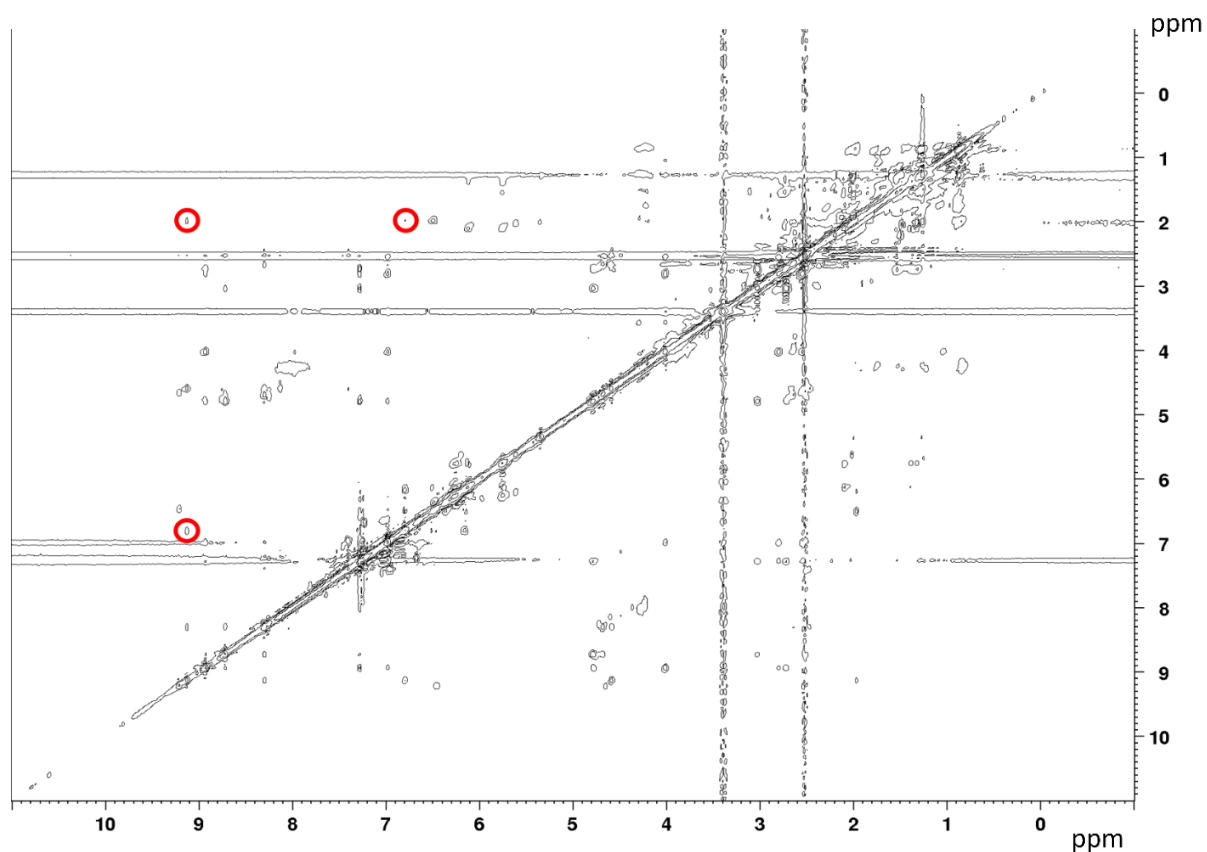
Extended Data Figures
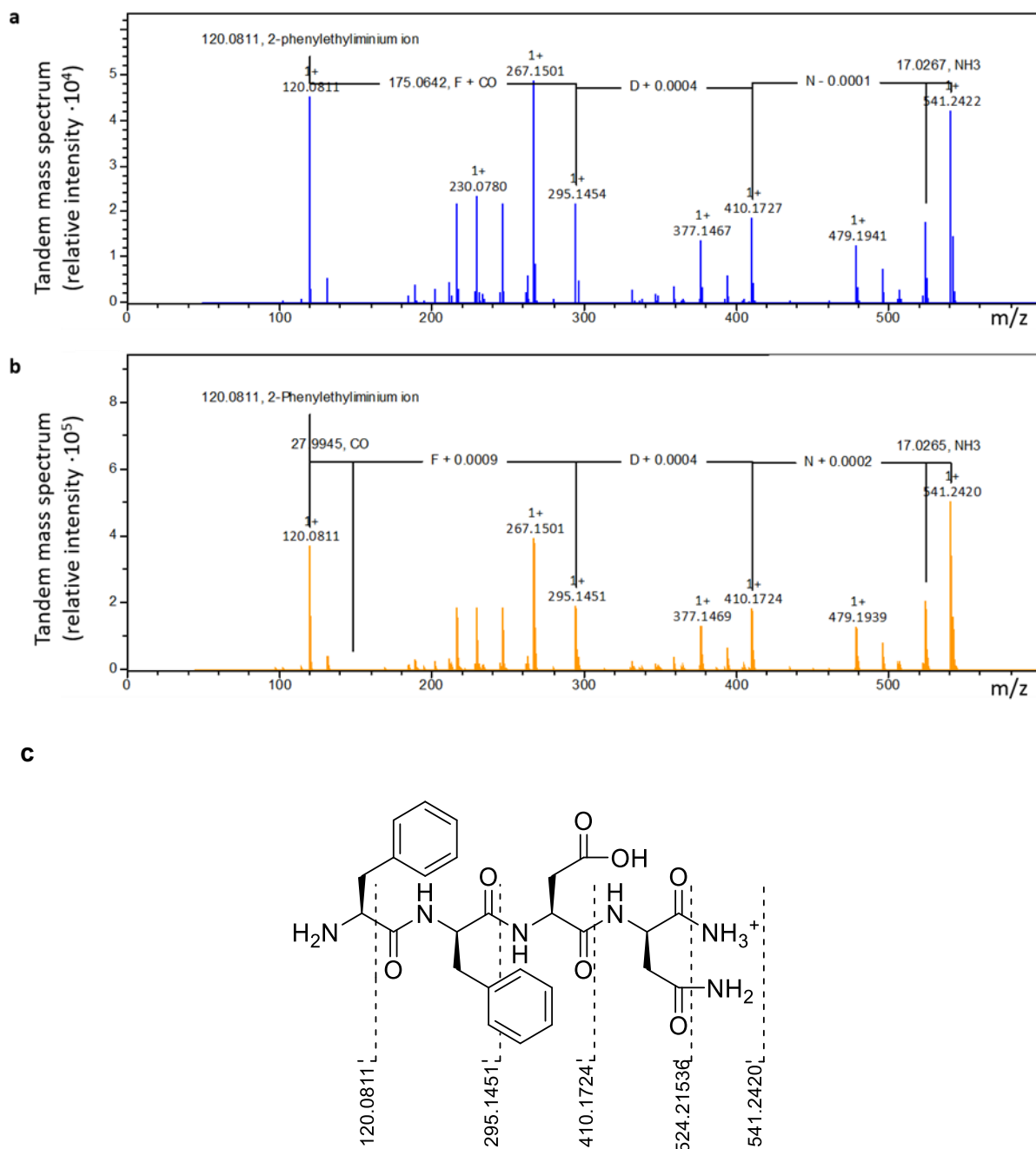
Extended Data Figure 1. Comparison of MS/MS spectra of the synthetic and natural peptide amide fragments of epifadin. a, MS/MS spectrum of the natural peptide amide after decomposition of epifadin. **b**, MS/MS spectrum of the synthetic peptide amide **2**. **c**, Fragmentation pattern of the synthetic and natural peptide amides **2**. Fragmentation pattern for the peptide amide **2** is shown in black. F, phenylalanine; D, aspartate; N, asparagine; CO, carbon monoxide; NH$_3$, ammonia.

a

b
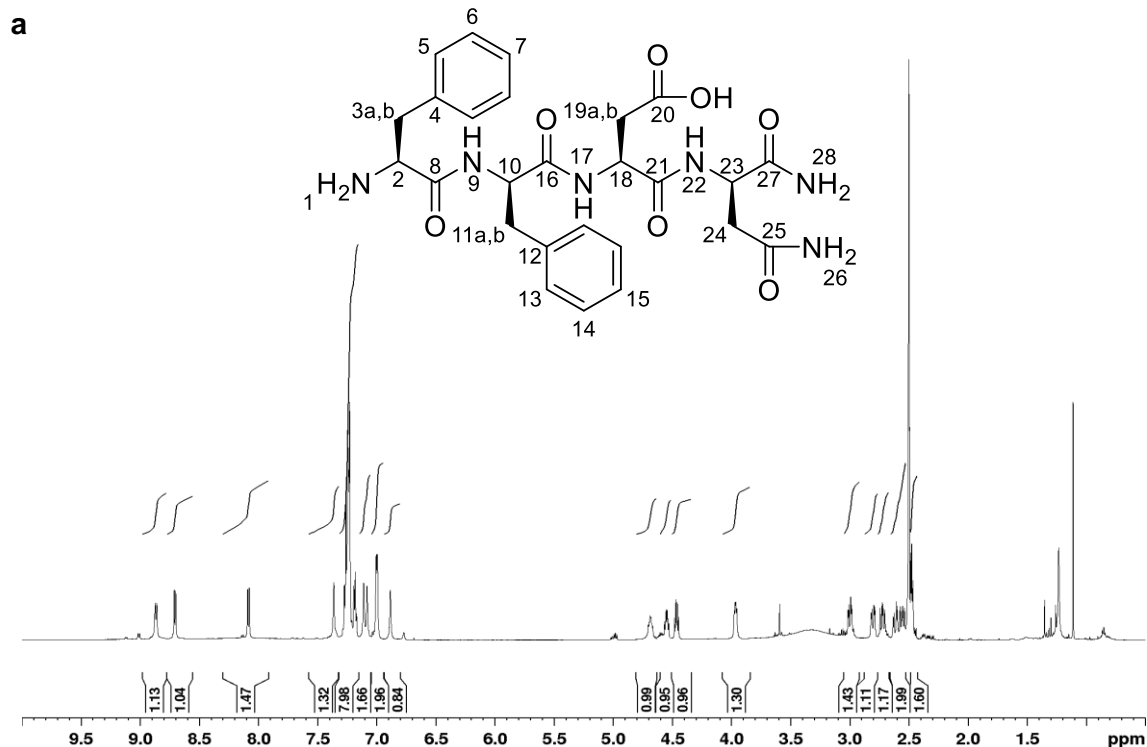
#	δ_H (mult., J)	δ_C	HMBC (H → #C)
1			
2	3.97 (m)	53.5	3, 4, 8
3a, 3b	2.56 (dd, 8.6, 14.2), 2.81(dd, 4.5, 14.2)	37.1	2, 4, 5, 8
4		134.9	
5	7.00 (d, 7.4)	129.4	3, 4, 5, 6, 7
6	7.23 (m)	128.4	4, 5, 7
7	7.23 (m)	127.0	4, 5, 6
8		168.3	
9	8.86 (d, 8.4)		8, 10, 11
10	4.69 (m)	54.0	11, 12, 16
11a, 11b	2.72 (dd, 10.0, 13.5), 3.00 (dd, 4.4, 14.2)	38.0	10, 12, 13, 16
12		137.3	
13	7.25 (m)	129.3	11, 12, 14, 15
14	7.26 (m)	128.1	12, 13, 15
15	7.18 (m)	126.5	12, 13, 14
16		170.8	
17	8.71 (d, 7.7)		16, 18, 19
18	4.55 (m)	49.6	16, 19, 20, 21
19a, 19b	2.62 (dd, 4.8, 16.7), 2.50 (overlapping with solvent)	36.4	18, 20, 21
20		171.7	
21		170.0	
22	8.09 (d, 8.2)		21, 23, 24
23	4.47 (m)	49.6	21, 24, 25, 27
24	2.48 (overlapping with solvent)	36.8	23, 25, 27
25		171.9	
26	6.88 (s), 7.36 (s)		24, 25
27		172.8	
28	7.08 (s), 7.11 (s)		23, 27

Extended Data Figure 2. Proton NMR spectrum (a) and signals (b) of the synthetic peptide amide FfDn-NH₂. (DMSO-d₆, 600MHz, 303K). The integrals of the proton signals are depicted as black curves. The scale shows the chemical shift δ in parts per million (ppm).

Extended Data Figure 3. ¹H-¹H-ROESY NMR spectrum of the purified epifadin in DMSO-d₆ (700 MHz, 303K). The red circles highlight coupling between the NH-proton and the protons of the methyl group of the alanine residue (9.14 ppm/1.95 ppm) and to the proton of the adjacent methine group (9.14 ppm/6.77 ppm). Also, the coupling of the protons of the methyl group from the alanine residue to the methine group is shown (6.77 ppm/1.95 ppm).
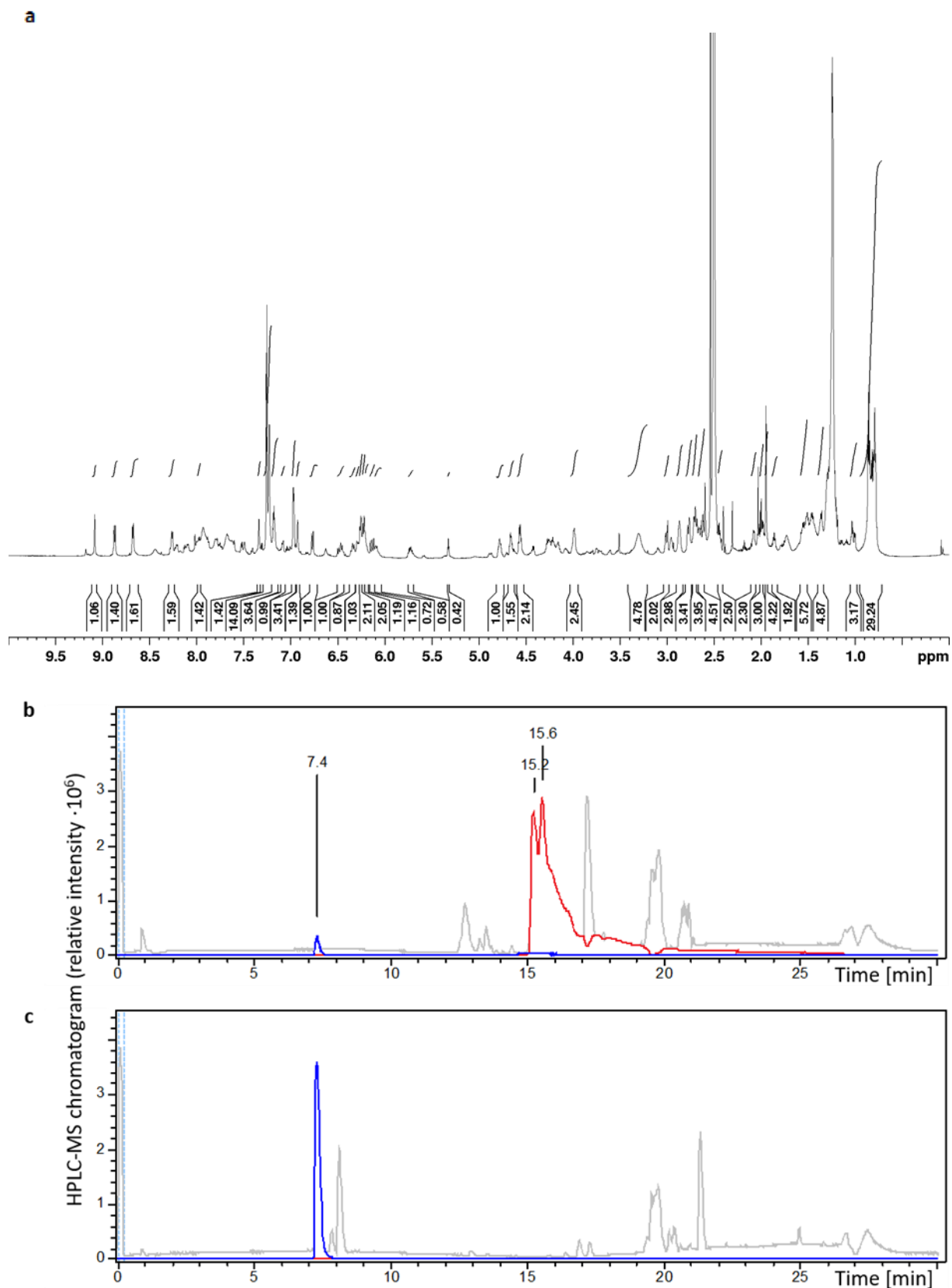
Extended Data Figure 4. ^{1}H NMR spectrum (DMSO-d$_6$, 700 MHz, 303 K) of purified epifadin and its decomposition analyzed by HPLC-MS. **a**, DMSO-d$_6$ signal at 2.50 ppm as reference. The integrals of the proton signals are depicted as black curves. The scale shows the chemical shift δ in parts per million (ppm)**. b,c**, The epifadin-enriched material was dissolved in a mixture of acetonitrile and water (1:1) with 0.05% trifluoroacetic acid, resulting

in a concentration of 0.2 mg·mL^{-1} and analyzed by HPLC-ESI-TOF-high resolution MS. The extracted ion chromatograms (EICs) of epifadin ($C_{51}H_{61}N_7O_{12}$ [M+H]$^+$, *m/z* 964.4451±0.005) are depicted in red (retention time 15.2 min and 15.6 min) and the base peak chromatograms (BPCs) in gray. EICs of the peptide amide ($C_{26}H_{32}N_6O_7$ [M+H]$^+$, *m/z* 541.2405±0.005) are depicted in blue (retention time 7.4 min) accumulating by strong decomposition of epifadin in the mentioned solvent after storage at -20°C. **b**, analyzed after purification. **c**, Analyzed after 14 days of storage at -20°C.
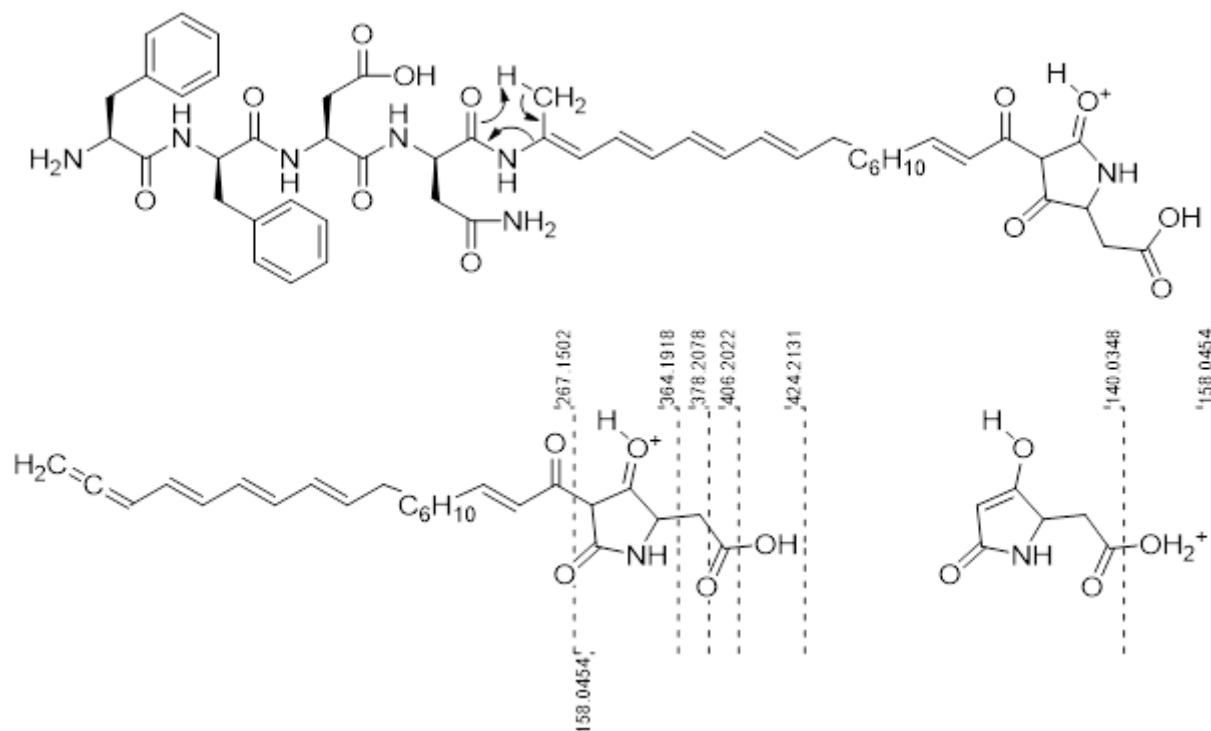

Extended Data Figure 5: Deduced fragmentation pattern for the peptide amide and the PKS/NRPS moiety. From a six-membered transition state a rearrangement results in a neutral loss of the peptide amide moiety. The newly formed allene (*m/z* 424.2131) decomposes into further fragments.

a

b
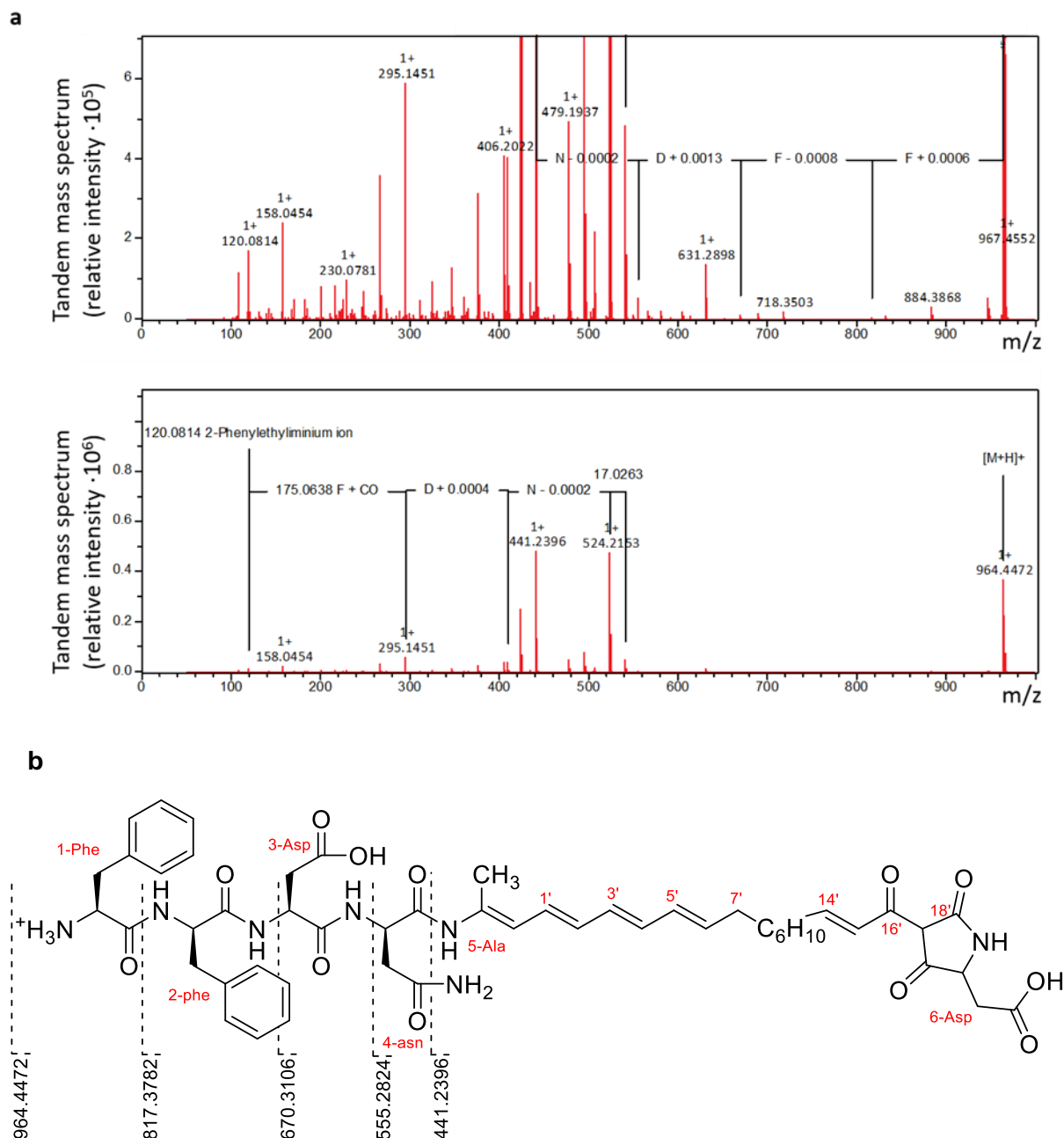
Extended Data Figure 6. MS/MS spectra of epifadin showing fragmentation products from ionization in MS. a, The mass of 964 Da corresponds to the intact proton adduct (m/z 964.4) of epifadin. 524 Da (*m/z* 524.2) corresponds to the proton adduct of the tetrapeptide EfiA product, and the mass of 441 Da (*m/z* 441.2) is assigned to the proton adduct of the EfiBCDE product. **b,** The fragmentation pattern for the peptide moiety in epifadin is shown in black. [M+H]+, monoisotopic positively charged ion; F, phenylalanine; D, aspartate; N, asparagine; CO, carbon monoxide. b, Numbering of amino acids and carbon atoms of PKS chain in red.
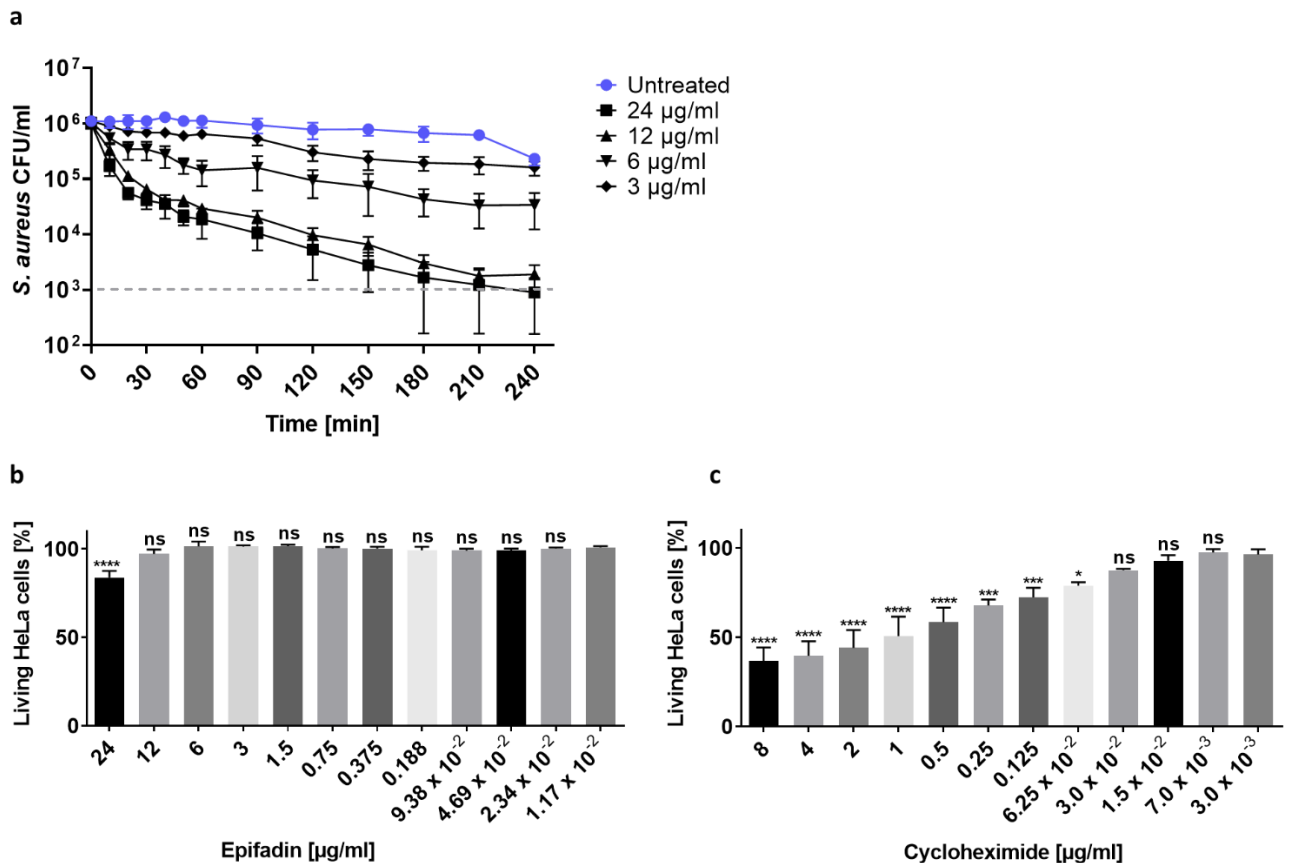
Extended Data Figure 7: Epifadin is bactericidal for susceptible bacterial cells but does not inhibit mammalian cells. a, Time-dependent elimination of *S. aureus* by epifadin. Incubation of *S. aureus* USA300 LAC with epifadin concentrations of 24 µg/mL and 12 µg/mL led to a fast decline of CFUs reaching the detection limit of 1×10^3 CFU/mL after 210 min. Data represent means with SEM of three independent experiments. **b,c**, Cytotoxicity assay. HeLa cells incubated with epifadin do not show increased cell death compared to mock-treated cells even at high concentrations of 12 µg/mL. Cycloheximide (CHM) was included as a positive control. Only at concentration of 24 µg/mL, epifadin shows a significant cytotoxic effect, still leaving 84% of HeLa cells intact. Data points represent the mean ± SD of three independent experiments. Significant differences between lowest compound concentrations and higher concentrations were analyzed by one-way ANOVA (*$P < 0.05$; **$P < 0.01$; ***$P < 0.001$; ****$P < 0.0001$).
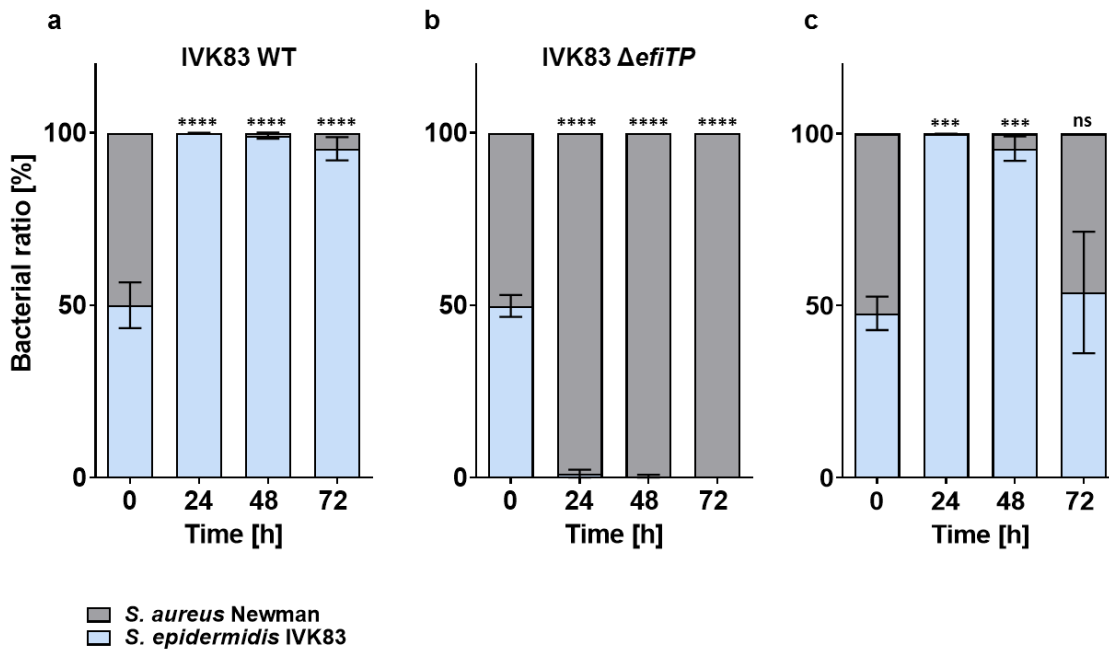
Extended Data Figure 8. Epifadin-producing *S. epidermidis* IVK83 restricts *S. aureus* growth *in vitro*. **a-c**, in *vitro* competition assays in TSB. **a,** *S. aureus* growth is inhibited by IVK83 wild type (grey or light blue bars, respectively) already after 24 h of incubation in TSB inoculated at ratios of ~50:50. **b,** in contrast, the mutant IVK83 Δ*efiTP* is overgrown by *S. aureus* over time when inoculated at a 50:50 ratio. **c,** Complemented strain overgrew S. aureus for 48 h, after 72 h, ratio of complemented strain and *S. aureus* were similar to starting conditions. Data points represent mean value ± SD of three independent experiments. Significant differences between the starting condition and the indicated time points were analyzed by one-way ANOVA (**$P < 0.01$; ***$P < 0.001$; ****$P < 0.0001$).
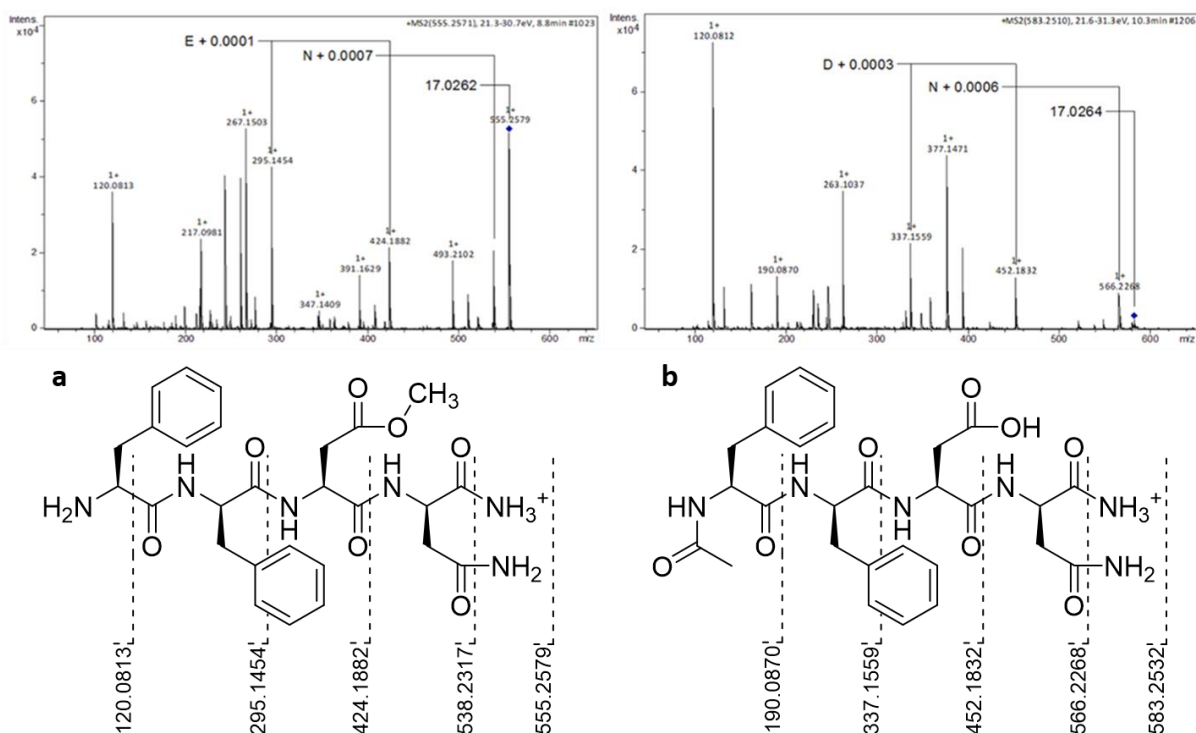
Extended Data Figure 9. Structures of semi-synthetic derivatives of peptide amide and MS/MS spectra of **a)** methyl ester of natural peptide amide and **b)** acetylated natural peptide amide.

Chapter 5

Acquisition of bacteriocin biosynthesis genes causes physiological burdens by disbalancing central metabolism

Sophia Krauss[a,b,c], Theresa Anisja Harbig[d], Johanna Rapp[b,e], Timm Schäfle[f], Mirita Franz-Wachtel[g], Leonie Reetz[a,b,c], Ahmed M. A. Elsherbini[a,b,c], Boris Macek[g], Stephanie Grond[f], Hannes Link[b,e], Kay Nieselt[d], Bernhard Krismer[a,b,c], Andreas Peschel[a,b,c], Simon Heilbronner[b,c,h]

[a] Department of Infection Biology, Interfaculty Institute of Microbiology and Infection Medicine, University of Tübingen, 72076 Tübingen, Germany.

[b] Cluster of Excellence EXC 2124 Controlling Microbes to Fight Infections, 72076 Tübingen, Germany.

[c] German Center for Infection Research (DZIF), partner site Tübingen.

[d] Interfaculty Institute for Bioinformatics and Medical Informatics (IBMI), University of Tübingen, 72076 Tübingen, Germany.

[e] Department of Bacterial Metabolomics, Interfaculty Institute of Microbiology and Infection Medicine, University of Tübingen, 72076 Tübingen, Germany.

[f] Institute of Organic Chemistry, University of Tübingen, 72076 Tübingen, Germany.

[g] Proteome Center Tübingen, University of Tübingen, 72076 Tübingen, Germany.

[h] Interfaculty Institute of Microbiology and Infection Medicine, Institute for Medical Microbiology and Hygiene, UKT Tübingen, 72076 Tübingen, Germany.

Abstract

Biosynthetic gene clusters (BGCs) encoding the production of bacteriocins are widespread amongst bacterial isolates and are important genetic determinants of competitive fitness within a given habitat. Staphylococci produce a tremendous diversity of compounds and the corresponding gene clusters (Staphylococcal Antibiosis Islands - SAbIs) are frequently associated with mobile genetic elements, suggesting acquisition and loss of biosynthetic capacity. Pharmaceutical biology has shown that compound production in heterologous hosts is often challenged by the lack of optimal precursor supplies. Accordingly, many recipients produce low compound amounts or show reduced growth rates. To assess whether transfer of SAbIs between closely related *S. aureus* strains has similar effects, we model intra species transfer of a SAbI encoding the ribosomally synthesized and post-translationally modified peptide (RiPP) Micrococcin P1 (MP1). We found that acquisition of the SAbI by *S. aureus* RN4220 did allow immediate MP1 production but also imposed a metabolic burden. Adaptive evolution selected for strains with increased TCA-cycle activity, which enhanced metabolic fitness and levels of compound production. Metabolome analysis showed that the adaptive mutation increased the levels of central metabolites including citrate and α-ketoglutarate. This was found to be essential to overcome SAbI associated growth defects. Our results indicate that acquisition of SAbIs requires genetic and metabolic predispositions allowing the integration of bacteriocin production into the cellular metabolism. Inappropriate metabolic characteristics of recipients can entail physiological burdens, negatively impacting the competitive fitness of SAbI recipients within natural bacterial communities.

Introduction

It is increasingly recognized that biosynthetic gene clusters (BGCs) allowing the production of antibacterial compounds are omnipresent in bacterial communities [1]. These antibacterial compounds are frequently referred to as bacteriocins. They can either be produced ribosomally or by non-ribosomal systems and are hugely diverse in terms of molecular size and structure [2]. In line with their structural diversity bacteriocins have diverse molecular targets and killing mechanisms entailing diverse spectra of bacterial species that can be affected [2, 3]. Bacteriocin-producing bacterial lineages have recently gained increasing attention for their potential to displace human pathogens from various human body sites thereby preventing infection [4-6].

Gram-positive staphylococci are one example in this regard. The genus comprises various predominantly apathogenic human commensals such as *S. epidermidis*, *S. capitis*, *S. lugdunensis* and *S. haemolyticus* but also the frequently invasive pathogen *S. aureus*. Many

staphylococcal isolates show inhibitory activity against a diverse range of human nasal commensals and pathogens [7-9]. Interestingly, most identified BGCs appear to be associated with mobile genetic elements such as plasmids, transposons, IS-elements, or chromosomal islands with G+C contents diverging from the genome average [1, 4, 7]. This suggests that the BGCs are transferred between strains and lineages. These BGCs and the produced antimicrobials create strain rather than species specific variation [1, 10, 11]. Therefore, we propose to name the mobile genetic elements of staphylococci "Staphylococcal Antibiosis Islands" (SAbIs).

Transfer of SAbIs between strains or species represents a natural system for heterologous expression of antibacterial compounds. However, transfer of BGCs between classic antibiotic-producing bacterial species (e.g., streptomyces) showed that heterologous hosts do frequently produce only limited amounts of compound and adaptive mutations or changes in nutritional supplies are needed to optimise compound production [12-14]. The same might be true in the context of naturally occurring transfer of SAbIs between strains and species. It has to be considered, that acquisition of bacteriocin BGCs can put a physiological burden on the recipient cell. The novel genetic material needs to be propagated and, if functionally expressed, it entails production and secretion of high amounts of toxic secondary metabolites. Precursor molecules need to be channelled from primary metabolism and cellular energy levels might be reduced., entailing metabolic costs for the producer [15]. Finally, suboptimal producer-immunity against the compound can further entail physiological burdens [16]. Accordingly, it seems plausible that SAbI acquisition might represent a mixed blessing for bacterial cells. On the one hand, compound production will provide a competitive advantage when susceptible competitors are present. On the other hand, compound/SAbI associated burdens might lead to a reduced fitness of the producer and might require adaptive evolution to optimize compound production and fitness. Physiological burdens and cellular integration of SAbIs in staphylococci remains unclear. However, knowledge about this phenomenon is key to understand why SAbIs are largely strain specific and not species-wide conserved traits. Future approaches to use bacteriocin-producing bacterial strains to displace pathogens from human microbiomes will crucially depend on the availability of "healthy" strains stably producing high levels of antibiotic molecules.

We modelled SAbI-transfer between closely related *S. aureus* strains using the naturally occurring plasmid pD4-19 which encodes the BGC for biosynthesis of the thiopeptide bacteriocin micrococcin P1 (MP1). Transfer of the plasmid in *S. aureus* RN4220 allowed immediate MP1 production but caused growth defects. *In vitro* evolution experiments selected for strains with increased activity of the tricarboxylic acid cycle (TCA) thereby leading to significant changes in the levels of central metabolic molecules including citrate, α-

ketoglutarate, and several amino acids. The adaptation significantly increased compound production and simultaneously allowed overcoming SAbI-associated growth defects. Our data indicate that strain-specific genetic and metabolic predispositions of SAbI recipients will determine the levels of bacteriocin production and strain fitness. In turn, this will most likely determine the success of a SAbI recipient in the context of competitive environments.

Results

Micrococcin P1-BGC as a model SAbI

We speculated that transfer of SAbIs, especially costly synthesized RiPPs, would have a significant impact on the fitness of the recipient and sought to investigate this by modelling SAbI transfer between strains of the same species. Screening of our extensive collection of nearly 1500 nasal isolates of diverse bacterial species resulted in the identification of two *S. aureus* strains showing intra-species inhibition against the test strain *S. aureus* USA300 LAC. Whole genome sequencing (WGS) and genome analysis with antiSMASH 5.0 (bacterial version) revealed the presence of plasmids encoding BGCs for aureocin A70 [17] in strain *S. aureus* P1-22 and for the thiopeptide micrococcin P1 (MP1) [18] in strain *S. aureus* D4-19. The MP1 encoding plasmid pD4-19 had a size of 28 391 bp (Fig. 1A) and besides the 11 kb BGC (Fig. 1B), it encoded a β-lactamase which we considered useful for *in vitro* transfer experiments. Therefore, we focused on pD4-19 as a model SAbI.

The thiopeptide RiPP MP1 is targeting the bacterial ribosome [19], and an alternative ribosomal subunit (*tclQ*) provides producer resistance against the compound [19-21]. The MP1 BGC that was present on pD4-19 showed an overall similarity of 99% to the gene cluster identified by Liu et al. in an *S. hominis* isolate [18], suggesting the production of the same compound and transferability of the BGC. To validate the production of MP1, a small-scale purification of the compound from *S. aureus* D4-19 cells was performed using methanol extraction and high-performance liquid chromatography/mass spectrometry (HPLC/MS) analysis (Fig. 1C). We identified the mass of MP1 (1144.4 Da with the sum formula $C_{48}H_{49}N_{13}O_9S_6$), confirming the production of MP1 by *S. aureus* D4-19. To prove that the identified BGC is responsible for the observed antimicrobial activity, we performed random transposon mutagenesis. Strains without antibiotic activity were found to carry the transposon within the MP1 BGC (Fig. S1) strongly suggesting that exclusively MP1 was responsible for the antibiotic activity of *S. aureus* D4-19.
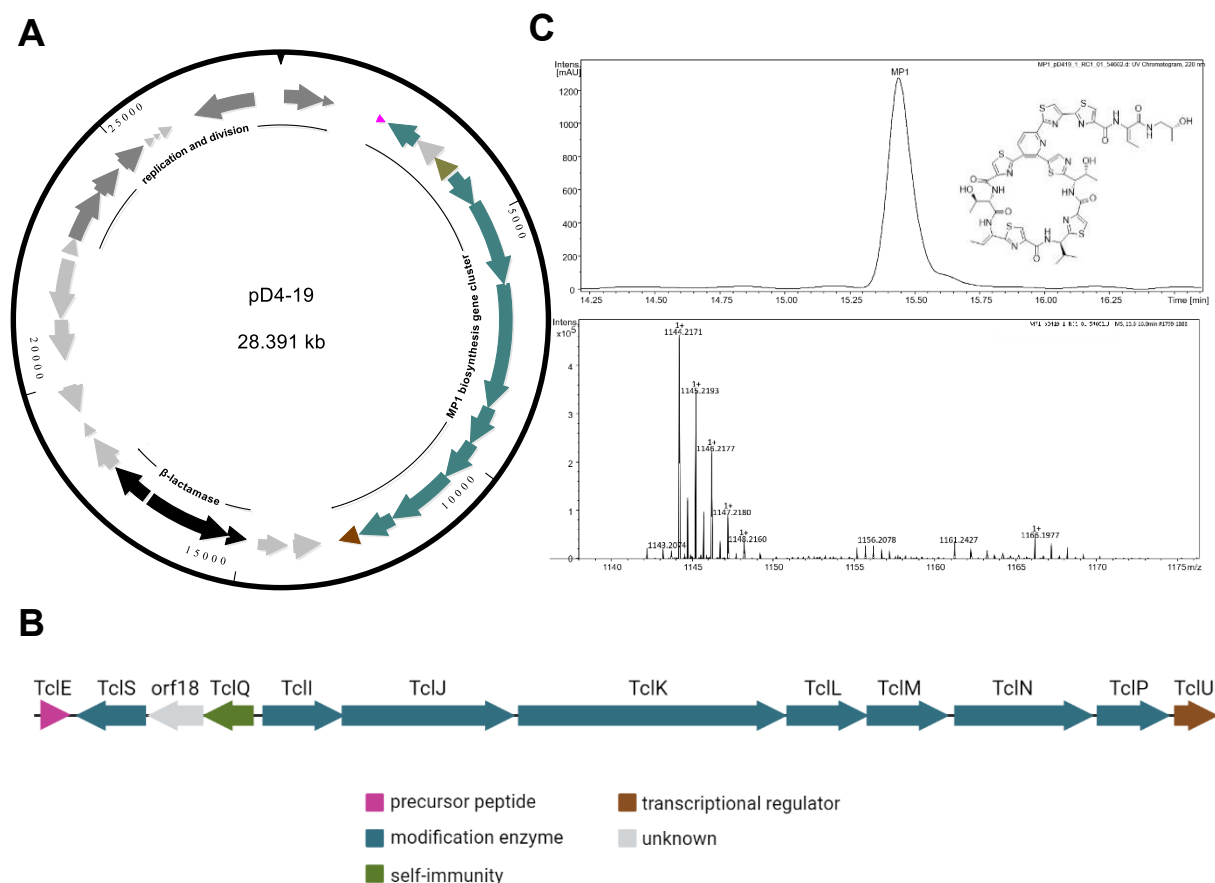
Figure 1: A) Map of plasmid pD4-19 that was identified in *S. aureus* D4-19 and that encoded the MP1 BGC (colour), a β-lactamase operon (black), several genes encoding for replication and division factors (dark grey) and hypothetical genes (light grey). **B)** Detailed view of the MP1 BGC. The annotated protein functions are indicated by different colours. **C)** HPLC-UV-chromatogram of extract from *S. aureus* D4-19 culture. Absorbance was measured in milli absorption units (mAU). MS spectrum confirming the mass of 1144.2171 $[MP1+H]^+$ for MP1. The final structure of MP1 is depicted.

Acquisition of the MP1 BGC confers the ability of compound production but also imposes a metabolic burden

We sought to investigate whether pD4-19 can be transferred to a related *S. aureus* strain and whether this entails significant physiological changes. *S. aureus* D4-19 belongs to clonal complex 8, and to avoid restriction modification (RM) barriers, we used the laboratory strain *S. aureus* RN4220 as recipient strain. This RM-deficient strain belongs to the same clonal complex, exhibits high transformation rates, and does not show inhibitory effects on other staphylococci. Finally, *S. aureus* RN4220 is highly sensitive to penicillin G (MIC = 0.015 µg/ml) allowing for the selection of pD4-19 which encodes a β-lactamase. The plasmid isolated from *S. aureus* D4-19 was used to transform *S. aureus* RN4220 by electroporation. After several unsuccessful attempts, we recovered a single individual transformant showing increased resistance to penicillin G. Plasmid isolation and restriction digestion confirmed that the strain *S. aureus* RN4220 had acquired the plasmid pD4-19 and propagated it as an

extrachromosomal element. As expected, *S. aureus* RN4220 pD4-19 showed antimicrobial activity against *S. aureus* USA300 LAC, most likely due to the acquired MP1-BGC (Fig 2A). However, the zone of inhibition was smaller than that of the original producer *S. aureus* D4-19. We speculated that the transformant produced less MP1 and analysed methanol extracts of cell pellets with identical cell numbers by HPLC-MS to confirm this. Interestingly, *S. aureus* RN4220 pD4-19 produced MP1 and additionally, a putative derivative of MP1 could be detected (Fig. 2B; Fig S2). However, the combined amount of MP1 and the putative derivative was threefold lower than the amount of MP1 produced by *S. aureus* D4-19 (Fig. 2C).

We performed growth curve analysis to investigate whether the acquisition of the MP1-BGC and the associated production of MP1 resulted in physiological changes and found *S. aureus* RN4220 pD4-19 to reach lower optical densities than the parental strain (Fig. 2D). To verify that the reduced growth was caused by MP1 production and not by other plasmid-associated effects, a mutant lacking the entire MP1 operon (*tclESQIJKLMNPU* + orf18) was constructed by allelic replacement. The resulting strain *S. aureus* RN4220 pD4-19 ΔMP1 lacked any antimicrobial activity against *S. aureus* USA300 LAC and reached a similar OD_{600} as the *S. aureus* RN4220 lacking the plasmid (Fig. S3A, S3B). This suggests that SAbI acquisition and the associated compound production represent a physiological burden to *S. aureus* RN4220. It has been reported that the production of antimicrobial compounds in staphylococci can be limited by insufficient immunity of the producer [16]. We therefore tested whether this phenomenon was also apparent here. We created mutants lacking the core peptide of the MP1 BGC (ΔPP) in the background of the original producer *S. aureus* D4-19 as well as in *S. aureus* RN4220 pD4-19. Accordingly, the mutants did not produce any MP1 but expressed the alternative ribosomal subunit (*tclQ*) that provides resistance. Using purified MP1 we found that the test strain *S. aureus* USA300 LAC and the WT *S. aureus* RN4220 were highly sensitive to the compound (MIC<0,2 µg/ml). In contrast, none of the MP1 concentrations used showed any inhibitory effect on the growth of the two ΔPP strains (MIC>100 µg/ml) (Fig. S4). This suggests that reduced resistance levels were not responsible for the impaired growth of *S. aureus* RN4220 pD4-19.
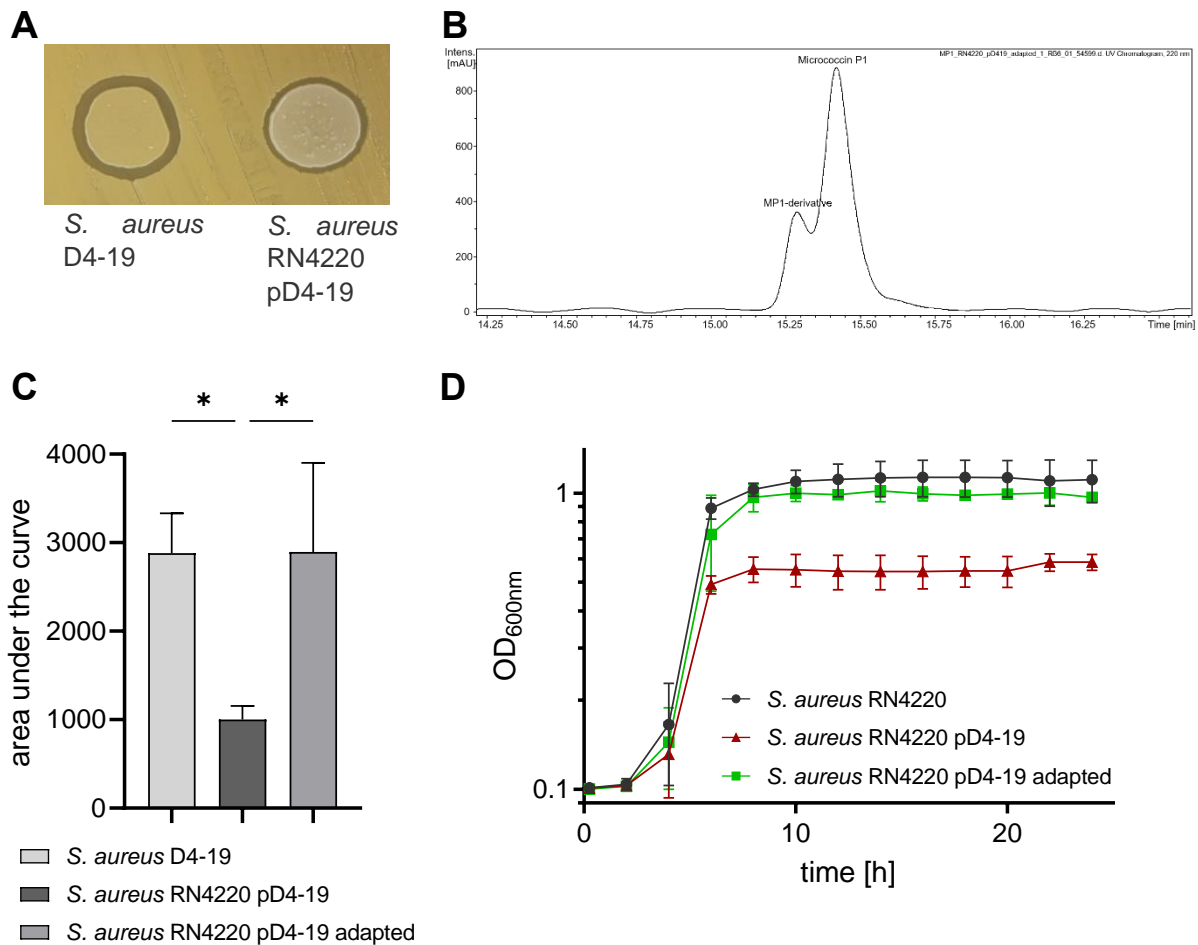
Figure 2: A) Spot assay of *S. aureus* D4-19 and *S. aureus* RN4220 pD4-19 on *S. aureus* USA300 LAC, demonstrating antimicrobial activity of both strains against the indicator strain. **B)** HPLC-UV-spectrum of cell pellet extracts of *S. aureus* RN4220 pD4-19, confirming the production of MP1 by this strain. A MP1-derivative, with slightly shorter retention time compared to MP1, is also produced by this strain. **C)** Calculation of relative quantity of MP1 produced by strains *S. aureus* D4-19, *S. aureus* RN4220 pD4-19 and *S. aureus* RN4220 pD4-19 adapted. MP1 amount is calculated as area under the curve. The adapted strain produces similar amounts as the nasal isolate. MP1 production is significantly reduced in the newly transformed strain *S. aureus* RN4220 pD4-19. **D)** Growth curves of *S. aureus* RN4220, *S. aureus* RN4220 pD4-19 and *S. aureus* RN4220 pD4-19 adapted grown in BM over 24 hours in a 24 well plate. *S. aureus* RN4220 pD4-19 showing a growth defect compared to the other two strains. Statistical significance was determined using an ordinary One-way ANOVA (Tukey's multiple comparisons test) (*$p < 0.05$).

Adaptive evolution increases compound production and relieves the metabolic burden

We speculated that the metabolism of *S. aureus* RN4220 might not be optimal to support the production of high levels of MP1 and that adaptational mutations might optimize compound yield and strain fitness over time. To test this, we performed an adaptive evolution experiment. Strain *S. aureus* RN4220 pD4-19 was inoculated into BM medium and passaged daily over 28 consecutive cultures. The colonies that were isolated from the evolution experiment were larger than those formed by the original transformant, and the recovered strain was named *S.*

aureus RN4220 pD4-19 adapted. Growth curve analysis confirmed that the new strain reached OD$_{600}$ values similar to those of the *S. aureus* RN4220 WT strain (Fig. 2D). Additionally, *S. aureus* RN4220 pD4-19 adapted produced comparable levels of MP1 as *S. aureus* D4-19 and 2,86-fold more than the parental strain *S. aureus* RN4220 pD4-19 (Fig. 2C). Interestingly, derivate appearance was observed despite the adaptation (Fig. S2) suggesting that this phenomenon was not associated with disturbed metabolic fluxes that might have caused biosynthesis intermediates to accumulate.

To identify mutations explaining the phenotypic differences between *S. aureus* RN4220 pD4-19 and RN4220 pD4-19 adapted, we performed whole genome analysis of both strains. Unexpectedly, we identified only a single point mutation in *S. aureus* RN4220 pD4-19 adapted which was located upstream of the annotated *S. aureus* RN4220 *citZ* gene (ACCFDFCE_01589) encoding citrate synthase. A more detailed analysis showed that the mutation in the adapted strain created a functional in frame start codon (ATG instead of ATA) extending the annotated open reading frame of *citZ* by 75 nucleotides (Fig. 3A). An "AG"-rich region resembling a putative ribosomal binding site (RBS) is present 6 bp upstream of the newly created start codon suggesting an appropriate translational start site. In contrast, the annotated shorter allele within the *S. aureus* RN4220 WT lacks an obvious Shine-Dalgarno sequence and relies on a "TTG" start codon which is rarely used in *S. aureus* [22]. Accordingly, we speculated that the *citZ* gene of strain *S. aureus* RN4220 is in fact truncated and potentially non-functional. To further investigate this, we compared the *citZ* allele of *S. aureus* RN4220 to those of other *S. aureus* strains and found that the shorter *citZ* allele appears to be conserved in the ancestral lineage of *S. aureus* RN4220 including strains NRS146, NRS133 and VC40 back to *S. aureus* NCTC8325, which was originally described in 1965 [23] (Fig. S5). All other 3 834 human associated *S. aureus* genome sequences of the NCBI database carry the full-length *citZ* allele as found in *S. aureus* RN4220 pD4-19 adapted.

Accordingly, we hypothesised that the adaptive mutation would allow production of the full-length protein compared to a truncated version in the *S. aureus* RN4220 WT, if translation is possible despite the missing RBS, and stimulate the central metabolism. To validate this, we cloned the natural *citZ* allele of the *S. aureus* RN4220 WT and that of the adapted mutant with a terminal hexahistidin-tag into the xylose-inducible expression vector pRB473-xylR. Importantly, for both alleles we included the entire annotated coding sequence and an additional stretch of DNA covering 41 bp upstream of the ATA/ATG codon affected by the adaptive mutation, to recreate the genetic context. Both constructs were transferred into *S. aureus* RN4220, and CitZ-His levels were assessed by infra-red western blotting. CitZ levels were strongly increased when the adapted allele was expressed (Fig. 3B). However, we also found the WT allele to allow low level production of apparently full-length CitZ (43 kDa),

suggesting that *S. aureus* RN4220 WT inefficiently uses "ATA" as a non-canonical start codon but produces full length citrate synthase.

This hypothesis was further confirmed by the subsequent proteome analysis. An eleven amino acid motif (GLEGVIAAETK) that can only be a fragment of full length CitZ protein was found in both strains. However, it was 20-fold more abundant in the adapted strain compared to the original transformant (Fig 3C). This confirmed that both strains translate the CitZ mRNA using the ATA/ATG codon affected by the point mutation. However, the efficiency of translation is strongly increased by the adaptive mutation entailing increased levels of CitZ.
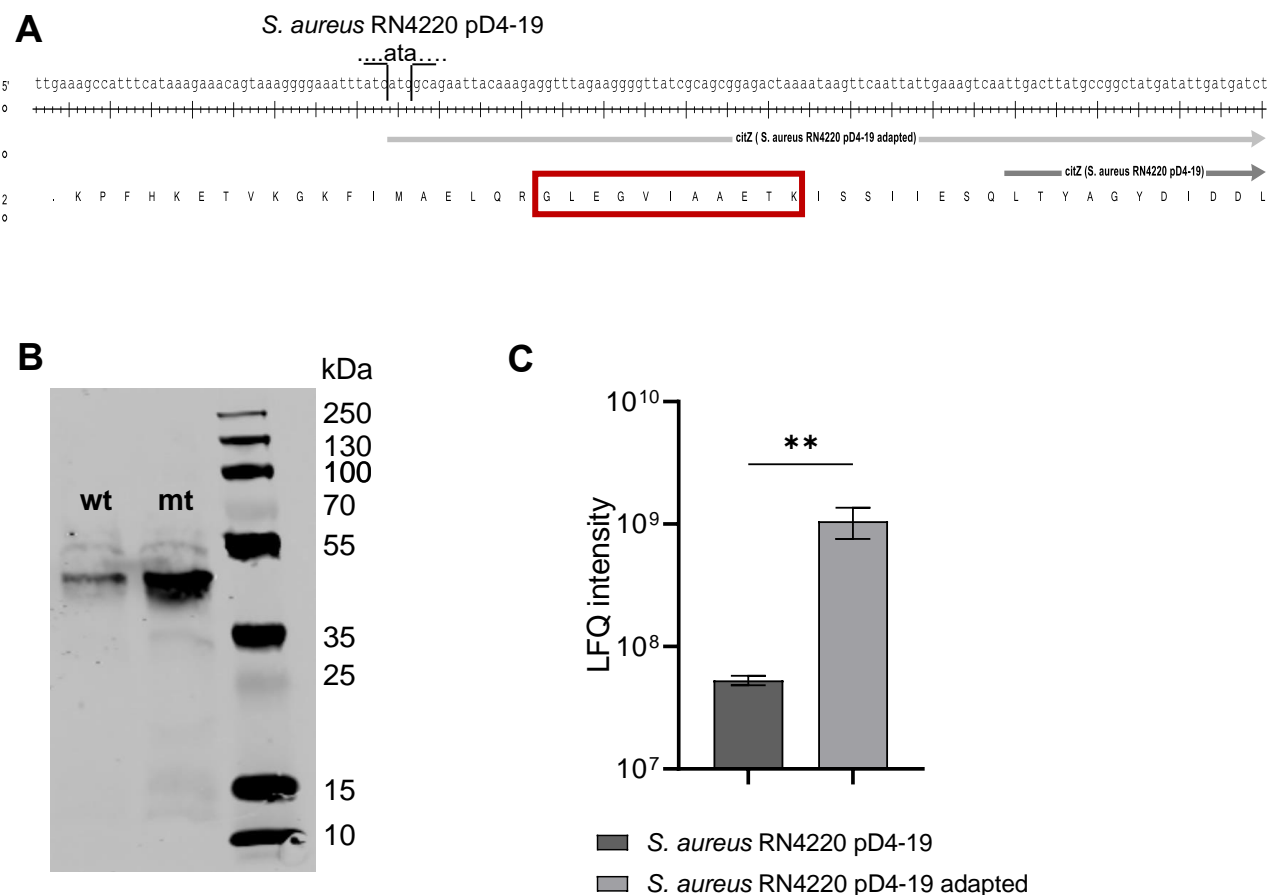
Figure 3: A) Promoter region and start site of *citZ* (ACCFDFCE_01589) gene from *S. aureus* RN4220 pD4-19 (wt) (dark grey) and *S. aureus* RN4220 pD4-19 adapted (mt) (light grey). The wt *citZ* has a delayed start codon compared to the mt allel, where ATA is exchanged to ATG, leading to an earlier transcription start of *citZ* in *S. aureus* RN4220 pD4-19 adapted. This mutation reverts CitZ to a full-size protein, similar to that of other staphylococci. The red box highlights the part of the amino acid sequence of CitZ that was used for the analysis shown in C). **B)** Western blot of cell extracts expressing the wt CitZ protein and the mt CitZ protein generated from *S. aureus* RN4220 pRB473-XylR-6xHis-*citZ* (wt) and *S. aureus* RN4220 pRB473-XylR-6xHis-*citZ* (mt). CitZ has a size of 42.6 kDa and can be detected in both extracts, but in higher amounts in the mt CitZ expressing strain, indicating leaky expression of wt CitZ. **C)** Proteome data were analysed for the presence of the protein fragment GLEGVIAAETK (depicted in A) to confirm leaky expression of wt CitZ with ATA as startcodon. The indicated fragment can be found in both proteomes, but with a 20-fold increase in *S. aureus* RN4220 pD4-19 adapted. Statistical significance was determined using an unpaired t-test (**$p < 0.01$).

Increased citrate levels allow overcoming the SAbI associated burden

We assumed that the increased CitZ levels would foster citrate biosynthesis and thereby stimulate the central metabolism of *S. aureus* RN4220 ultimately leading to improved compound production and growth. Measuring the intracellular concentration of citrate confirmed increased levels of the metabolite in the adapted strain compared to the original transformant (Fig. 4A). Additionally, exogenous addition of 5 mM sodium citrate allowed the original *S. aureus* RN4220 pD4-19 to overcome the bacteriocin-associated growth defects (Fig. 4B). These results indicated that appropriate integration of MP1 production into the cellular metabolism is dependent on appropriate citrate availability. Most likely MP1 production disbalances the pool of TCA cycle derived metabolites causing growth defects when citrate biosynthesis is too low.
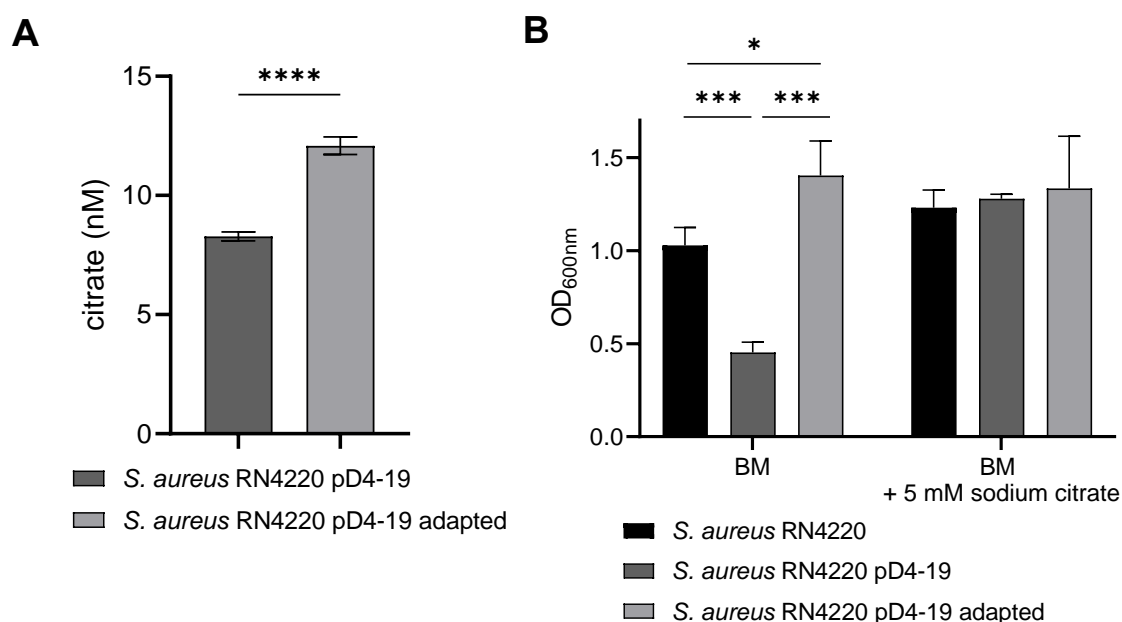

Figure 4: A) Significantly reduced citrate levels in *S. aureus* RN4220 pD4-19 compared to *S. aureus* RN4220 pD4-19 adapted were determined using the citrate assay kit (MAK057) from Sigma-Aldrich. Statistical significance was calculated using an unpaired t-test (****$p < 0.0001$). **B)** Endpoint OD_{600nm} of *S. aureus* RN4220, *S. aureus* RN4220 pD4-19 and *S. aureus* RN4220 pD4-19 adapted in standard growth medium and supplemented with 5 mM sodium citrate grown in a 24 well plate. OD_{600nm} after 24 hours shows restoration of growth by the addition of sodium citrate for *S. aureus* RN4220 pD4-19. Statistical significance was calculated using an ordinary One-way ANOVA (Tukey's multiple comparisons test) (*$p < 0.05$, **$p < 0.01$, ***$p < 0.001$, ****$p < 0.0001$).

Adaptive mutation increases metabolic activity of the MP1 producer

We reasoned that MP1 production, and the associated increasing demands of cellular citrate might have pleiotropic effects on the bacterial physiology. To gain insights into the general levels of metabolites, we performed Flow Injection Mass Spectrum (FI-MS)-based untargeted metabolomics of cell lysates of *S. aureus* RN4220 WT, the initial transformant as well as the

adapted strain, and analysed the datasets using hierarchical clustering (Fig 5). The analysis showed that the metabolic profiles of the *S. aureus* RN4220 WT and of the adapted strain clustered together while the profile of the initial transformant was dissimilar. This strongly suggested that acquisition of the SAbI-encoding plasmid impacts the general metabolism of the recipient, and these effects are widely corrected by the adaptive mutation of *citZ*.
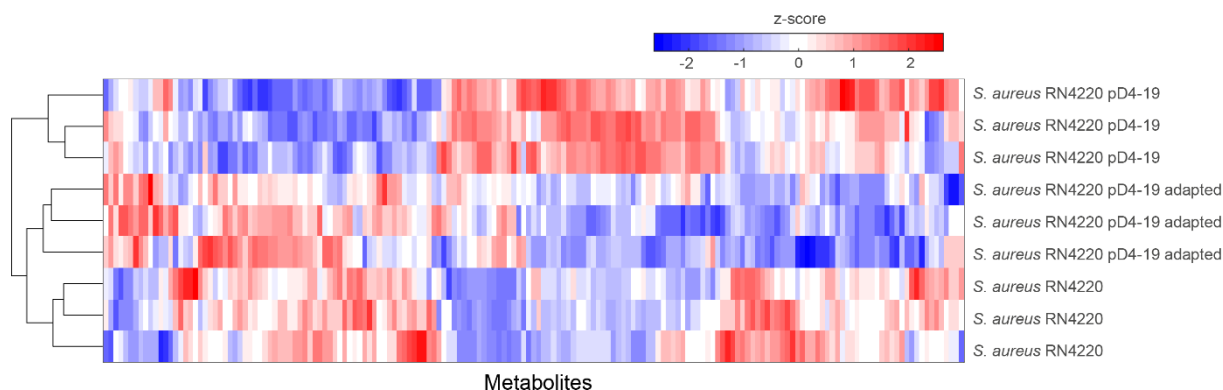

Figure 5: Hierarchical cluster plot of metabolites obtained via FI-MS analysis. All metabolites [M+H]$^+$ measured via FI-MS are depicted, [M-H]$^-$ values of metabolites cysteine, citrate (and isobars isocitrate and 5-dehydro-4-deoxy-D-glucarate), α-ketoglutarate, fumarate, malate, oxaloacetate, pyruvate, acetate, glucose (and isobars galactose, allose, fructose, mannose and myo-inositol) and lactate (and its isobars glyceraldehyde and dihydroxyacetone) were added to the analysis. The colours in the heat map reflect the relative metabolite abundance level according to the z-score.

We speculated that especially central metabolites of glycolysis, tricarboxylic acid cycle (TCA) as well as of amino acid biosynthesis and turnover might be relevant in the context of MP1 production. We used a combination of LC-MS/MS and FI-MS analysis to investigate the levels of these central metabolites (Fig. 6A/B, S6, S7, S8, S9). Although our analysis did not allow to distinguish between citrate and its two isobars (isocitrate, 5-Dehydro-4-deoxy-D-glucarate), the metabolomic data confirmed the citrate levels as measured via the citrate assay kit (Fig. 4A) and suggested a decrease in citrate levels upon plasmid acquisition and a strong increase upon adaptive mutation (Fig. 6A). Besides this observation, levels of glycolysis intermediates (3-phosphoglycerate, phosphoenolpyruvate, pyruvate, acetyl-CoA) showed an increase upon plasmid acquisition, suggesting insufficient feeding of the TCA cycle. Upon adaptive mutation, levels of these metabolites decreased to WT levels or even lower. Additionally, the levels of α-ketoglutarate raised, all suggesting increased activity of the central metabolism (Fig. 6B, S7). Interestingly, we found that pD4-19 acquisition accounts for the accumulation of various amino acids (aspartate and asparagine, alanine, tyrosine and tryptophan, threonine, glycine, and histidine) pointing to a reduced protein biosynthesis rate [24]. This general accumulation of amino acids was not observed in the CitZ adapted strain. In contrast, amino acid levels of the latter were frequently reduced compared to the WT, suggesting their efficient usage in protein biosynthesis (Fig. 6B, S6). An exception to this general observation were the levels of

glutamate, glutamine and proline which were increased in both, the initial transformant and adapted strain. Glutamate and glutamine serve as precursors for several amino acids (including proline) and bacteria create glutamate or glutamine by condensation of α-ketoglutaric acid or glutamate with ammonium as a means to store nitrogen. Accordingly, their levels are regarded as an indicator of nitrogen availability [25] and connect the urea cycle to amino acid biosynthesis. Accumulation of urea cycle intermediates (ornithine, citrulline, argininosuccinate) was only observed in *S. aureus* pD4-19 and was abrogated upon adaptive mutation, suggesting that the intermediates are efficiently used to feed the TCA cycle and with-it amino acid biosynthesis in this strain (Fig. 6B, S8).

Besides the provision of precursors for metabolic processes, the activity of the TCA cycle is crucially important for the aerobic generation of ATP. In the presence of glucose, *S. aureus* produces ATP by fermentation and produces predominantly acetate which is secreted. Only after glucose is depleted, acetate is consumed and decarboxylated using the TCA cycle and the respiratory chain [26, 27]. This metabolic switch has been reported to occur after approximately 5 hours of growth [27] which matches the observed starting point of growth deficiency in our experiments. We noted that the intracellular levels of acetate were increased within the transformant (Fig. 6B, S9), supporting the idea that TCA cycle activity might not be sufficient in this strain to generate sufficient ATP. We failed to detect ATP in our metabolome analysis, therefore we quantified extracellular acetate levels of strains as an indirect means to assess TCA-cycle dependent generation of ATP (Fig 6C). We found acetate to accumulate in the culture supernatants of *S. aureus* RN4220 and *S. aureus* pD4-19 while accumulation was strongly reduced in the adapted strain and dropped quickly after 6h of growth, suggesting an increased rate of oxidative decarboxylation upon restoration of the *citZ* allele.
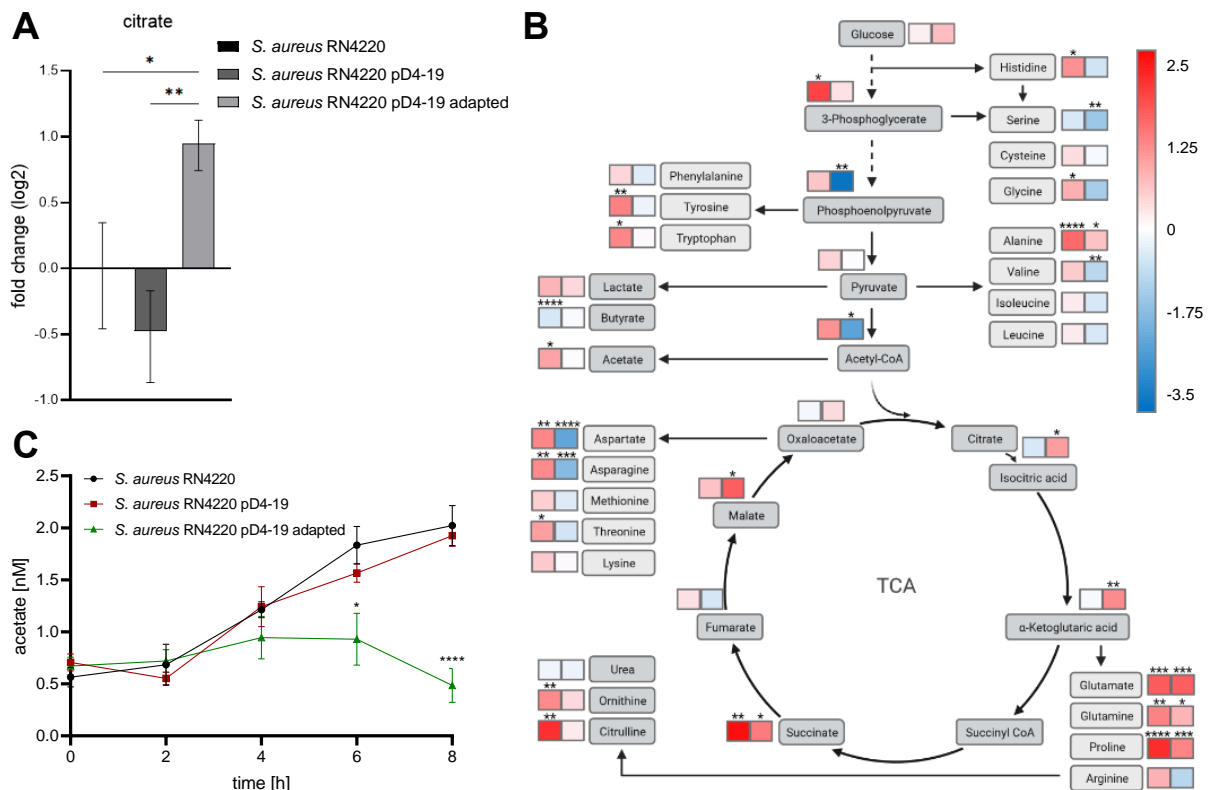
Figure 6: A) Changes (log2-fold) of cytoplasmic citrate levels in *S. aureus* RN4220 pD4-19 (dark grey) and *S. aureus* RN4220 pD4-19 adapted (light grey) compared to *S. aureus* RN4220 (black). Citrate and its isobars isocitrate and 5-dehydro-4-deoxy-D-glucarate [M-H]⁻ were measured via FI-MS. **B)** Metabolic differences, depicted as log2-fold changes, of *S. aureus* RN4220 pD4-19 (left box) and *S. aureus* RN4220 pD4-19 adapted (right box) compared to *S. aureus* RN4220. Red: Increase in metabolite levels compared to *S. aureus* RN4220. Blue: Decrease of metabolite level compared to *S. aureus* RN4220. Metabolic pathways are not depicted in detail. **C)** Extracellular acetate levels were measured in *S. aureus* RN4220, *S. aureus* RN4220 pD4-19 and *S. aureus* RN4220 pD4-19 adapted after 0, 2, 4, 6 and 6 hours of growth in BM with the acetate assay kit (MAK086) from Sigma-Aldrich. The p-values were calculated using an ordinary One-way ANOVA (Tukey's multiple comparisons test). Statistical significance is indicated by $*p < 0.05$, $**p < 0.01$, $***p < 0.001$, $****p < 0.0001$.

Transcriptomic signatures support increased metabolic activity upon adaptive mutation

We performed transcriptome analysis of the strains, to investigate whether increased compound production upon adaptation might be the result of differential expression of pD4-19 associated genes. Expression of all plasmid genes did not differ significantly between the transformant and the adapted strain (Fig. S10A). This suggests that the metabolic changes rather than increased expression of MP1 biosynthesis genes or resistance determinants contribute to the increased growth.

To analyse this further, we extracted differentially regulated genes between the transformant and the adapted strain and performed GO term analysis to identify the general cellular

functions altered in response to the adaptive mutation in *citZ*. The results supported our hypothesis that the increased citrate levels enhanced the cellular and metabolic activity of the strain. The adaptive mutation in *citZ* increased transcription of the translational machinery (30S and 50S ribosomal subunits), pointing to a generally enhanced protein biosynthesis (Fig. 7). This was accompanied by upregulation of pathways for the biosynthesis of the cofactors folate (*folPBK*), thiamine (*thiEM*) and riboflavin (*ribAB*). Increased amino acid turnover was indicated by upregulation of the L-tryptophan-biosynthesis pathway (*trpCDEFG*) as well as of catabolic pathways for threonine (*ilvA*) and alanine (*ald1*). Additionally, upregulation of the genes encoding the urea transporter Utp and each gene of the urease operon (*ureABCEFGD*), catalysing the hydrolysis of urea into carbon dioxide and ammonia, was observed (Fig. 7, S10B). This indicates increased generation of ammonia, most likely to fuel the urea cycle and to stimulate the TCA cycle and amino acid biosynthesis as discussed above (Fig. S8). We observed upregulation of the twin-arginine translocation (Tat) pathway in the adapted mutant (Fig. 7). The Tat system was described to be responsible for the translocation of the iron-dependent peroxidase (FepB) which is involved in iron uptake [28]. Acquisition of iron is important for bacteria as iron is essential for many cellular processes like transcription, metabolism, and energy generation via respiration. Upregulation of the TAT system might contribute to satisfy increased energy demands of the adapted mutant.

Transcriptional analysis also revealed that the balance of osmoprotective molecules was impacted by the adaptive mutation, as we found transcription of the carnitine transporter *opuC* (*opuCA/CB/CC/CD*) to be downregulated in *S. aureus* RN4220 pD4-19, which is in line with reduced carnitine levels detected via metabolome analysis (Fig. S9, Fig. S10) [29]. Instead, the osmoprotectant choline was increased in both, the original transformant and the CitZ adapted strain. Since several amino acids act as osmoprotectants (especially proline and glycine) [30, 31], we assume that accumulation of these amino acids in response to pD4-19 acquisition was responsible for the altered osmoprotective balance. Our transcriptome analysis identified several genes that were differentially expressed upon pD4-19 acquisition and whose expression retained altered upon adaptive evolution, arguing for intrinsic effects of the plasmid. Among those genes several were associated with virulence and immune interference including hemolysins (*hlgB/C*, *hlY*), the capsule biosynthesis operon *cap,* the serine protease locus *spl*, and the type seven secretion system *ess* (Fig S10).
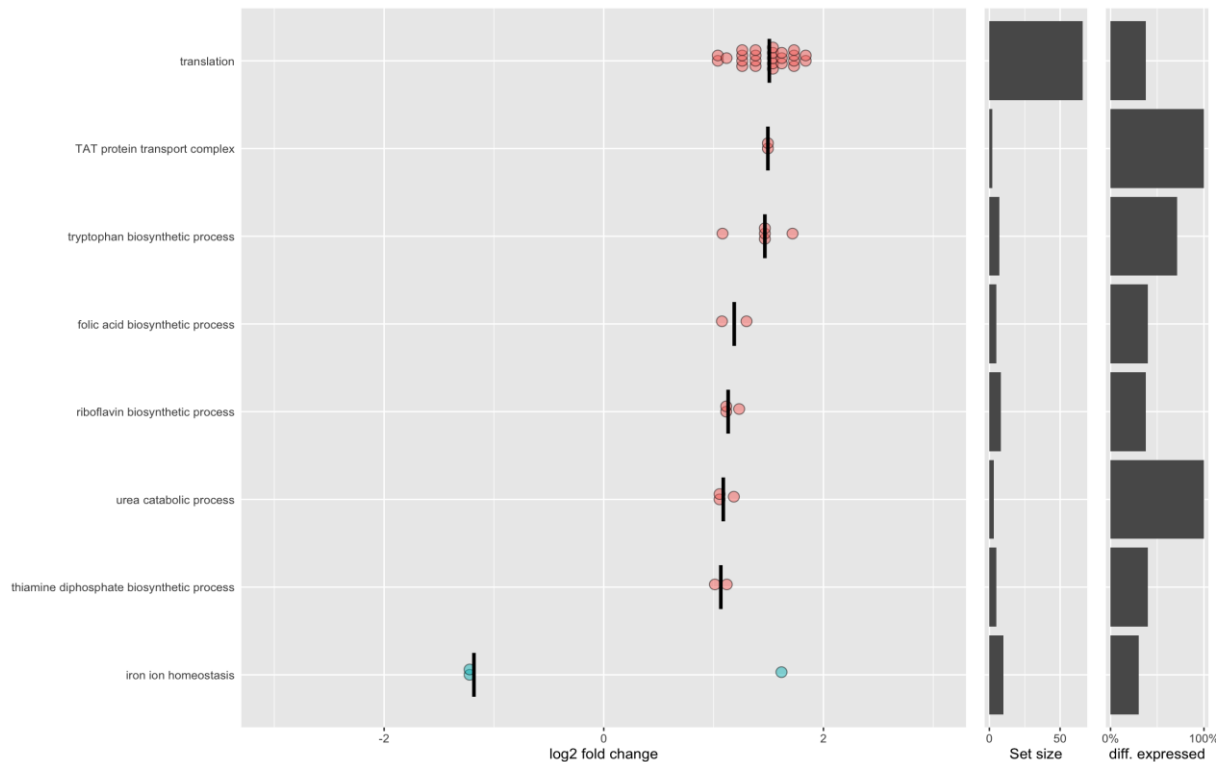
Figure 7: Selection of significantly enriched Go terms and the corresponding differentially expressed genes obtained via RNAseq. Depicted is the log2 fold change in expression levels of *S. aureus* RN4220 pD4-19 adapted compared to *S. aureus* RN4220 pD4-19. Increased median expression is indicated in red, decreased median expression in blue. The set size indicates the number of genes covered by the GO term. The last column indicates how many genes of the set are differentially expressed (in %).

SAbl acquisition and adaptive evolution influence biofilm formation

Amongst the transcriptionally increased virulence factors, we also identified the *icaADBC* operon encoding the synthesis of the polysaccharide intercellular adhesin (PIA) and thereby responsible for biofilm formation (Fig. S10). Transcriptomic analysis showed the *icaADBC* genes to be upregulated upon pD4-19 acquisition and the strain showed indeed strongly increased levels of biofilm (Fig 8). Interestingly, this phenotype was reverted upon adaptive evolution although transcription of *icaADBC* remained elevated and only the transcriptional levels of *icaD* decreased (Fig. 8, Fig S10). This suggests that the *icaD* gene product is crucial for biofilm formation which has been suggested previously [32] The reduced biofilm formation of the adapted strain might also be the consequence of the downregulation of *msa*, a modulator of s*arA* expression. Indeed, inactivation of *msa* has been shown to result in reduced and unstable biofilm formation which can explain our observations [33].
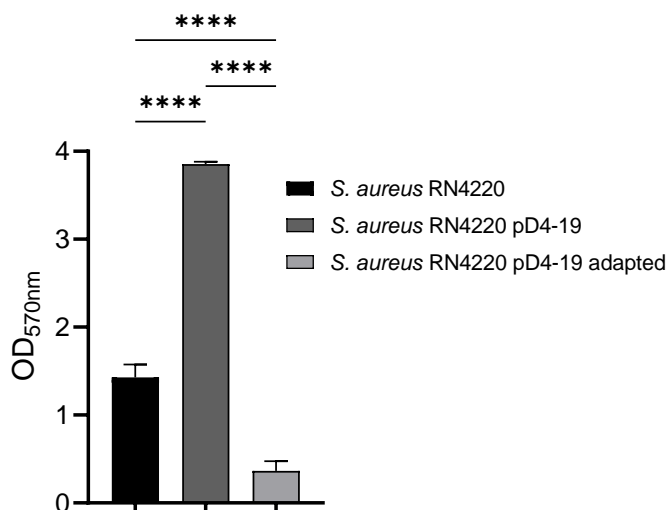
Figure 8: Biofilm formation of *S. aureus* RN4220, *S. aureus* RN4220 pD4-19 and *S. aureus* RN4220 pD4-19 adapted grown in BM. Statistical significance was calculated using an ordinary One-way ANOVA (Tukey's multiple comparisons test) (****$p < 0.0001$).

Discussion

Using our collection of nasal staphylococcal isolates, we identified the *S. aureus* strain D4-19 carrying a plasmid encoding the MP1 BGC. A number of studies identified MP1-BGCs in a variety of staphylococcal species, including *S. aureus* [34], *S. epidermidis* [35], *S. equorum* [36], *S. pseudintermedius* [37], *S. agnetis*, and *S. hominis* [18]. Also, an isolate from *Mammaliicoccus sciuri* (former *Staphylococcus sciuri*) [38] showed production of MP1. Additionally, the NCBI database includes various homologous sequences from distantly related *S. aureus* strains as well as many coagulase-negative staphylococci. This suggests intra- and inter-species horizontal transfer of the BGC, a perception that is supported by the fact that the so far identified MP1 gene clusters in staphylococci are located on plasmids which are per definition mobile genetic elements.

It is well recognised that bacteriocin production is associated with metabolic costs for the producing cell and expression is therefore frequently regulated in complex ways and dependent on cell densities or on the presence of competitors [39, 40]. Compound-production generates metabolic burdens as the responsible gene cluster needs to be propagated, precursors need to be channelled from the primary metabolism and sufficient self-immunity needs to be established. This concept might be of special relevance for RiPPs such as MP1 as their production relies on cellular tRNA pools and sudden expression upon SAbI acquisition might therefore disturb metabolic fluxes. It seems therefor likely that cellular fitness in the context of bacteriocin-production requires adjustments of metabolic pathways. Our

experiments showed that acquisition of the plasmid pD4-19 enabled production of bioactive MP1. However, the BGC-recipient produced significantly less compound than the original host of the plasmid while simultaneously a growth defect compared to the parental strain was apparent. Increased availability of citrate, of exogenous or endogenous origin, improved compound production and abrogated any growth defects. Interestingly, we found *S. aureus* RN4220 to carry a malfunctioning *citZ* allele, limiting the levels of citrate synthase, of citrate and most likely also the activity of the entire TCA cycle. Importantly, the entire lineage of *S. aureus* NCTC8325 (parental lineage of *S. aureus* RN4220) developed and maintained the malfunctioning *citZ* allele. Although *S. aureus* RN4220 has been used for decades to study *S. aureus* physiology and virulence, obvious fitness defects compared to other environmental isolates have never been reported, suggesting that low-level production of CitZ is in general sufficient for the lineage. However, the acquisition of pD4-19 made the metabolic shortcomings of the lineage apparent. The most prominent phenotype of TCA cycle deficient mutants is a growth defect that manifests after approximately 5 hours of growth in glucose containing medium [27]. This is due to the fact that *S. aureus* preferentially degrades glucose via glycolysis or the pentose phosphate pathway and fermentation to produce acetate [26, 27]. Concurrently, catabolite repression of glucose inhibits the TCA cycle [41]. Only after glucose is consumed, acetate catabolism demands TCA cycle activity to create ATP and to sustain growth [27]. Interestingly we observed that pD4-19 and the associated MP1 production entailed premature growth arrest as well as increased levels of pyruvate and acetyl-CoA as well as extracellular accumulation of acetate all of which are hallmarks of TCA cycle-deficient strains [27]. It is tempting to speculate that MP1 production entailed excessive channelling of TCA intermediates into the biosynthesis of amino acids, going along with increased needs of ATP, ultimately leading to premature growth arrest of the strain. Restoration of a fully functional *citZ* allele restored the growth defect, reduced acetyl-CoA levels and increased the levels of citrate and α-ketoglutarate. Simultaneously, accumulation of extracellular acetate was limited and dropped rapidly after 6 hours of growth. This strongly suggests increased levels of oxidative decarboxylation and an associated increase in the cellular ATP levels, although we failed to assess ATP-levels in our metabolomic analysis. Restoration of the *citZ* allele also entailed a strong increase in expression of the translational machinery, cofactor biosynthesis, and of the urea cycle, all suggesting an increase of protein biosynthesis and turnover supporting the positive effect of the mutation on the cellular metabolism.

Restoration of the *citZ* allele did also enhance MP1 produced by the lineage. It is well accepted, that expression of antibiotic BGCs in heterologous hosts can be limited due to inappropriate supply of cellular precursors. This is of special relevance for the production of NRPS-PKS-derived compounds that frequently rely on special precursors such as none-proteinogenic amino acids or unusual carbohydrates. Exemplarily, overexpression of rhamnose and

forosamine biosynthetic pathways improved 1000-fold the biosynthesis of the polyketide antibiotic spinosad [42], and medium optimisation to provide appropriate precursors has proven to be an efficient strategy to enhance compound production [12]. Similarly, optimisation of the microbial central metabolic processes including glucose, amino acid or fatty acid metabolism can boost compound production in heterologous hosts [43]. For RiPPs like MP1, the relevance of this concept is less clear, as the compounds are produced using the ribosomal machinery which relies on the cellular pool of aminoacyl-tRNAs. This ensures that precursor molecules are generally available, and compound-production is possible. However, it seems plausible that RiPP production can disbalance the pool of aminoacyl-tRNAs thereby limiting compound production or even impacting cellular fitness. This hypothesis is supported by the finding that addition of the amino acids glutamate, glycine, serine and threonine as well as the addition of maltose enhanced the production of the RiPP gallidermin [44]. However, our metabolic analysis showed that at the time point of growth arrest, amino acid levels were not depleted in the pD4-19 recipient arguing against amino acid limitation as the underlying reason and suggesting ATP limitation to be responsible.

The relevance of inappropriate TCA cycle activity is further underlined by the fact that the initial transformant produced high levels of biofilm which was abrogated upon adaptive mutation in *citZ*. Several studies associate TCA cycle activity with the capacity of Staphylococci to form biofilms. A major factor determining staphylococcal biofilm formation is the production of the polysaccharide intracellular adhesin (PIA) [45, 46]. We found the responsible *ica* genes to be strongly upregulated upon pD4-19 acquisition. Vuong et al. described that reduced TCA cycle activity increased PIA production in *Staphylococcus epidermidis* [47], and TCA-deficient mutants showed regular expression of the *ica* genes and the channelling of carbohydrates into PIA-synthesis [48]. Additionally, it was described that citrate as well as TCA cycle intermediates can stimulate expression of the fibronectin-binding proteins FnbA and FnbB leading to *ica*-independent biofilm formation [49]. However, we did not observe differences in *fnbA/fnbB* expression levels in our experiments, suggesting that this mechanism is not relevant for biofilm formation in *S. aureus* RN4220 pD4-19.

Finally, it also has to be considered that effects that are independent of cellular metabolites might impact the fitness of antibiotic producers. Similar to our experiments, it has been observed that production of the lantibiotics epidermin and gallidermin represent a physiological burden to the producing staphylococcal strain [16]. This effect was attributed to insufficient immunity of the producer strains entailing increased cell lysis. We did not observe different levels of resistance to MP1 between the different strains used in our study, suggesting that insufficient immunity does not substantially contribute to the observed phenotypes. Most likely due to the different modes of action and the associated resistance mechanisms. Lantibiotics

target lipid I, II, III in the bacterial membrane, ultimately damaging the integrity of the cell envelope and inducing lysis [16, 50]. Resistance is imperfect and relies on the active efflux of lantibiotics [51, 52]. In contrast, MP1 targets the bacterial ribosome [19] and full resistance is provided by the expression of an alternative L11 ribosomal subunit [53]. Interestingly, accumulation of amino acids similar to that observed in the pD4-19 recipient is known to be induced by antibiotic compounds targeting the bacterial ribosome [24]. However, expression of the plasmid associated-resistance determinant did not change upon adaptive mutation in *citZ* suggesting that altered levels of autoimmunity are not causative for the observed increase of cellular fitness.

In general, our observations support a model in which pD4-19 acquisition and associated compound production drain the levels of TCA-cycle intermediates along with the levels of cellular ATP and entail pleiotropic effects including growth deficiency, reduced compound production and increased biofilm formation .

Material and Methods

Strains and growth conditions

The *Staphylococcus* strains used in this study were *S. aureus* D4-19, *S. aureus* RN4220*, S. aureus* USA300 LAC. Further strains generated during this study were *S. aureus* RN4220 pD4-19, *S. aureus* RN4220 pD4-19 adapted, *S. aureus* RN4220 ΔPP, *S. aureus* RN4220 ΔMP1. Overexpression strains were constructed in *S. aureus* RN4220 background carrying the plasmid pRB473-xylR-6xHis-citZ, with *citZ* deriving from either *S. aureus* RN4220 pD4-19 or *S. aureus* RN4220 pD4-19 adapted. The construction of the plasmids and knockouts is described below. *Escherichia coli* DC10B or *E. coli* Sa08B were used as the cloning host for further transformation in *S. aureus* D4-19 or *S. aureus* RN4220.

Basic medium (BM; 1% soy peptone A3 [Organotechnie SAS, France], 0.5% Ohly Kat yeast extract [Deutsche Hefewerke GmbH, Germany], 0.5% NaCl, 0.1% glucose, and 0.1% K_2HPO_4, pH 7.2) was used as the standard growth medium. If necessary, antibiotics were supplemented at a concentration of 10 µg ml^{-1} for chloramphenicol, 2.5 µg ml^{-1} for erythromycin or 0.5 µg ml^{-1} for penicillin G. *E. coli* transformants were grown in lysogeny broth (LB; Lennox) medium (1% tryptone, 0.5% yeast extract, and 0.5% NaCl; Carl Roth GmbH, Germany) supplemented with 10 µg ml^{-1} chloramphenicol or on BM agar with 10 µg ml^{-1} chloramphenicol. BM without glucose (B_0) was used for expression of *citZ*.

To monitor growth over time, strains were grown overnight in BM under continuous shaking at 37°C. Each strain was adjusted to an optical density at 600 nm (OD_{600}) of 1 in BM, and 5 µl of

the bacterial stock solutions were pipetted to 1 ml BM into a 24-well microtiter plate. If necessary, 5 mM sodium citrate was added to each well. The plates were incubated for 24 h under continuous shaking in a microplate reader, and OD_{600} was measured every 15 minutes.

Cloning

DNA manipulation, isolation of plasmid DNA, and transformation of *E. coli* and *S. aureus* were performed by using standard procedures. Enzymes for molecular cloning were obtained from Thermo Fisher Scientific.

Transposon mutagenesis

To identify the biosynthetic gene cluster responsible for antimicrobial activity of *S. aureus* D4-19, the strain was transformed with the plasmid pBTn and mutants were generated by transposon insertion as described previously [54]. To identify the insertion site of the transposon in clones, that had lost antimicrobial activity, genomic DNA was isolated, and an inverse PCR was performed. Therefore, 5 µg gDNA were digested with the restriction enzyme BspHI for 3h at 37°C. After purification of the digest, 2 µg of DNA were religated in 100 µl total volume for 2-3 hours and 2 µl of the ligation mixture were used for standard PCR (in 25 µl volume) with pBTn up and down primers (Table 1). Analyse the PCR products on an analytical gel, isolate strong bands, and sequence with pBTn up/down primers.

Generation of *S. aureus* RN4220 pD4-19 and adapted mutant

Plasmid DNA was isolated from *S. aureus* D4-19 and transferred into *S. aureus* RN4220. Positive transformants were selected on BM plates containing 0.5 µg ml^{-1} Penicillin G and screened by PCR with primers binding in the BGC and the β-lactamase gene cluster (Table 1). To generate a mutant that had adapted to MP1 production, *S. aureus* RN4220 pD4-19 was passaged for 28 days by inoculating fresh BM medium every day with 10 µl of overnight culture.

Generation of knockout mutants

For the generation of knockout mutants, the temperature-sensitive shuttle vector pIMAY was used, and mutants were generated by allelic replacement as described previously [55]. Flanking regions of the genes to be deleted were amplified by PCR (Table 1) and ligated into pIMAY after digestion with suitable restriction enzymes. Cloning was performed in *E. coli*

DC10B or *E. coli* Sa08B. Sequence-verified plasmids were transferred in the target strains, *S. aureus* D4-19 and *S. aureus* RN4220 pD4-19. Successful knockouts were confirmed by PCR with respective primers and sequencing of the PCR product covering the area of the knocked-out gene.

Overexpression of *citZ*

To overexpress *citZ*, a novel xylose-inducible plasmid was constructed on the basis of the shuttle vector pRB473. The regulatory unit containing the *xylR* repressor gene and about 200 nucleotides at its 3'-end encompassing the regulated promotor were amplified with primers pTX15 Hind and pTX15 Sma and plasmid pTX15 as template. From the resulting PCR product, the required fragment was generated via HindIII and BamHI digestion, which was subsequently ligated to the equally digested pRB473 resulting in pRB473-xylR. Furthermore, a 6xHis tag was inserted into the plasmid to get a C-terminally tagged protein. Therefore, plasmid pPSHG3 was used as template to amplify the 6xHis tag with the primers His-term down and His-term up (Table 1). The insert and pRB473-xylR were digested with EcoRI and BamHI and after ligation, *E. coli* DC10B was transformed. *citZ* was amplified from *S. aureus* RN4220 pD4-19 and *S. aureus* RN4220 pD4-19 adapted using the primers citZ_overex_fwd and citZ_overex_rev_new. After restriction digestion with BamHI and SacI, the inserts were ligated into pRB473-xylR-6xHis. Sequence verified plasmids were transferred into *S. aureus* RN4220. To check the expressed protein levels, strains were grown overnight in BM, inoculated to $OD_{600}=0.1$ in B_0 and grown to $OD_{600}=0.5$. After induction with 0.5% xylose, samples were taken at time points 0 h, 2 h and 4 h. Samples were loaded on an SDS-Page (12% pre-cast gel, BioRad) after incubation with 4x Laemmli Sample Buffer (BioRad, add. 355 mM 2-mercaptoethanol) at 95°C for 5 min and centrifugation for 10 min at 16.000 xg. PageRuler Prestained (ThermoScientific) was used, and the gel was run at 120 V for 1 h. For Western Blotting, a nitrocellulose membrane was cut to the size of the gel and the blotting paper, and the membrane were equilibrated in transfer buffer. Blotting paper, gel, membrane, and blotting paper were stacked in a blotting chamber of the BioRad Transblot Turbo. To detect the His-Tag, the membrane was incubated in blocking buffer and then washed with PBS-T (PBS-Tween) and PBS. After incubation with the primary antibody from QIAGEN (Penta-His Antibody, 1:1000 dilution) at RT for 1 h under shaking, the membrane was washed again, 3x with PBS-T and 1 with PBS. The secondary antibody from LICOR (IRDye® 680RD Goat anti-Rabbit IgG, 1:10000 dilution) was added and after incubation for 1h at RT with shaking, washed again as mentioned before. The membrane was analysed using LI-COR Odyssey. Protein amounts were calculated using the LI-COR Odyssey imaging tools.

Table 1: Primers used for transposon mutagenesis and generation of knockout mutants.

Primer	Sequence (5'-3')	assignment
pBTn seq up	ACCAACATGACGAATCCCTCC	inverse PCR and sequencing
pBTn seq down	CCCGCCATACCACAGATGTT	inverse PCR and sequencing
TclS	GCATCAGACACCTGTTCACTTATT	pD4-19 sequencing
BlaR1-fwd	CTATGGCTGAATGGGATGTTAT	pD4-19 sequencing
WT_KO_PP_up_fwd	CGAGGGTCGACTAAACTTAAACCTGACTGTCATTGT	Deletion of MP1 precursor peptide (*tclE*) and MP1 BGC
WT_KO_PP_up_rev	CCTAACTAAATTATTATTACGAGCACCACCTTTACTTAGAT	Deletion of MP1 precursor peptide (*tclE*)
WT_KO_PP_dw_fwd	GGTGGTGCTCGTAATAATAATTTAGTTAGGTATAAATTA	Deletion of MP1 precursor peptide (*tclE*)
WT_KO_PP_dw_rev	CTGCAGGAATTCAGAATATCTAGTATCGAAGATTT	Deletion of MP1 precursor peptide (*tclE*)
KO_MP1_up_rev	TTTAATATAATTGTATGGAGGTTAGTTACGAGCACCACCTTTACTTAGAT	Deletion of MP1 BGC
KO_MP1_down_fwd	ATCTAAGTAAAGGTGGTGCTCGTAACTAACCTCCATACAATTATATTAAA	Deletion of MP1 BGC
KO_MP1_down_rev	ATATGAATTCATCGAGTTGTCGAAATGTTAGAA	Deletion of MP1 BGC
pTX15 Hind	CGTTATCACAAGTGGTCACCACTCT	Construction of pRB473-xylR
pTX15 Sma	GCTTCCGGCTCGTATGTTGTGTGG	Construction of pRB473-xylR
His-term down	GGCTAGCGGATCCTCGAGTCGACTACCGAGCTCAGATCTCATC	Insertion if 6xHis in pRB473-xylR
His-term up	AGTTAGAATTCTGCAGTTTCATGAATATTACAAACAAAAAGC	Insertion if 6xHis in pRB473-xylR
citZ_overex_fwd	AATGTAGGATCCAATTGTTGCACATATAATGCCAGTT	Amplification of *citZ* with promotor region

citZ_overex_rev_new	AGATCTGAGCTCTTTTCTTTC TTCAAGCGGGATATAC	Amplification of *citZ* with promotor region

MIC assay

Strains used for MIC determinations were grown overnight in BM under continuous shaking at 37°C. Each strain was adjusted to OD_{600}=0.00125 in BM and 100 µl were pipetted in each well of a 96-well microtiter plate. The MP1 stock solution was serially diluted in this 96-well microtiter plate and the plates were incubated at 37°C for 21 h under continuous shaking (160 rpm). OD_{600} of cultures in each well was measured with a microplate reader, and the lowest concentration of MP1 leading to no bacterial growth was defined as the MIC value.

Citrate assay

Citrate levels were measured using the Citrate Assay Kit (MAK057) from Sigma-Aldrich. Samples were prepared as follows. Strains were grown over night in BM, diluted into fresh BM to OD=0.1 and grown for 5 h at 37°C under continuous shaking. For each strain, $1x10^8$ cells in 100 µl citrate assay buffer were homogenised in a 1.5 ml microcentrifuge tube containing 100 µl glass beads with a Fast prep at 6.5 m/s for 60 s. After centrifugation for 10 min at maximum speed, 30 µl of supernatant were pipetted in a 96 well plate. 20 µl of citrate assay buffer was added to reach the final volume of 50 µl described in the kit manual. Reaction mixes were prepared, and the analysis was carried out as described in the manufacturer's manual.

Acetate assay

Acetate levels were measured using the Acetate Colorimetric Assay Kit (MAK086) from Sigma-Aldrich. Samples were prepared as follows. Strains were grown over night in BM, fresh BM was inoculated to OD=0.1 and grown for 8 h at 37°C under continuous shaking. At time points 0, 2, 4, 6 and 8 hours, 1 ml of culture were centrifuged at 11 000 xg for 5 min and the supernatant was transferred into a fresh tube. Samples were 1000-fold diluted, reaction mixes were prepared, and the analysis was carried out as described in the manufacturer's manual.

Spot assay

Antimicrobial activity was assessed, by resuspending the sensitive *S. aureus* USA300 in 200 µl BM and spreading it with a cotton swab on a BM plate. Producer strains were also

resuspended in BM and 10 µl of the suspension were spotted on the prepared indicator plate. Once the spots were dry, the plates were incubated at 37°C overnight.

Purification of MP1

Cell bound MP1 can be isolated as follows. 50 ml overnight culture were centrifuged at 6 000 xg for 10 min, the pellet was washed two times with 15 ml PBS and then resuspended in 3 ml methanol. After incubation on a spinning wheel for 1 h and a centrifugation step at 6 000 xg for 10 min, the supernatant was transferred in a fresh falcon and used for HPLC or MS/MS analysis.

LC-MS analysis of MP1

LC-MS analysis of culture extracts was performed with a HPLC (Ultimate 3000, Thermo Fischer) and subsequent HR-ESI-TOF-MS (Maxis 4G, Bruker). For HPLC analysis, LC-MS-grade water (with 0.01 % formic acid) and LC-MS-grade methanol (with 0.06 % formic acid) were used and fractionation was performed with a gradient from 10% to 100% over 20 min and a flow rate of 0.3 ml/min. A nucleoshell RP18 column with a column length of 150 mm, an inner diameter of 2 mm and a particle size of 2.7 µm, prewarmed to 40°C was used. For HR-ESI-TOF-MS sodium formate was used as calibrant.

Sample preparation for metabolome analysis

For the preparation of samples for metabolome analysis, strains were grown over night, inoculated in fresh medium (20 ml) to OD_{600}=0.1 and grown for 5 h at 37°C under continuous shaking. OD_{600} was measured and all strains were set to the lowest OD measured. The culture was filtered through a 0.22 µm bottle-top sterile filter (250 ml, Nalgene) via vacuum. The filter was washed with 0.6 % ice-cold NaCl, cut in 4 pieces and incubated at -20°C for 20 min with 5 ml ice-cold 40:40:20 (v/v/v) methanol:acetonitrile:water in a glass bottle. 1 ml of filtrate was transferred into a microcentrifuge tube bead beaten 2x 30 s at 6.5 m/s with 0.5 ml glass beads. Samples were kept on ice in between. After centrifugation for 5 min at 4°C with maximum speed, 600 µl of supernatant were stored at -80°C.

Metabolite analysis by flow injection MS (FI-MS)

Metabolites were analyzed by flow injection into a high-resolution quadrupole time-of-flight (QTOF) mass spectrometer (Agilent QTOF 6546) as described previously [56]. 3 µL of the sample was injected with an Agilent 1290 Bio Multisampler (G7137A) into the mobile phase that was a 60:40 (v/v-%) mixture of isopropanol (LiChrosolv Supelco hypergrade for LC-MS, 1.02781.2500) and ultrapure water (Omnia Pure, stakpure), buffered with 10 mM ammonium carbonate ($(NH_4)_2CO_3$, Sigma-Aldrich, 3799-10 G) and 0.04% ammonium hydroxide (NH_4OH, Honeywell/Fluka TraceSELECT Ultra, 16748-250 ML). The flow rate of the mobile phase was 0.15 mL*min^{-1}. Mass spectra were separately recorded in positive- and negative ionization profile mode from *m/z* 50 to *m/z* 1700 with an acquisition rate of 1.4 ms/spectrum using the highest resolving power (10 GHz-High Sensitivity). Online mass axis correction was performed with purine and hexakis(1H,1H,3H- tetrafluoropropoxy)phosphazine (HP-0921, Agilent Technologies). The source gas temperature of the ESI ion source was 225 °C, with 11 l*min^{-1} drying gas and a nebulizer pressure of 20 psi. The sheath gas temperature was 350 °C, and the flow rate was 10 l*min^{-1}. Electrospray nozzle and capillary voltages were 2,000 and 3,500 V, respectively. Fragmenter and skimmer voltages were 120 and 65 V, respectively. Ion peaks were annotated by matching the mass-to-charge ratios to calculated, single (de-) protonated masses of metabolites listed in a genome scale model of Escherichia coli K12 (iML1515) [57]. Hierarchical cluster plot was generated using MATLAB.

Metabolite analysis by LC-MS/MS

LC-MS/MS was performed with an Agilent 6495 triple quadrupole mass spectrometer (Agilent Technologies) as described previously [58]. An Agilent 1290 Infinity II UHPLC system (Agilent Technologies) was used for liquid chromatography using two columns: i) an Acquity UPLC BEH Amide (Waters) for acidic conditions and ii) an iHILIC-Fusion(P) (HILICON AB) for basic conditions. The column oven was at 30°C. LC solvents were: solvent A: water with ammonium formate (10 mM) and formic acid (0.1 % v/v) for acidic conditions, and water with ammonium carbonate (10 mM) and ammonium hydroxide (0.2 %) for basic conditions; solvents B: acetonitrile with formic acid (0.1% v/v) for acidic, and acetonitrile for basic conditions. The LC gradient was: 0 min 90% B, 1.3 min 40% B, 1.5 min 40% B, 1.7 min 90% B, 2 min 90 % B. The flow rate was 0.4 mL/min. The injection volume was 3 µL. Settings of the ESI source were: 200 °C source gas, 14 L/min drying gas and 24 psi nebulizer pressure. The sheath gas temperature was at 300 °C and flow at 11 L/min. The electrospray nozzle was set to 500 V and capillary voltage to 2500 V. All samples were mixed with a 13-C labelled internal standard and the ratio of 12-C and 13-C peak heights was used to quantify metabolites. 12C/13C ratios were normalized to the OD-specific cell volume at the time point of sampling.

Sample preparation for proteome analysis

Strains were grown over night, inoculated in fresh medium to OD_{600}=0.1 and grown for 5 h at 37°C under continuous shaking. 1.5 ml were centrifuged, the pellet was resuspended in 1 ml SDS buffer (4% w/v sodium dodecyl sulfate (SDS), in 100 mM tris(hydroxymethyl)aminomethane (Tris)/HCl; pH 8). Homogenise cells at 6.5 m/s for 2x40s by using a Fast Prep, incubate on ice for 2 min in between. Centrifuge at maximum speed for 1 min and transfer the supernatant into a fresh Eppendorf tube. To reduce cysteine disulfide bonds, 10 mM Dithiothreitol (DTT) was added to the samples and incubated for 45 min shaking at 650 rpm at room temperature (RT). 5.5 mM Iodoacetamide (IAA) were added to alkylate reduced cysteine thiol groups. Incubate for 45 min at RT with shaking at 650 rpm in the dark. After centrifugation of the samples at 12.000xg for 15 min, the supernatant was transferred in a new tube. One volume of supernatant was mixed with 7 volumes of ice cold 8:1 acetone:methanol, vortexed and incubated over night at -20°C. Centrifugation of the precipitated proteins for 5 min at 1000xg was followed by two washing steps with 80% acetone at RT. The protein pellet was air dried for 10-15 min and rehydrated in denaturation buffer (6 M urea, 2 M thiourea in 10 mM Tris/HCl; pH 7.5).

LC-MS/MS analysis of proteome samples

Ten microgram of proteins per sample were digested in solution with trypsin as described previously [59]. Desalted peptides [60] were separated on an Easy-nLC 1200 system coupled to a quadrupole Orbitrap Exploris 480 mass spectrometer (all Thermo Fisher Scientific) as described previously [61] with slight modifications: peptides were separated using an 87-minute segmented gradient from 10-33-50-90% of HPLC solvent B (80% acetonitrile in 0.1% formic acid) in HPLC solvent A (0.1% formic acid) at a flow rate of 200 nl/min. The mass spectrometer was operated in data-dependent mode, collecting MS spectra in the Orbitrap mass analyser (60,000 resolution, 300-1750 *m/z* range) with an automatic gain control (AGC) set to standard and a maximum ion injection time set to automatic. The 20 most intense precursor ions were sequentially fragmented with a normalized collision energy of 28 in each scan cycle using higher energy collisional dissociation (HCD) fragmentation. In all measurements, sequenced precursor masses were excluded from further selection for 30 s. MS/MS spectra were recorded with a resolution of 15,000, whereby fill time was set to automatic. Acquired MS spectra were processed with MaxQuant software package version 1.6.14.0 [62] with integrated Andromeda search engine [63]. Database search was performed against a *Staphylococcus aureus* (allStrains) protein database (downloaded on 7th of October 2020, 216,059 entries), and 286 commonly observed contaminants. Endoprotease trypsin was defined as protease with a maximum of two missed cleavages. Oxidation of methionine, and

protein N-terminal acetylation were specified as variable modifications. Carbamidomethylation on cysteine was set as fixed modification. Initial maximum allowed mass tolerance was set to 4.5 parts per million (ppm) for precursor ions and 20 ppm for fragment ions. Peptide, protein and modification site identifications were reported at a false discovery rate (FDR) of 0.01, estimated by the target-decoy approach [64]. The iBAQ (Intensity Based Absolute Quantification) and LFQ (Label-Free Quantification) algorithms were enabled, as was the "match between runs" option [65, 66].

RNA isolation for transcriptome analysis

Strains were grown over night, inoculated in fresh medium to OD_{600}=0.1 and grown for 5 h at 37°C under continuous shaking. 1/10 volume EtOH/Phenol was added to 500 μl of sample and mixed for 1 min. After incubation on ice for 5 min, the samples were centrifuged for 1 min at 20 000 xg at 4°C. The supernatant was discarded, and the pellet was resuspended in 1 ml TRIzol. Each sample was transferred to one screw-cap tube with glass beads and cells were lysed via bead-beating for 2x 6.5 ms/s for 30 s. In between the two runs the cells were kept on ice for 2 min. 200 μl chloroform was added to the samples, mixed and incubated 2-3 min before centrifugation of the samples for 15 min, 12 000 xg, 4°C. The aqueous supernatant was taken, mixed with 500 μl isopropanol and samples were centrifuged for 10 min, 21 000 xg, 4°C. The supernatant was discarded, and the pellet was resuspended in 500 μl 75% EtOH. After centrifugation for 5 min, 20 000 xg, 4°C, the supernatant was discarded, and the pellet was dried at RT. The pellet was resuspended in 100 μl RNA-grade water and RNA was concentrated via the MN RNA clean up kit (Machery-Nagel) and RNA was eluted in 60 μl RNA-grade water. After quantification with a Nanodrop, RNA was stored at -80°C.

DNA isolation and sequencing

DNA isolation, library preparation and sequencing was performed by the Institute for Medical Microbiology (part of the NGS Competence Center NCCT, Tübingen, Germany). DNA was extracted using the Qiagen Genomic Tip 20/G Kit, following the manufacturer's instructions. The genomic DNA was quantified with a Qubit dsDNA BR Assay Kit (Thermo Fisher).

ONT library preparation was performed following the instructions manual Native barcoding genomic DNA (with EXP-NBD196 and SQK-LSK109, Oxford Nanopore) with an input of 250 ng DNA. 12 μl template DNA was supplemented with the required reagents from the NEBNext Ultra II End Repair/dA Tailing kit (E7546S, NEB) and was first incubated at 20°C for 5 minutes and then at 65°C for 5 minutes. For the barcode ligation 3 μl of nuclease-free water, 0.75 μl

End-prepped DNA, 1 µl Native Barcode (Native Barcoding Expansion 96, EXP-NBD196) and 5 µl Blunt/TA Ligase Master Mix (NEB Blunt/TA Ligase Master Mix, M0367) were combined in a new reaction vessel and incubated for 20 minutes at room temperature. 1 µl of 0.5 M EDTA was added and samples were pooled in a new reaction tube. The pool was cleaned-up by using AMPure XP Beads (Agencourt), washed twice with 70% ethanol and resuspended in nuclease-free water. For barcode ligation 5 µl Adapter Mix II, 10 µl NEBNext Quick Ligation Reaction Buffer (5X) and 5 µl Quick T4 DNA Ligase were added to the pool and incubated for 10 minutes at room temperature. The pool was cleaned up using AMPure XP Beads, washed twice with Long Fragment Buffer and eluted in Elution Buffer. The library pool was loaded on a MinION device (Oxford Nanopore Technology, ONT) and stopped at 39 Gb output. Base calling was performed using the ONT's Guppy basecaller version 4.1.1.

Libraries for Illumina short-read sequencing were prepared using the Illumina Nextera™ DNA Flex Library Preparation Kit with IDT for Illumina DNA/RNA UD indexes, tagmentation according to the manufacturer's protocol with 500 ng DNA input and 5 cycles indexing PCR. Libraries were checked for correct fragment length on an Agilent 2100 Bioanalyzer and pooled equimolarly and quantified with Qubit DNA HS Assay Kit (ThermoFisher). Equimolarly pooled libraries were sequenced on a MiSeq Reagent Kit v2 (300 cycles) flow cell (Illumina) with 2 x 150 bp read length.

DNA data assessment and analysis

Sequencing statistics including the quality per base and adapter content assessment of Illumina reads were conducted with FastQC v0.11.8 (http://www.bioinformatics.babraham.ac.uk/projects/fastqc, accessed June 2022).

Unicycler v0.5.0 [67] with default parameters was used for a hybrid assembly of the Oxford Nanopore and Illumina reads of the *Staphylococcus aureus* RN4220 pD419 genome. The resulting genome was annotated using prokka v1.14.6 [68] with the additional parameters to add gene features in the annotation and searching for non-coding RNAs (parameters --addgenes and --rfam). The quality of the assembly was assessed using quast v5.1.0 [69].

Illumina reads of *Staphylococcus aureus* RN4220 pD419 adapted were compared against the assembled genome using EAGER v1.92.56 [70] to extract SNPs.

RNA isolation and processing

Library Prep and Sequencing was performed by the Institute for Medical Microbiology (part of the NGS Competence Center NCCT (Tübingen, Germany)). RNA samples were DNase I

digested (DNase I recombinant, Rnase-free, Millipore Sigma), cleaned up (RNA Clean & Concentrator-5, Zymo Research), quantified (Qubit RNA BR Assay Kit, ThermoFisher) and normalized to 100 ng in 11 µl nuclease-free water. Library preparation was performed according to the Illumina Stranded Total RNA Prep, Ligation with Ribo-Zero Plus Reference Guide. Library concentration was measured with Qubit DNA HS Assay Kit, (ThermoFisher) on a Qubit Fluorometer (invitrogen) and fragment length was assessed with an Agilent 2100 Bioanalyzer (Agilent High sensitivity DNA Kit, Agilent). Samples were equimolarly pooled and sequenced on NextSeq™ 500 High Output Kit v2.5 (75 cycles) flow cell (Illumina) with 1 x 75 bp read length.

RNA-Seq data assessment and analysis

Sequencing statistics including the quality per base and adapter content assessment of resulting transcriptome sequencing data were conducted with FastQC v0.11.8 (http://www.bioinformatics.babraham.ac.uk/projects/fastqc, accessed June 2022). All reads mappings were performed against the previously assembled reference strain *Staphylococcus aureus* RN4220 pD4-19 (SRA Bioproject ID PRJNA855446). The mappings of all samples were conducted with HISAT2 v2.1.0 [71]. As parameters spliced alignment of reads was disabled and strand-specific information was set to reverse complemented (HISAT2 parameter --no-spliced-alignment and --rna-strandness "R"). The resulting mapping files in SAM format were converted to BAM format using SAMtools v1.9 [72]. Mapping statistics, including strand specificity estimation and percentage of mapped reads, were conducted with the RNA-Seq module of QualiMap2 v2.2.2-a [73]. Gene counts for all samples were computed with featureCounts v1.6.4 [74] based on the annotation of the respective reference genome, where the selected feature type was set to transcript records (featureCounts parameter -t transcript). To assess variability of the replicates of each time series, a principal component analysis (PCA) was conducted with the DESeq2 package v1.28.1 [75].

Normalization and differential gene expression

For the computation of genes differentially expressed between the two different strains (pD4-19 and pD4-19 adapted) and the wild type strain, DESeq2 v1.20.0 [75] was applied to the absolute gene counts as computed with featureCounts. For differences between the two strains and the wildtype strain, genes with an adjusted p-value (FDR) < 0.05 and absolute log2 fold change (FC) > 1 were reported as differentially expressed.

Gene set enrichment analysis

The genome was annotated functionally using FACoP (http://facop.molgenrug.nl/). Gene set enrichment analysis was performed on differentially expressed genes (adjusted q-value <0.05, Fold enrichment >1) using FUNAGE-Pro (http://gseapro.molgenrug.nl/).

Biofilm assay

Strains were grown over night in tryptic soy broth and adjusted to the OD_{600} of the strain with the lowest OD_{600}. 5 µl were added to 995 µl of BM containing 1% (v/v) glucose. 200 µl were transferred to triplicate wells of a fibrinogen coated Nunclon Delta surface microtiter plate. The plate was incubated at 37°C for 24 h, in non-shaking conditions. Control wells with broth and no bacteria were included. The supernatant was discarded, and wells were washed three times with 200 µl PBS. The plate was inverted for 30 min to dry. 100 µl crystal violet was added to each well and washed off after 1 min (3-5 times with PBS). 100 µl of 5% acetic acid was added to the wells and the plate was placed on a shaker for 5 min to dissolve the cells. Subsequently the absorbance at 570 nm was measured using the FLUOstar Optima.

Phylogenetic tree generation

A database was generated containing 3 839 human *S. aureus* genome sequences downloaded from the PATRIC database. To extract *citZ* gene sequences with start codon mutation, *in silico* PCR (https://github.com/egonozer/in_silico_pcr) was performed with primers 5'-ATAGCAGAATTACAAAGAGGTT-3' and 5'-TTATTTTCTTTCTTCAAGCGGG-3' allowing 5 mismatches/indels. To show the phylogenetic relationship of *citZ* mutants among selected *S. aureus* from different lineages, Prokka (v.1.14.6) [68] was used to retrieve the annotated protein faa files from whole genomes. A maximum likelihood tree was drawn via the RaxML program (v.8.2.12) [76] and applied to the PhyloPhlAn (v.3.0.60) pipeline [77] using its default database. After rooting the tree from the strain *S. aureus* ST398 isolate 2012-3, the tree was visualized via iTOL (v.5) [78].

Statistical analysis

Statistical analyses were performed using GraphPad Prism 9.02.

Data availability

Upload of proteome and transcriptome raw data was initiated. Metabolome data can be accessed at Metabolights via the identifier MTBLS5196. Data for *S. aureus* RN4220 pD4-19 and *S. aureus* RN4220 pD4-19 adapted were deposited in BioProject under accession number PRJNA855446 and the plasmid sequence of pD4-19 (from *S. aureus* D4-19) has the GenBank accession number ON936820.

Acknowledgements

References.

1. Heilbronner, S., et al., *The microbiome-shaping roles of bacteriocins.* Nat Rev Microbiol, 2021.
2. Cotter, P.D., R.P. Ross, and C. Hill, *Bacteriocins - a viable alternative to antibiotics?* Nat Rev Microbiol, 2013. **11**(2): p. 95-105.
3. Simons, A., K. Alhanout, and R.E. Duval, *Bacteriocins, Antimicrobial Peptides from Bacterial Origin: Overview of Their Biology and Their Impact against Multidrug-Resistant Bacteria.* Microorganisms, 2020. **8**(5).
4. Zipperer, A., et al., *Human commensals producing a novel antibiotic impair pathogen colonization.* Nature, 2016. **535**(7613): p. 511-6.
5. Claesen, J., et al., *A Cutibacterium acnes antibiotic modulates human skin microbiota composition in hair follicles.* Sci Transl Med, 2020. **12**(570).
6. Kim, S.G., et al., *Microbiota-derived lantibiotic restores resistance against vancomycin-resistant Enterococcus.* Nature, 2019. **572**(7771): p. 665-669.
7. Janek, D., et al., *High Frequency and Diversity of Antimicrobial Activities Produced by Nasal Staphylococcus Strains against Bacterial Competitors.* PLoS Pathog, 2016. **12**(8): p. e1005812.
8. Newstead, L.L., et al., *Staphylococcal-Produced Bacteriocins and Antimicrobial Peptides: Their Potential as Alternative Treatments for Staphylococcus aureus Infections.* Antibiotics (Basel), 2020. **9**(2).
9. Carson, D.A., et al., *Bacteriocins of Non-aureus Staphylococci Isolated from Bovine Milk.* Appl Environ Microbiol, 2017. **83**(17).
10. Tang, X., et al., *Cariogenic Streptococcus mutans Produces Tetramic Acid Strain-Specific Antibiotics That Impair Commensal Colonization.* ACS Infect Dis, 2020. **6**(4): p. 563-571.
11. Ceotto, H., et al., *Aureocin A70 production is disseminated amongst genetically unrelated Staphylococcus aureus involved in bovine mastitis.* Lett Appl Microbiol, 2012. **54**(5): p. 455-61.
12. Huo, L., et al., *Heterologous expression of bacterial natural product biosynthetic pathways.* Nat Prod Rep, 2019. **36**(10): p. 1412-1436.
13. Barbuto Ferraiuolo, S., et al., *Streptomycetes as platform for biotechnological production processes of drugs.* Appl Microbiol Biotechnol, 2021. **105**(2): p. 551-568.
14. Bekiesch, P., P. Basitta, and A.K. Apel, *Challenges in the Heterologous Production of Antibiotics in Streptomyces.* Arch Pharm (Weinheim), 2016. **349**(8): p. 594-601.
15. Blanchard, A.E., C. Liao, and T. Lu, *An Ecological Understanding of Quorum Sensing-Controlled Bacteriocin Synthesis.* Cellular and Molecular Bioengineering, 2016. **9**(3): p. 443-454.
16. Ebner, P., et al., *Lantibiotic production is a burden for the producing staphylococci.* Sci Rep, 2018. **8**(1): p. 7471.
17. Netz, D.J., et al., *Molecular characterisation of aureocin A70, a multi-peptide bacteriocin isolated from Staphylococcus aureus.* J Mol Biol, 2001. **311**(5): p. 939-49.
18. Liu, Y., et al., *Skin microbiota analysis-inspired development of novel anti-infectives.* Microbiome, 2020. **8**(1): p. 85.
19. Rosendahl, G. and S. Douthwaite, *The antibiotics micrococcin and thiostrepton interact directly with 23S rRNA nucleotides 1067A and 1095A.* Nucleic Acids Res, 1994. **22**(3): p. 357-63.
20. Porse, B.T., E. Cundliffe, and R.A. Garrett, *The antibiotic micrococcin acts on protein L11 at the ribosomal GTPase centre.* J Mol Biol, 1999. **287**(1): p. 33-45.
21. Ciufolini, M.A. and D. Lefranc, *Micrococcin P1: structure, biology and synthesis.* Nat Prod Rep, 2010. **27**(3): p. 330-42.
22. Starmer, J., et al., *Predicting Shine-Dalgarno sequence locations exposes genome annotation errors.* PLoS Comput Biol, 2006. **2**(5): p. e57.
23. Novick, R.P. and M.H. Richmond, *Nature and Interactions of the Genetic Elements Governing Penicillinase Synthesis in Staphylococcus Aureus.* J Bacteriol, 1965. **90**: p. 467-80.

24. Hancock, R., *Accumulation of pool amino acids in Staphylococcus aureus following inhibition of protein synthesis.* Biochim Biophys Acta, 1960. **37**: p. 47-55.

25. Kloosterman, T.G., et al., *Regulation of Glutamine and Glutamate Metabolism by GlnR and GlnA in Streptococcus pneumoniae*.* Journal of Biological Chemistry, 2006. **281**(35): p. 25097-25109.

26. Blumenthal, H.J., C.F. Huettner, and F.A. Montiel, *Comparative aspects of glucose catabolism in Staphylococcus aureus and S. epidermidis.* Ann N Y Acad Sci, 1974. **236**(0): p. 105-14.

27. Somerville, G.A., et al., *Staphylococcus aureus aconitase inactivation unexpectedly inhibits post-exponential-phase growth and enhances stationary-phase survival.* Infect Immun, 2002. **70**(11): p. 6373-82.

28. Biswas, L., et al., *Role of the twin-arginine translocation pathway in Staphylococcus.* J Bacteriol, 2009. **191**(19): p. 5921-9.

29. Schuster, C.F., et al., *The second messenger c-di-AMP inhibits the osmolyte uptake system OpuC in Staphylococcus aureus.* Sci Signal, 2016. **9**(441): p. ra81.

30. Alreshidi, M.M., et al., *Amino acids and proteomic acclimation of Staphylococcus aureus when incubated in a defined minimal medium supplemented with 5% sodium chloride.* Microbiologyopen, 2019. **8**(6): p. e00772.

31. Ming, T., et al., *iTRAQ-Based Quantitative Proteomic Profiling of Staphylococcus aureus Under Different Osmotic Stress Conditions.* Front Microbiol, 2019. **10**: p. 1082.

32. Gotz, F., *Staphylococcus and biofilms.* Mol Microbiol, 2002. **43**(6): p. 1367-78.

33. Sambanthamoorthy, K., et al., *The Role of msa in Staphylococcus aureus Biofilm Formation.* BMC Microbiol, 2008. **8**: p. 221.

34. Kassem, M.A., et al., *Exploring clinically isolated Staphylococcus sp. bacteriocins revealed the production of amonabactin, micrococcin, and alpha-circulocin.* Iran J Microbiol, 2021. **13**(2): p. 212-224.

35. Bennallack, P.R., et al., *Characterization of a novel plasmid-borne thiopeptide gene cluster in Staphylococcus epidermidis strain 115.* J Bacteriol, 2014. **196**(24): p. 4344-50.

36. Ovchinnikov, K.V., et al., *A Strong Synergy Between the Thiopeptide Bacteriocin Micrococcin P1 and Rifampicin Against MRSA in a Murine Skin Infection Model.* Front Immunol, 2021. **12**: p. 676534.

37. O'Neill, A.M., et al., *Antimicrobials from a feline commensal bacterium inhibit skin infection by drug-resistant S. pseudintermedius.* Elife, 2021. **10**.

38. Van der Veken, D., et al., *Genome-Based Characterization of a Plasmid-Associated Micrococcin P1 Biosynthetic Gene Cluster and Virulence Factors in Mammaliicoccus sciuri IMDO-S72.* Appl Environ Microbiol, 2022. **88**(4): p. e0208821.

39. Maldonado-Barragan, A. and S.A. West, *The cost and benefit of quorum sensing-controlled bacteriocin production in Lactobacillus plantarum.* J Evol Biol, 2020. **33**(1): p. 101-111.

40. Gonzalez, D. and D.A.I. Mavridou, *Making the Best of Aggression: The Many Dimensions of Bacterial Toxin Regulation.* Trends Microbiol, 2019. **27**(11): p. 897-905.

41. Strasters, K.C. and K.C. Winkler, *Carbohydrate Metabolism of Staphylococcus Aureus.* J Gen Microbiol, 1963. **33**: p. 213-29.

42. Tan, G.Y., et al., *Heterologous Biosynthesis of Spinosad: An Omics-Guided Large Polyketide Synthase Gene Cluster Reconstitution in Streptomyces.* ACS Synth Biol, 2017. **6**(6): p. 995-1005.

43. Olano, C., et al., *Improving production of bioactive secondary metabolites in actinomycetes by metabolic engineering.* Metab Eng, 2008. **10**(5): p. 281-92.

44. Kempf, M., U. Theobald, and H.P. Fiedler, *Correlation between the consumption of amino acids and the production of the antibiotic gallidermin by Staphylococcus gallinarum.* Biotechnology Letters, 1999. **21**(11): p. 959-963.

45. Mack, D., et al., *The intercellular adhesin involved in biofilm accumulation of Staphylococcus epidermidis is a linear beta-1,6-linked glucosaminoglycan: purification and structural analysis.* J Bacteriol, 1996. **178**(1): p. 175-83.

46.   Cramton, S.E., et al., *The intercellular adhesion (ica) locus is present in Staphylococcus aureus and is required for biofilm formation.* Infect Immun, 1999. **67**(10): p. 5427-33.

47.   Vuong, C., et al., *Staphylococcus epidermidis polysaccharide intercellular adhesin production significantly increases during tricarboxylic acid cycle stress.* J Bacteriol, 2005. **187**(9): p. 2967-73.

48.   Sadykov, M.R., et al., *Tricarboxylic acid cycle-dependent regulation of Staphylococcus epidermidis polysaccharide intercellular adhesin synthesis.* J Bacteriol, 2008. **190**(23): p. 7621-32.

49.   Shanks, R.M., et al., *Genetic evidence for an alternative citrate-dependent biofilm formation pathway in Staphylococcus aureus that is dependent on fibronectin binding proteins and the GraRS two-component regulatory system.* Infect Immun, 2008. **76**(6): p. 2469-77.

50.   Brotz, H., et al., *Role of lipid-bound peptidoglycan precursors in the formation of pores by nisin, epidermin and other lantibiotics.* Mol Microbiol, 1998. **30**(2): p. 317-27.

51.   Peschel, A. and F. Gotz, *Analysis of the Staphylococcus epidermidis genes epiF, -E, and -G involved in epidermin immunity.* J Bacteriol, 1996. **178**(2): p. 531-6.

52.   Otto, M., A. Peschel, and F. Gotz, *Producer self-protection against the lantibiotic epidermin by the ABC transporter EpiFEG of Staphylococcus epidermidis Tu3298.* FEMS Microbiol Lett, 1998. **166**(2): p. 203-11.

53.   Baumann, S., et al., *Molecular determinants of microbial resistance to thiopeptide antibiotics.* J Am Chem Soc, 2010. **132**(20): p. 6973-81.

54.   Li, M., et al., *Staphylococcus aureus mutant screen reveals interaction of the human antimicrobial peptide dermcidin with membrane phospholipids.* Antimicrob Agents Chemother, 2009. **53**(10): p. 4200-10.

55.   Monk, I.R., et al., *Transforming the Untransformable: Application of Direct Transformation To Manipulate Genetically Staphylococcus aureus and Staphylococcus epidermidis.* Mbio, 2012. **3**(2).

56.   Fuhrer, T., et al., *High-throughput, accurate mass metabolome profiling of cellular extracts by flow injection-time-of-flight mass spectrometry.* Anal Chem, 2011. **83**(18): p. 7074-80.

57.   Monk, J.M., et al., *iML1515, a knowledgebase that computes Escherichia coli traits.* Nat Biotechnol, 2017. **35**(10): p. 904-908.

58.   Guder, J.C., et al., *Time-Optimized Isotope Ratio LC-MS/MS for High-Throughput Quantification of Primary Metabolites.* Anal Chem, 2017. **89**(3): p. 1624-1631.

59.   Zittlau, K.I., et al., *Temporal Analysis of Protein Ubiquitylation and Phosphorylation During Parkin-Dependent Mitophagy.* Mol Cell Proteomics, 2022. **21**(2): p. 100191.

60.   Rappsilber, J., M. Mann, and Y. Ishihama, *Protocol for micro-purification, enrichment, pre-fractionation and storage of peptides for proteomics using StageTips.* Nat Protoc, 2007. **2**(8): p. 1896-906.

61.   Bekker-Jensen, D.B., et al., *A Compact Quadrupole-Orbitrap Mass Spectrometer with FAIMS Interface Improves Proteome Coverage in Short LC Gradients.* Mol Cell Proteomics, 2020. **19**(4): p. 716-729.

62.   Cox, J. and M. Mann, *MaxQuant enables high peptide identification rates, individualized p.p.b.-range mass accuracies and proteome-wide protein quantification.* Nat Biotechnol, 2008. **26**(12): p. 1367-72.

63.   Cox, J., et al., *Andromeda: a peptide search engine integrated into the MaxQuant environment.* J Proteome Res, 2011. **10**(4): p. 1794-805.

64.   Elias, J.E. and S.P. Gygi, *Target-decoy search strategy for increased confidence in large-scale protein identifications by mass spectrometry.* Nat Methods, 2007. **4**(3): p. 207-14.

65.   Schwanhausser, B., et al., *Global quantification of mammalian gene expression control.* Nature, 2011. **473**(7347): p. 337-42.

66.   Luber, C.A., et al., *Quantitative proteomics reveals subset-specific viral recognition in dendritic cells.* Immunity, 2010. **32**(2): p. 279-89.

67.   Wick, R.R., et al., *Unicycler: Resolving bacterial genome assemblies from short and long sequencing reads.* PLoS Comput Biol, 2017. **13**(6): p. e1005595.

68. Seemann, T., *Prokka: rapid prokaryotic genome annotation.* Bioinformatics, 2014. **30**(14): p. 2068-9.
69. Gurevich, A., et al., *QUAST: quality assessment tool for genome assemblies.* Bioinformatics, 2013. **29**(8): p. 1072-5.
70. Peltzer, A., et al., *EAGER: efficient ancient genome reconstruction.* Genome Biol, 2016. **17**: p. 60.
71. Kim, D., B. Langmead, and S.L. Salzberg, *HISAT: a fast spliced aligner with low memory requirements.* Nat Methods, 2015. **12**(4): p. 357-60.
72. Li, H., et al., *The Sequence Alignment/Map format and SAMtools.* Bioinformatics, 2009. **25**(16): p. 2078-9.
73. Okonechnikov, K., A. Conesa, and F. Garcia-Alcalde, *Qualimap 2: advanced multi-sample quality control for high-throughput sequencing data.* Bioinformatics, 2016. **32**(2): p. 292-4.
74. Liao, Y., G.K. Smyth, and W. Shi, *featureCounts: an efficient general purpose program for assigning sequence reads to genomic features.* Bioinformatics, 2014. **30**(7): p. 923-30.
75. Love, M.I., W. Huber, and S. Anders, *Moderated estimation of fold change and dispersion for RNA-seq data with DESeq2.* Genome Biol, 2014. **15**(12): p. 550.
76. Stamatakis, A., *RAxML version 8: a tool for phylogenetic analysis and post-analysis of large phylogenies.* Bioinformatics, 2014. **30**(9): p. 1312-3.
77. Asnicar, F., et al., *Precise phylogenetic analysis of microbial isolates and genomes from metagenomes using PhyloPhlAn 3.0.* Nat Commun, 2020. **11**(1): p. 2500.
78. Letunic, I. and P. Bork, *Interactive Tree Of Life (iTOL) v5: an online tool for phylogenetic tree display and annotation.* Nucleic Acids Res, 2021. **49**(W1): p. W293-W296.
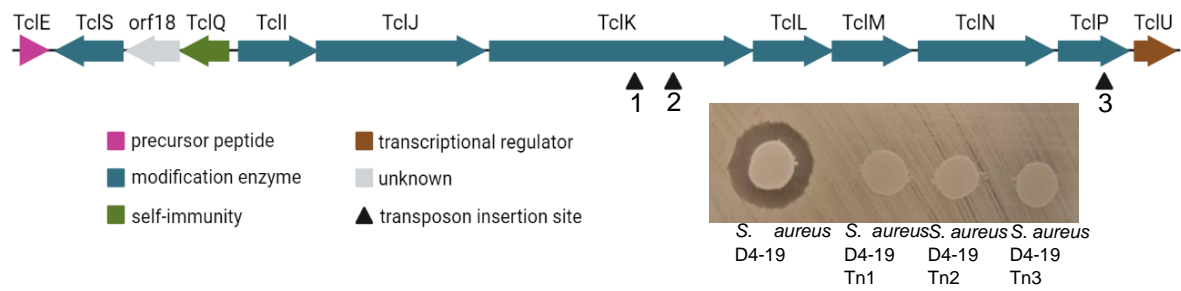
Supplemental information

Figure S1: Transposon insertion sites indicted in the MP1 gene cluster of *S. aureus* D4-19 as indicated by arrowheads and spot assay of these mutants on *S. aureus* USA300 LAC to confirm loss of antimicrobial activity.
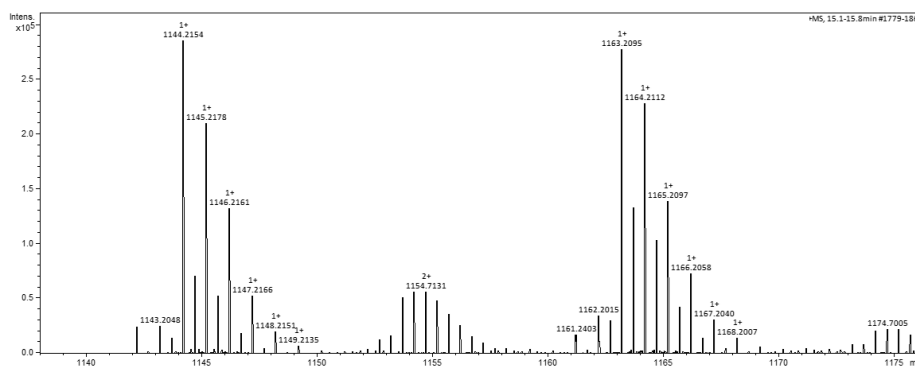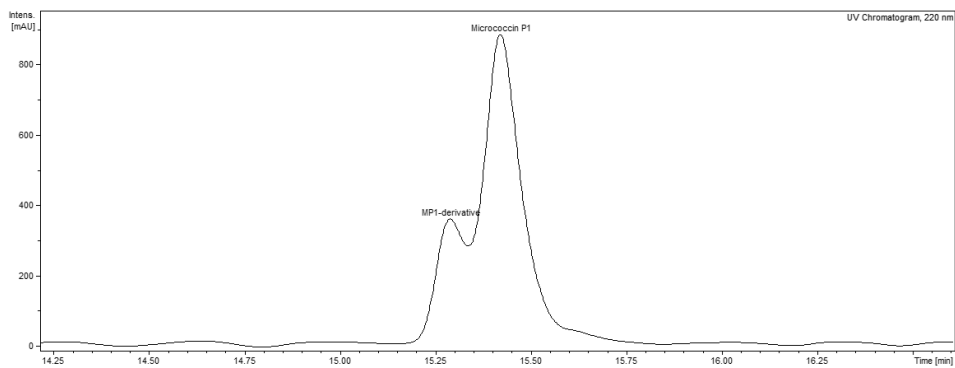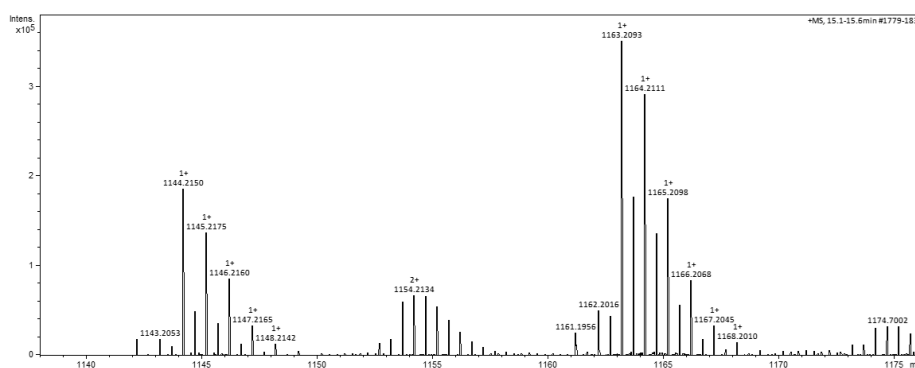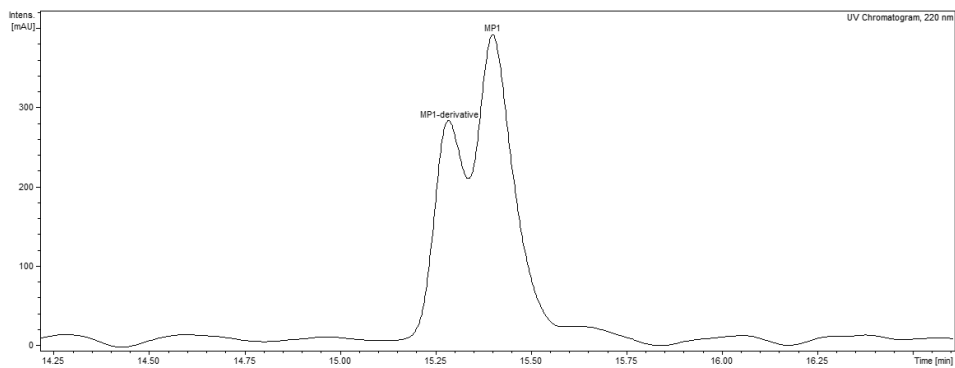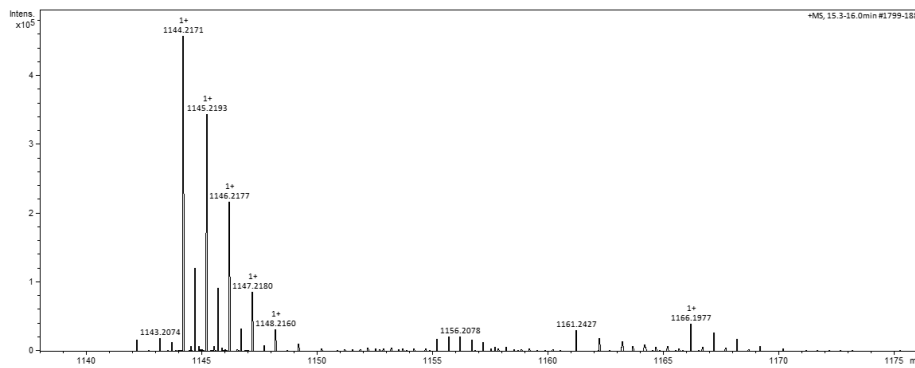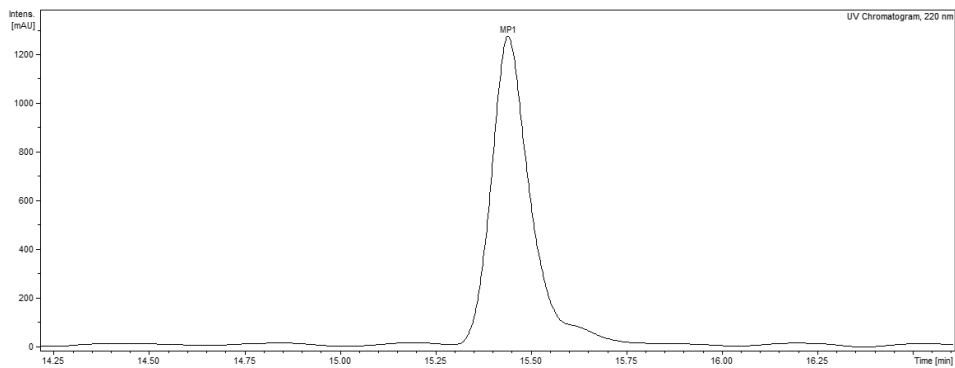
Figure S2: HPLC-UV spectrum (left) and MS spectrum (right) of *S. aureus* D4-19 (top), *S. aureus* RN4220 pD4-19 (middle) and *S. aureus* pD4-19 adapted (bottom). The UV spectra confirm the presence of MP1 in all three strains, and of a derivative in *S. aureus* RN4220 pD4-19 and *S. aureus* pD4-19 adapted. The MP1 peak has a mass of 1144.2154 $[M+H]^+$ and the derivate of 1163.2095 $[M+H]^+$.
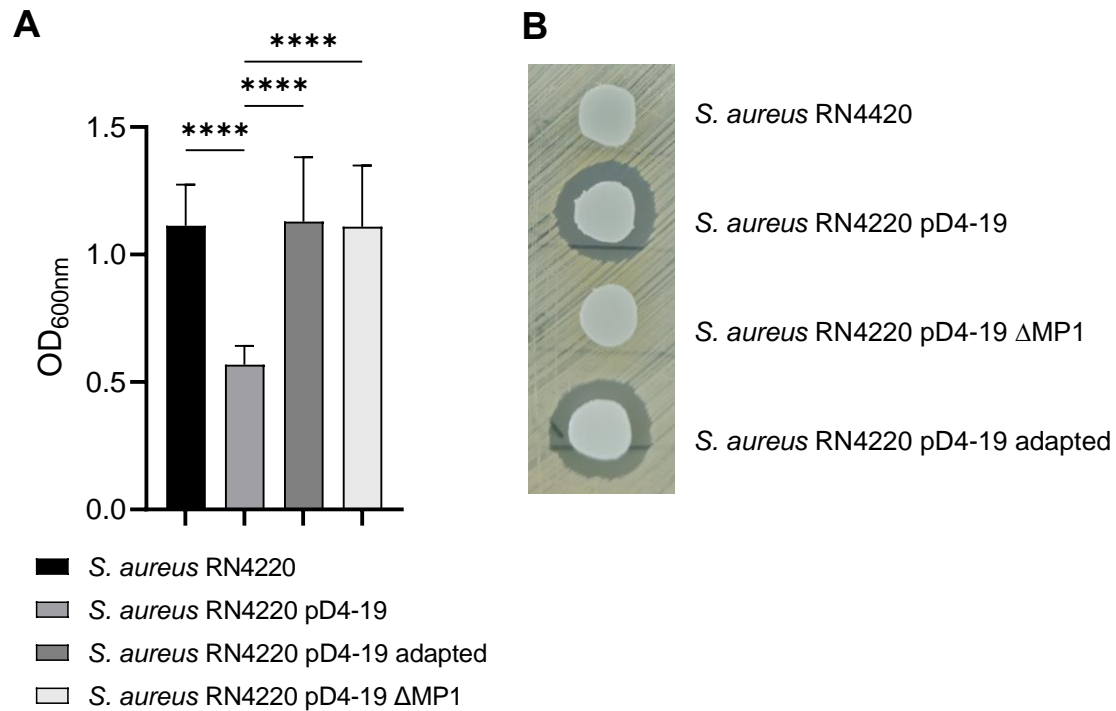

Figure S3: A) Endpoint OD_{600nm} of *S. aureus* RN4220, *S. aureus* RN4220 pD4-19, *S. aureus* RN4220 pD4-19 adapted and *S. aureus* RN4220 pD4-19 ΔMP1 after 20 h in a 24-well microtiter plate. **B)** Spot assay of *S. aureus* RN4220, *S. aureus* RN4220 pD4-19, *S. aureus* RN4220 pD4-19 adapted and *S. aureus* RN4220 pD4-19 ΔMP1 on BM plate with *S. aureus* USA300 LAC as indicator strain. Statistical significance was calculated using an ordinary One-way ANOVA (Tukey's multiple comparisons test)(****$p < 0.0001$).

	100 µg/ml	50 µg/ml	25 µg/ml	12.5 µg/ml	6.25 µg/ml	3.13 µg/ml	1.56 µg/ml	0.78 µg/ml	0.39 µg/ml	0.2 µg/ml	GC
S. aureus USA 300	0.156	0.099	0.043	0.035	0.025	0.021	0.012	0.019	0.130	-0.001	1.402
S. aureus RN4220	0.121	0.069	0.025	0.010	0.004	0.000	0.008	0.004	0.009	0.006	0.969
S. aureus RN4220 pD4-19	1.243	1.261	1.175	0.928	1.219	1.026	1.020	1.085	1.277	1.257	1.305
S. aureus RN4220 pD4-19 ΔPP	1.326	1.275	1.229	1.267	1.264	1.271	1.240	1.248	1.331	1.260	1.306
S. aureus D4-19	1.385	1.434	1.414	1.433	1.403	1.432	1.418	1.427	1.424	1.428	1.370
S. aureus D4-19 ΔPP	1.341	1.381	1.356	1.354	1.337	1.334	1.354	1.329	1.356	1.343	1.341

Figure S4: MIC values of purified MP1 were assessed against *S. aureus* USA300, *S. aureus* RN4220, *S. aureus* RN4220 pD4-19, *S. aureus* RN4220 pD4-19 ΔPP, *S. aureus* D4-19, *S. aureus* D4-19 ΔPP. The highest concentration of MP1 (100 µg/ml) leads to the formation of a precipitate which explains the higher OD values for the two wild type strains at this MP1 concentration. A growth control (GC) is included where no MP1 was added to the well.
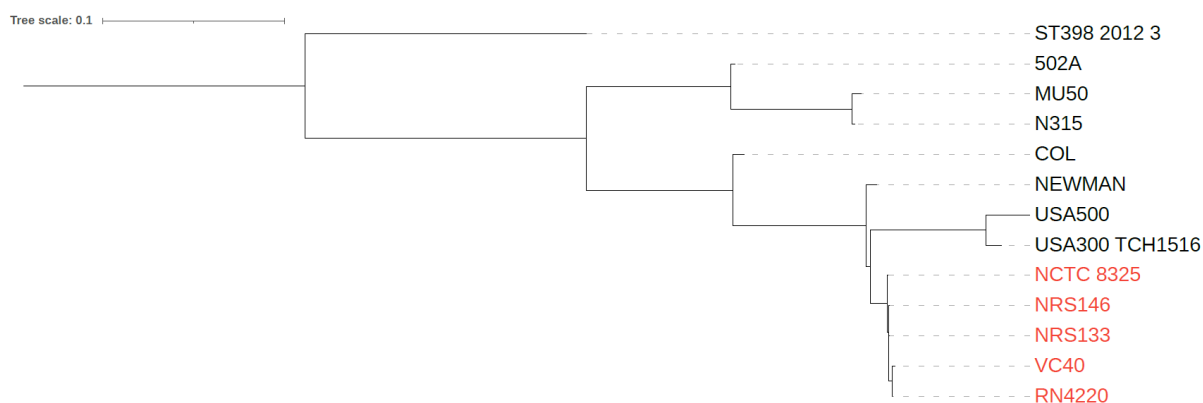

Figure S5: Phylogenetic tree of selected *S. aureus* strains from different lineages based on the identity of the *citZ* gene. *S. aureus* RN4220 with the ancestor strain NCTC8325 and three other strains also deriving from NCTC8325 show a mutated start codon (from "ATG" to "ATA") in *citZ* compared to other representatives of the *S. aureus* clade.
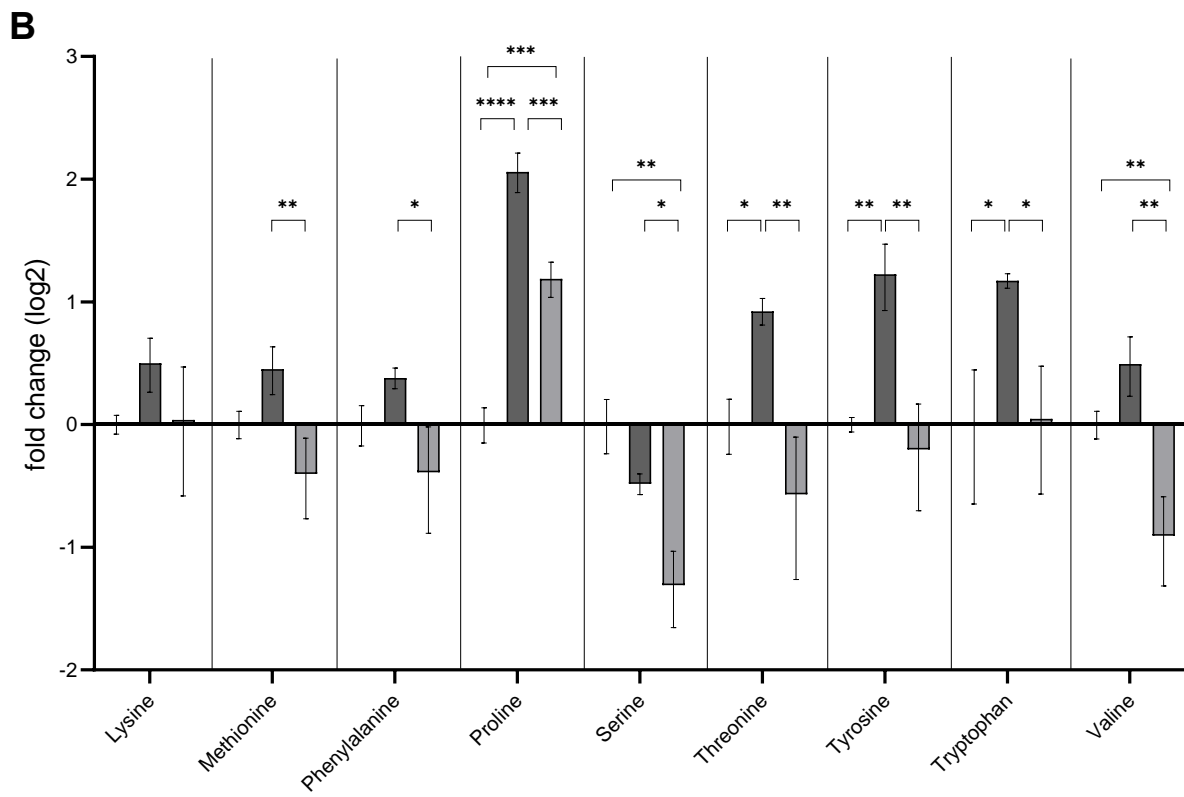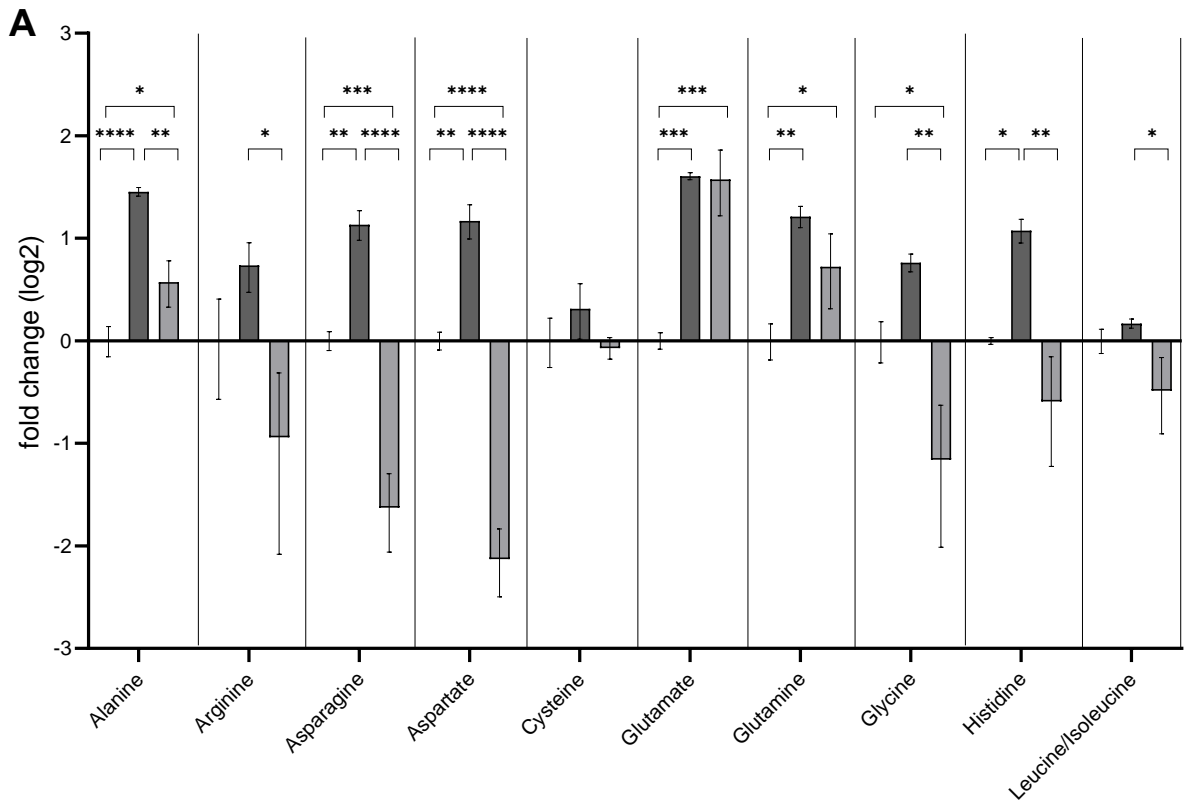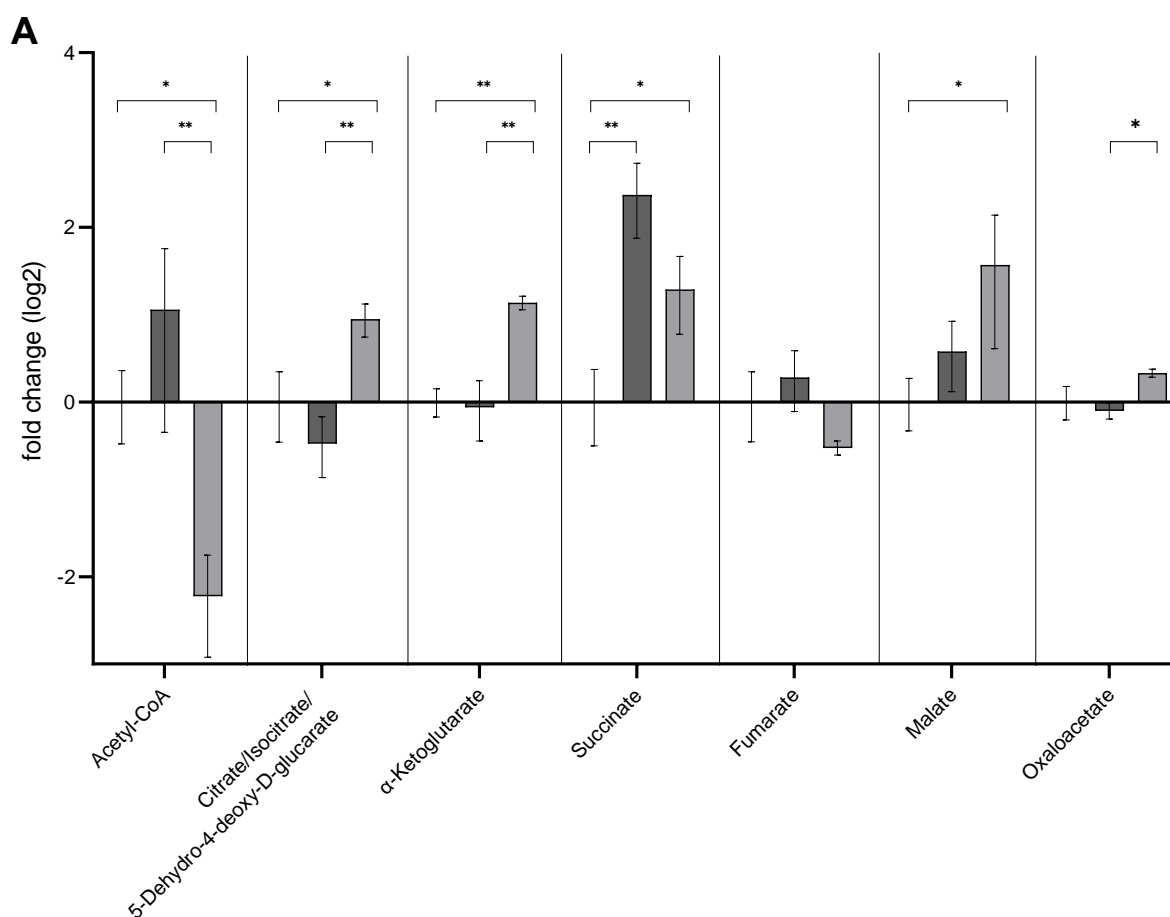
Figure S6: A) Amino acid levels as measured via metabolome analysis in *S. aureus* RN4220 (black), *S. aureus* RN4220 pD4-19 (dark grey) and *S. aureus* RN4220 pD4-19 adapted (light grey). Metabolite concentrations (for LC-MS/MS method) or ion intensities (for FI-MS) are shown as log2-fold changes that are normalized to *S. aureus* RN4220. Amino acids (except cysteine) were measured using LC-MS/MS, cysteine [M-H]⁻ levels were measured via FI-MS. **B)** Amino acid levels as detected via metabolome analysis in *S. aureus* RN4220 (black), *S. aureus* RN4220 pD4-19 (dark grey) and *S. aureus* RN4220 pD4-19 adapted (light grey). Metabolite concentrations (for LC-MS/MS method) are shown as log2-fold changes that are normalized to *S. aureus* RN4220. All amino acids were measured using LC-MS/MS. The p-values were calculated using an ordinary One-way ANOVA (Tukey's multiple comparisons test). Statistical significance is indicated by *p < 0.05, **p < 0.01, ***p < 0.001, ****p < 0.0001.
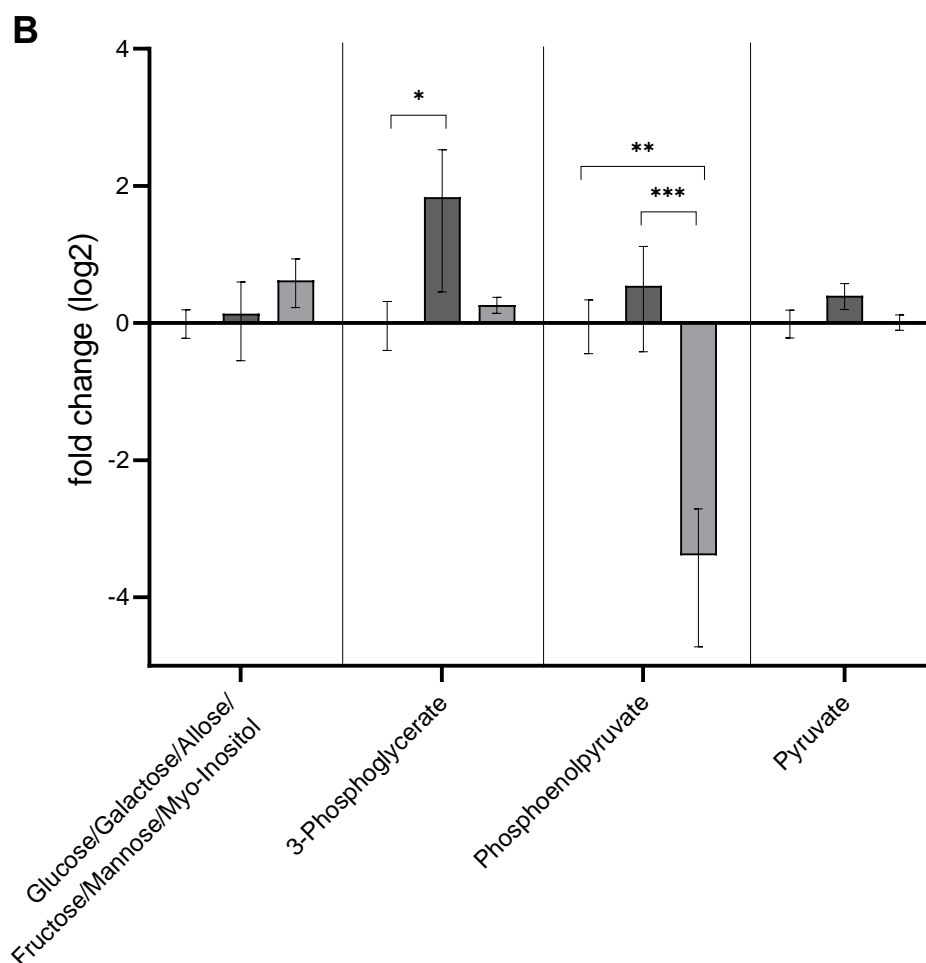
Figure S7: A) TCA intermediates as measured via metabolome analysis in *S. aureus* RN4220 (black), *S. aureus* RN4220 pD4-19 (dark grey) and *S. aureus* RN4220 pD4-19 adapted (light grey). Metabolite concentrations (for LC-MS/MS method) or ion intensities (for FI-MS) are shown as log2-fold changes that are normalized to *S. aureus* RN4220. The FI-MS method was used to measure citrate and its isobars isocitrate and 5-Dehydro-4-deoxy-D-glucarate [M-H]⁻, α-ketoglutarate [M-H]⁻, fumarate [M-H]⁻, malate [M-H]⁻, oxaloacetate [M-H]⁻. The rest was measured using LC-MS/MS. **B)** Glycolysis intermediates detected via metabolome analysis in *S. aureus* RN4220 (black), *S. aureus* RN4220 pD4-19 (dark grey) and *S. aureus* RN4220 pD4-19 adapted (light grey). Metabolite concentrations (for LC-MS/MS method) or ion intensities (for FI-MS) are shown as log2-fold changes that are normalized to *S. aureus* RN4220. The FI-MS method was used to measure pyruvate [M-H]⁻ and glucose [M-H]⁻ (and its isobars galactose, allose, fructose, mannose and myo-inositol), LC-MS/MS was used for the other metabolites. The p-values were calculated using an ordinary One-way ANOVA (Tukey's multiple comparisons test). Statistical significance is indicated by *p < 0.05, **p < 0.01, ***p < 0.001, ****p < 0.0001.
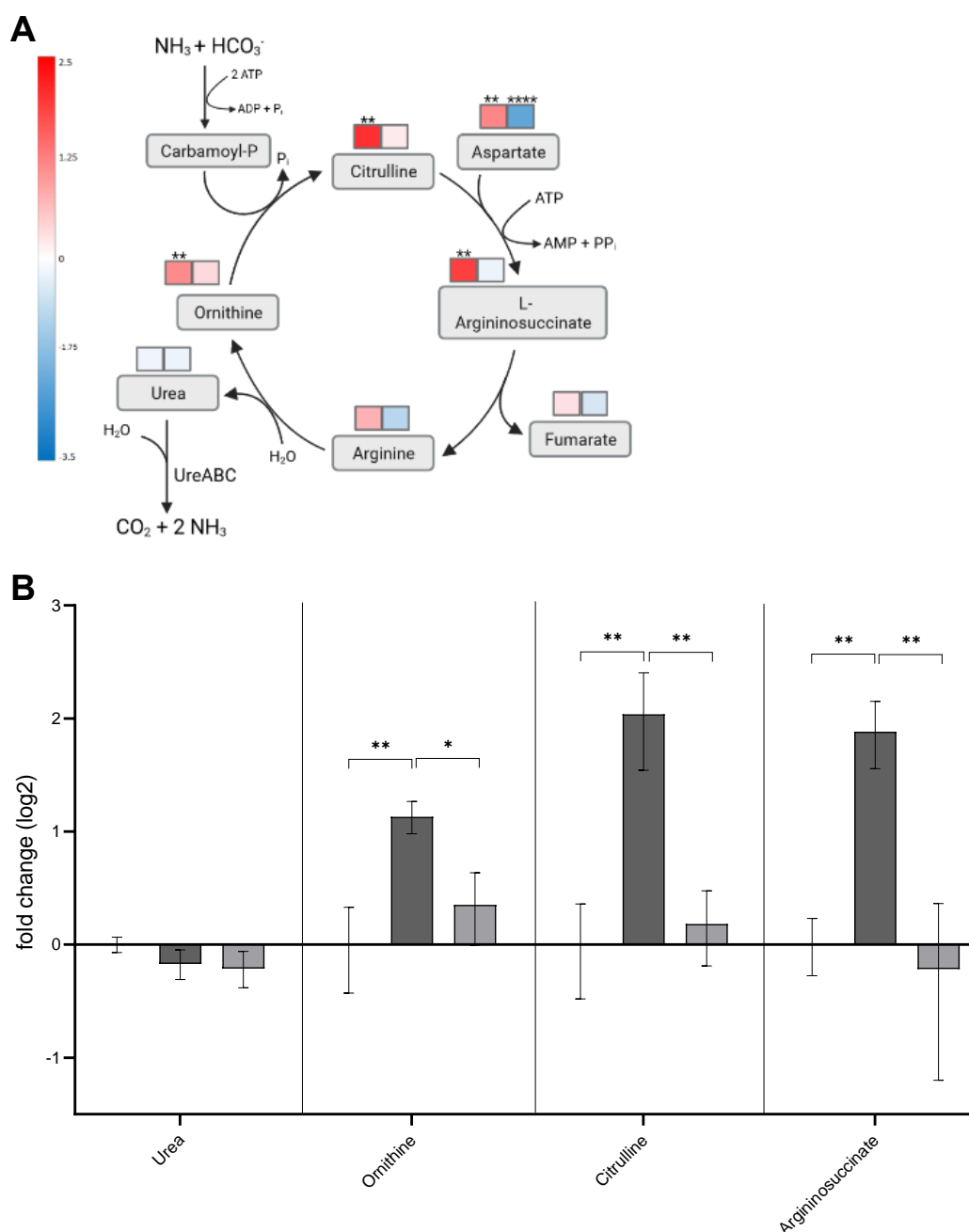
Figure S8: A) Summary of the metabolic differences in urea cycle intermediated between *S. aureus* RN4220 pD4-19 and *S. aureus* RN4220 pD4-19 adapted. The indicated log2 fold changes were calculated for *S. aureus* RN4220 pD4-19 (left box) and *S. aureus* RN4220 pD4-19 adapted (right box) vs. *S. aureus* RN4220, respectively. The fold change is indicated by different colours: a decrease in metabolite levels compared to *S. aureus* RN4220 is depicted in blue, an increase in metabolite levels compared to *S. aureus* RN4220 is depicted in red. **B)** Urea cycle intermediates as measured via metabolome analysis in *S. aureus* RN4220 (black), *S. aureus* RN4220 pD4-19 (dark grey) and *S. aureus* RN4220 pD4-19 adapted (light grey). Metabolite concentrations (for LC-MS/MS method) or ion intensities (for FI-MS) are shown as log2-fold changes that are normalized to *S. aureus* RN4220. The FI-MS method was used to measure citrulline $[M+H]^+$. Urea, ornithine and argininosuccinate were measured using LC-MS/MS. The p-values were calculated using an ordinary One-way ANOVA (Tukey's multiple comparisons test). Statistical significance is indicated by *$p < 0.05$, **$p < 0.01$, ***$p < 0.001$, ****$p < 0.0001$.
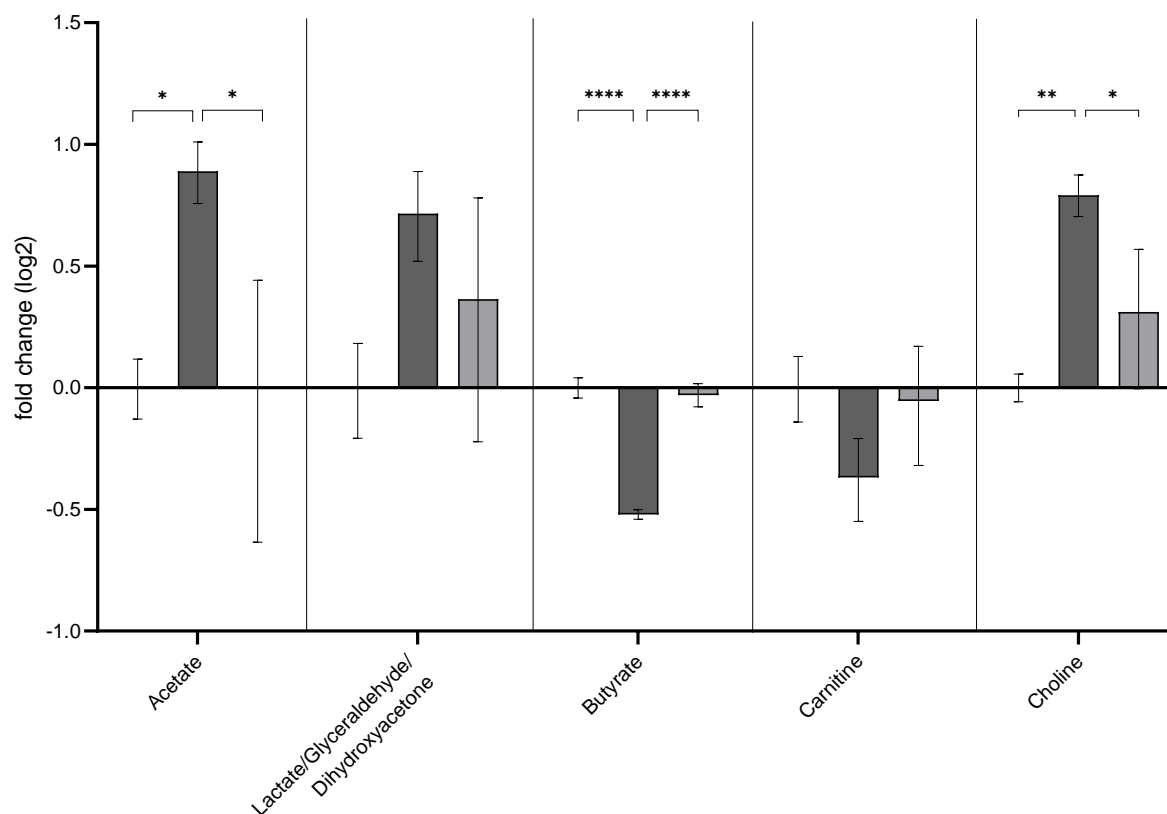
Figure S9: Fermentation products and osmoprotectants as measured via metabolome analysis in *S. aureus* RN4220 (black), *S. aureus* RN4220 pD4-19 (dark grey) and *S. aureus* RN4220 pD4-19 adapted (light grey). Metabolite concentrations (for LC-MS/MS method) or ion intensities (for FI-MS) are shown as log2-fold changes that are normalized to *S. aureus* RN4220. The FI-MS method was used to measure acetate [M-H]⁻, lactate and its isobars glyceraldehyde and dihydroxyacetone [M-H]⁻, butyrate [M+H]⁺, carnitine [M+H]⁺, and choline [M+H]⁺. The p-values were calculated using an ordinary One-way ANOVA (Tukey's multiple comparisons test). Statistical significance is indicated by *$p < 0.05$, **$p < 0.01$, ***$p < 0.001$, ****$p < 0.0001$.
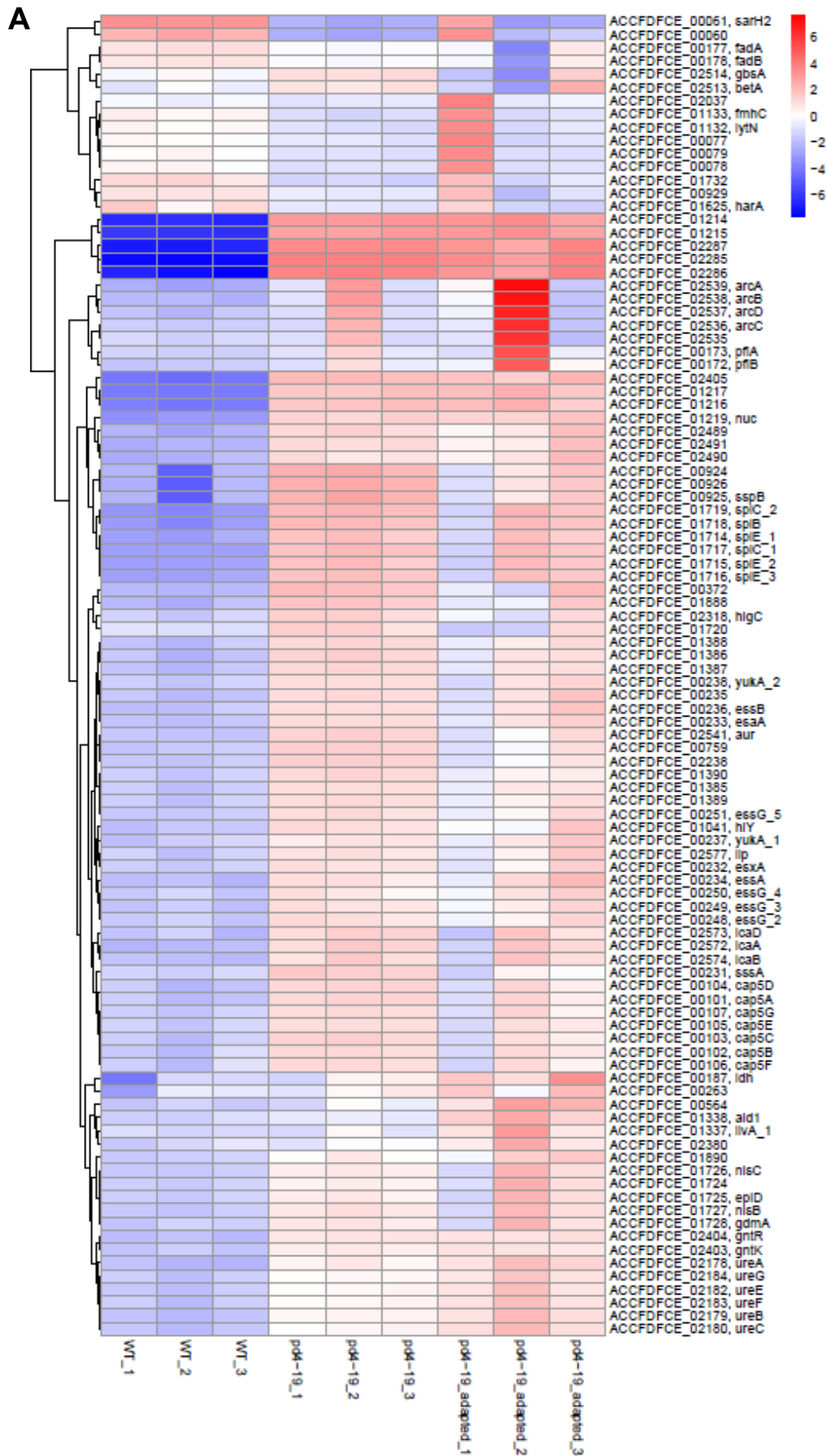
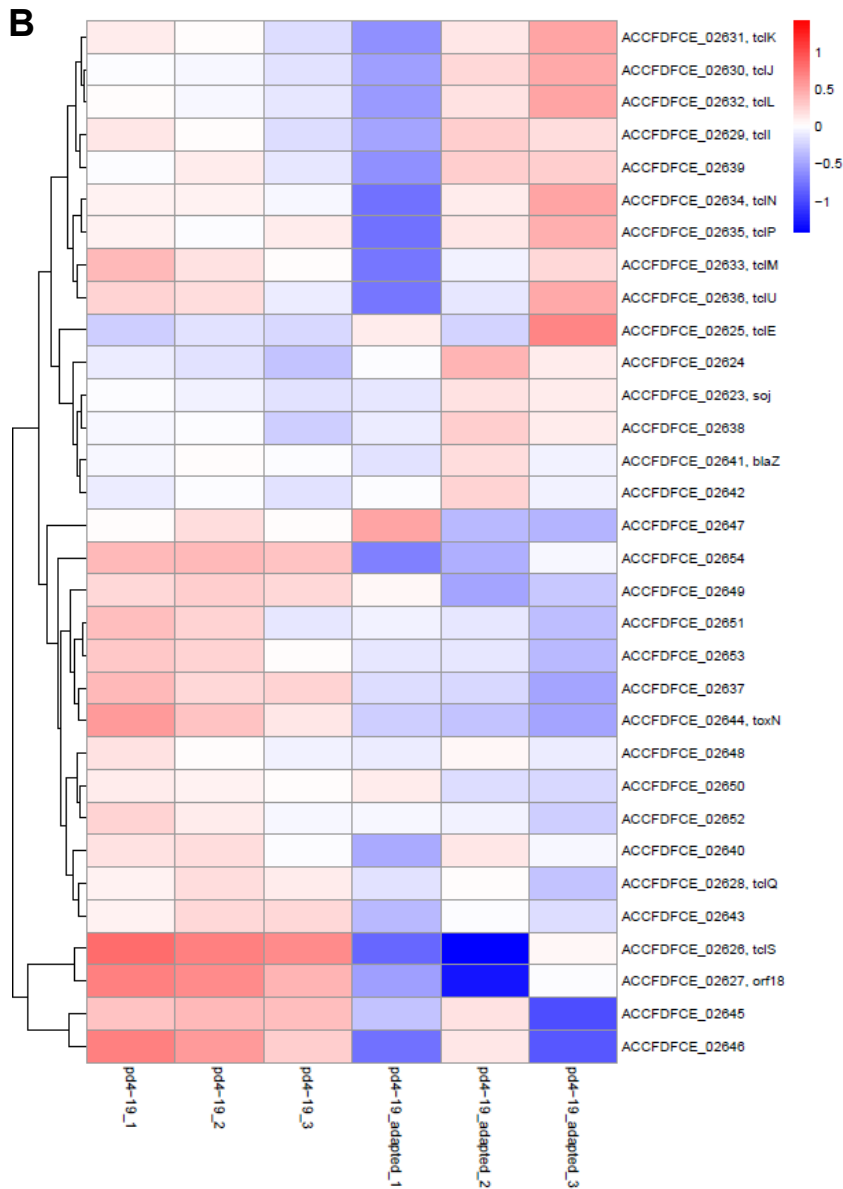**Figure S10:** Heat maps showing normalized expression (variance stabilizing transformation) centred on the mean of each row. **A)** Heat map of the 100 most differentially expressed genes in *S. aureus* RN4220 (WT), *S. aureus* RN4220 pD4-19 and *S. aureus* RN4220 pD4-19 adapted. **B)** Heat map of all genes expressed on pD4-19 in *S. aureus* RN4220 pD4-19 and *S. aureus* RN4220 pD4-19 adapted.

Chapter 6 – General Discussion

Bacteriocin BGCs frequently found and exchanged in nasal microbiome

The human microbiome has long been an understudied field, due to the non-culturability of most members of the microbiome under lab conditions [1, 2]. Cataloguing of human microbial communities from various body sites by the Human Microbiome Project was a key step defining the basic composition of the human microbiome. The authors concluded that the microbiome is highly individual and changes over time and between body sites [3-5]. Recent studies revealed that the composition of microbial communities has a great influence on the overall human health and disease development [6-9].

A distinct community of bacterial species comprises the human nasal microbiome, where most of the inhabitants act as commensals, but some also as pathobionts, which can switch between commensal and pathogenic state causing a variety of infections [10]. One of them is *S. aureus,* colonizing the anterior nares of approximately 30% of the human population, which is a risk factor for infection [10-12]. The nasal carriage of *S. aureus* is a highly dynamic and complex process and relies on the interaction of the bacterium with the nasal microbiota and the host [13-15]. Why only a subset of individuals is permanently colonized by *S. aureus* remains unclear. Identifying the factors which promote or prevent pathogen colonization and the underlying mechanisms which shape the microbiome composition, are of great interest.

The human microbiome composition is strongly influenced by microbe-microbe and microbe-host interactions. Mainly mediated by secondary metabolites and other public goods, these interactions can be advantageous or unfavourable for the producer or recipient [16-18]. To overcome competitors and to finally achieve niche occupation, bacteria produce antimicrobial compounds like bacteriocins inhibiting competing bacteria in the vicinity of the producer cell [15, 19, 20]. Donia et al. performed a systematic metagenome analysis of BGCs in the human microbiome and confirmed, that the human microbiome is a rich source of diverse BGCs for in general secondary metabolites or public goods, distributed across different bacterial taxa and with most of them never described before [21]. This study highlights the importance to deepen our knowledge about the human microbiome and the influence of secondary metabolites on the overall microbiota composition and to acknowledge it as a rich source of novel compounds.

Bacteria not only kill each other via the production of bacteriocins, but also share the genetic information or the BGCs via HGT with bacteria in their surroundings. Bacteriocin BGCs are often located on MGEs, like plasmids or transposons, facilitating the exchange of these BGC

via different mechanisms like transformation, conjugation, or transduction. This is indicated by the frequent acquisition and loss of bacteriocin BGCs. Thus, HGT is a major driver of bacterial adaptation, genetic variation, and evolution and makes bacteriocin production a strain-specific more than a species-specific trait [22-25].

Especially staphylococci seem to be a rich source for bacteriocin BGCs, as a study from Janek et al. could show that out of 89 nasal staphylococcal strains, 84% showed bacteriocin-like inhibitory activities against various test strains. Exhibiting rather narrow but distinct antimicrobial activity spectra, reflecting the identification of different BGCs, these BGCs also seem to be frequently transferred via HGT, due to their localisation on plasmids or flanking by MGEs on the chromosome [26]. This highlights the importance of HGT in shaping the human nasal microbiome by facilitating the dissemination of bacteriocin BGCs in the bacterial community.

In this follow up study we could confirm the findings from Janek et al., where 15 different BGCs could be identified in nasal staphylococci (Supplementary data, Table 1). Among them are already well known bacteriocins like epidermin [27] or micrococcin P1 [28], but also a set of poorly or non-characterised compounds. 60% of the identified BGCs are located on a plasmid indicating potential mobility of these BGCs via HGT. Chromosomally encoded BGCs would need to be further analysed for the presence of MGE in the vicinity of the BGC. Interestingly, in some strains more than one BGC could be identified, sometimes even located on distinct plasmids, highlighting the advantage and frequency of BGC acquisition. However, the reasons for this costly maintenance of two plasmids remain to be elucidated [29]. For some *E. coli* strains it is already described, that different bacteriocins co-associate in one strain [30]. This study could confirm that the nasal microbiota is a rich source for antimicrobials, with still a lot of compounds to discover and that HGT is an important factor for BGC distribution.

Three of the identified BGCs are of major interest due to their antimicrobial activity against methicillin-resistant *S. aureus* (MRSA) and their location on MGEs. First, the lugdunin BGC found in *S. lugdunensis* IVK28, which is the first microbiome derived non-ribosomal peptide (NRP) and belongs to the newly described group of fibupeptides. Second, the epifadin BGC identified in *S. epidermidis* IVK83, which is the first staphylococcal bacteriocin synthesized by NRP synthetases (NRPS) and polyketide synthases (PKS). And third, the micrococcin P1 (MP1) BGC found in *S. aureus* D4-19, where HGT of this BGC led to physiological burdens by disbalancing the central metabolism.

Lugdunin, the first fibupeptide antibiotic isolated from human nasal microbiome

The lugdunin BGC comprises the biosynthetic *lugABCD* genes, the putative regulator gene *lugR* and the *lugIEFGH* genes associated with export and producer immunity. Furthermore, some accessory genes like *lugT*, encoding a putative type-II thioesterase, *lugZ*, encoding a homolog to 4'-phosphopantetheinyl transferases and further downstream, probably forming a separate transcriptional unit, *lugM*, which encodes a putative monooxygenase with a yet unknown influence on the synthesis, are part of the BGC [31]. Just recently, the exact roles of the two ABC transporters LugEF and LugGH have been elucidated. We could demonstrate the distinct, but also overlapping roles of the two transporters in lugdunin secretion (LugEF) and self-resistance (LugGH), and the contributing role of the small accessory putative membrane protein LugI. Interestingly, the two transporters and LugI are needed to generate full-level resistance.

The G+C content of the BGC is significantly lower compared to the rest of the chromosome, indicating that this BGC was acquired from a species with lower G+C content via horizontal gene transfer [32, 33]. Genetic analysis of producing and non-producing *S. lugdunensis* isolates revealed that the lugdunin BGC is located at the same genetic position in all isolates, and that the adjacent genes can also be found in the non-producing strains (unpublished data). These findings indicate, that the lugdunin BGC was frequently transferred and integrated into *S. lugdunensis* genomes in a highly conserved way. However, it might also be the case, that at speciation of the first *S. lugdunensis* strain, the BGC was either taken up or already present in that strain and that it got lost over time during evolution in a few strains due to cessation of selection pressure. To clarify this, it would be necessary to determine the distribution of the lugdunin BGC in different clonal complexes, to see if a certain lineage has lost the BGC. Notably, the BGC was never found in another bacterial species than *S. lugdunensis,* leading to the assumption that this BGC is a very species-specific trait.

When acquiring a bacteriocin BGC, producer-immunity is an elementary feature which needs to come with the BGC. Immunity is mainly limited to the produced compound or derivatives and achieved via export by transporters, expression of altered target proteins or proteases which inactivate the compound [34, 35]. ABC transporters which rely on accessory proteins like LugI, to achieve full export function and immunity, were already described for lantibiotic BGCs. In general, the LanFEG ABC transporter relying on the extracellular lipoprotein LanI, the LanFE(G) ABC transporter requiring the accessory protein LanH and the LanTH ABC transporter, which can provide immunity in the presence of any accessory protein, are described for various lantibiotics [27, 36-40]. The ISK-1 BGC, for example, encodes the membrane protein NukH, which acts together with the NukFEG ABC transporter to achieve full level producer-immunity. Heterologous expression of *nukFEG* or *nukH* conferred only partial

self-resistance against nukacin ISK-1, suggesting that NukH, similar to LugI, contributes to self-protection mediated by NukFEG or LugEFGH respectively [41, 42].

Unlike multidrug transporters (MDR) that export structurally distinct molecules, ABC transporters conferring producer-immunity appear to be specific for their substrates [43]. This can also be seen for LugIEFGH, which is only capable to mediate immunity against lugdunin and, already with lower efficacy, to some but not all derivatives. Future structure elucidation studies would help to identify potential interactions between lugdunin, the transporters LugEF and LugGH and the accessory membrane protein LugI.

Epifadin, an extremely short-lived antimicrobial

In contrast to the lugdunin BGC, which is present in most *S. lugdunensis* genomes, the epifadin BGC is encoded on a plasmid in a strain-specific manner. Five *S. epidermidis* strains, belonging to four different multi-locus sequence types, were found to harbour the epifadin BGC with almost 100% sequence identity. The strains were isolated in three different countries from different body sites of the skin and nose, indicating a widespread ecological relevance of the epifadin BGC. In public genome databases the plasmid itself and the epifadin BGC were absent from all available *S. epidermidis* genomes, indicating that the BGC is an infrequent accessory genetic element.

All the identified plasmids encode a relaxase gene of the newly described Mob_L family, which is exclusively found in Firmicutes [44]. Relaxases are essential for mobilization of genetic elements via conjugation [45], thus indicating, that the plasmids might have been horizontally exchanged between the different *S. epidermidis* clonal groups via conjugation. Furthermore, the plasmids seem to be highly stable since the size of the plasmids and the BGC sequences are almost identical.

Besides in *S. epidermidis,* the epifadin encoding plasmid could be identified in two *Staphylococcus saccharolyticus* genomes with high similarity indicating HGT also across species boundaries [46]. Clusters with similar gene organization can be found in the genome of plant-associated *Lactococcus lactis* strains [47, 48] and on a genomic island identified in oral *Streptococcus mutans* strains [49]. Structural information for the streptococcal and lactococcal compound are lacking, making it impossible to conclude if these BGCs also produce epifadin or only resemble the epifadin biosynthesis. However, if epifadin would be synthesised by these strains, it would be another example of HGT of a bacteriocin BGC between bacterial classes in the human microbiome.

Micrococcin P1, horizontal gene transfer leads to metabolic changes in the producer

The micrococcin P1 (MP1) BGC has already been identified in various different species, including *Micrococcus sp.* [50], *Bacillus pumilus* [51], *Staphylococcus equorum* WS2733 [52], *Bacillus cereus* ATCC14579 [53], *Macrococcus caseolyticus* 115 [54], *Staphylococcus hominis* S34-1 [55], *Mammaliicoccus sciuri* IMDO-S72 [56] and *S. aureus* MK65 [57]. The NCBI database, furthermore, includes homologous sequences to the MP1 BGC in distantly related *S. aureus* isolates. The BGC is mainly located on plasmids and is associated with mobilization genes highlighting the multiple and frequent inter- and intra-species transfer of this BGC via HGT. These clear hints for MGE and HGT underline the advantage of acquisition and production of MP1 in various different ecological niches.

However, little is known about the costs and consequences of HGT especially when MGEs encode antibiosis islands like MP1. In general, HGT is one of the major drivers of evolution in bacterial populations because the transfer of foreign DNA allows the acquisition of new functions and ecologically important traits and thus rapid adaptation to novel environments [58-60]. One of the best examples for the effectiveness of HGT is the rapid dissemination of antibiotic resistance genes throughout bacterial populations [61]. HGT can occur between taxonomically distinct bacterial lineages, and even between kingdoms blurring the boundaries between clades and driving bacterial speciation [62-64].

Plasmids are key elements of HGT and, from an evolutionary perspective, considered as selfish genetic elements, as they encode genes controlling their own replication and transmission. They can exist independently of the host bacterial genome, with fitness or evolutionary purposes that do not necessarily align with the interests of the bacterial host [59, 65, 66]. As already mentioned, plasmids consist of a backbone containing essential genes controlling core plasmid functions, and furthermore, more importantly, accessory genes, which are potentially beneficial for the host and provide the currency of HGT [59, 67]. Accessory genes are often carried on smaller MGEs embedded on the plasmid, allowing mobilization within and between plasmids and integration into the host chromosome. Virulence genes, genes conferring resistance to antimicrobials, like antibiotics and heavy metals, genes for antimicrobial or bacteriocin biosynthesis and genes for metabolic functions represent the majority of accessory genes on plasmids [68, 69].

Newly acquired DNA must provide a strong enough benefit or low enough fitness cost to be maintained within a population and not being lost due to genetic drift or selection. However, due to conflicts within the new genomic background, recently acquired DNA can be energetically or physiologically costly despite the great evolutionary benefits [70, 71]. Successful bacteriocin production in a strain, which freshly acquired the responsible genes via HGT, depends on many factors, like plasmid stability, expression of secretion systems,

bacteriocin immunity and plasmid copy numbers [69, 72]. We could indeed demonstrate that sudden MP1 production imposes a strong burden on the producer *S. aureus* RN4220 visible by impaired growth. It is already well known that after the transfer of a plasmid strains experience a metabolic burden associated with the plasmid. This is indicated by lengthening of lag phase, decrease in maximum growth rates or cell densities, or changes in oxygen consumption or biofilm formation [73-77]. However, deletion of the MP1 precursor peptide and thus termination of MP1 biosynthesis could reverse the observed phenotype, indicating that indeed MP1 production and not the maintenance of pD4-19 is the limiting factor.

In general, gene product synthesis for lots of cellular functions involves high energetic or nutritional costs which can reduce bacterial cell densities [78-80]. Protein biosynthesis, for example, consumes intracellular energy resources like GTP, nutrients as building blocks and cellular machineries like ribosomes, polymerases, and chaperones whose availability might be limited [81-83]. Bacteriocins are, as their alternative name "ribosomally synthesized and post-translationally modified peptides" (RiPPs) already indicates, using the host protein biosynthesis machinery for synthesis. Ribosomal translation of the precursor peptide, and especially of the modifying enzymes and, in case of MP1, synthesis of the self-immunity protein needs to be integrated into the cellular metabolism of the new producer strain [54, 84, 85].

Only a few studies exist on how bacteriocin production impacts the fitness of the producer, but in general, production rates of bacteriocins strongly correlate with the growth rate of the producer. Supplementation of growth medium with carbohydrate and/or nitrogen sources (amino acids and peptides) and salts can result in increased growth and bacteriocin production [86, 87]. This already indicates that bacteriocin production disturbs the usual metabolic fluxes of the producer cell and leads to an intracellular resource partition between growth and bacteriocin production [88]. Maldonado-Barragán et al. could show that constitutive production of plantaricin in *Lactobacillus plantarum* negatively impacts growth rates and that the strain reduces bacteriocin production when growing alone, to avoid costly production of plantaricin when the benefit of killing competitors is not existent [89].

Coevolutionary changes in both the plasmid and the host resulting in increased fitness have been described to occur after long-term association between plasmids and their hosts [90, 91]. Since bacteriocins are often located on plasmids, one could assume, that bacterial strains can adapt not only to the plasmid, but also to bacteriocin production. Indeed, plasmid-encoded colicin producing *Escherichia coli* showed increased fitness after 800 generations of growth in glucose-limited medium compared to plasmid-free strains [92]. Kloos et al. could show that compensatory mutations in the carbon catabolite repression and the aerobic respiration control in extraintestinal pathogenic *E. coli* strains are reversing deleterious effects of a multidrug-resistance plasmid. The authors conclude that these mutations led to transcriptional rewiring

which facilitate niche adaptation with plasmid maintenance as a side effect [93]. This is in line with our finding that the compensatory mutation in *citZ,* which occurred during the adaptation process, leads to reversion of the observed phenotype. This single mutation led to general changes observable in the transcriptome and metabolome and, in summary, to metabolic adaptation to MP1 production.

To conclude, HGT of bacteriocin BGCs comes with both benefits and costs for the new host. The benefit of competing against other bacteria in their ecological niche via bacteriocin production is affected by the extent of how strongly usual metabolic fluxes of the producer cell are disturbed by resource partition for growth and bacteriocin production. Compensatory mutations can lead to amelioration of the negative influence of bacteriocin production on the central metabolism. In general, the MP1 BGC seems to be highly mobile since it can be found in various different bacterial genera. These findings highlight the advantage of acquisition and production of MP1 in different ecological niches, despite its initial negative effects on bacterial fitness.

Final conclusions

This study highlights the frequency of HGT of bacteriocin BGCs in the human nasal microbiome. With HGT being the major driver of bacterial evolution, it allows bacteria in the nasal microbiome to rapidly acquire bacteriocin BGCs to either remain or invade new ecological niches by successfully competing against other bacteria. We were able to identify the same bacteriocin BGCs in taxonomically distinct bacterial lineages, highlighting the strong impact of HGT on bacterial speciation. The metabolic costs, which are associated with bacteriocin production after HGT, can be compensated by mutations to reverse the initial negative effect of production. In summary it can be said that the human nasal microbiome is a rich source of many unknown BGCs, which await to be explored to further deepen our knowledge in the field of microbiome research.

1.   Blum, H.E., *The human microbiome.* Adv Med Sci, 2017. **62**(2): p. 414-420.
2.   Rogers, K., *"human microbiome",* in *Encyclopedia Britannica.* 2022.
3.   Turnbaugh, P.J., et al., *The human microbiome project.* Nature, 2007. **449**(7164): p. 804-10.
4.   Proctor, L.M., *The Human Microbiome Project in 2011 and beyond.* Cell Host Microbe, 2011. **10**(4): p. 287-91.
5.   Human Microbiome Project, C., *Structure, function and diversity of the healthy human microbiome.* Nature, 2012. **486**(7402): p. 207-14.
6.   Aagaard, K., *The Human Microbiome of Local Body Sites and Their Unique Biology*, in *Mandell, Douglas, and Bennett's Principles and Practice of Infectious Diseases.* 2014.
7.   Le Chatelier, E., et al., *Richness of human gut microbiome correlates with metabolic markers.* Nature, 2013. **500**(7464): p. 541-6.
8.   Nejman, D., et al., *The human tumor microbiome is composed of tumor type-specific intracellular bacteria.* Science, 2020. **368**(6494): p. 973-980.
9.   Arrieta, M.C., et al., *The intestinal microbiome in early life: health and disease.* Front Immunol, 2014. **5**: p. 427.
10.   Lemon, K.P., *Human nasal microbiota.* Curr Biol, 2020. **30**(19): p. R1118-R1119.
11.   Kluytmans, J., A. van Belkum, and H. Verbrugh, *Nasal carriage of Staphylococcus aureus: epidemiology, underlying mechanisms, and associated risks.* Clin Microbiol Rev, 1997. **10**(3): p. 505-20.
12.   von Eiff, C., et al., *Nasal carriage as a source of Staphylococcus aureus bacteremia. Study Group.* N Engl J Med, 2001. **344**(1): p. 11-6.
13.   Brown, A.F., et al., *Staphylococcus aureus Colonization: Modulation of Host Immune Response and Impact on Human Vaccine Design.* Front Immunol, 2014. **4**: p. 507.
14.   Johannessen, M., J.E. Sollid, and A.M. Hanssen, *Host- and microbe determinants that may influence the success of S. aureus colonization.* Front Cell Infect Microbiol, 2012. **2**: p. 56.
15.   Krismer, B., et al., *Nutrient limitation governs Staphylococcus aureus metabolism and niche adaptation in the human nose.* PLoS Pathog, 2014. **10**(1): p. e1003862.
16.   Otto, M., *Staphylococci in the human microbiome: the role of host and interbacterial interactions.* Curr Opin Microbiol, 2020. **53**: p. 71-77.
17.   Krismer, B., et al., *The commensal lifestyle of Staphylococcus aureus and its interactions with the nasal microbiota.* Nat Rev Microbiol, 2017. **15**(11): p. 675-687.
18.   Torres Salazar, B.O., et al., *Secondary Metabolites Governing Microbiome Interaction of Staphylococcal Pathogens and Commensals.* Microb Physiol, 2021. **31**(3): p. 198-216.
19.   Hibbing, M.E., et al., *Bacterial competition: surviving and thriving in the microbial jungle.* Nat Rev Microbiol, 2010. **8**(1): p. 15-25.
20.   Brugger, S.D., L. Bomar, and K.P. Lemon, *Commensal-Pathogen Interactions along the Human Nasal Passages.* PLoS Pathog, 2016. **12**(7): p. e1005633.
21.   Donia, M.S., et al., *A systematic analysis of biosynthetic gene clusters in the human microbiome reveals a common family of antibiotics.* Cell, 2014. **158**(6): p. 1402-1414.
22.   Cotter, P.D., R.P. Ross, and C. Hill, *Bacteriocins - a viable alternative to antibiotics?* Nat Rev Microbiol, 2013. **11**(2): p. 95-105.
23.   Smillie, C.S., et al., *Ecology drives a global network of gene exchange connecting the human microbiome.* Nature, 2011. **480**(7376): p. 241-4.
24.   Gogarten, J.P. and J.P. Townsend, *Horizontal gene transfer, genome innovation and evolution.* Nat Rev Microbiol, 2005. **3**(9): p. 679-87.
25.   Hall, J.P.J., M.A. Brockhurst, and E. Harrison, *Sampling the mobile gene pool: innovation via horizontal gene transfer in bacteria.* Philos Trans R Soc Lond B Biol Sci, 2017. **372**(1735).
26.   Janek, D., et al., *High Frequency and Diversity of Antimicrobial Activities Produced by Nasal Staphylococcus Strains against Bacterial Competitors.* PLoS Pathog, 2016. **12**(8): p. e1005812.
27.   Bierbaum, G., et al., *The biosynthesis of the lantibiotics epidermin, gallidermin, Pep5 and epilancin K7.* Antonie Van Leeuwenhoek, 1996. **69**(2): p. 119-127.

28.	Ciufolini, M.A. and D. Lefranc, *Micrococcin P1: structure, biology and synthesis.* Nat Prod Rep, 2010. **27**(3): p. 330-42.

29.	San Millan, A. and R.C. MacLean, *Fitness Costs of Plasmids: a Limit to Plasmid Transmission.* Microbiol Spectr, 2017. **5**(5).

30.	Gordon, D.M. and C.L. O'Brien, *Bacteriocin diversity and the frequency of multiple bacteriocin production in Escherichia coli.* Microbiology (Reading), 2006. **152**(Pt 11): p. 3239-3244.

31.	Zipperer, A., et al., *Human commensals producing a novel antibiotic impair pathogen colonization.* Nature, 2016. **535**(7613): p. 511-6.

32.	Zhang, R., et al., *Identification of Horizontally-transferred Genomic Islands and Genome Segmentation Points by Using the GC Profile Method.* Curr Genomics, 2014. **15**(2): p. 113-21.

33.	Nelson, K.E., et al., *Evidence for lateral gene transfer between Archaea and bacteria from genome sequence of Thermotoga maritima.* Nature, 1999. **399**(6734): p. 323-9.

34.	Kjos, M., et al., *Target recognition, resistance, immunity and genome mining of class II bacteriocins from Gram-positive bacteria.* Microbiology (Reading), 2011. **157**(Pt 12): p. 3256-3267.

35.	Heilbronner, S., et al., *The microbiome-shaping roles of bacteriocins.* Nat Rev Microbiol, 2021. **19**(11): p. 726-739.

36.	Smits, S.H.J., L. Schmitt, and K. Beis, *Self-immunity to antibacterial peptides by ABC transporters.* FEBS Lett, 2020. **594**(23): p. 3920-3942.

37.	Hille, M., et al., *Dual role of GdmH in producer immunity and secretion of the Staphylococcal lantibiotics gallidermin and epidermin.* Appl Environ Microbiol, 2001. **67**(3): p. 1380-3.

38.	Peschel, A., et al., *Secretion of the lantibiotics epidermin and gallidermin: sequence analysis of the genes gdmT and gdmH, their influence on epidermin production and their regulation by EpiQ.* Mol Gen Genet, 1997. **254**(3): p. 312-8.

39.	Pozzi, R., et al., *Distinct mechanisms contribute to immunity in the lantibiotic NAI-107 producer strain Microbispora ATCC PTA-5024.* Environ Microbiol, 2016. **18**(1): p. 118-32.

40.	Diaz, M., et al., *Characterization of a new operon, as-48EFGH, from the as-48 gene cluster involved in immunity to enterocin AS-48.* Appl Environ Microbiol, 2003. **69**(2): p. 1229-36.

41.	Aso, Y., et al., *A novel type of immunity protein, NukH, for the lantibiotic nukacin ISK-1 produced by Staphylococcus warneri ISK-1.* Biosci Biotechnol Biochem, 2005. **69**(7): p. 1403-10.

42.	Okuda, K., et al., *Characterization of functional domains of lantibiotic-binding immunity protein, NukH, from Staphylococcus warneri ISK-1.* FEMS Microbiol Lett, 2005. **250**(1): p. 19-25.

43.	Clemens, R., et al., *Insight into Two ABC Transporter Families Involved in Lantibiotic Resistance.* Front Mol Biosci, 2017. **4**: p. 91.

44.	Ramachandran, G., et al., *Discovery of a new family of relaxases in Firmicutes bacteria.* PLoS Genet, 2017. **13**(2): p. e1006586.

45.	Soler, N., et al., *Characterization of a relaxase belonging to the MOBT family, a widespread family in Firmicutes mediating the transfer of ICEs.* Mob DNA, 2019. **10**: p. 18.

46.	Bruggemann, H., et al., *Staphylococcus saccharolyticus Isolated From Blood Cultures and Prosthetic Joint Infections Exhibits Excessive Genome Decay.* Front Microbiol, 2019. **10**: p. 478.

47.	Golomb, B.L., et al., *The Lactococcus lactis KF147 nonribosomal peptide synthetase/polyketide synthase system confers resistance to oxidative stress during growth on plant leaf tissue lysate.* Microbiologyopen, 2018. **7**(1).

48.	Khayatt, B.I., V. van Noort, and R.J. Siezen, *The Genome of the Plant-Associated Lactic Acid Bacterium Lactococcus lactis KF147 Harbors a Hybrid NRPS-PKS System Conserved in Strains of the Dental Cariogenic Streptococcus mutans.* Curr Microbiol, 2020. **77**(1): p. 136-145.

49. Wu, C., et al., *Genomic island TnSmu2 of Streptococcus mutans harbors a nonribosomal peptide synthetase-polyketide synthase gene cluster responsible for the biosynthesis of pigments involved in oxygen and H2O2 tolerance.* Appl Environ Microbiol, 2010. **76**(17): p. 5815-26.

50. Su, T.L., *Micrococcin, an antibacterial substance formed by a strain of Micrococcus.* Br J Exp Pathol, 1948. **29**(5): p. 473-81.

51. Abraham, E.P., et al., *Probable identity of an antibiotic produced by a spore-bearing bacillus of the B. pumilus group with micrococcin.* Nature, 1956. **178**(4523): p. 44-5.

52. Carnio, M.C., et al., *The macrocyclic peptide antibiotic micrococcin P(1) is secreted by the food-borne bacterium Staphylococcus equorum WS 2733 and inhibits Listeria monocytogenes on soft cheese.* Appl Environ Microbiol, 2000. **66**(6): p. 2378-84.

53. Wieland Brown, L.C., et al., *Thirteen posttranslational modifications convert a 14-residue peptide into the antibiotic thiocillin.* Proc Natl Acad Sci U S A, 2009. **106**(8): p. 2549-53.

54. Bennallack, P.R., et al., *Characterization of a novel plasmid-borne thiopeptide gene cluster in Staphylococcus epidermidis strain 115.* J Bacteriol, 2014. **196**(24): p. 4344-50.

55. Liu, Y., et al., *Skin microbiota analysis-inspired development of novel anti-infectives.* Microbiome, 2020. **8**(1): p. 85.

56. Van der Veken, D., et al., *Genome-Based Characterization of a Plasmid-Associated Micrococcin P1 Biosynthetic Gene Cluster and Virulence Factors in Mammaliicoccus sciuri IMDO-S72.* Appl Environ Microbiol, 2022. **88**(4): p. e0208821.

57. Kassem, M.A., et al., *Exploring clinically isolated Staphylococcus sp. bacteriocins revealed the production of amonabactin, micrococcin, and alpha-circulocin.* Iran J Microbiol, 2021. **13**(2): p. 212-224.

58. Treangen, T.J. and E.P. Rocha, *Horizontal transfer, not duplication, drives the expansion of protein families in prokaryotes.* PLoS Genet, 2011. **7**(1): p. e1001284.

59. Harrison, E. and M.A. Brockhurst, *Plasmid-mediated horizontal gene transfer is a coevolutionary process.* Trends Microbiol, 2012. **20**(6): p. 262-7.

60. Levin, B.R., *The accessory genetic elements of bacteria: existence conditions and (co)evolution.* Curr Opin Genet Dev, 1993. **3**(6): p. 849-54.

61. Bennett, P.M., *Plasmid encoded antibiotic resistance: acquisition and transfer of antibiotic resistance genes in bacteria.* Br J Pharmacol, 2008. **153 Suppl 1**: p. S347-57.

62. Wiedenbeck, J. and F.M. Cohan, *Origins of bacterial diversity through horizontal genetic transfer and adaptation to new ecological niches.* FEMS Microbiol Rev, 2011. **35**(5): p. 957-76.

63. Ochman, H., J.G. Lawrence, and E.A. Groisman, *Lateral gene transfer and the nature of bacterial innovation.* Nature, 2000. **405**(6784): p. 299-304.

64. Peng, Y., et al., *Multiple inter-kingdom horizontal gene transfers in the evolution of the phosphoenolpyruvate carboxylase gene family.* PLoS One, 2012. **7**(12): p. e51159.

65. Werren, J.H., U. Nur, and C.I. Wu, *Selfish genetic elements.* Trends Ecol Evol, 1988. **3**(11): p. 297-302.

66. Rankin, D.J., E.P. Rocha, and S.P. Brown, *What traits are carried on mobile genetic elements, and why?* Heredity (Edinb), 2011. **106**(1): p. 1-10.

67. Rodriguez-Beltran, J., et al., *Beyond horizontal gene transfer: the role of plasmids in bacterial evolution.* Nat Rev Microbiol, 2021. **19**(6): p. 347-359.

68. Petrovski, S. and V.A. Stanisich, *Embedded elements in the IncPbeta plasmids R772 and R906 can be mobilized and can serve as a source of diverse and novel elements.* Microbiology (Reading), 2011. **157**(Pt 6): p. 1714-1725.

69. Lozo, J., L. Topisirovic, and M. Kojic, *Natural bacterial isolates as an inexhaustible source of new bacteriocins.* Appl Microbiol Biotechnol, 2021. **105**(2): p. 477-492.

70. Chou, H.H., et al., *Diminishing returns epistasis among beneficial mutations decelerates adaptation.* Science, 2011. **332**(6034): p. 1190-2.

71. Park, C. and J. Zhang, *High expression hampers horizontal gene transfer.* Genome Biol Evol, 2012. **4**(4): p. 523-32.

72. Ebner, P., et al., *Lantibiotic production is a burden for the producing staphylococci.* Sci Rep, 2018. **8**(1): p. 7471.

73. Diaz Ricci, J.C. and M.E. Hernandez, *Plasmid effects on Escherichia coli metabolism.* Crit Rev Biotechnol, 2000. **20**(2): p. 79-108.

74. Gaillard, M., et al., *Host and invader impact of transfer of the clc genomic island into Pseudomonas aeruginosa PAO1.* Proc Natl Acad Sci U S A, 2008. **105**(19): p. 7058-63.

75. Heuer, H., R.E. Fox, and E.M. Top, *Frequent conjugative transfer accelerates adaptation of a broad-host-range plasmid to an unfavorable Pseudomonas putida host.* FEMS Microbiol Ecol, 2007. **59**(3): p. 738-48.

76. van Rensburg, E., et al., *The metabolic burden of cellulase expression by recombinant Saccharomyces cerevisiae Y294 in aerobic batch culture.* Appl Microbiol Biotechnol, 2012. **96**(1): p. 197-209.

77. San Millan, A., et al., *Integrative analysis of fitness and metabolic effects of plasmids in Pseudomonas aeruginosa PAO1.* ISME J, 2018. **12**(12): p. 3014-3024.

78. Pinhal, S., et al., *Acetate Metabolism and the Inhibition of Bacterial Growth by Acetate.* J Bacteriol, 2019. **201**(13).

79. Ruparell, A., et al., *The fitness burden imposed by synthesising quorum sensing signals.* Sci Rep, 2016. **6**: p. 33101.

80. Wortel, M.T., et al., *Metabolic enzyme cost explains variable trade-offs between microbial growth rate and yield.* PLoS Comput Biol, 2018. **14**(2): p. e1006010.

81. Kurland, C.G., *Translational accuracy and the fitness of bacteria.* Annu Rev Genet, 1992. **26**: p. 29-50.

82. Scott, M., et al., *Interdependence of cell growth and gene expression: origins and consequences.* Science, 2010. **330**(6007): p. 1099-102.

83. Kafri, M., et al., *The Cost of Protein Production.* Cell Rep, 2016. **14**(1): p. 22-31.

84. Ortega, M.A. and W.A. van der Donk, *New Insights into the Biosynthetic Logic of Ribosomally Synthesized and Post-translationally Modified Peptide Natural Products.* Cell Chem Biol, 2016. **23**(1): p. 31-44.

85. Arnison, P.G., et al., *Ribosomally synthesized and post-translationally modified peptide natural products: overview and recommendations for a universal nomenclature.* Nat Prod Rep, 2013. **30**(1): p. 108-60.

86. Biswas, S.R., et al., *Influence of Growth Conditions on the Production of a Bacteriocin, Pediocin AcH, by Pediococcus acidilactici H.* Appl Environ Microbiol, 1991. **57**(4): p. 1265-7.

87. Sidooski, T., et al., *Physical and nutritional conditions for optimized production of bacteriocins by lactic acid bacteria - A review.* Crit Rev Food Sci Nutr, 2019. **59**(17): p. 2839-2849.

88. Blanchard, A.E., C. Liao, and T. Lu, *An Ecological Understanding of Quorum Sensing-Controlled Bacteriocin Synthesis.* Cellular and Molecular Bioengineering, 2016. **9**(3): p. 443-454.

89. Maldonado-Barragan, A. and S.A. West, *The cost and benefit of quorum sensing-controlled bacteriocin production in Lactobacillus plantarum.* J Evol Biol, 2020. **33**(1): p. 101-111.

90. Bouma, J.E. and R.E. Lenski, *Evolution of a bacteria/plasmid association.* Nature, 1988. **335**(6188): p. 351-2.

91. Lenski, R.E., S.C. Simpson, and T.T. Nguyen, *Genetic analysis of a plasmid-encoded, host genotype-specific enhancement of bacterial fitness.* J Bacteriol, 1994. **176**(11): p. 3140-7.

92. Modi, R.I. and J. Adams, *Coevolution in Bacterial-Plasmid Populations.* Evolution, 1991. **45**(3): p. 656-667.

93. Kloos, J., et al., *Piggybacking on Niche Adaptation Improves the Maintenance of Multidrug-Resistance Plasmids.* Mol Biol Evol, 2021. **38**(8): p. 3188-3201.

Appendix

The precursor of a red pigment produced by nasal *Staphylococcus epidermidis* isolates exhibits antimicrobial activity

Introduction

As mentioned previously, sequencing of nasal microbiome isolates with antimicrobial activity against *E. coli* DH5α revealed several *S. epidermidis* strains (e.g., *S. epidermidis* D2-30, used in this study as model organism) harbouring the gene cluster for pulcherriminic acid biosynthesis either on a plasmid or chromosomally. Pulcherriminic acid has been described to be the precursor of pulcherrimin, which spontaneously forms when pulcherriminic acid binds to ferric iron in the environment [1, 2]. The 3.7 kb large gene cluster encodes a MarR family transcriptional regulator (*pacR*), a transporter belonging to the major facilitator superfamily (*pacT*), a tRNA-dependent cyclodipeptide synthase (*pacS*) and a cytochrome P450 oxidase (*pacO*) (Fig. 1). The nomenclature of published pulcherriminic acid genes is not consistent, which is why we introduce "**p**ulcherriminic **ac**id", short *pac,* for the annotation of the genes in *S. epidermidis.*
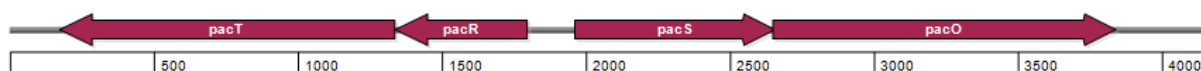

Figure 1: Biosynthetic gene cluster for pulcherriminic acid production and secretion found in S. epidermidis D2-30.

Biosynthesis starts with two L-leucyl tRNAs which are modified by PacS to form cyclodileucine (cLL), and further oxidation by PacO leads to the formation of pulcherriminic acid. After release into the environment, most likely by PacT, pulcherriminic acid spontaneously binds to two Fe^{3+} molecules to form pulcherrimin (Fig. 2) [3, 4].
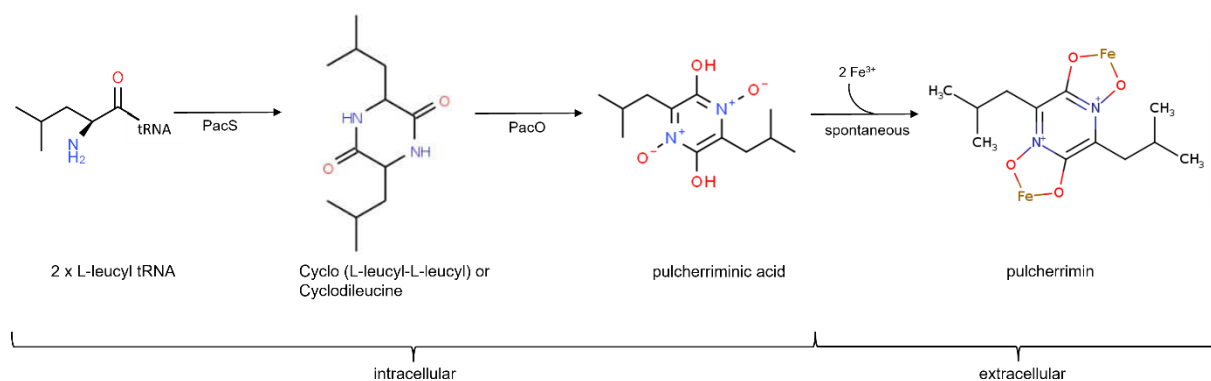
Figure 2: Biosynthesis pathway for pulcherriminic acid and pulcherrimin formation.

The first description of pulcherrimin dates back to 1901, when it was isolated from *Candida pulcherrima* grown on wine grapes [5]. Literature focuses on the description of the red pigment pulcherrimin, which forms when pulcherriminic acid, first described as a colourless chromogen, binds to ferric iron ions in the medium [1, 6, 7]. The pulcherriminic acid BGC was subsequently found in various yeast species, *Bacillus subtilis* and *Bacillus licheniformis* [8-12]. The oldest hypothesis about the mode of action of pulcherriminic acid suggests, that it binds ferric iron in the medium to protect the producer from harmful iron concentrations [6]. Newer assumptions are that pulcherriminic acid is an iron chelator and that the observed antimicrobial effect of pulcherrimin is based on iron starvation for competing bacteria [9, 12-15]. Siderophore characteristics were also postulated for pulcherrimin isolated from *Kluyveromyces lactis,* but most studies conclude that there is no uptake or utilization of pulcherrimin [8, 13]. Only a few authors briefly mentioned, that pulcherriminic acid itself might also have inhibitory capacity besides the extracellular iron binding ability [9, 16, 17]. Antimicrobial activity against mainly plant pathogens like fungi and yeasts and some bacteria, in the context of iron deprivation, was already described [9, 10, 14, 18]. Binding of pulcherriminic acid to iron leads to the formation of pulcherrimin, large complexes or aggregates which establish because one pulcherriminic acid molecule can bind two iron ions (Fig. 3) [7, 19]. These red complexes are insoluble in almost all solvents [6, 19].
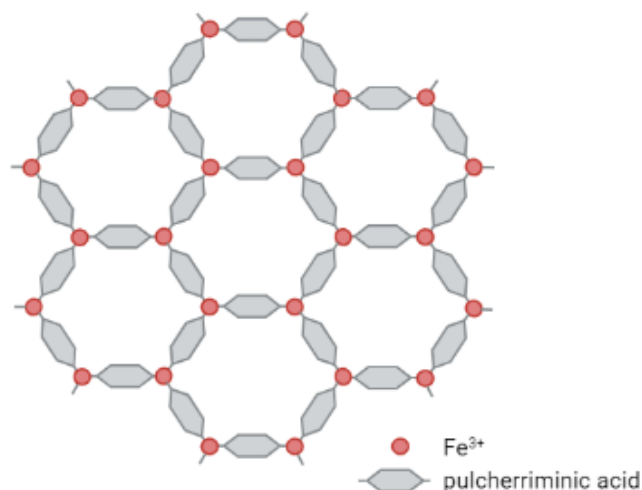
Figure 3: Molecular pattern of the pulcherrimin complex. Red dots represent iron atoms and the grey hexagons pulcherriminic acid molecules.

Only a few studies focused on the regulation of pulcherriminic acid so far. In *Bacillus subtilis* experiments showed that there is no iron-dependent pulcherriminic acid production and the main regulator, the MarR like repressor YvmB, is upregulated under iron limiting conditions [20, 21]. These findings speak against the hypothesis that pulcherrimin is involved in iron acquisition [17]. Randazzo et al. thus speculate, that pulcherriminic acid might generally interfere with iron-dependent intracellular processes, leading to yet unknown changes in the cell [21]. In *Metschnikowia pulcherrima* (former *Candida pulcherrima*), the gene *snf2* has been identified as regulator of pulcherriminic acid biosynthesis and antifungal activity, with no further information of how *snf2* itself is regulated [17]. A study, published by Wang et al. in 2018, presents contradictory results to previously published data, stating that three regulators are necessary to regulate pulcherriminic acid biosynthesis in iron-rich environments in *Bacillus licheniformis* and that cells stop pulcherriminic acid biosynthesis under iron starvation [12].

A lot of different studies on pulcherriminic acid and pulcherrimin have been published in over 100 years of research, describing the gene cluster and compounds in various species. This study is the first to describe pulcherriminic acid production in staphylococci, indicating the wide distribution of this gene cluster over species boundaries. But also raising the question if the compound, regulation of biosynthesis and mode of action of pulcherriminic acid is the same in the different species. This study presents clear evidence that the mode of action of pulcherriminic acid does not rely on iron binding in the environment and thus iron starvation for competing bacteria. Results indicate that production of pulcherriminic acid in *S. epidermidis* is iron-independent and it is hypothesised that pulcherriminic acid might act intracellularly in the target cell.

Material & Methods

Culturing pulcherriminic acid producer strains

To obtain good production of pulcherriminic acid, strains were grown in basic medium (BM; 1% soy peptone A3 [Organotechnie SAS, France], 0.5% Ohly Kat yeast extract [Deutsche Hefewerke GmbH, Germany], 0.5% NaCl, 0.1% glucose, and 0.1% K_2HPO_4, pH 7.2). For culturing in minimal medium like RPMI-1640 (R6504, Sigma-Aldrich), 0.1 % Casamino acids (Bacto™, Life technologies) were added before sterile filtering the RPMI. Also, preculturing in BM was performed and strains were washed twice with RPMI before inoculating RMPI to OD_{600}=0.1 for overnight culturing.

Construction of heterologous expression strain *S. epidermidis* 1457 pRB473-*pacTRSO*

To check if the biosynthetic gene cluster identified via sequencing and antiSMASH analysis is responsible for antimicrobial activity, the four genes *pacTRSO* were amplified from *S. epidermidis* D2-30 DNA using the primers Sepi_pulch 1 and Sepi_pulch 3 (table 1). After restriction digestion of the plasmid pRB473 with BamHI and SacI and of the insert with BglII and SacI, vector and insert were ligated and *E. coli* DC10B was transformed. After confirmation of the correct plasmid sequence via sequencing, the plasmid (Fig. 4) was brought into the lab strain *S. epidermidis* 1457 via electroporation.

Figure 4: Plasmid map of pRB473-pacTRSO

Generation of *E. coli* DH5α expressing *pacTR*

The *pacTR* genes were cloned into pRB473 using the primers Sepi_pulch1 and transporter_473 (table 1) and restriction digestion of vector and insert with SacI and HindIII. *E. coli* DH5α was transformed with the ligation mix, and positive clones were confirmed by sequencing.

Generation of *pacR* deletion mutant *S. epidermidis* 1457 pRB473-*pacTSO*

A MarR transcriptional regulator (*pacR*) deletion mutant was generated to check if pulcherriminic acid production still occurs without regulation. Due to literature, pulcherrimin production is reported to be iron dependent, deletion of the regulator would lead to a constitutively expressing strain. Therefore, pRB473-*pacTRSO* was used as template to amplify the plasmid without *pacR* with the primers Gibson_MarR_fwd and Gibson_MarR_rev (table 1). The PCR product was digested with DpnI for 3 hours at 37°C, the enzyme was heat inactivated at 80°C for 20 min. Gibson Assembly Master Mix (New England Biolabs) was used to ligate the plasmid. After incubation at 50°C for 45 min, *E. coli* DC10B was transformed with the master mix. The plasmid was sent for sequencing and afterwards, brought into *S. epidermidis* 1457 via electroporation.

Heterologous expression of *pacTRSO* from other nasal isolates

Handling different strains which possess the *pacTRSO* operon verified via sequencing, it could be observed, that not all strains are turning red on BM agar plates. One strain showing this behaviour is *S. lugdunensis* IVK28, already known as lugdunin producer [22]. To investigate this phenotype, another pulcherriminic acid producer, *S. epidermidis* 17-20, turning slightly red on plate was chosen for heterologous expression. Therefore, *pacTRSO* was amplified from *S. lugdunensis* IVK28 gDNA with the primers IVK28_pulch_fwd_new and IVK28_pulch_rev_new and from *S. epidermidis* 17-20 gDNA with the primers 17-20_pulch_fwd and 17-20_pulch_rev (Table 1). pRB473 and the two inserts were digested with SacI and PstI, ligated and *E. coli* DC10B was transformed. After sequencing and confirmation of successful cloning, the two plasmids were brought into *S. epidermidis* 1457 via electroporation.

Table 1: Primers used in this study

Primer	Sequence (5'-3')	Amplified gene
Sepi_pulch 1 (SacI)	CGTGTCATA**GAGCTC**ATGTATAAAACCTG	5' of *pacT*
Sepi_pulch 3 (BglII)	ACAGGGTAAAGCA**AGATCT**ATCGAGTCG	3' of *pacO*
transporter_473 (HindIII)	AAA**AAGCTT**AGTGTAAGCAATTGCATTTGAC	3' of *pacR*
Gibson_MarR_fwd	TTAGAAATTCAATGATAGTTTCCATTTATTGTTAACCGGTTAACAATATT	5' of *pacO*
Gibson_MarR_rev	AATATTGTTAACCGGTTAACAATAAATGGAAACTATCATTGAATTTCTAA	3' of *pacT*
IVK28_pulch_fwd_new (SacI)	ATTC**GAGCTC**GGGTTTGATTGTAGACAAA	5' of *pacT*
IVK28_pulch_rev_new (PstI)	ATGC**CTGCAG**GAATCTATTGGATTATTAAATATA	3' of *pacO*
17-20_pulch_fwd (SacI)	ATTC**GAGCTC**GTGATGTAAGTACTAAATATATACC	5' of *pacT*
17-20_pulch_rev (PstI)	ATGC**CTGCAG**TAAAGTGGTAATTAGCTATA	3' of *pacO*

Purification

Pulcherriminic acid can be purified using two different methods. Either ethyl acetate or 1-butanol can be used to extract the compound. Therefore, an overnight culture of the producer and negative control were generated in BM. BM or RPMI + 0.1% casamino acids were inoculated with OD_{600}=0.1 and incubated overnight at 37°C at 120 rpm. Extraction with 1-butanol was performed with 3:1 v/v overnight culture:butanol and for ethyl acetate with 1:1 v/v. After adding the solvent, the culture was incubated for one hour at 37°C under continuous shaking. After centrifugation for 10 min at 4.700 x g, the upper phase/solvent phase was transferred in a glas flask for subsequent evaporation of the solvent via rotary evaporator (KNF group). To check for antimicrobial activity of the extract on agar plate, the dried extract was dissolved in DMSO and pipetted in holes punched out of the agar plate with a cork borer. A sensitive indicator strain was streaked out on plate with a cotton swab prior to punching the holes. Plates were incubated overnight at 37°C. Ethyl acetate or 1-butanol extracts, still in solution, were analysed by AG Grond, Institute for Organic Chemistry, University of Tübingen, by HPLC/MS.

Gradient plates

Plates with an iron gradient were generated to check for iron dependent production or activity of pulcherriminic acid. Therefore, a square Petri dish (120 x 120 x 17 mm, Greiner Bio-One) was placed on the lid of a round Petri dish to slant the square Petri dish. For BM based gradient plates, two different kinds of plates were generated. Either 40 ml BM agar (50°C) were supplemented with 100 µM $FeSO_4$ and 10 µg ml^{-1} chloramphenicol and poured into the square Petri dish. Or 2x BM was supplemented with 7% w/v Chelex®100 (a chelating agent, with high selectivity for copper, iron, and other heavy metal ions over monovalent cations, SigmaAldrich) and put on a stirrer overnight at 4°C. After sterile filtering, the 2X BM was supplemented with

10 µM EDDHA (chelating agent for metal ions, Fluorochem) and 10 µg ml^{-1} chloramphenicol and mixed with preheated 2x agar (50°C) 1:1 to reach final volume of 40 ml. Let stand until agar is completely solid. Remove square Petri dish from the lid of the round Petri dish and cover the generated inclined agar with 40 ml of standard BM agar with 10 µg ml^{-1} chloramphenicol (50°C). Dry plates for one hour under the clean bench with closed lid, to allow diffusion between the two different agar layers. For gradient plates based on RPMI agar, 2x RPMI (+ 0.1% casamino acids) and 2x agar were preheated to 50°C, mixed 1:1 to reach final volume of 40 ml. 100 µM $FeSO_4$ and 10 µg ml^{-1} chloramphenicol were added and the agar was poured into the plate as described before. For the top layer, again 2x RPMI (+ 0.1% casamino acids) and 2x agar were mixed 1:1 (50°C) to reach final volume of 40 ml, 10 µg ml^{-1} chloramphenicol was added and poured onto the other agar layer. To proceed, 1 µl of an overnight culture of the indicator/background strain (OD_{600}=~10) *S. aureus* JE2 NE773 is diluted in 1 ml BM and streaked out on the square Petri dish with a cotton swab in three different directions. The producer strains *S. epidermidis* pRB473-*pacTRSO* and *S. epidermidis* pRB473-*pacTSO* and the empty plasmid control *S. epidermidis* pRB473 are set to OD_{600}=10 and 50 µl of these suspensions are evenly dispensed on plate according to the gradient with an electric multichannel pipette.

Competition assay

The effect of the production of pulcherriminic acid by *S. epidermidis* D2-30 on colony forming units (CFU) of a sensitive and resistant strain was checked via competition assays. Therefore *S. epidermidis* D2-30, *S. aureus* JE2 and *S. aureus* JE2 NE773 were grown in BM overnight. 1 ml was centrifuged at 4700 x g, 5 min and the pellet was resuspended in RPMI + 0.1 % casamino acids. This step was repeated twice and afterwards OD_{600} was measured, and the producer strain was set to 1.8×10^8 in 1 ml and *S. aureus* JE2 and *S. aureus* JE2 NE773 to 1×10^8 in 1 ml to reach a final 60:40 ratio of producer and target strain. To check for the right ratio, the start CFU was determined by diluting 20 µl of the 1.8×10^8 or 1×10^8 suspensions in 180 µl BM in a 96 well plate and further dilution to 10^{-8}. 10 µl of each dilution were spotted on BM agar plates twice with a multichannel pipette. To start the competition, mix 100 µl of producer with 100 µl of each target strain and spot 10 µl on RPMI + 0.1 % casamino acids plate with or without 50 µM or 100 µM $FeSO_4$. Let grow for 24, 48, 72 hours at 37°C. At each timepoint, one spot was scraped off, resuspended in 200 µl BM and diluted for CFU determination on BM agar plate as described before. Colonies were counted at the same dilution to determine the ratio between producer and target strain.

Results & Discussion

Plasmid of *S. epidermidis* D2-30

Whole genome sequencing revealed that the pulcherriminic acid biosynthesis gene cluster of *S. epidermidis* D2-30 is located on a 45 kb large plasmid (Fig. 5). The BGC has a G+C content of 26% and does thus not stand out from the rest of the plasmid (Fig. 6). A set of transposases and integrases is encoded as well, indicating mobility of genetic elements of the plasmid and some transporter genes, showing some similarity to ABC-type multidrug transporter systems, are located on the plasmid. Adjacent to the BGC, genes associated with replication can be found. Interestingly, the replication protein (RepA) located on the plasmid seems to be non-functional according to the sequence. Further investigations revealed that *S. epidermidis* D2-30 harbours a second plasmid, mainly only encoding a replication gene, which seems to overtake the role of the non-functional RepA protein on pD2-30. Only little is known about this kind of replication, with plasmid pLS20 from *Bacillus subtilis* being the only described plasmid with no own replication protein and most likely using the host encoded DnaA protein for initiation of replication [23, 24]. In general, the plasmid carries a lot of hypothetical genes or genes with unknown function. These findings seem to underline the advantage of pulcherriminic acid biosynthesis for the producer, since it keeps a quite large plasmid, which is additionally dependent on another plasmid for replication.
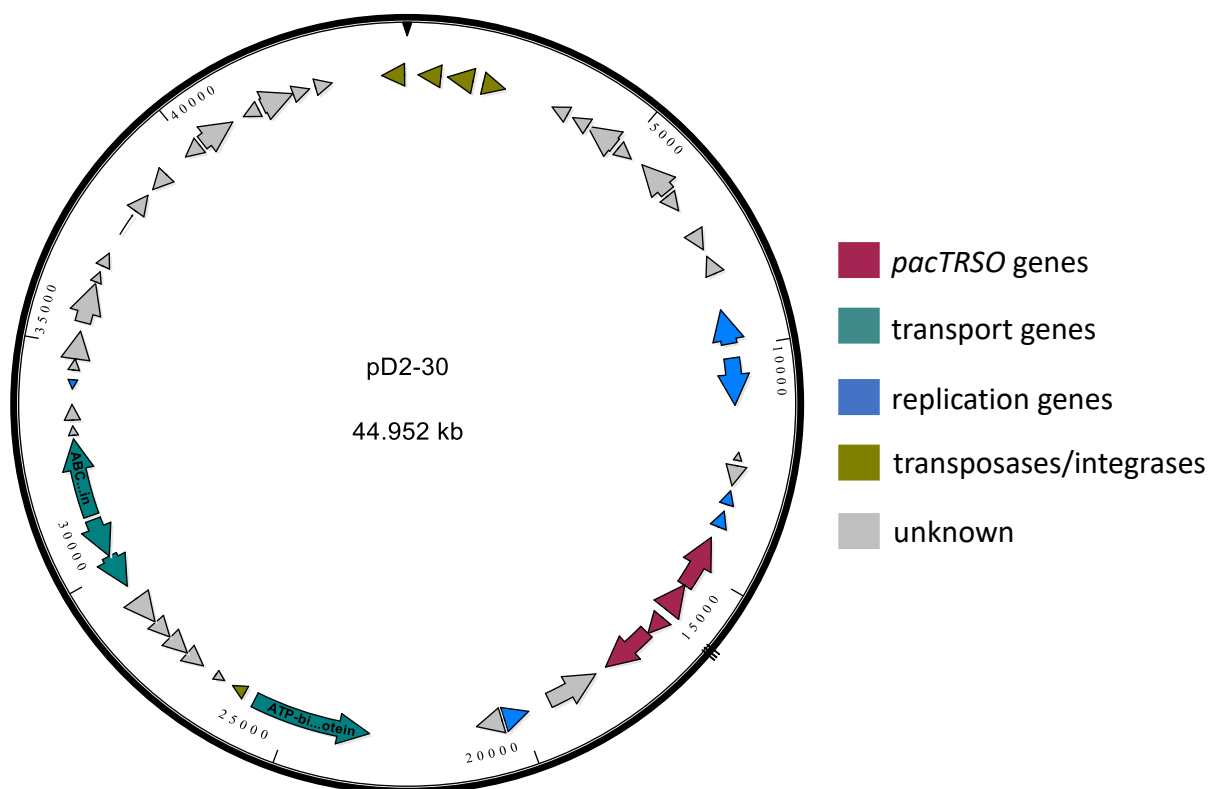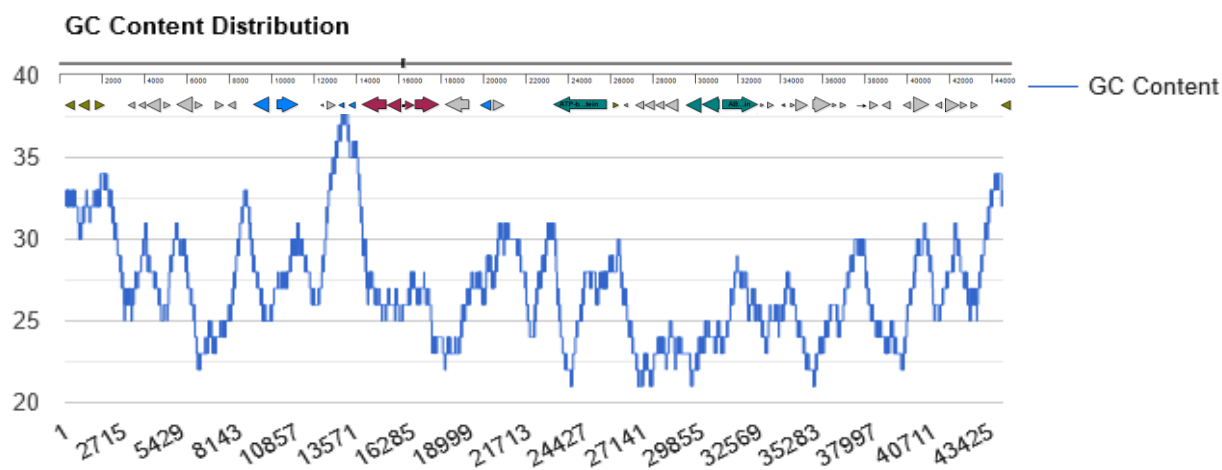

Figure 5: Plasmid map of pD2-30 identified in S. epidermidis D2-30.

Figure 6: GC content of pD2-30 calculated with BIOLOGICS International Corp, GC content calculator. pacTRSO is indicated in purple above the curve for the GC content.

Prevalence of pulcherriminic acid BGC and evidence of horizontal gene transfer

Bioinformatic analysis showed an underrepresentation of the pulcherriminic acid BGC in *S. epidermidis* in public databases compared to the number of strains found during this study. PacTRSO was detected in 11 assemblies of *S. epidermidis* genomes, which corresponds to 1% calculated on all available *S. epidermidis* genomes. Our study was able to identify 6 *S. epidermidis* strains with the pulcherriminic acid BGC in a collection of approximately 2000 human nasal isolates. For *S. aureus pacTRSO* could be found in 17 assemblies, which equates ~0.1% of available genome sequences. In *S. lugdunensis*, 22 assemblies (58%) were *pacTRSO* positive. The BGC was also found in 2 assemblies of *S. hominis* (1%), 17 assemblies of *S. haemolyticus* (5%) and 1 assembly of *S. simulans* (1.5%). In all species the BGC was either found on the chromosome or a plasmid, only in *S. epidermidis* it can be found in both. For *S. aureus*, the BGCs had the identical chromosomal integration site, which consists of ~1 kb of non-coding DNA. A group II intron reverse transcriptase/maturase and transposase, both with premature stop codons, were identified in this region. About 40% of roughly 12,000 *S. aureus* genome assemblies in the NCBI database contained only *pacTR*, also at the same chromosomal position. A phylogenetic analysis did not show widespread evidence of the cluster jumping from one species to another, although *S. epidermidis* promiscuously accepts various cluster positions in the genome. In summary, the pulcherriminic acid BGC is widespread amongst staphylococci and is most often found on plasmids (Unpublished data, Jeffrey J. Power).

Heterologous expression of *pacTRSO* and *pacTR*

S. epidermidis 1457 was chosen as heterologous host, because this strain is not producing any antimicrobial compound and is an easy-to-handle lab strain. After transformation of *S. epidermidis* 1457 with pRB473-*pacTRSO*, the strain showed antimicrobial activity on BM plates against the sensitive strain *E. coli* DH5α (Fig. 7) leading to the conclusion that indeed the four genes *pacTRSO* and their product pulcherriminic acid are responsible for the antimicrobial effect exhibited by *S. epidermidis* D2-30.
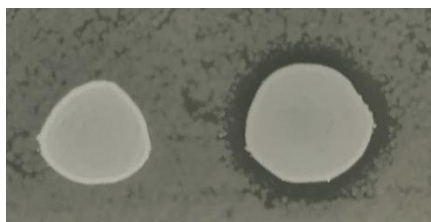

Figure 7: S. epidermidis 1457 pRB473 (left) and S. epidermidis pRB473-pacTRSO (right) spotted on E. coli DH5α.

Further activity tests showed that resistant as well as sensitive *S. aureus* strains can be found, one of the pulcherriminic acid resistant strains being *S. aureus* JE2. A closer look into the genome revealed that this strain has the *pacTR* genes on the chromosome. To investigate the effect of the deletion of *pacT* and *pacR* in this strain, the Nebraska transposon library of *S. aureus* JE2 was used, where an erythromycin (erm) cassette is randomly integrated into non-essential genes of *S. aureus* JE2. *S. aureus* JE2 NE773 is a *pacT* deletion mutant and *S. aureus* JE2 NE281 is a *pacR* mutant and both isolates showed sensitivity against *S. epidermidis* D2-30 on BM agar plate (Fig. 8). The zone of inhibition (ZOI) is clearer for the *pacT* deletion mutant compared to the *pacR* mutant. This does not fit to the assumption that deletion of *pacR* would lead to a constitutive expression of *pacT*, leading to a fully resistant strain. However, the regulatory effect of *pacR* is still unclear and a negative effect of the inserted erm cassette cannot be ruled out and might be an explanation for this intermediate resistant phenotype. A clean knockout of *pacR* and *pacT* in *S. aureus* JE2 might be useful to rule out these side effects. In summary, these findings demonstrate, that PacT confers resistance to pulcherriminic acid with a possible involvement of PacR.

Figure 8: S. epidermidis D2-30 spotted on S. aureus JE2 (left), S. aureus JE2 NE773 (middle) and S. aureus JE2 NE281 (right).

To further confirm this finding, the sensitive *E. coli* DH5α was transformed with the plasmid pRB473-*pacTR* to see, if the strain gets resistant when expressing the regulator and the transporter of the pulcherriminic acid gene cluster. Indeed, no ZOI can be seen around *S. epidermidis* D2-30 when spotted on *E. coli* DH5α pRB473-*pacTR*, confirming the previous results, that PacTR are sufficient to confer resistance against pulcherriminic acid (data not shown).

Deletion mutant *S. epidermidis* 1457 pRB473-*pacTSO*

Deletion of *pacR*, without affecting the functionality of *pacT,* in *S. epidermidis* 1457 pRB473-*pacTRSO* generated a deregulated strain, still producing pulcherriminic acid (Fig. 9a). As visible in Fig. 9, the *pacR* deletion mutant shows strong signs of lysis on plate and the ZOI is smaller compared to *S. epidermidis* 1457 pRB473-*pacTRSO*. This indicates that deletion of *pacR* leads to a sick phenotype, also visible by the formation of very small and (dark) red colonies on plate. Most MarR type transcriptional regulators are described to be repressors, also the *pacR* homologue *yvmB* identified in *Bacillus subtilis* is described to be a transcriptional repressor of the operon expressing pulcherriminic acid in *B. subtilis* [21, 25]. Deregulation of pulcherriminic acid biosynthesis by deletion of *pacR* in *S. epidermidis* 1457 pRB473-*pacTRSO* thus leads to a strain, which produces more pulcherriminic acid under normal culture conditions, but resistance to the own compound, mediated by the transporter, seems to be insufficient for the high amount of produced compound leading to lysis of the cells. It is assumed that pulcherriminic acid accumulates in the producer cells, causing cell death. Growth curves also support the sick phenotype, showing that the *pacR* deletion mutant reaches a maximum OD_{600nm}=2-3 in BM overnight, compared to OD_{600nm}=~8 reached by *S. epidermidis* 1457 pRB473-*pacTRSO and* OD_{600nm}=13 by *S. epidermidis* 1457 pRB473 (Fig. 9b). In summary it can be said that an overproduction strain was generated, but due to the sickness of the strain, an advantage of this overproduction for example for purification of pulcherriminic acid seems to be questionable.
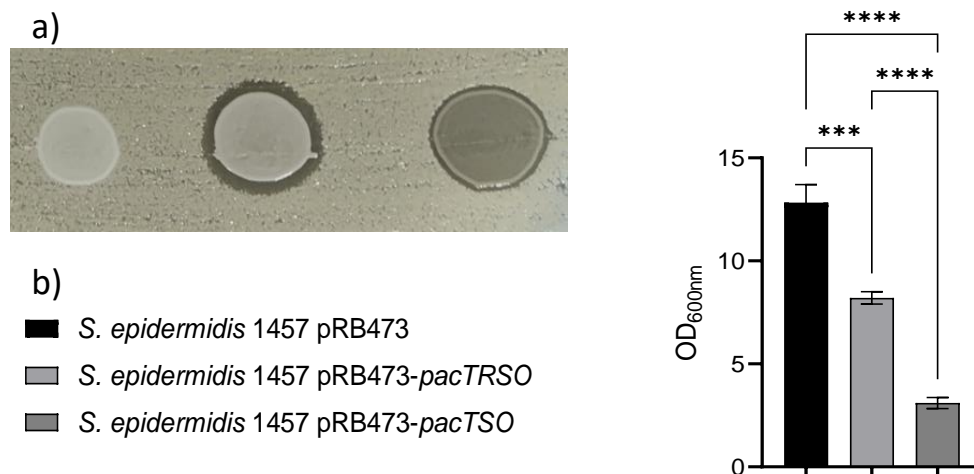
Figure 9: a) S. epidermidis 1457 pRB473 (left), S. epidermidis 1457 pRB473-pacTRSO (middle) and S. epidermidis 1457 pRB473-pacTSO (right) on BM agar plates. S. aureus JE2 NE773 as indicator strain. b) Endpoint OD_{600nm} of S. epidermidis 1457 pRB473 (black), S. epidermidis 1457 pRB473-pacTRSO (light grey) and S. epidermidis 1457 pRB473-pacTSO (dark grey) after 24 hours of growth in BM.

Activity spectrum of *S. epidermidis* D2-30 and *S. epidermidis* 1457 pRB473-*pacTRSO*

The antimicrobial activity of *S. epidermidis* D2-30 and *S. epidermidis* 1457 pRB473-*pacTRSO* against various staphylococci, some members of the nasal microbiome and Gram-negative bacteria was determined via spot assay on BM plate (Fig. 10).

strain	S. epidermidis D2-30	S. epidermidis 1457 pRB473-pacTRSO
S. epidermidis IVK83	grey	grey
S. aureus COL	grey	yellow
S. aureus USA300	grey	yellow
S. aureus SA113	grey	yellow
S. pseudintermedius	yellow	orange
S. haemolyticus	yellow	yellow
S. saprophyticus	yellow	yellow
S. auricularis	yellow	yellow
S. xylosus	grey	grey
B. thuringiensis	grey	grey
B. brevis	grey	grey
B. subtilis	grey	yellow
B. megaterium	yellow	orange
S. agalactiae	grey	grey
S. salivarius	grey	grey
L. monocytogenes	grey	grey

strain	S. epidermidis D2-30	S. epidermidis 1457 pRB473-pacTRSO
L. grayi	grey	grey
C. propinquum 44885	yellow	orange
C. propinquum 44286	yellow	orange
C. accolens 44278	yellow	yellow
C. accolens 44279	yellow	yellow
P. stutzeri	grey	yellow
P. aeruginosa	grey	grey
E. faecalis	grey	grey
E. faecalis VRE	grey	grey
E. faecium	grey	grey
E. coli DH5α	yellow	orange
K. pneumoniae	grey	grey
K. oxytoca	orange	orange
M. cattarhalis	orange	red
P. damselae	orange	red

grey	no inhibition
yellow	up to 1 mm
orange	1-3 mm
red	3 mm - 1 cm

Figure 10: Activity spectrum of S. epidermidis D2-30 and S. epidermidis 1457 pRB473-pacTRSO on BM plate against various bacterial strains. Grey indicates no antimicrobial activity, yellow slight antimicrobial activity, orange intermediate activity and red strong activity.

The results show that the pulcherriminic acid producers have quite a broad spectrum of activity, acting against Gram-positive as well as Gram-negative bacteria. Also, members of the nasal microbiome like corynebacteria or *Moraxella catarrhalis* are inhibited. The difference in antimicrobial activity between the wild type *S. epidermidis* D2-30 and the heterologous host is

most likely due to higher expression of the operon in *S. epidermidis* 1457 pRB473-*pacTRSO* in consequence of the higher copy number.

Purification of pulcherriminic acid

Different attempts were made to purify pulcherriminic acid from liquid culture and agar plates. So far only extraction of liquid cultures (BM and RPMI-1640) with ethyl acetate or 1-butanol led to the identification of pulcherriminic acid via HPLC/MS analysis. Extraction with ethyl acetate of the empty plasmid control and the deregulated strain grown in RPMI-1640 was performed and analysed for all masses, which can be detected in the extracts (Fig. 11). The precursor cLL as well as pulcherriminic acid and its derivatives can be identified in the base peak chromatogram (BPC) of the deregulated strain after 11 minutes until 15 minutes, highlighted by a red box. Cyclodileucine is the strongest peak compared to the peaks marked with (B), (C) and (D), which are abbreviations for the incompletely oxidised version of pulcherriminic acid also named dihydro-pulcherriminic acid (B) and two degradation products (C+D) which already have a broken aromatic ring [17]. Chemical structures for these detected compounds are displayed in figure 12. Peaks for pulcherriminic acid and degradation products can only be seen in the extract of the producer strain, as expected.
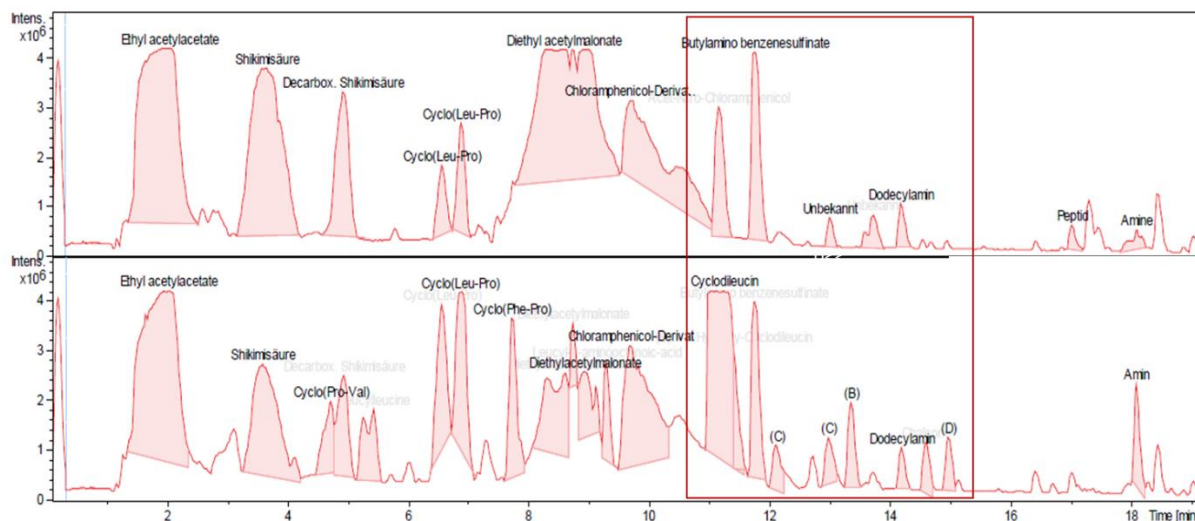

Figure 11: Base peak chromatogram of ethyl acetate extracts of S. epidermidis pRB473 (top) and S. epidermidis pRB473-pacTSO (bottom). Indicated is the relative intensity.
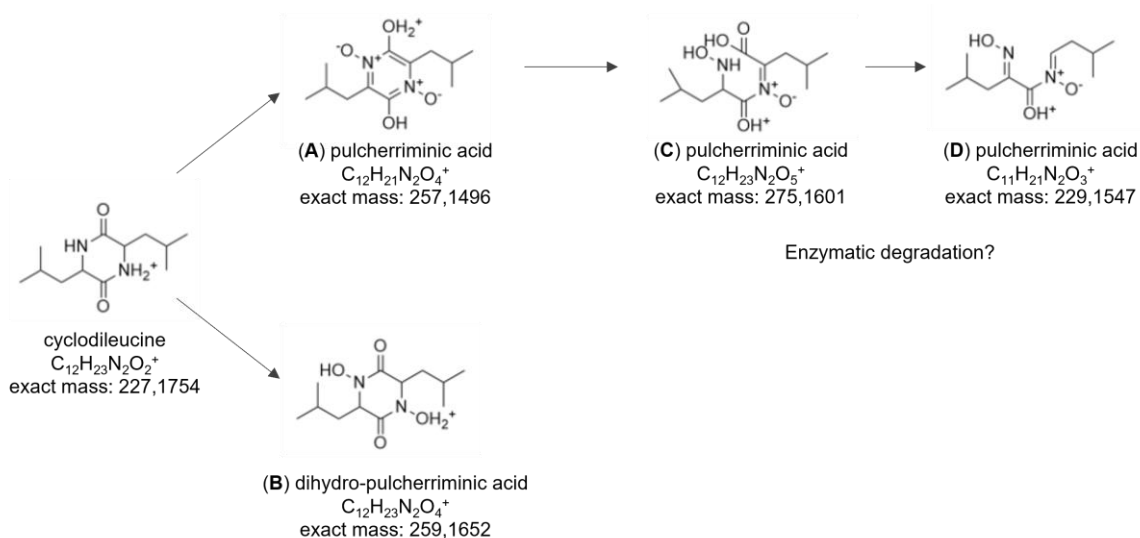
Figure 12: Chemical structures for cyclodileucine, pulcherriminic acid variants (A, B) and degradation products (C, D) which can be detected in HPLC/MS analysis. Modified from Gore-Llyod et al., 2019.

Having a look at the UV spectrum, no peaks resembling the masses detected in the MS can be found in the HPLC analysis between minutes 11 and 15 (Fig. 13). This might be due to very small amounts of compound present in the extract. Also supported by the finding, that no antimicrobial activity can be obtained on plate with the generated extract (data not shown). Another reason for unsuccessful detection of pulcherriminic acid via HPLC might be that the settings were not suitable, and the measurement was performed at the wrong wavelength. As a side note, the ethyl acetate extract exhibits a quite strong acidity effect on plate, which is not connected to pulcherriminic acid as it can also be seen for the empty plasmid control (data not shown).
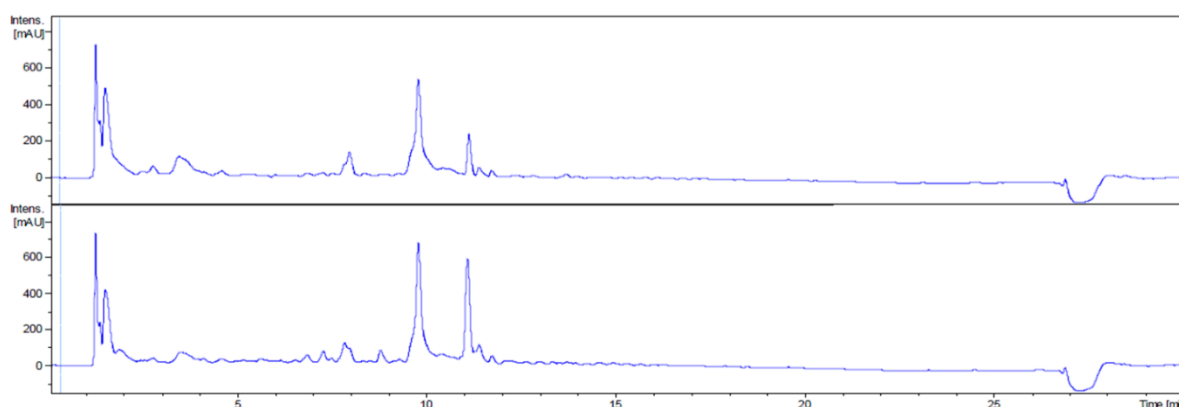

Figure 13: UV spectrum of the ethyl acetate extract of S. epidermidis pRB473 (top) and S. epidermidis pRB473-pacTSO (bottom). The peaks of interest should appear between minutes 11 and 15. Absorbance was measured in milli absorptions units (mAU).

All detected compounds in the extracts are also displayed in the following table (Table 2). Highlighting again, that pulcherriminic acid variants and derivates can only be found in the extract of the producer strain. Interestingly, also some other compounds are unique for the producer strain, which might be related to *pacTRSO*. For example, different cyclic dipeptides can be detected, indicating that PacS is not acting only on L-leucyl-tRNA but also on other

amino acids like proline, phenylalanine and valine. However, the obtained data also show that extracts of the negative control *S. epidermidis* 1457 pRB473 also contain cyclic dipeptides, like cyclo(leucyl-prolyl), which are obviously unrelated to *pacTRSO.*

Table 2: List of all detected compounds in the ethyl acetate extract of S. epidermidis pRB473 and S. epidermidis pRB473-pacTSO grown in RPMI-1640.

Peak	*S. epidermidis* 1457 pRB473	*S. epidermidis* 1457 pRB473-*pacTSO*
1	Ethyl acetylacetate (131,0703; $C_6H_{10}O_3$)	Ethyl acetylacetate (131,0703; $C_6H_{10}O_3$)
2	Shikimic acid (175,0601; $C_7H_{10}O_5$)	Shikimic acid (175,0601; $C_7H_{10}O_5$)
3	x	Cyclo(Pro-Val) (197,1286; $C_{10}H_{16}N_2O_2$)
4	Decarboxylated shikimic acid (129,0546; $C_6H_9O_3$)	Decarboxylated shikimic acid (129,0546; $C_6H_9O_3$)
5	x	Leucylleucine (245,1862; $C_{12}H_{24}N_2O_3$)
6	Cyclo(Leu-Pro) (211,1446; $C_{11}H_{18}N_2O_2$)	Cyclo(Leu-Pro) (211,1446; $C_{11}H_{18}N_2O_2$)
7	Cyclo(Leu-Pro) (211,1446; $C_{11}H_{18}N_2O_2$)	Cyclo(Leu-Pro) (211,1446; $C_{11}H_{18}N_2O_2$)
8	x	Cyclo(Phe-Pro) (245,1284; $C_{14}H_{17}N_2O_2$)
9	Diethyl acetylmalonate (203,0915; $C_9H_{14}O_5$)	Diethyl acetylmalonate (203,0915; $C_9H_{14}O_5$)
10	Diethyl acetylmalonate (203,0915; $C_9H_{14}O_5$)	Diethyl acetylmalonate species (201,1120; $C_{10}H_{16}O_4$ (M-H_2O)/219,1227; $C_{10}H_{18}O_5$) (ident. MS/MS)
11	Diethyl acetylmalonate (203,0915; $C_9H_{14}O_5$)	Diethyl acetylmalonate (203,0915; $C_9H_{14}O_5$)
12	x	Leu-aminoctanoic-acid (273,2173; $C_{14}H_{28}N_2O_3$)
13	Chloramphenicol derivate (355,0638; $C_{22}H_{12}ClN_2O$)	Chloramphenicol derivate (355,0638; $C_{22}H_{12}ClN_2O$)
14	Acet-chloramphenicol with nitro group (424,0670; $C_{15}H_{19}Cl_2N_3O_7$/ 347,0194; $C_{13}H_{12}Cl_2N_2O_5$) (ident. MS/MS)	Cyclodileucine (227,1755; $C_{12}H_{22}N_2O_2$)
15	x	(**B**) Dihydro-pulcherriminic acid (259,1653; $C_{12}H_{22}N_2O_4$) and N-hydroxy-cyclodileucine (243,1699; $C_{12}H_{22}N_2O_3$)
16	Butylamino benzenesulfinate (214,0898; $C_{10}H_{15}NO_2S$)	Butylamino benzenesulfinate (214,0898; $C_{10}H_{15}NO_2S$)
17	x	(**C**) pulcherriminic acid (275,1600; $C_{12}H_{22}N_2O_5$)
18	x	(**C**) pulcherriminic acid (275,1604; $C_{12}H_{22}N_2O_5$)
19	x	(**B**) Dihydro-pulcherriminic acid (259,1653; $C_{12}H_{22}N_2O_4$)
20	Dodecylamine (186,2220; $C_{12}H_{27}N$)	Dodecylamine (186,2220; $C_{12}H_{27}N$)
21	x	Chalcone (209,0961; $C_{15}H_{12}O$)
22	x	(**D**) pulcherriminic acid (229,1547; $C_{11}H_{20}NO_3$)
23	x	Amine (354,4103; $C_{24}H_{51}N$)

To avoid the acidity effect seen with the ethyl acetate extract, 1-butanol extracts were generated, and HPLC/MS analysis confirmed that extraction with 1-butanol worked comparably to the one with ethyl acetate (data not shown). However, antimicrobial activity tests on plate could not obtain any ZOI for the 1-butanol extract. But to further clarify the differences in pulcherriminic acid production between *S. epidermidis* pRB473-*pacTRSO* and *S. epidermidis* pRB473-*pacTSO* and the influence of the growth medium, 1-butanol extracts were generated from both strains grown either in BM or RPMI-1640 (+ 0.1% casamino acids). The BPC, the extracted ion chromatogram (EIC) and the UV spectrum for butanol extracts of *S. epidermidis* pRB473, *S. epidermidis* pRB473-*pacTRSO* and *S. epidermidis* pRB473-*pacTSO* grown in BM show, that the precursor cLL can be detected also in the negative control, and that the pulcherriminic acid variant (B) and derivates (C) and (D) can only be detected in the producer extracts (Fig. 14). In an EIC the masses for one or more molecules of interest are recovered ("extracted") from the entire data set for a separate chromatographic run, to provide clean chromatograms of compounds of interest, in our case (A), (B), (C) and (D). The extract of *S. epidermidis* pRB473-*pacTSO* grown in BM shows slightly reduced amounts of pulcherriminic acid variant (B) and derivates compared to *S. epidermidis* pRB473-*pacTRSO*. cLL can be detected in both samples in similar amounts and is also the only molecule of interest which can be detected in the UV spectrum.
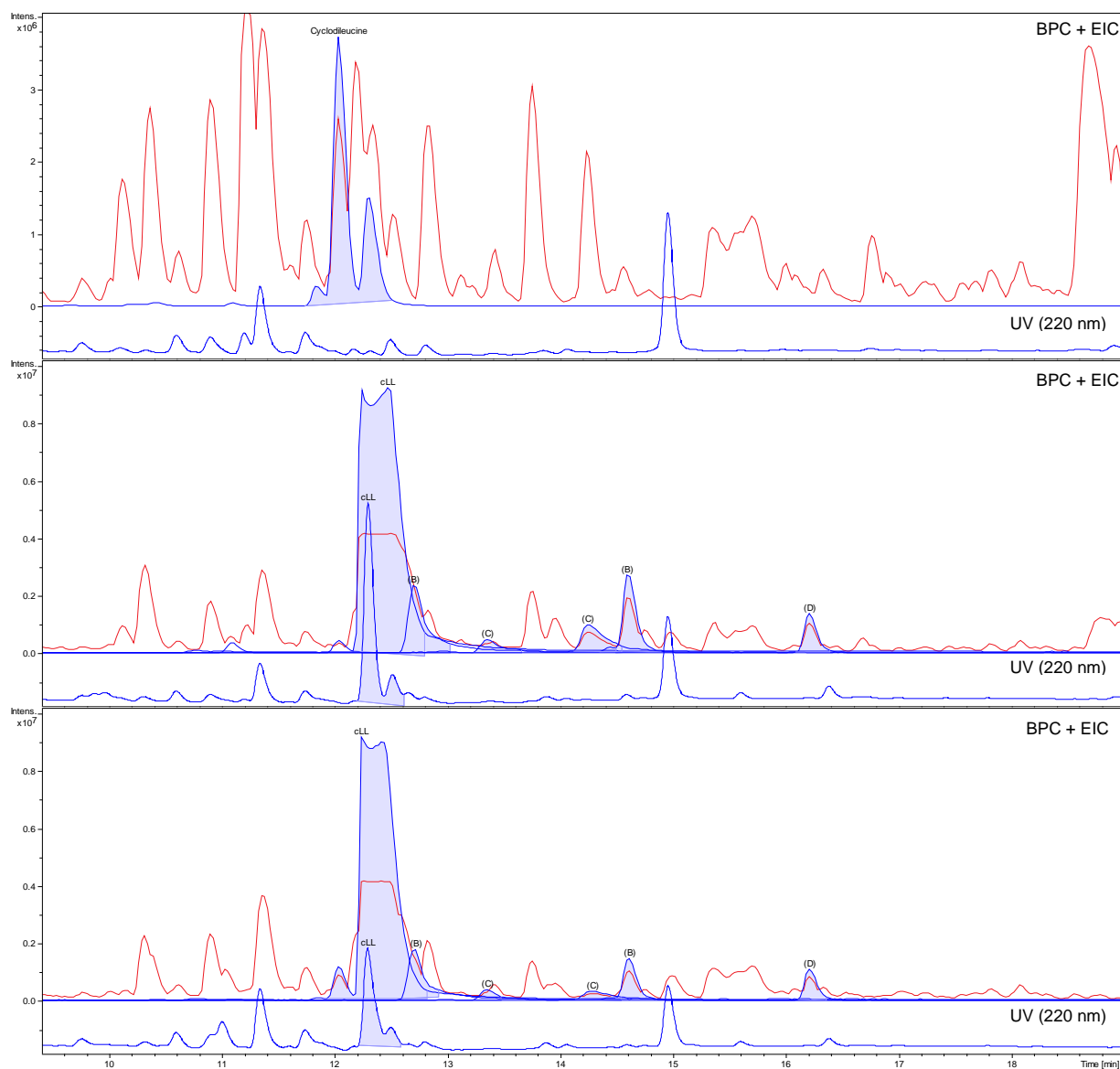
Figure 14: 1-butanol extracts of S. epidermidis pRB473 (upper panel), S. epidermidis pRB473-pacTRSO (middle) and S. epidermidis pRB473-pacTSO (lower panel) grown in BM. BPC (red) + EIC (blue) is shown in the upper part of diagram and UV spectrum is shown underneath. Indicated is the relative intensity.

Comparing the RMPI extracts, it is obvious that in general, less molecules could be isolated from the culture, indicated by a reduced number of peaks also for the negative control (Fig. 15). The extract of *S. epidermidis* pRB473-*pacTRSO* shows only very small peaks for (B), (C) and (D) and also the EIC is not congruent with the BPC, indicating very little amounts of compounds in the extract. For *S. epidermidis* pRB473-*pacTSO* however, the extract contains good amounts of the compounds of interest, also indicated by EICs which are congruent with the BPCs.
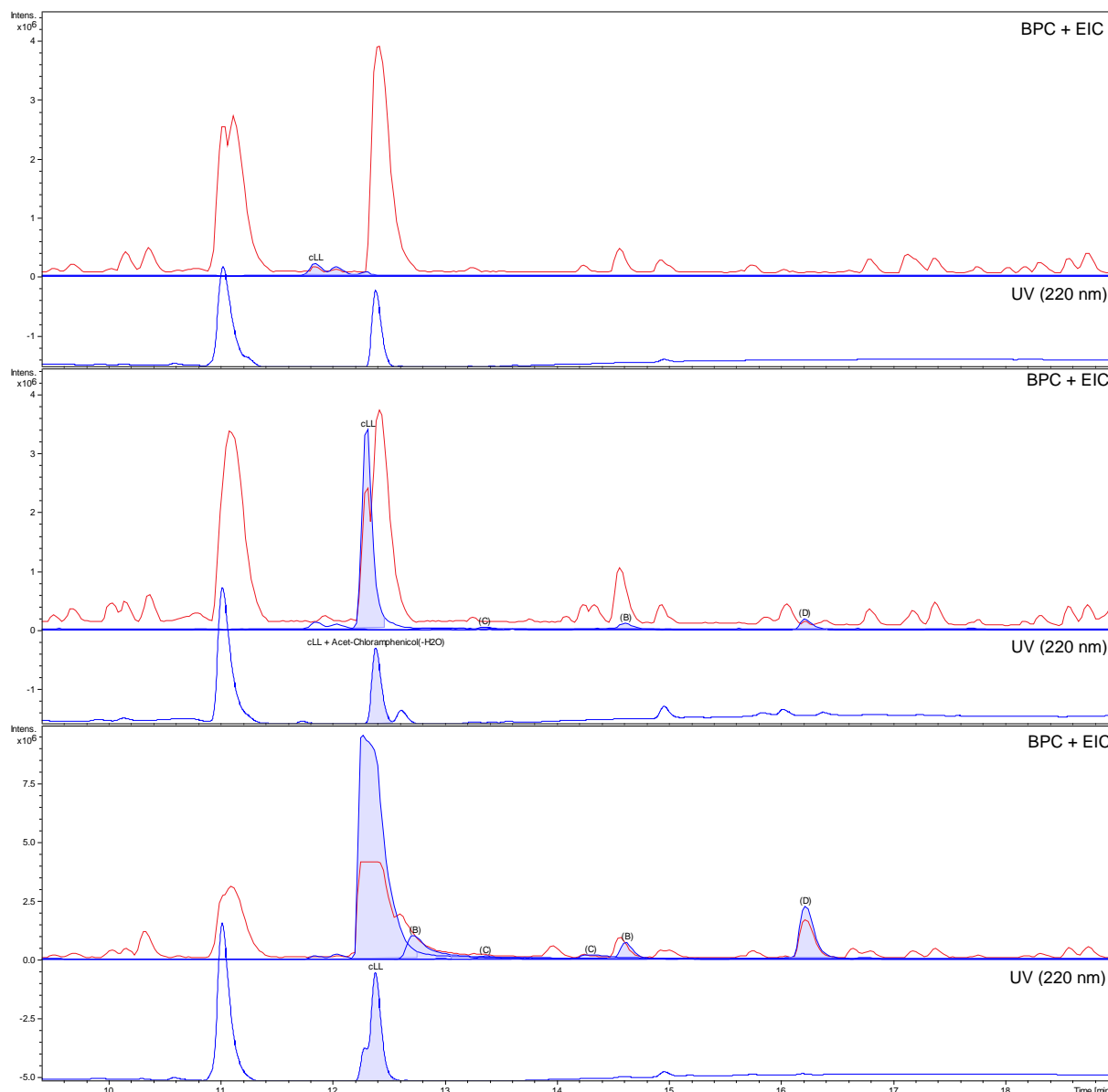
Figure 15: 1-butanol extracts of S. epidermidis pRB473 (upper panel), S. epidermidis pRB473-pacTRSO (middle) and S. epidermidis pRB473-pacTSO (lower panel) grown in RPMI-1640. BPC (red) + EIC (blue) is shown in the upper part of diagram and UV spectrum is shown underneath. Indicated is the relative intensity.

To summarize, the (A) variant of pulcherriminic acid cannot be detected in any of the extracts. But because we can detect (C) and (D), one could assume, that the (A) form of pulcherriminic acid was produced by the strains. It might be, that (A) can bind iron more efficient than (B), due to the aromatic centre and the differentially located electron orbitals, which facilitate stronger iron complexation and that all produced (A) pulcherriminic acid is immediately "inactivated" by iron. It might also be the case, that (A) is instable or rapidly degraded by an unknown mechanism. These results also show that the purification method is still not optimal, especially because no antimicrobial activity can be obtained with the extracts. However, the expected masses can be detected only in the producer strains via HPLC/MS analysis, confirming that pulcherriminic acid is generated by PacTRSO. The deletion of *pacR* does not

seem to be a big advantage for purification, but the results show that the *pacR* deletion mutant shows better production in iron limited medium than the full cluster strain, confirming the constitutive expression of the gene cluster by the deletion of *pacR*. The full cluster strain shows better production in BM, which is interesting, because one would assume that a lot of produced pulcherriminic acid gets bound by the iron present in BM and making it undetectable in the HPLC/MS analysis. Interestingly, the amount of the precursor cLL does not vary a lot between the producer strains and the growth conditions, raising the question why only a small amount of cLL gets converted into the final product. However, it might also be the case that there is proportional conversion into pulcherriminic acid, but due to the instability of pulcherriminic acid only little amounts can be extracted with 1-butanol, which might also be the reason why chemical synthesis was not successful so far.

Investigations on iron dependent or independent antimicrobial activity

Gradient plates

Three different kinds of gradient plates were generated. Two plates, BM and RPMI-1640, which were supplemented with 100 μM $FeSO_4$, were made to get an idea about antimicrobial activity and production under high iron conditions as described in literature. And one plate, where free metal ions, especially iron ions, were chelated by usage of EDDHA and Chelex®100, was made, to see what happens under iron limited conditions. RMPI-1640 itself can be considered as iron poor medium, especially with the reduced amount of casamino acids used in this study. The RPMI-1640 plate supplemented with iron thus resembles on the one side iron limited conditions and on the other side iron rich conditions.

On BM plates supplemented with 100 μM $FeSO_4$ it is obvious, that antimicrobial activity is decreasing with increasing iron concentrations (Fig. 16). From top to bottom, *S. epidermidis* pRB473, *S. epidermidis* pRB473-*pacTSO*, *S. epidermidis* pRB473-*pacTRSO* can be seen on plate, with *S. aureus* NE773 as indicator strain in the background. On the far left of the plate, normal BM conditions are displayed and for *S. epidermidis* pRB473-*pacTRSO* a ZOI is visible. The ZOI increases a little bit to the middle of the plate with increasing iron concentrations and then decreases again with increasing iron concentrations and is hardly visible at 100 μM $FeSO_4$. The red coloration of the colonies, indicating pulcherriminic acid production with subsequent binding of the iron in the environment, is clearly visible, also for normal BM conditions when compared to the non-producing empty vector control *S. epidermidis* pRB473. Under these conditions, it is obvious, that *S. epidermidis* pRB473-*pacTSO* shows a sick phenotype, with signs of lysis of the cells. Despite no ZOI is visible, production can be seen by the strong red coloration of the strain with increasing iron concentrations. But due to the

sickness of the strain and the resulting decreased cell density compared to *S. epidermidis* pRB473-*pacTRSO*, the amount of produced pulcherriminic acid is most likely not high enough to diffuse into the agar and kill *S. aureus* JE2 NE773. It is also possible that due to immediate formation of pulcherrimin complexes in the proximity of the producer cells, *S. epidermidis* pRB473-*pacTSO* cells and also *S. epidermidis* pRB473-*pacTRSO* cells get sort of encapsulated at high iron concentrations, which enhances cell death due to reduced availability of nutrients [26]. Previous experiments however showed, that *S. epidermidis* pRB473-*pacTSO* is at least able to generate a ZOI under normal BM conditions, which is not visible on this plate. This might be due to a small amount of iron diffusing also in the area which can be considered as normal BM conditions, already leading to binding of all produced pulcherriminic acid und thus subsequent inactivation of the compound.
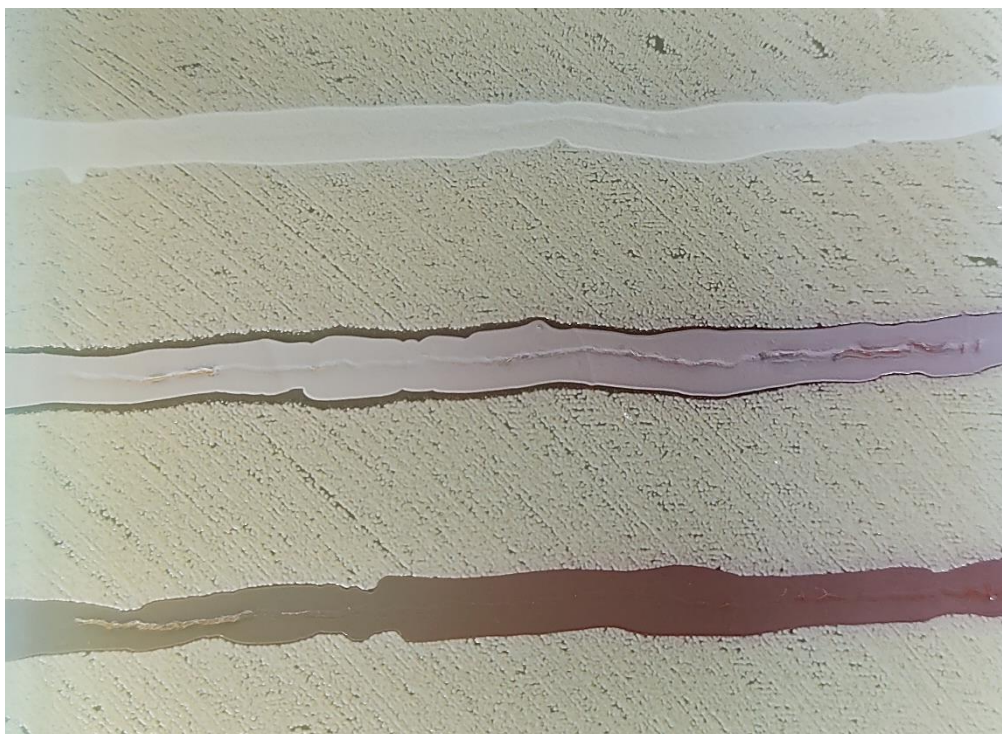

Figure 16: BM gradient plate with increasing FeSO$_4$ concentrations to the right (100 µM FeSO$_4$). Normal BM culture conditions are resembled on the far left of the plate. S. epidermidis pRB473 (top), S. epidermidis pRB473-pacTRSO (middle), S. epidermidis pRB473-pacTSO (bottom). S. aureus JE2 NE773 is used as indicator strain. (n=3)

On the BM gradient plates, deprived of any free iron on the far right of the plate, it is visible, that *S. epidermidis* pRB473-*pacTSO* is again able to generate a ZOI under normal BM conditions, resembled on the far left of the plate (Fig. 17). The ZOI of the deregulated strain as well as of the strain with the whole *pacTRSO* BGC increases with decreasing iron concentrations. It is to note that the indicator strain *S. aureus* JE2 NE773 seems to have some growth difficulties with increasing iron limitation. However, it seems as pulcherriminic acid can diffuse better in the agar when less iron is present in the environment, because *S. aureus* JE2

NE773 can be killed in more distance, indicated by the larger ZOI. Pulcherriminic acid is not inactivated by iron complexation in the medium but can instead act on the target cell by an unknown mechanism.
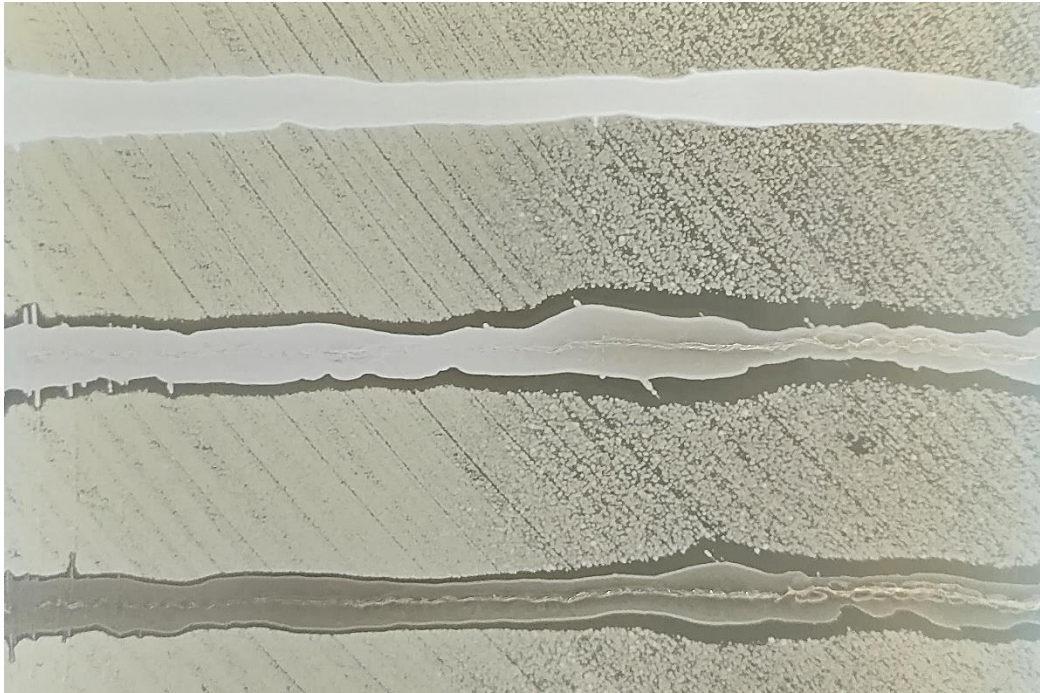

Figure 17: BM gradient plate with decreasing iron concentrations to the right. Normal BM culture conditions are resembled on the far left of the plate. S. epidermidis pRB473 (top), S. epidermidis pRB473-pacTRSO (middle), S. epidermidis pRB473-pacTSO (bottom). S. aureus JE2 NE773 is used as indicator strain. (n=3)

The RPMI-1640 plates supplemented with 100 µM $FeSO_4$ nicely summarize the previous findings. It can be observed, that both pulcherriminic acid producers show best antimicrobial activity under iron limited conditions (Fig. 18), resembled here by normal RPMI-1640 on the far left of the plate. The smaller ZOI for *S. epidermidis* pRB473-*pacTSO* might be due to the reduced OD_{600} the strain is able to reach and the general sick phenotype. The red coloration of the colonies can also be seen here and again supporting the previous results, that antimicrobial activity is not related to red colour formation or pulcherrimin formation to be more precise. It indeed seems like antimicrobial activity is best when no free environmental iron is present in the vicinity of the producer cell, so that pulcherriminic acid can diffuse in the agar to reach the target cell. The finding that *S. epidermidis* pRB473-*pacTRSO* is able to produce pulcherriminic acid under iron restriction indicates that the BGC might actually not be iron regulated [20, 21].
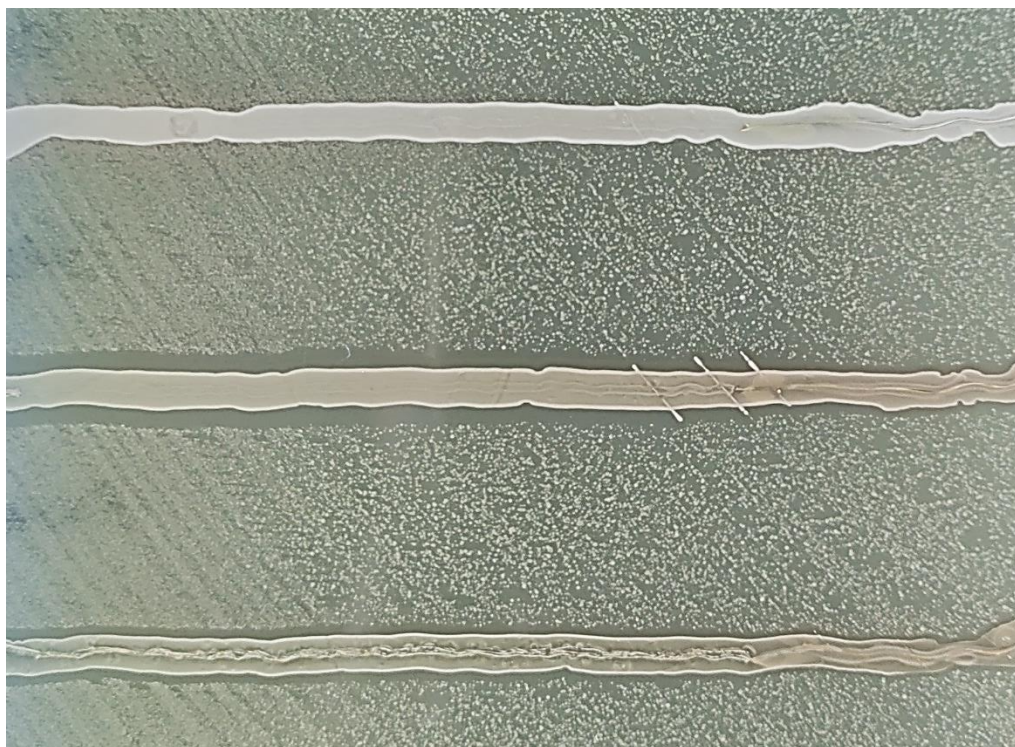
Figure 18: RPMI-1640 gradient plate with increasing iron concentrations to the right (100 µM FeSO₄). Normal RPMI culture conditions are resembled on the far left of the plate. S. epidermidis pRB473 (top), S. epidermidis pRB473-pacTRSO (middle), S. epidermidis pRB473-pacTSO (bottom). S. aureus JE2 NE773 is used as indicator strain. (n=3)

To summarize, these results indicate, that *pacTRSO* might not be iron regulated and that antimicrobial activity of pulcherriminic acid is not based on iron binding in the environment and subsequent growth inhibition of the target cell by iron starvation as described in literature [9, 12, 13, 15]. Recent studies only focused on the red colour, which only forms under iron presence, but the presented data show that pulcherriminic acid production and antimicrobial activity are not dependent on environmentally present iron. This arises the question of the actual mode of action of pulcherriminic acid. Another hint for an intracellular antimicrobial activity is the finding that sensitive strains can become resistant by expressing *pacTR*, which cannot be explained with inhibition by iron complexation.

Competition assay

Competition assays were performed to see, if pulcherriminic acid is bacteriostatic or bactericidal, how fast its antimicrobial activity is detectable and to confirm previous results that pulcherriminic acid acts independently of environmental iron. Therefore, *S. epidermidis* D2-30 was mixed with either *S. aureus* JE2 or *S. aureus* JE2 NE773 and bacterial ratios were determined after incubation on standard RMPI-1640, RPMI-1640 + 50 µM FeSO₄ or RPMI-1640 + 100 µM FeSO₄. To begin with, under normal RPMI-1640 conditions, *S. epidermidis* D2-

30 is able to overgrow *S. aureus* JE2 NE773 already after 24 hours whereas the resistant *S. aureus* JE2 starts to outcompete the producer (Fig. 19). But interestingly, the producer grows back after 48 hours and reaches almost 50% after 72 hours. This might be due to insufficient resistance of *S. aureus* JE2, and already previous experiments showed, that PacTR cannot protect from pulcherriminic acid to 100%. In general, the results of this competition assays show that pulcherriminic acid has a quite strong antimicrobial activity, which seems to be bactericidal. These findings also support the earlier mentioned assumption, that pulcherriminic acid is formed and acts on the target cell iron-independent also in the wild type isolate.
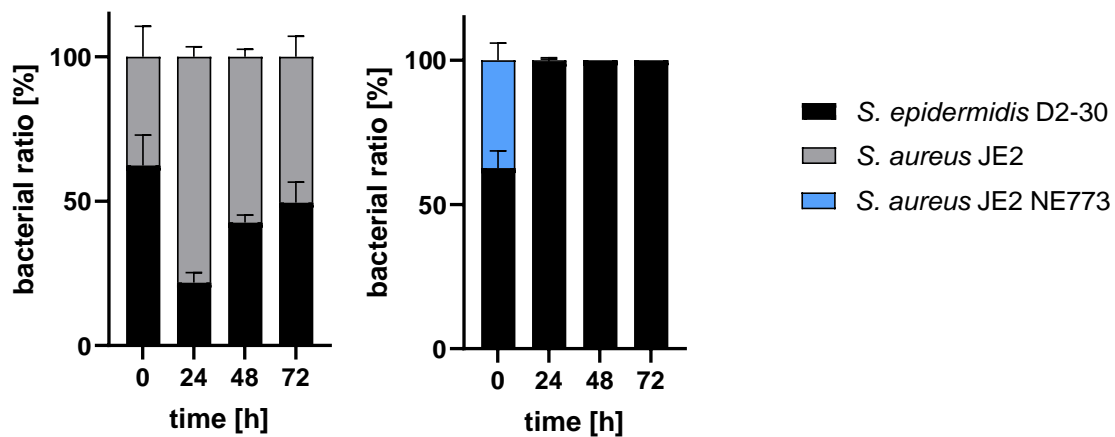

Figure 19: Bacterial ratios in percent, at timepoint 0, 24, 48 and 72 hours of cocultivation on RMPI-1640 + 0.1% casamino acids. (n=3)

At iron presence, the bacterial ratios only show slight variations compared to the iron-limited conditions (Fig. 20), indicating that free iron or iron in the medium/environment is dispensable for the antimicrobial effect of pulcherriminic acid.
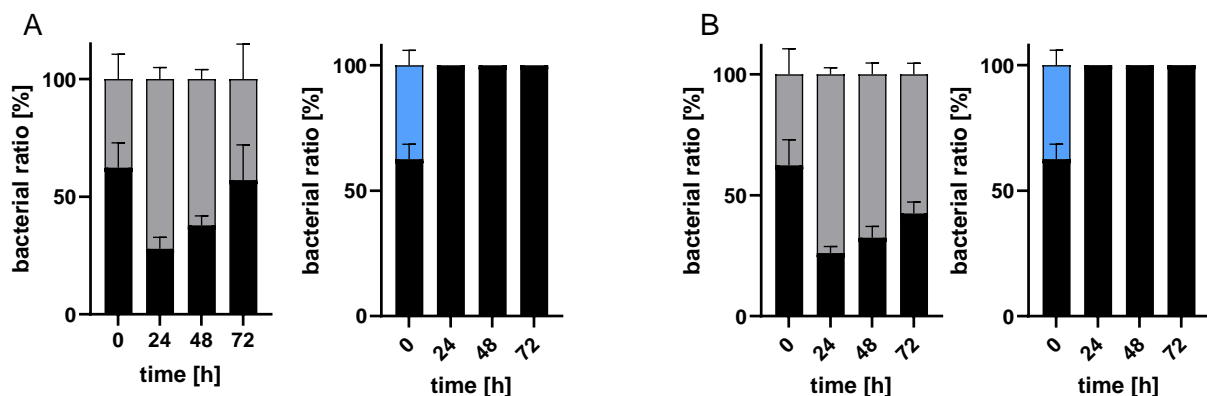

Figure 20: (A) Bacterial ratios in percent, at timepoint 0, 24, 48 and 72 hours of cocultivation on RMPI-1640 + 0.1% casamino acids supplemented with 50 μM FeSO₄. (B) Bacterial ratios in percent, at timepoint 0, 24, 48 and 72 hours of cocultivation on RMPI-1640 + 0.1% casamino acids supplemented with 100 μM FeSO₄. Grey: S. aureus JE2, blue: S. aureus JE2 NE773, black: S. epidermidis D2-30. (n=3)

In summary, the results from the gradient plates and the competition assay lead to the assumption that pulcherriminic acid biosynthesis seems to be iron independent and also antimicrobial activity is independent of environmentally present iron. With high amounts of free iron in the medium, all produced pulcherriminic acid is immediately bound and pulcherrimin complexes are formed. The active compound thus cannot diffuse into the agar and cannot reach the target cell. It seems like the formation of these pulcherrimin complexes is also not very beneficial for the producer, because at least on agar it gets sort of encapsulated in pulcherrimin complexes, cutting it off from the environment. This is already described in one of the first publications that pigmented cells are non-viable [6, 26]. The mode of action remains unclear, but it is most likely still related to some kind of iron binding. Maybe pulcherriminic acid binds iron intracellularly of the target cell leading to iron starvation, however on the supposition that pulcherriminic acid would also bind to Fe^{2+}, which is the more abundant form of iron in the cell [27]. In general, it can be said, that it is not the iron restriction in the environment, which leads to killing of the target cell and that the red colour formation is rather a side effect, also enforced by unphysiological iron concentrations under lab conditions.

Expression of pulcherriminic acid BGC found in other nasal isolates

Handling of different nasal isolates and analysis of different genomes revealed that *S. lugdunensis* IVK28, known as lugdunin producer [22], possesses the *pacTRSO* gene cluster, but is not showing the classical red colony phenotype on BM agar plates. Comparison of the BGC of *S. lugdunensis* IVK28 with *S. epidermidis* D2-30 revealed that *S. lugdunensis* IVK28 has a deletion of seven amino acids in PacO (Fig. 21). PacO sequences from different pulcherriminic acid producers (*S. epidermidis* D2-30, P4-45, 14-4, 17-20) were aligned with the PacO sequence of *S. lugdunensis* IVK28, showing a quite conserved sequence. PacO from *S. epidermidis* 17-20 seems to be an intermediate between PacO from *S. epidermidis* D2-30/P4-45/14-4 and *S. lugdunensis* IVK28, also visible in the phylogenetic tree. *S. epidermidis* D2-30/P4-45/14-4, in contrast to *S. lugdunensis* IVK28, all turn strongly red on plate.

Figure 21: Alignment of the protein sequences of PacO from different S. epidermidis (D2-30, P4-45, 14-4, 17-20) strains and one S. lugdunensis strain (IVK28). Sequences between the S. epidermidis strains seem to be quite conserved, only S. lugdunensis IVK28 exhibits the deletion of seven amino acids. The phylogenetic tree of CytX proteins from S. epidermidis (D2-30, P4-45, 14-4, 17-20) strains and one S. lugdunensis strain (IVK28) show clustering of the S. epidermidis D2-30, P4-45 and 14-4 sequence and with a more genetic distance the proteins from S. epidermidis 17-20 and S. lugdunensis IVK28.

To further investigate and to check for antimicrobial activity of these strains, *pacTRSO* from *S. epidermidis* 17-20 and *S. lugdunensis* IVK28 were heterologously expressed in *S. epidermidis* 1457. Heterologous expression was chosen, because both strains, *S. epidermidis* 17-20 and *S. lugdunensis* IVK28, are producers of other antimicrobial compounds besides pulcherriminic acid. Expression of *pacTRSO* in *S. epidermidis* 1457 from *S. epidermidis* 17-20 led to the generation of a ZOI on *S. aureus* JE NE773, but not of *pacTRSO* from *S. lugdunensis* IVK28 (Fig. 22).
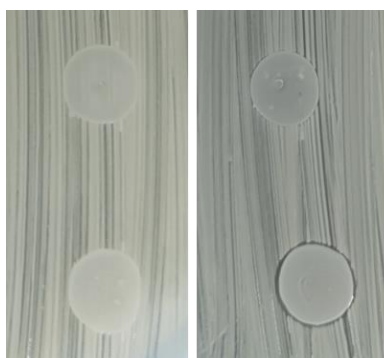

Figure 22: Spot assay of S. epidermidis 1457 pRB473-pacTRSO[IVK28] (upper row) and S. epidermidis 1457 pRB483-pacTRSO[17-20] (lower row) on S. aureus JE2 (left) and S. aureus JE2 NE773 (right).

Butanol extracts from *S. epidermidis* 1457 pRB473-pacTRSO[IVK28] were prepared, to confirm that pulcherriminic acid cannot be detected in the sample. The BPC chromatogram confirms that only the precursor cLL can be detected in the samples, but no pulcherriminic acid or derivatives (important time frame marked by red box) (Fig. 23). The relevant peaks, from minute 11 to 13, are shown in more detail in figure 24. The empty plasmid control *S. epidermidis* 1457 pRB473 (upper panel) does indeed also produce cyclic dipeptides without

the *pacTRSO* gene cluster, indicating again that *S. epidermidis* 1457 itself is also producing cyclic dipeptides. Analysis showed that cyclodileucine and cyclophenylleucine are produced by *S. epidermidis* 1457 pRB473. However, expression of pacTRSO[IVK28] (two lower panels) leads to an increase of the third peek visible in the BPC, which is now dominated by cyclodileucine instead of cyclophenylleucine, making it clearly distinguishable, which peak or compound originates from the strain itself or from *pacTRSO*. The obtained data thus indicate a stereospecific synthesis of cyclodileucine by *pacTRSO*.
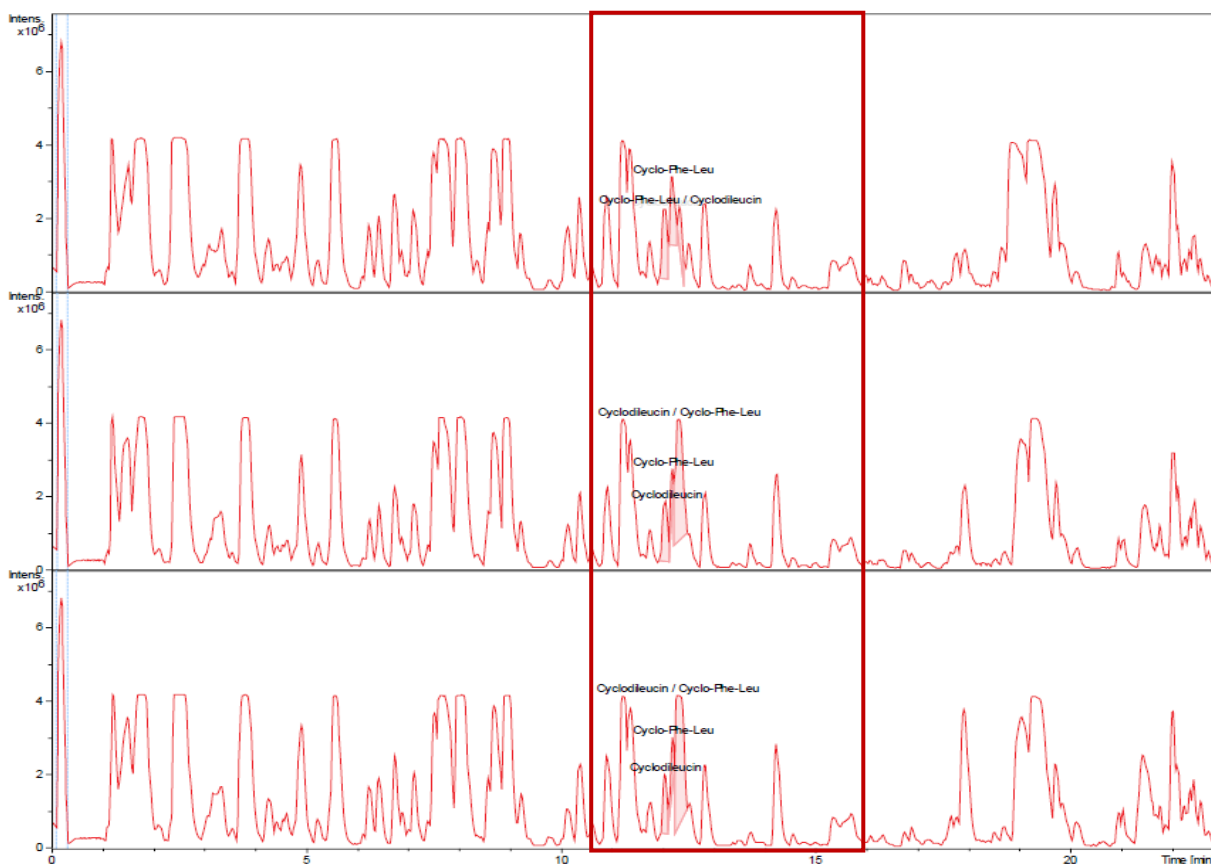

Figure 23: Chromatogram of 1-butanol extracts of S. epidermidis 1457 pRB473 (top) and two independent replicates of S. epidermidis 1457 pRB473-pacTRSO[IVK28] (middle and bottom). Indicated is the relative intensity.

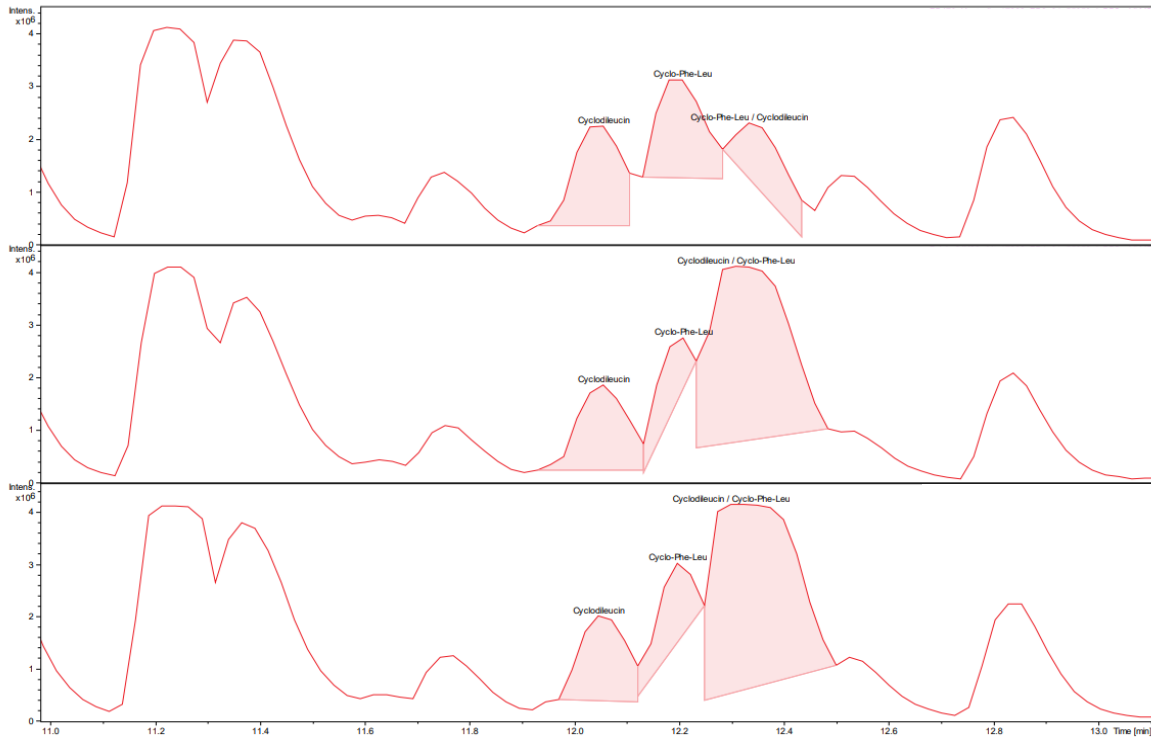*Figure 24: Chromatogram of 1-butanol extracts of S. epidermidis 1457 pRB473 (top) and two independent replicates of S. epidermidis 1457 pRB473-pacTRSO^{IVK28} (middle and bottom) zoomed in on minutes 11 to 13. Indicated is the relative intensity.*

Results obtained from the HPLC analysis can also be confirmed with MS data, showing a dominant peak for cyclophenylleucine (~261,16) in the *S. epidermidis* 1457 pRB473 sample and for cyclodileucine (~227,17) in the *S. epidermidis* 1457 pRB473-pacTRSO^{IVK28} extract (Fig. 25).
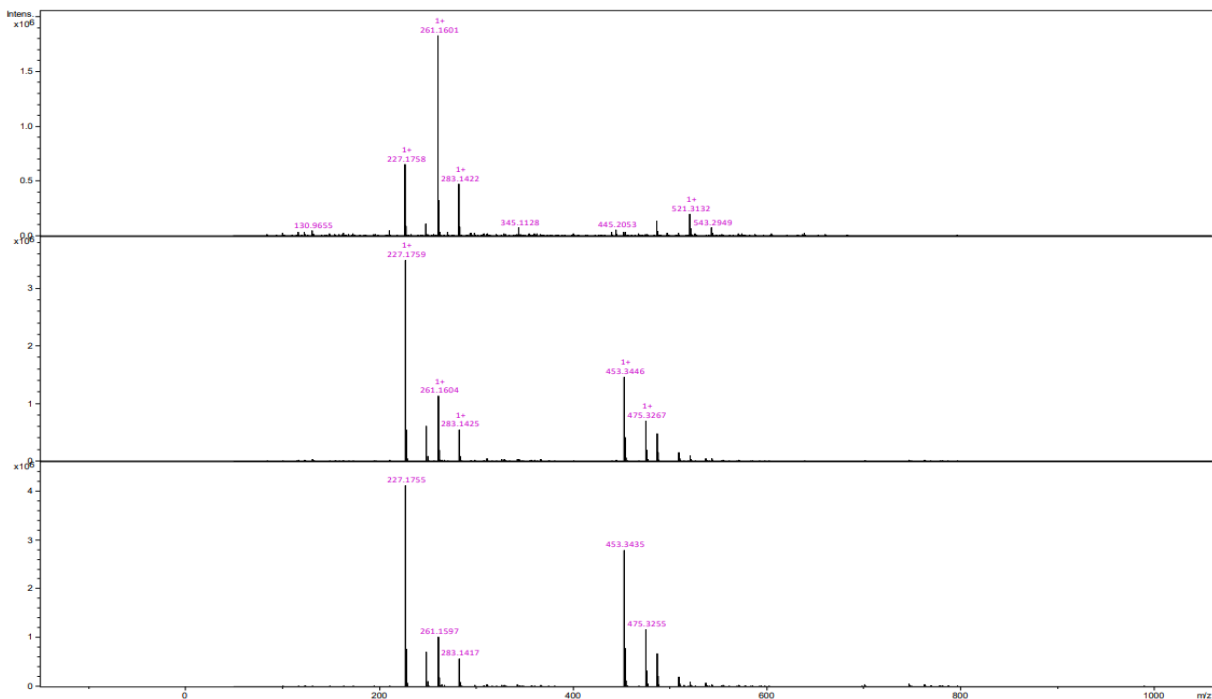

Figure 25: MS spectrum for 1-butanol extracts of S. epidermidis 1457 pRB473 (top) and two independent replicates of S. epidermidis 1457 pRB473-pacTRSO^{IVK28} (middle and bottom). Indicated is the relative intensity.

In summary, these results indicate that the mutation in PacO found in *S. lugdunensis* IVK28 leads to a non-functional protein abolishing final oxidation to pulcherriminic acid, but PacS is generating the precursor cLL, suggesting that the gene cluster itself is functional. Leading to the assumption that *S. lugdunensis* IVK28 might keep the gene cluster not for competing with other bacteria but for protecting itself via PacT.

Outlook

Further studies on pulcherriminic acid structure and function are necessary to finally confirm the antimicrobially active compound and to elucidate the mode of action. Therefore, chemical synthesis of pulcherriminic acid would be a huge milestone as purification from culture does not seem to yield enough compound. Furthermore, a knockout of the gene cluster in the wildtype strain *S. epidermidis* D2-30 would be useful to confirm the data obtained with the heterologous expressing strain. Based on the findings from the competition assay, transcriptome analysis could be performed from cocultures of *S. epidermidis* D2-30 with a target strain at different time points to see if specific genes are up- or downregulated in the target cell after contact to pulcherriminic acid. Electron microscopy of a target cell in close contact to a producer cell might also be helpful to get a hint about the mode of action of pulcherriminic acid. In summary it can be said, that pulcherriminic acid seems to be a very interesting but also challenging molecule and despite the over hundred years of research, only very little is known about it.

1. Cook A. H., S.C.A., *The Structure of Pulcherrimin.* J. Chem. Society, 1956: p. 4133-4135.
2. Cook, A.H., *Metabolism of "wild" yeasts. The chemical nature of pulcherrimin.* Brewing Industry Research Foundation, 1954. **60**: p. 213-217.
3. MacDonald, J.C., *Biosynthesis of pulcherriminic acid.* Biochem J, 1965. **96**(2): p. 533-8.
4. Bonnefond, L., et al., *Structural basis for nonribosomal peptide synthesis by an aminoacyl-tRNA synthetase paralog.* Proc Natl Acad Sci U S A, 2011. **108**(10): p. 3912-7.
5. Lindner, P., *Mikroskopische Betriebskontrolle in den Gärungsgewerben. Mit einer Einführung in die technische Biologie, Hefenreinkultur und Infektionslehre.* 1901: Paul Parey.
6. Beijerinck, M.W., *Pigment producing yeast. A new biologic reaction with iron.* Arch. Neerland. physiol., 1908. **2**: p. 609.
7. Canale-Parola, E., *A red pigment produced by aerobic sporeforming bacteria.* Archiv. Mikrobiol., 1963. **46**: p. 414-427.
8. Krause, D.J., et al., *Functional and evolutionary characterization of a secondary metabolite gene cluster in budding yeasts.* Proc Natl Acad Sci U S A, 2018. **115**(43): p. 11030-11035.
9. Sipiczki, M., *Metschnikowia strains isolated from botrytized grapes antagonize fungal and bacterial growth by iron depletion.* Appl Environ Microbiol, 2006. **72**(10): p. 6716-24.
10. Pawlikowska, E., et al., *Biocontrol capability of local Metschnikowia sp. isolates.* Antonie Van Leeuwenhoek, 2019. **112**(10): p. 1425-1445.
11. Uffen, R.L. and E. Canale-Parola, *Synthesis of pulcherriminic acid by Bacillus subtilis.* J Bacteriol, 1972. **111**(1): p. 86-93.
12. Wang, D., et al., *Regulation of the Synthesis and Secretion of the Iron Chelator Cyclodipeptide Pulcherriminic Acid in Bacillus licheniformis.* Appl Environ Microbiol, 2018. **84**(13).
13. Arnaouteli, S., et al., *Pulcherrimin formation controls growth arrest of the Bacillus subtilis biofilm.* Proc Natl Acad Sci U S A, 2019. **116**(27): p. 13553-13562.
14. Saravanakumar D, C.A., Spadaro D, Garibaldi A, Lodovica Gullino M, *Metschnikowia pulcherrima strain MACH1 outcompetes Botrytis cinerea, Alternaria alternata and Penicillium expansum in apples through iron depletion.* Postharvest Biology and Technology, 2008. **49**(1): p. 121-128.
15. Melvydas, V., et al., *In vitro inhibition of Saccharomyces cerevisiae growth by Metschnikowia spp. triggered by fast removal of iron via two ways.* Braz J Microbiol, 2020. **51**(4): p. 1953-1964.
16. Horvath, E., et al., *The antagonistic Metschnikowia andauensis produces extracellular enzymes and pulcherrimin, whose production can be promoted by the culture factors.* Sci Rep, 2021. **11**(1): p. 10593.
17. Gore-Lloyd, D., et al., *Snf2 controls pulcherriminic acid biosynthesis and antifungal activity of the biocontrol yeast Metschnikowia pulcherrima.* Mol Microbiol, 2019. **112**(1): p. 317-332.
18. Janisiewicz, W.J., T.J. Tworkoski, and C.P. Kurtzman, *Biocontrol Potential of Metchnikowia pulcherrima Strains Against Blue Mold of Apple.* Phytopathology, 2001. **91**(11): p. 1098-108.
19. Kluyver, A.J., J.P. van der Walt, and A.J. van Triet, *Pulcherrimin, The Pigment of Candida Pulcherrima.* Proc Natl Acad Sci U S A, 1953. **39**(7): p. 583-93.
20. Kupfer, D.G., R.L. Uffen, and E. Canale-Parola, *The role of iron and molecular oxygen in pulcherrimin synthesis by bacteria.* Arch Mikrobiol, 1967. **56**(1): p. 9-21.
21. Randazzo, P., et al., *The MarR-like protein PchR (YvmB) regulates expression of genes involved in pulcherriminic acid biosynthesis and in the initiation of sporulation in Bacillus subtilis.* BMC Microbiol, 2016. **16**(1): p. 190.
22. Zipperer, A., et al., *Human commensals producing a novel antibiotic impair pathogen colonization.* Nature, 2016. **535**(7613): p. 511-6.

23. Meijer, W.J., et al., *Characterization of the replication region of the Bacillus subtilis plasmid pLS20: a novel type of replicon.* Nucleic Acids Res, 1995. **23**(16): p. 3214-23.
24. Val-Calvo, J., et al., *pLS20 is the archetype of a new family of conjugative plasmids harboured by Bacillus species.* NAR Genom Bioinform, 2021. **3**(4): p. lqab096.
25. Grove, A., *MarR family transcription factors.* Curr Biol, 2013. **23**(4): p. R142-3.
26. Roberts, C., *The effect of iron and other factors on the production of pigment by the yeast Torulopsis pulcherrima.* Am J Bot, 1946. **33**(4): p. 237-44.
27. Frawley, E.R. and F.C. Fang, *The ins and outs of bacterial iron metabolism.* Mol Microbiol, 2014. **93**(4): p. 609-16.

Supplementary data

Table 3: Overview of sequenced nasal isolates and identified BGCs.

ID	Species	Identified gene cluster(s) by antiSMASH	bacteriocin class	Location of BGC
3-17	*S. aureus*	BsaA1 and BsaA2	lantibiotic	chromosome
6-9/12	*S. warneri*	epilancin	lantibiotic	chromosome
6-14	*S. epidermidis*	epidermin	lantibiotic	chromosome
7-7	*S. epidermidis*	Blp family class II bacteriocin	class II	plasmid
9-14	*S. epidermidis*	unknown 3 peptide bacteriocin cluster	-	chromosome
10-20	*S. epidermidis*	epidermin	lantibiotic	plasmid
12-9	*S. epidermidis*	pulcherriminic acid	-	chromosome
14-4	*S. epidermidis*	epifadin + pulcherriminic acid	- -	plasmid plasmid
16-9	*S. capitis*	capidermicin	class II	chromosome
17-20	*S. epidermidis*	unknown 3 peptide bacteriocin cluster + pulcherriminic acid	- -	chromosome plasmid
17-29	*S. epidermidis*	unknown NRPS	-	chromosome
18-19	*S. warneri*	nukacin ISK-1	lantibiotic	plasmid
P1-22	*S. aureus*	aureocin A70	class II	plasmid
D4-19	*S. aureus*	micrococcin P1	thiopeptide	plasmid
D2-30	*S. epidermidis*	pulcherriminic acid	-	plasmid
P4-45	*S. epidermidis*	pulcherriminic acid	-	plasmid
P5-23	*S. epidermidis*	pulcherriminic acid + unknown BGC	-	plasmid
D2-37	*S. lugdunensis*	lugdunin	fibupeptide	chromosome
W1-7	*S. epidermidis*	pulcherriminic acid + lactococcin G	- class II	plasmid plasmid
W2-13	*S. epidermidis*	epifadin + pulcherriminic acid	- -	plasmid plasmid

Contributions to publications

Chapter 3 – Secretion of and self-resistance to the novel fibupeptide antimicrobial lugdunin by distinct ABC transporters in _Staphylococcus lugdunensis_

For this publication, I constructed plasmids and strains and performed MIC tests.

Chapter 4 – Extremely short-lived peptide-polyene antimicrobial enables nasal commensal to eliminate _Staphylococcus aureus_ (in revision)

I provided two _S. epidermidis_ strains harboring a plasmid highly similar to pIVK83 and the corresponding plasmid and genome sequences.

Chapter 5 – Acquisition of bacteriocin biosynthesis genes causes physiological burdens by disbalancing central metabolism (ready for submission)

I performed all experiments (by myself or in cooperation) but the following:

Chemical analysis of micrococcin P1 (Schäfle T, Grond S), analysis of proteome data (Franz-Wachtel M, Macek B), bioinformatic analysis of transcriptome and proteome data (Harbig TA, Nieselt K), chemical analysis of metabolome data (Rapp J, Link H), phylogenetic analysis of _citZ_ in _S. aureus_ (Elsherbini A).

Curriculum vitae

removed